Université de Montréal

Calcium dynamics and related alterations in pulmonary hypertension associated with heart failure

par Nour Dayeh

Département de Médecine
Faculté de Médecine

Thèse présentée à la Faculté de Médecine
en vue de l'obtention du grade de *Philosophiae Doctor* (Ph.D)
en Sciences biomédicales
option générale

Août, 2018

Cette thèse intitulée :

Calcium dynamics and related alterations in pulmonary hypertension associated with heart failure

Présentée par :

Nour Dayeh

a été évaluée par un jury composé des personnes suivantes :

Dr Anique Ducharme, président-rapporteur

…….

Dr Jocelyn Dupuis, directeur de recherche

…….

Dr Jonathan Ledoux, co-directeur de recherche

…….

Dr Guy Rousseau, membre du jury

…….

Dr Sébastien Bonnet, examinateur externe

…….

Résumé

L'insuffisance cardiaque (IC) représente un problème de santé important au Canada. La plupart des patients atteints d'IC développent une hypertension pulmonaire (HP), qui est un marqueur de la progression de la maladie et de son mauvais pronostic. Des progrès significatifs ont été réalisés pour le traitement de l'IC. Néanmoins, la morbidité et la mortalité chez les patients atteints d'IC avancée, qui ont développé l'HP reste élevée.

L'augmentation de la pression vasculaire pulmonaire (PVP) observée en HP entraîne une augmentation du tonus vasculaire et un remodelage vasculaire associés à des réponses vasodilatatrices altérées. En effet, une diminution des réponses vasodilatatrices a été observée dans l'HP. La dysfonction endothéliale est au cœur des altérations vasodilatatrices. Cette caractéristique de la plupart des maladies cardiovasculaires est associée à des altérations de l'homéostasie du calcium (Ca^{2+}).

Bien que le Ca^{2+} global joue un rôle dans un grand nombre de fonctions cellulaires, la présente thèse est concentrée sur l'impact de la signalisation calcique locale dans les cellules endothéliales (CE). Parmi les différents types de signaux calciques locaux, les pulsars ont été identifiés. Les pulsars calciques sont des évènements endothéliaux locaux dont l'activité est finement régulée par des agents physiologiques qui modulent les niveaux intracellulaires d'inositol 1,4,5-triphosphate (IP_3) et de Ca^{2+}. Les pulsars ont un effet sur plusieurs fonctions cellulaires importantes. Dans les artères mésentériques, les pulsars induisent une relaxation des cellules musculaires lisses vasculaires. Jusqu'à présent, les mécanismes de régulation des pulsars Ca^{2+} restent à découvrir. Les caractéristiques spatio-temporelles des pulsars suggèrent qu'ils pourraient jouer un rôle dans le contrôle du tonus vasculaire pulmonaire, impliquant potentiellement plus de canaux ioniques transmembranaires, ainsi que des protéines régulatrices. Les canaux TRP de la famille vanilloïde 4 (TRPV4) sont des canaux cationiques méchanosensitifs, non sélectifs, largement exprimés dans un nombre de tissus. L'activation des canaux TRPV4 permet l'entrée de Ca^{2+} dans la cellule. Des études ont montré l'implication de TRPV4 ainsi que d'autres canaux de la famille TRP dans l'HP.

Les mécanismes physiopathologiques liés au Ca^{2+} endothélial modulant le tonus vasculaire pulmonaire et conduisant au développement de l'HP du groupe II sont mal définis. En outre, la

rareté des études explorant la physiopathologie et les thérapies de l'HP du groupe II réside dans l'absence de modèles animaux validés pour l'étude de l'HP du groupe II, avec une détermination adéquate de la présence et de la sévérité de l'HP.

Les travaux issus de cette thèse ont identifié et caractérisé pour la première fois des pulsars Ca^{2+} intracellulaires dans l'endothélium pulmonaire et leurs altérations dans un modèle de souris cliniquement significatif de l'HP de groupe II qui a été développé. En outre, ce travail a révélé l'implication des canaux TRPV4 endothéliaux dans la dérégulation des pulsars Ca^{2+} dans l'HP du groupe II.

Mots-clés :

Hypertension pulmonaire, Insuffisance cardiaque , Calcium, Pulsars, TRPV4

Abstract

Congestive heart failure (CHF) represents an important Canadian health problem. Most patients with CHF develop pulmonary hypertension (PH), which is an important marker that signals progression of the disease and its poor outcome. Significant advances have been made for the treatment of heart failure (HF). Nevertheless, the morbidity and mortality among patients with advanced heart HF, who have developed PH remains high.

Increased pulmonary vascular pressure (PVP) observed in PH leads to increased vascular tone and vascular remodelling associated with altered vasodilatory responses. It is noteworthy that a decrease in vasodilatory responses has been observed in PH. At the core of vasodilatory alterations lies endothelial dysfunction. This hallmark of most cardiovascular diseases is associated with alterations in calcium (Ca^{2+}) homeostasis.

Although global Ca^{2+} plays a role in a wide range of cellular functions, this thesis work focused on the impact of local Ca^{2+} signalling in endothelial cells (ECs). Among the different types of local Ca^{2+} signals, Ca^{2+} pulsars were identified. Ca^{2+} pulsars are local endothelial Ca^{2+} signals whose activity is finely regulated by physiological agents that modulate intracellular levels of inositol 1,4,5-triphosphate (IP3) and Ca^{2+}. Ca^{2+} pulsars have been shown to have an effect on several important cellular functions. In mesenteric arteries, Ca^{2+} pulsars induce endothelium-induced relaxation of vascular smooth muscle cells. Up until now, the regulatory mechanisms of Ca^{2+} pulsars remain to be uncovered. The spatio-temporal characteristics of Ca^{2+} pulsars suggest that they could play a role in the control of pulmonary vascular tone, potentially involving more transmembrane ion channels, as well as regulatory proteins. Transient receptor potential vanilloid 4 (TRPV4) channels are non-selective mechanosensitive osmo-regulated cation channels broadly expressed in a number of tissues. Activation of TRPV4 channels allows Ca^{2+} entry into the cell. A number of studies have shown the implication of TRPV4 as well as other channels from the TRP family in PH.

Endothelial Ca^{2+}-related pathophysiological mechanisms modulating pulmonary vascular tone and leading to the development of group II PH are poorly defined. In addition, the scarcity of studies exploring the pathophysiology and therapies of group II PH resides in the lack of validated small animal models with an adequate determination of the presence and severity of PH.

The work in this thesis identified and characterized for the first time intracellular Ca^{2+} pulsars in pulmonary endothelium and their alterations in a clinically relevant mouse model of group II PH that was developed. In addition, this work revealed the implication of endothelial TRPV4 channels in Ca^{2+} pulsars dysregulation in group II-PH.

Keywords:
Pulmonary hypertension, Heart failure , Calcium, Pulsars, TRPV4

Table of contents

List of tables

List of figures

List of abbreviations

PH	Pulmonary hypertension
HF	Heart failure
mPAP	Mean pulmonary arterial pressure
PVR	Pulmonary vascular resistance
Group I-PAH	Pulmonary arterial hypertension
PH-LHD	Pulmonary hypertension associated to left heart disease
PA	Pulmonary artery
PV	Pulmonary vein
EC	Endothelial cell
NO	Nitric oxide
PGI_2	Prostacyclin
ET-1	Endothelin-1
Ang II	Angiotensin II
TxA_2	Thromboxane A_2
IEL	Internal elastic lamina
MEP	Myoendothelial projection
SMC	Smooth muscle cell
Ca^{2+}	Calcium
CaM	Calmodulin
MLCK	Myosin light chain kinase
MLC20	Myosin light chain
ATP	Adenosine triphosphate
MLCP	Myosin light chain phosphatase
PVSMC	Pulmonary vascular smooth muscle cell
NANC	Non-adrenergic non-cholinergic system
PAP	Pulmonary arterial pressure
NOS	Nitric oxide synthase
sGC	Soluble guanylate cyclase
cGMP	Cyclic guanosine monophosphate

PKG	cGMP-dependent protein kinase
NCX	Na^+/Ca^{2+} exchanger
K^+	Potassium
AA	Arachidonic acid
Cox	Cyclooxygenase
cAMP	Cyclic adenosine monophosphate
PKA	Cyclic adenosine monophosphate-dependent protein kinase A
BKca	Large conductance calcium-activated potassium channel (Kca 1.1)
Kir	Inward rectifying potassium channel
Kv	Voltage-dependent potassium channel
EDHF	Endothelium-derived hyperpolarizing factors
EETs	Epoxyeicosatrienoic acids
H_2O_2	Hydrogen peroxide
IK	Intermediate conductance Ca-activated K channel
SK	Small conductance Ca-activated K channel
MEGJ	Gap junctions at the MEP level
TGF-β	Transforming growth factor β
ET_A	Endothelin receptor A
ET_B	Endothelin receptor B
COPD	Chronic obstructive pulmonary disease
PLC	Phospholipase C
IP_3	Inositol triphosphate
DAG	Diacylglycerol
ACE	Angiotensin converting enzyme
5-HT	Serotonin
PAH	Pulmonary arterial hypertension
ER	Endoplasmic reticulum
IP_3R	inositol 1,4,5-triphosphate receptor
RRy	Ryanodine receptors
CaMKII	Ca/CaM-dependent protein kinase II
SERCA	Sarco-endoplasmic reticulum calcium ATPase

SR	Sarcoplasmic reticulum
NFAT	Nuclear factor of activated T-cells
HUVEC	Human umbilical vein endothelial cells
HPAEC	Human pulmonary artery endothelial cells
PIP_2	Phosphatidylinositol 4,5-biphosphate
eNOS	Endothelial nitric oxide synthase
STOC	Spontaneous transient outward current
VDCC	Voltage-dependent Ca^{2+} channels
TRPV4	Transient receptor potential vanilloid 4
TRP	Transient receptor potential
TRPC	Transient receptor potential canonic
TRPM	Transient receptor potential melastatin
TRPP	Transient receptor potential polycyctine
TRPML	Transient receptor potential mucopiline
TRPA	Transient receptor potential ankyrine
TRPN	Transient receptor potential nompC
CNS	Central nervous system
DRG	Dorsal root ganglia
NGF	Nerve growth factor
PI3K	Phosphatidylinositol-3-kinase
OTRPCA4	Osm-9-like TRP channel 4
VR-OAC	Vanilloid receptor-related osmitically activated channel
CaM-BD	Calmodulin-binding domain
CYP450	Cytochrome P450
4α-PDD	4α-phorbol-12,13-didecanoate
GSK1016790A	N-((1S)-1-3-hydroxypropanoyl)-1-piperazinyl]carbonyl}-3-methylbutyl)-1-benzothiophene-2-carboxamide
HC067047	2-Methyl-1-[3-(4-morpholinyl)propyl]-5-phenyl-*N*-[3-(trifluoromethyl)phenyl]-1*H*-pyrrole-3-carboxamide
WHO	World health organization
Group II-PH	PH associated with left heart failure

Group III-PH	PH associated with chronic disease and/or hypoxia
Group IV-PH	PH associated with chronic thromboembolic disease
Group V-PH	PH due to multifactorial mechanisms
BMPR2	Bone morphogenic protein receptor 2
ACVRL1	Activin kinase receptor type 1
HFrEF	Heart failure with reduced ejection fraction
HFpEF	Heart failure with preserved ejection fraction
LV	Left ventricle
PCWP	Pulmonary capillary wedge pressure
TPG	Transpulmonary gradient
IPF	Idiopathic pulmonary fibrosis
CPFE	Pulmonary fibrosis combine with emphysema
PHCTE	PH related to chronic thromboembolic disease
PDE	Phosphodiesterase
VIP	Vasoactive intestinal peptide
CO	Cardiac output
MCT	Monocrotaline
(HIF-1α)-k^+	Mitochondrial reactive oxygen species inducible factor α
PAB	Pulmonary artery banding
RV	Right ventricle
SU-5416	Semaxinib
VEGF	Vascular endothelial growth factor
RVH	RV hypertrophy
RVSP	RV systolic pressure
TAC	Transverse aortic constriction
LVEDP	Left ventricular end diastolic pressure
RVEDP	Right ventricular end diastolic pressure
PPHN	Persistent PH of the newborn
PAAT	Pulmonary artery acceleration time
TAPSE	Tricuspid annular plane systolic excursion
TNF- α	Tumor necrosis factor α

To my family.

Acknowledgements

I would like to thank members of my jury, Dr. *Anique Ducharme*, Dr. *Guy Rousseau*, and Dr. *Sébastien Bonnet* for taking part in the completion of this thesis.

I would like to thank my supervisor Dr. *Jocelyn Dupuis* and my co-supervisor Dr. *Jonathan Ledoux* for their dedication to the realization of my thesis. I have experienced growth on a personal and intellectual level.

I would like to thank Dr. *Dupuis* for his guidance, mentorship, wise advice and his belief in my capacities at times when I did not believe in myself. I would like to thank Dr. *Ledoux* for his commitment, for constantly pushing me to think deeper and creatively, for his great ideas in my project, and for allowing me the chance to participate in different projects in his lab.

I would like to thank *Emma Dedelis*. I am very thankful for your sense of humour and sarcasm, which got me through some very rough times. And, of course thank you for your great technical assistance. Some experiments were humanly impossible for one person to do and you were always there. Thank you for the chocolate, and candy, and cookies etc…

Thank you to everyone who participated in my project, Yanfen Shi, Marc-Antoine Gillis, Louis Villeneuve, and to all members of both labs I was part of.

To Dr *Yahye Merhi*, thank you for not letting me give up, for being a listening ear and for your wise advice.

To my friends, *Hneineh*, *Mira*, *Hiba*, *Hassan*, and *Omar*. Thank you for being there for better or for worse. To friends I made at the Montreal Heart Institute, *Sam*, *Celia*, *Sherine*, *Anh-tuan*, and *Nassiba*, thank you for making MHI a pleasant and happy place to work at. I will cherish these times forever.

Mira, the bestie, the partner in crime, you give a completely new meaning to the word friendship!

To *Peter*, I am beyond words. Thank you for your patience, constant support and encouragement, and for being the most understanding at difficult times.

To my parents and two brothers, who have been my constant support system, thank you for your unconditional love and unlimited support. *Joumana* and *Riad*, everything I am and everything I will be is thanks to both of you. I love you and forever will be grateful.

To every single person who has brought happiness to my heart, thank you from the bottom of mine.

I am seeking. I am striving. I am in it with all my heart.

Vincent Van Gogh

I. Chapter I: Introduction

Pulmonary hypertension (PH) is a common complication in heart failure (HF). It is considered as group II according to international clinical guidelines [1, 2]. It is characterized by a progressive increase in mean pulmonary arterial pressure (mPAP) and pulmonary vascular resistance (PVR) successively inducing right ventricular hypertrophy and death. The disease is under-diagnosed and clinically detectable in its later stage. Current clinically approved pharmacological treatments only slow the progression of the disease without treating it permanently and are primarily limited to pulmonary arterial hypertension (group I-PAH). Extensive ongoing clinical trials are yet to confirm their validity for the treatment of pulmonary hypertension associated to left heart disease (PH-LHD). PH-LHD therefore remains an important public health problem and a better understanding of the cellular and molecular mechanisms underlying this condition is necessary for the development of innovative and effective therapies.

1. The pulmonary system

The main function of the cardio-pulmonary apparatus is to provide tissues with oxygen rich blood, thus allowing their proper functioning. Deoxygenated blood coming from the right ventricle reaches the lungs through the right and left pulmonary arteries (PAs). It circulates the arteries, arterioles, reaching the pulmonary capillaries. Gas exchange occurs within the alveolar-capillary surface, and oxygen rich blood returns through the pulmonary veins to the left heart.

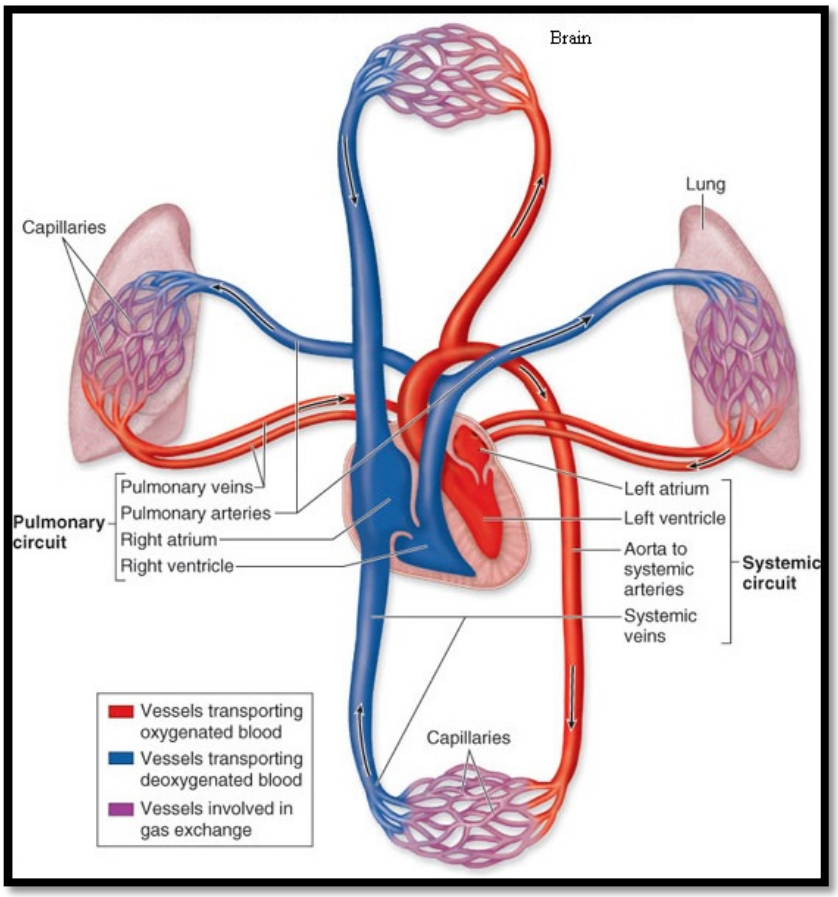

Figure 1 The systemic and pulmonary circulations (http://academic.kellogg.cc.mi.us)

1.1. Anatomical and functional organization of the lungs

In the thoracic cavity, the lungs are enclosed by the pleural membrane, which is composed of two layers: an outer membrane (the parietal pleura) that lines the chest wall and diaphragm, and an inner membrane (visceral pleura) separated by an inter-pleural space which contains fluid

secreted by both membranes. The right lung is divided into three lobes (superior, middle, and inferior), while the left lung is composed of two lobes (superior and inferior).

The lungs are connected to the trachea by the right and left bronchi that branch from the main bronchus. Each lobe in the lung is supplied by a bronchopulmonary segment. A lobe subdivides into smaller lobules separated by a septum with the branching of bronchi into bronchioles. Inside a lobule, a bronchiole subdivides into multiple branches.

Blood supply to the lungs begins with the PA that arises from the pulmonary trunk carrying deoxygenated arterial blood to the alveoli. The PA branches in parallel with the bronchi reaching the level of smaller arterioles. One arteriole and an accompanying vein supply and drain one pulmonary lobule. As they approach the alveoli, pulmonary arterioles become the pulmonary capillary network. At the level of the alveolar-capillary membrane, where the capillary wall meets the alveolar wall, gas exchange occurs.

1.2 Cellular composition of the lungs and airways

The trachea, bronchi, and bronchioles are lined with ciliated columnar epithelial cells, intercepted by serous cells, as well as club cells with a macrophage-like role. Starting at the level of terminal bronchioles, pulmonary epithelial cells lose their cilia and are intercepted by goblet cells capable of producing mucus.

The walls of alveoli are lined with two types of cells termed alveolar cells type I (squamous pneumocyte) and type II (granular pneumocyte), supported by a thin layer of connective tissue. Type I alveolar cells, which are the main cells paving the structure of alveoli, have extremely thin walls that allow easy gas exchange. Type II alveolar cells have a cuboidal shape, possess microvilli, and produce and secrete lung surfactant. Lung surfactant mainly composed of lipids and proteins, is secreted into the alveolar space. It has a number of functions that include prevention of lung collapse during expiration, supporting inspiratory opening of the lungs, and balancing hydrostatic filtration forces to prevent lung oedema formation. In addition to its biophysical functions, lung surfactant possesses immunological functions [3], and protects the lungs from micro-organisms and toxins. Macrophages are also found inside the alveoli and are responsible for keeping the lungs free of pathogens and other foreign matter that can enter

the alveoli with inhaled air. All the epithelial cells lining the respiratory tract except for type I alveolar cells secrete epithelial lining fluid, which covers the mucosa of the alveoli and airways. The pulmonary circulation comprises several cell types that compose the different layers of pulmonary vessels depending on vessel calibre and type.

1.3 Structure of pulmonary arteries, arterioles and capillaries

The pulmonary vasculature has a low pressure and low resistance under normal conditions. It accommodates 100% of the cardiac output [4]. Therefore, the structure of PAs and pulmonary veins (PVs) differ from the systemic one on a variety of levels. In general, pulmonary vessels are more compressible and distensible than systemic ones. Additionally, pulmonary vessels are thin-walled compared to their systemic counterparts, and have less vascular smooth muscle [5]. Similarly to systemic arteries, PAs are composed of three histologically distinct layers: the tunica intima, the tunica media, and the tunica adventitia.

1.3.1 The tunica intima

The tunica intima is the inner layer of PAs, as well as the only layer forming pulmonary capillaries [6]. It is a monolayer of endothelial cells (ECs) separated by intercellular tight junctions resting on a basal membrane that is secreted by ECs. It is responsible for gas exchange at the alveolar-capillary level, as well as endothelial control of the pulmonary circulation through the release of a number of molecules and factors (Nitric oxide (NO), prostacyclin (PGI_2), endothelin 1 (ET-1), angiotensin II (Ang II), thromboxane A_2 (TxA_2). Pulmonary vascular ECs are aligned in the direction of blood flow, and exclusively express a number of proteins like lung endothelial cell adhesion molecule-1 and endothelial specific molecule-1 [7]. The pulmonary endothelium is a metabolically active surface that plays an important role in immunologic and inflammatory events [8]. Endothelial dysfunction is a major contributor to a wide range of diseases [9], notably PH . In fact, several studies have revealed that pulmonary ECs abnormalities (in morphology and function) were major contributors and sole initiators of the pulmonary remodelling process [10] [11] [12].

1.3.2 The internal elastic lamina

The internal elastic lamina (IEL) consists of elastic fibers and its thickness varies according to vessel diameter and vascular bed. The structure of the IEL can vary as well. Some IEL contain holes termed fenestrations. It general, the size and density of fenestrations are inversely proportional to vessel calibre and greatly dependent on vessel function [13, 14] [15] [16]. In the pulmonary circulation, the IEL is fenestrated and through its fenestrations, extensions from ECs pass and are in contact with smooth muscle cells (SMCs). These myoendothelial projections (MEPs) (around 0.5 μm width and 0.5 μm depth variable from one vascular bed to another) have been shown to play an important role in the control of vascular function through the release and diffusion of vasoactive substances [17] [18]. Additionally, it has been shown that modulation in the number of IEL holes occurs in pathological conditions [13], including PH [14]. Results regarding hole density in pathological states have varied. In some hypertensive rat models, hole density was found to be lower compared to normotensive rats in some stains, while it remained the same for both groups in other strains [13]. In PH, a study on patients with congenital cardiac shunts revealed that the number of IEL gaps in peripheral pulmonary arteries was lower in pre-acinar arteries compared to a control group[14].

1.3.3 The tunica media

The tunica media is the middle layer of PAs. It is mainly composed of longitudinally arranged SMCs, connective tissue, collagen and elastic fibers. It is separated from the tunica intima by the IEL. In PAs, the contribution of the media to the total wall thickness varies with vessel diameter. Additionally, the number and alignment of elastic lamina varies according to diameter and type. Pulmonary vascular SMCs are responsible for the maintenance of pulmonary vascular tone, vascular resistance, as well as contractile response upon stimulation. An increase in intracellular calcium (Ca^{2+}) levels leads to its binding to the (Ca^{2+})-binding protein calmodulin (CaM). The then formed Ca^{2+}-CaM complex binds to and activates myosin light chain kinase (MLCK) via the C-terminal domain of CaM. Activated MLCK phosphorylates myosin light chain (MLC20) resulting in the interaction of myosin and actin filaments in an ATP-dependent manner [19] [20]. De-phosphorylation of MLC20 by myosin light chain

phosphatase (MLCP) inhibits the interactions between myosine and actine filaments, and consequently ends vascular contraction.

1.3.4 The tunica adventitia

The tunica adventitia of PAs, the outermost layer, is separated from the media by the external elastic lamina. It is loosely organized, composed of fibroblasts and a collagen matrix that reinforces vessels and protects their integrity. The tunica adventitia of larger vessels contains vasa vasorum, a capillary network that nourishes the external tissues of the blood vessel wall [6]. In the pulmonary circulation, fibroblasts of the tunica adventitia have been shown to play an important role in the response to environmental stimuli [21].

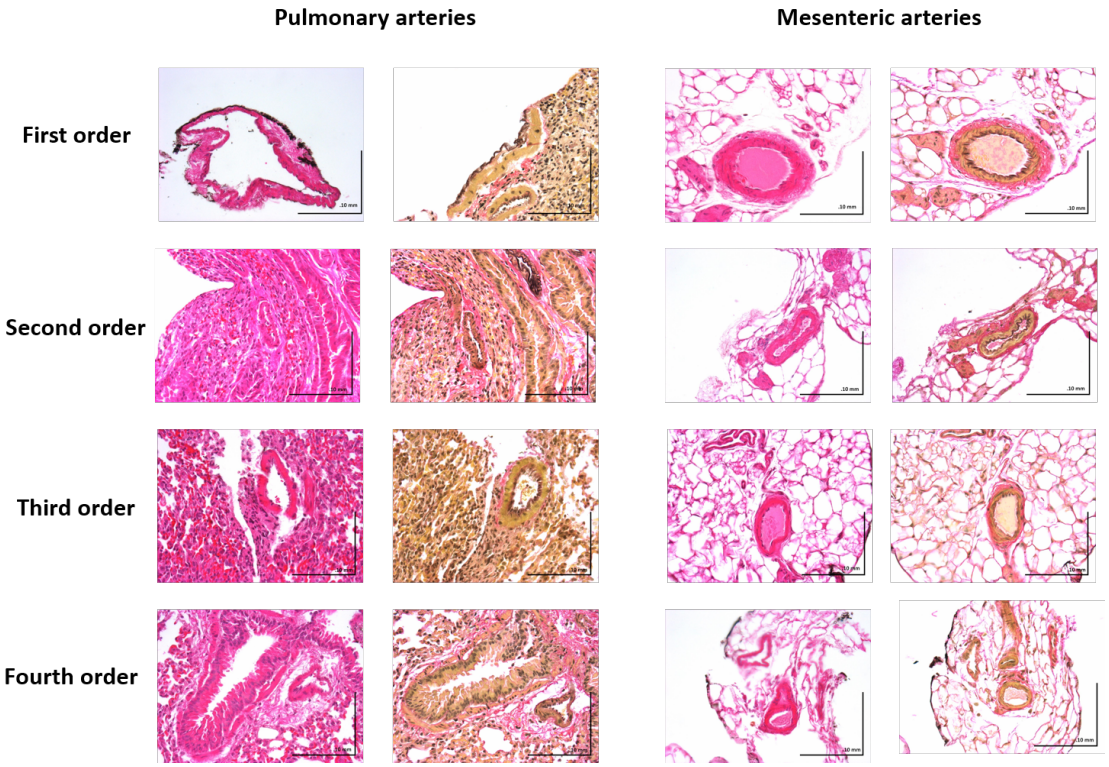

Figure 2 Structural differences between pulmonary arteries and mesenteric arteries of mice

Hematoxylin and eosin staining of cross-sections of mouse pulmonary and mesenteric arteries of different orders (scale bar: 10 mm).

1.4 Pulmonary veins

PVs run inferior to PAs throughout the lungs and are not accompanied by an airway. PVs arise from the pulmonary capillary network and carry oxygenated blood from the lungs to the heart. Unlike systemic vessels, PVs are not so physiologically and structurally distinct from PAs. Additionally, they possess a similar density of MEPs to that observed in PAs [22]. Small differences between PAs and PVs lie within the histological level, where PVs have thinner and less well organized walls than PAs of the same calibre [23]. Additionally, EC nuclei shapes are not similar between PAs and PVs: while ECs of PAs have an elliptical shape, ECs of PVs have a polygonal shape [24] [25].

Studies have confirmed the contribution of PVs to the total PVR [26] [27] [28].

1.5 The bronchial circulation

The bronchial circulation is smaller than the pulmonary circulation. Bronchial vessels usually originate from the aorta (90%) or intercostal arteries [29]. They enter the lungs at the hilum and supply the lower trachea, bronchi, bronchial branches, esophagus, and visceral pleura with oxygen and nutriments [30]. Additionally, they supply blood to the vasa vasorum of the thoracic aorta and pulmonary arteries and veins, as well as the nerves and lymph nodes in the thorax [30] that are not supplied by the pulmonary circulation. The bronchial circulation terminates at the level of terminal bronchioles where it joins pulmonary capillaries and venules. Bronchial arteries receive around 1% of the total cardiac output, and are high resistance, low capacitance vessels [30].

1.6 Lymphatic vessels

The lungs possess two sets of lymphatic vessels. Surface lymphatic vessels are located beneath the pleura, while deep lymphatic vessels parallel blood vessels in the lungs and extend along the bronchi and are not present in the walls of alveoli. They are responsible for clearing fluid and particulates.

1.7 Regulation and distribution of blood flow

A passive regulation of blood flow exists in the lung. The lung is divided into three zones determined by the relative values of the pulmonary arterial (P_a), pulmonary venous (P_v), and alveolar (P_A) pressure. In an upright position, blood flow in the upper portion of the lung (zone 1) is extremely low due to the fact that alveolar pressure is greater than both P_a and P_v ($P_A > P_a > P_v$). Zone 2 is the middle portion of the lung where $P_a > P_A > P_v$, and blood flow remains impaired. Zone 3 is the lowest zone in the lung where the level of vessel recruitment is the greatest at rest because the arterial and venous pressures are both higher than the alveolar pressure allowing vessels to be maximally distended at all times. Following an increase in blood flow, there is blood vessel recruitment in zones 1 and 2, resulting in an even blood flow distribution throughout the lung.

In addition to passive flow regulation, an active regulatory system that includes sympathetic innervation, humoral mechanisms, and respiratory gases, is a key determinant of vascular pressure.

1.8 Pulmonary vascular tone

In contrast to the systemic circulation where a relatively elevated vascular tone participates in the regulation of arterial pressure, the basal pulmonary vascular tone is low under normal conditions. Pulmonary vascular ECs play an undisputed role in the maintenance of a low resting vascular tone [31]. Extensive work has shown that the low tone is attributed to a continuous circulating and local production of vasodilators like a tonic endothelial release of NO and PGI_2 [32], as well as vasoconstrictors with the balance tipped in favour of vasodilators. Additionally, the control of pulmonary vascular tone happens via the autonomic nervous system where parasympathetic innervation (cholinergic) is responsible for the vasodilator effect, and sympathetic innervation (adrenergic) is responsible for the vasoconstrictor effect [33]. A non-adrenergic non-cholinergic (NANC) system also regulates pulmonary vascular tone [34]. Pulmonary vascular tone can be raised in response to a number of stimuli like changes in O_2 pressures, which can result in vasoconstriction, as well as acidosis [35].

1.9 Pulmonary vascular resistance

The mean pressure in human PAs is around 15 mmHg. When reaching the pulmonary capillaries, the pressure drops to about 5 mmHg. Vascular resistance is defined as the pressure drop divided by the flow, which is identical in both systemic and pulmonary circulations. However, the pressure drop in the pulmonary circulation is much lower. Therefore, the pulmonary circulation has low resistance.

PVR is about 1/8 to 1/10 of systemic vascular resistance. According to Poseuille's law ($\Delta P = 8\eta LQ / \pi r^4$), small variations in radius are to the fourth, and can therefore significantly affect flow (Q), and consequently PVR [36]. In PAs, variations of PAP have direct consequences on PVR. A sustained increase in PVR is a contributor to disease progression in a number of pathologies including PH [37] [38]. PVR can also increase in pulmonary veins following fluctuations in pressure.

1.10 Endothelial control of the pulmonary circulation

1.10.1 Endothelium-dependent vasodilation

Nitric oxide (NO)

NO is produced by a biochemical reaction triggered by the activity of the enzyme NO-synthase (NOS) on L-arginine [39]. Briefly, the completion of the reaction consumes oxygen and produces NO and H_2O by conversion of L-arginine to L-citrulline. Three NOS isoforms have been described. Neuronal NOS (NOS-I), constitutively expressed in neuronal cells, inducible NOS (NOS-II), and endothelial NOS (NOS-III), found throughout the vascular endothelium, all three of which are expressed in the lung [40].

Newly synthesized NO diffuses through the cell membrane into the cytoplasm of adjacent SMCs, where it activates sGC and increases intracellular levels of cGMP [41]. The latter activates PKG, consequently causing a decrease in intracellular Ca^{2+} concentration due to inhibition of voltage and receptor-operated Ca^{2+} channels accompanied by increased cellular extrusion of Ca^{2+} through Ca^{2+}- ATPase pumps and the Na^+ / Ca^{2+} exchanger. PKG activity also

causes the activation of Ca^{2+}-dependent K^+ channels leading to cellular hyperpolarization. Additionally, PKG activates MLCP leading to SMC relaxation.

Prostacyclin (PGI_2)

PGI_2 is synthesized from arachidonic acid (AA) by the cyclooxygenase pathway (Cox). Once synthesized, PGI_2 diffuses and binds to its receptors. These receptors activate the enzyme adenylyl cyclase located at the membrane level, resulting in an increase in the formation of cyclic AMP (cAMP). cAMP thus produced activates cAMP –dependent protein kinase A (PKA), capable of inducing relaxation of SMCs. On the other hand, PGI_2 is capable of activating ATP-dependent K^+ channels, Ca^{2+} dependent K^+ channels, large conductance (BKca), inwardly rectifying K^+ channels (Kir), and voltage-dependent K^+ channels (Kv), all participating in relaxation of the vascular smooth muscle [42].

Endothelium-derived hyperpolarizing factors (EDHF)

While NO signalling appears to play a major role in the vasoreactivity of arteries, the dominant responses in small resistance arteries are related to the EDHF pathway [43]. Several factors are included in EDHF signalling, including electrical signalling through MEPs, an increase in intracellular Ca^{2+} levels that activates intermediate and small conductance K^+ channels, IK and SK, and produces endothelial hyperpolarization, the extracellular accumulation of K^+, Epoxyeicosatrienoic acids (EETs), hydrogen peroxide (H_2O_2), and type C natriuretic peptide. Endothelial hyperpolarization propagates along the blood vessels via homocellular gap junctions, and communicated to adjacent SMCs by communicating junctions at the level of the MEPs [44]. Gap junctions at the MEP level are composed of proteins called connexins that physically connect the cytoplasm of ECs and SMCs, which allows electrical and chemical coupling between the two cell types. Cyclic AMP facilitates the electrical transmission of endothelial hyperpolarization of smooth muscle layers by increasing the conductance of gap junctions of smooth muscle. In addition, activation of endothelial K^+ channels also leads to accumulation of K^+ ions in the intercellular space. The increase in extracellular K^+ concentration can activate Na^+/K^+ ATPase and Kir which also produces hyperpolarization of the vascular SMC [45].

1.10.2 Endothelium-dependent vasoconstriction

Endothelin-1

Endothelin-1 is produced mainly by ECs [46] from a precursor, pre-endothelin, transformed into inactive big-ET and then into ET by the endothelin conversion enzyme. ET-1 production is increased by several stimuli, such as shear forces and hypoxia as well as by a number of neurohumoral factors and cytokines including AngII, vasopressin, catecholamines and transforming growth factor- β (TGF-β) [47] [48]. ET_A and ET_B are two G protein-coupled receptors (GPCR) that mediate the effects of ET-1. ET_B is mainly found on ECs. Its activation leads to vasorelaxation. While ET-1 can be responsible for vasodilation when it binds to endothelial ET_B receptors, its main role in vasoconstriction is mediated by its receptors on SMCs. Pulmonary vascular SMCs express both ET_A and ET_B receptors. Activation of these receptors induces contraction that contributes to the increase of vascular tone, and to the reduction of the flow. Briefly, activation of both receptors leads to vasoconstriction through the activation of phospholipase C (PLC), generation of inositol triphosphate (IP_3) and diacylglycerol (DAG), and the consequent increase in intracellular Ca^{2+} followed by the activation of the vascular SMCs' contractile system. Additionally, ET-1 can promote vascular remodelling by triggering SMC proliferation and collagen deposition.

In various pathological conditions affecting the pulmonary circulation, such as pulmonary arterial hypertension, chronic obstructive pulmonary disease (COPD), and Hypoxia, an increased synthesis of ET-1 is at the basis of the increase in tone [49] [50].

Thromboxane A_2

TXA_2 is synthetized through the activation of the COX1-2 pathway and has a half-life of a few seconds. Briefly, binding of TXA_2 to its GPCRs, prostanoid receptor T_1 and prostanoid receptor T_2 (TP_1 and TP_2) leads to the activation of PLC and induces intracellular Ca^{2+} increase thus leading to vascular SMC contraction. Under physiological conditions, the production of TxA_2 is countered by a production of PGI_2. However, this equilibrium can be shifted in the presence of pathologies affecting endothelial function.

Angiotensin II

Ang II is synthetized in the lung as a result of the enzymatic conversion of angiotensin I by the endothelial angiotensin converting enzyme (ACE) [51]. It causes vasoconstriction through its binding to its receptors AT_1 and AT_2 on the surface of VSMCs. Briefly, binding of Ang II to its receptors results in the activation of PLC and the generation of IP_3 and an increase in intracellular Ca^{2+} levels.

Serotonin

Serotonin (5-HT) is synthesized via the hydroxylation and subsequent decarboxylation of its precursor tryptophan. After synthesis, 5-HT is stocked in platelet dense granules and is released upon their activation. Serotonin induces vasoconstriction following its binding to its specific GPCR of several subtypes (14 distinct subtypes including: 1B/D, 2A and 2) abundantly expressed within the lung on pulmonary arterial SMCs. Serotonin has been implicated in a number of pathologies including PAH, where studies have clearly shown that drugs (ex: appetite suppressant fenfluramine and aminorex) that affected serotonin signalling had a marked effect on PAH progression [52, 53].

1.11 Vasoactive properties of pulmonary veins

In the pulmonary circulation, vasoactive mediators have effects on veins. In fact, PVs seem to have a stronger response than PAs to certain vasoactive factors [54] [55]. NO was shown to be produced by ECs of PVs of a number of animal models. Vascular response to NO revealed to be greater in PVs than PAs [56]. This effect was due to a higher amount and activity of NOS in PVs [56] [57]. Other animal studies have attributed this same effect to a more pronounced phosphodiesterase activity as well as a prominent role of PKG [58]. Additionally, PGI_2 production was shown to be the same in adult ovine pulmonary arteries and veins [26]. A variety of studies showed that PVs possess greater sensitivities than arteries to a number of vasoconstrictors and vasoconstrictor stimuli like ET, thromboxane, leukotriennes, and hypoxia. In fact, in a number of animal models as well as in humans, ET-1 seems to be a more potent constrictor of pulmonary veins than arteries with a more notable effect in small veins [59] [60]

[61] [62]. Finally, TXA_2 was found to be a constrictor of PVs in a number of animal models as well as humans [63] [64] [28]. It was found to induce vasoconstriction of human PVs through prostanoid receptor subtypes TP and EP_1 [65].

Whether causing dilation or constriction, vasoactive molecules exert their effects on vascular tone through their control of Ca^{2+} levels. For example, vascular dilation through EDHF can happen via IK and SK channels, activated following an increase in intracellular Ca^{2+}. Additionally, can Ca^{2+} initiate the production of vasoactive molecules like NO for example through the activation of eNOS. Ca^{2+} is required for the control and regulation of a variety of cellular functions of the endothelium. It is at the base of the genesis of various endothelial factors that control resting pulmonary vascular tone and react to any variations caused by internal and/or external stimuli. Therefore, the regulatory mechanisms of endothelial intracellular Ca^{2+} levels have a significant impact on vascular dynamics.

2. Intracellular calcium homeostasis

Variations of intracellular Ca^{2+} concentration are at the core of a multitude of cellular processes. Ca^{2+}- dependent mechanisms include cellular differentiation, proliferation, contraction, secretion, gene expression and apoptosis [66]. Ca^{2+} homeostasis is the equilibrium between influx and efflux of Ca^{2+}. In arteries (ECs and SMCs), Ca^{2+} plays an indispensable role; it is at the basis of the generation of molecules and factors responsible for vascular contraction and relaxation. These processes require a cross talk between ECs and SMCs. Bidirectional communication between both cell types is conferred by the presence of MEP [67].

2.1 Intracellular calcium sources and transporters

Ca^{2+} is present in the nucleus, mitochondria, endoplasmic reticulum (ER), and the Golgi apparatus. The ER is the most important intracellular Ca^{2+} reserve. In the ER, Ca^{2+} is present at a concentration of around 1 mM, while it is less concentrated in the cytoplasm (10-100 nM). In cellular compartments, Ca^{2+} can be present in a free form or bound to chelating proteins. In the ER/SR, Ca^{2+} exists under two forms: free Ca^{2+} or bound to a Ca^{2+} binding protein like calreticuline or calsequestrin. In the cytoplasm Ca^{2+} can also be bound to proteins like calmodulin and calcineurin.

2.1.1 Inositol 1,4,5-triphosphate receptors

Structure and expression of inositol 1,4,5-triphosphate receptors

The inositol 1,4,5-triphosphate receptor (IP_3R) is a tetrameric protein of 250-300 KDa that possesses six transmembrane segments and a Ca^{2+}-passing pore. The protein consists of an NH_2-terminal ligand and Ca^{2+}- binding domain, a central modulatory domain, and a COOH-terminal [68]. The N and C terminals are on the cytoplasmic side. In addition, the IP_3R protein possesses several phosphorylation sites [69]. Several homologues of IP_3Rs exist (IP_3R1, IP_3R2, and IP_3R3). Four IP_3Rs subunits assemble to form a functional channel. Subunits can assemble to form homo- or hetero-tetrameric channels. Each receptor subtype has a different IP_3-binding (affinity, specificity, and Ca^{2+} sensitivity) and modulation (phosphorylation and calmodulin-

binding) properties. IP_3Rs were found to form clusters on the ER membrane when cytoplasmic Ca^{2+} concentrations elevate [70] [71].

Properties of inositol 1,4,5-triphosphate receptors

Activation of IP_3Rs requires both IP_3 and Ca^{2+} [72] [73]. A functional channel is activated following the binding of four IP_3 molecules and Ca^{2+}. In fact, the effect of Ca^{2+} on IP_3Rs is biphasic. Modest increases in cytosolic Ca^{2+} concentration (up to 300nM) enhance the efficiency of IP_3 binding to IP_3R, whereas higher Ca^{2+} concentrations (μM) are inhibitory [74] [72]. IP_3R3 is Ca^{2+}- independent. Additionally, IP_3R activity can be regulated by variety of proteins including PKA, Ca^{2+}/CaM-dependent protein kinase II (CaMKII) and tyrosine kinases.

2.1.2 Ryanodine receptors

Structure of ryanodine receptors

Ryanodine receptors (RyR) were initially identified in the sarcoplasmic reticulum (SR) of skeletal muscle [75]. They are tetrameric proteins with a molecular weight of around 550 kDa [76] [77]. Their C and N terminals are within the cytoplasm having the pore region contained within the C-terminal. The C-terminal is also responsible for channel selectivity while the N-terminal is responsible for the binding of Ca^{2+} and CaM [78]. Additionally, the N-terminal contains several phosphorylation sites. Three RyR isoforms exist: RyR1, RyR2, and RyR3. All three isoforms are expressed in pulmonary vascular SMCs [79] [80].

Activity of ryanodine receptors

RyR activity is modulated by intracellular cytoplasmic Ca^{2+} concentrations (1-10μM), as well as Ca^{2+} concentrations within the SR. High Ca^{2+} concentrations inhibit RyR activity (1-10mM) [81]. RyR are also inhibited by cytoplasmic Mg^{2+} through competitive binding against Ca^{2+} [82]. Additionally, RyR can be activated by free cytosolic ATP [83]. Similarly, CaM has a double effect on RyR [84]. Other molecules can affect the activity of RyR like PKA and CaMKII via phosphorylation [85] [86].

2.1.3 SERCA pumps

Ca^{2+} that has exited the sarco/endoplasmic reticulum is returned back via sarco-endoplasmic reticulum calcium ATPase (SERCA) pumps. SERCA pumps are located within the sarco/endoplasmic membrane, and exist in three identified isoforms: SERCA1, 2 and 3. They are 100 kDa proteins with a cytoplasmic loop and several transmembrane domains forming a pore. Ca^{2+} transfer into the sarco/endoplasmic reticulum happens through ATP breakdown allowing the translocation of two Ca^{2+} ions per one hydrolyzed ATP molecule [87] [88].

SERCA2 (SERCA2a and SERCA2b) isoform was found to be expressed in PVSMCs, with SERCA2a and SERCA2b being differentially distributed [89, 90]. SERCA2 and SERCA3 were found to be expressed in human pulmonary artery ECs [91].

2.1.4 Plasma membrane Ca^{2+}-ATPase and Na^{+}/Ca^{2+} exchanger

Plasma membrane Ca^{2+}-ATPase are 120 to 140 kDa proteins with ten transmembrane domains and cytoplasmic N and C-terminal domains. Plasma membrane Ca^{2+}-ATPase transporters are expressed on the plasma membrane and transport Ca^{2+} outside of the cell through ATP breakdown (1:1 ratio) and aid in maintaining the Ca^{2+} concentration gradient. Ca^{2+}-ATPase transporters are the main factors responsible for maintaining intracellular Ca^{2+} concentrations at rest. They are activated by CaM [87].

The Na^{+}/Ca^{2+} exchanger (NCX) is an 110kDa protein composed of nine transmembrane domains separated in two groups: five on the N-terminal side and four on the C-terminal side. In the middle, there is an intracellular loop [92]. NCX transports one Ca^{2+} ion into the extracellular space in exchange of three Na^{+} ions. NCX can also function in the opposite direction under certain conditions like membrane depolarization or an increase in intracellular Na^{+} during which the NCX exchanger lets one Ca^{2+} ion inside the cell in exchange for three Na^{+} ions [93].

2.1 Extracellular calcium

Under resting conditions, intracellular Ca^{2+} is kept at very low levels (≈ 100 nM) relative to an extracellular concentration of around 1-2 mM making the extracellular space a highly important Ca^{2+} source. At the level of the plasma membrane, different types of channels and pumps control the exchange of Ca^{2+} ions between the intra- and extracellular media.

2.1.1 Ca^{2+} influx from the extracellular space

A wide array of proteins controls the passage of Ca^{2+} into the intracellular space. The list of channels includes several G-protein coupled receptors, typosine kinase recptors, and transient receptor potential channels (TRP), which will be discussed in part three of this thesis introduction. Additionally, Ca^{2+} entry into the cell is dependent upon the SOCE (store-operated Ca^{2+} entry) mechanism. In fact, a decrease in Ca^{2+} from the ER is sensed by a membrane protein called stromal interaction molecule 1 (STIM1) whose N-terminal region contains an EF-hand Ca^{2+}-binding motif, while its C-terminal region contains a sequence involved in protein-protein interactions and activation of membrane channels leading to their opening and subsequent Ca^{2+} entry.

2.2 Calcium signalling

Intracellular Ca^{2+} signals are diverse and are defined and characterized based on several parameters represented by the localization, kinetics, and amplitude of Ca^{2+} increases. The nature and characteristics of an increase in Ca^{2+} can generate different physiologic responses. An intracellular Ca^{2+} increase can occur in a specific region within the cell or can extend throughout the entire cell generating a Ca^{2+} wave. The duration of an increase in intracellular Ca^{2+} has also consequences on the cellular response. For example, a transitory Ca^{2+} increase can lead to the translocation of certain transcription factors like nuclear factor of activated T-cells (NFAT) [94], while a sustained Ca^{2+} increase was shown to have variable effects like the proliferation of human umbilical vein endothelial cells (HUVEC) and human pulmonary artery endothelial cells (HPAEC) [95], and apoptosis of other cell types like proximal tubular renal cells [96].

2.2.1 Global calcium signalling

In ECs, a global cellular increase in Ca^{2+} occurs in two phases; one that is represented by a rapid and restricted in time Ca^{2+} increase, while the second phase is represented by a longer sustained increase in intracellular Ca^{2+}. The first phase is the consequence of the activation of GPCRs or tyrosine kinase activated receptors, or mechanical forces like shear stress. Activation of those receptors leads to the production of IP_3 and DAG from phosphatidylinositol 4,5-biphosphate (PIP2) via the activity of PLC. Activation of IP_3Rs by IP_3 and Ca^{2+} leads to the release of Ca^{2+} from the ER [97]. Liberated Ca^{2+} will further activate more IP_3Rs leading to Ca^{2+}-induced Ca^{2+} release causing increases in Ca^{2+} throughout the cell (Ca^{2+} wave). The depletion of the ER from Ca^{2+} initiates the second phase termed store operated Ca^{2+} entry (SOCE), responsible for the sustenance of elevated Ca^{2+} levels. In fact, as mentioned in a previous section, ER depletion of Ca^{2+} causes a the activation of Ca^{2+} permeable channels within the cell membrane (TRPs, ORAI1), as well as the ER membrane (STIM1), leading to a global intracellular Ca^{2+} increase [98].

In SMCs, voltage-dependent Ca^{2+} channels mainly, mediate extracellular Ca^{2+} entry into the cell. However, other types of channels like TRP and ionotropic purinergic receptors (P2X) can also lead to Ca^{2+} entry into the cell. Ca^{2+} entry from the extracellular space is followed by Ca^{2+} release from the SR. Ca^{2+} store depletion is succeeded by the activation of STIM-ORAI causing a sustained Ca^{2+} increase [99].

2.2.2 Local calcium signalling

Although global Ca^{2+} plays a role in a wide range of cellular functions, in this thesis work we focus on the impact of local Ca^{2+} signalling. Several types of oscillatory localized Ca^{2+} patterns have been identified. Based on their spatial/temporal characteristics as well as their localization, Ca^{2+} transients are divided into several types: Ca^{2+} blips, Ca^{2+} puffs, Ca^{2+} sparklets, Ca^{2+} sparks, Ca^{2+} pulsars, and Ca^{2+} wavelets.

Calcium blips

Ca^{2+} blips are spontaneous Ca^{2+} increases generated following the activation of one IP_3R in the presence of a low concentration of IP_3 [100] [101]. These events have a low duration of approximately 100 ms, and an amplitude measured at around 23 nM in cultured bovine pulmonary ECs [102]. Ca^{2+} blips have been observed in a number of vascular beds [103].

Calcium puffs

Ca^{2+} puffs are larger that blips and result from the concerted opening of a few IP3 channels in the same cluster. They were first observed in Xenopus oocytes [104] [105] and later on in HeLa cells [106]. They have been visualized in non-excitable cells [107]. Puffs have amplitudes ranging from ~ 50-500 nM, a spatial spread of ~ 2-4 μm^2, and a total duration of ~ 1 second. A number of studies have concluded that the temporally and spatially coordinated recruitment of Ca^{2+} puffs is responsible for the generation of repetitive Ca^{2+} waves and oscillations [101] [108].

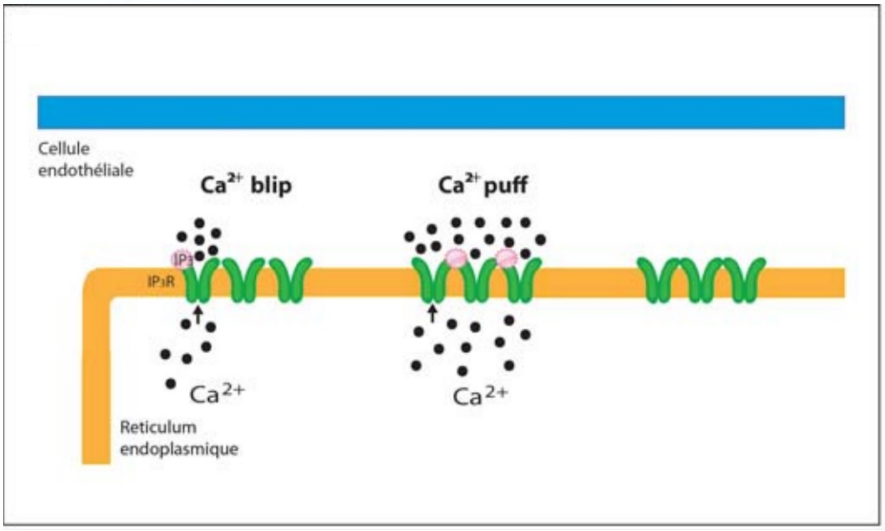

Figure 3 Calcium blips and puffs (Charbel et al., 2013)

Ca^{2+}: Calcium

Calcium sparks

Ca^{2+} sparks are localized transient increases in Ca^{2+} that can occur after agonist stimulation as well as under basal conditions following its release through RyR. They have been

initially identified in cardiac cells [109]. Since then, Ca^{2+} sparks have been described in several cell types like SMCs and skeletal muscle cells [110]. Sparks display variable spatial distribution with every occurrence. On average, Ca^{2+} sparks have a spatial spread ~ 12-14 μm^2. The fusion of sparks generates propagating Ca^{2+} waves. Spontaneous spark activity results in a K^+ current termed spontaneous transient outward current (STOC) [111]. Ca^{2+} sparks play a role in muscle contraction, as well as a negative feedback to muscle contraction by inactivating voltage-dependent Ca^{2+} channels. Additionally, Ca^{2+} sparks activate SMCs large conductance Ca^{2+}-activated K^+ channels affecting vascular tone [112] [113].

Calcium sparklets

Ca^{2+} sparklets are intiated following Ca^{2+} entry through membrane bound Ca^{2+}-permeable channels [114] [115]. Ca^{2+} sparklets were initially identified in vascular SMCs of animals, and cardiac cells of animals, as well as ECs in mesenteric arteries of mice. Extensive investigations had previously concluded that sparklets generally depended on the opening of voltage-dependent Ca^{2+} channels (VDCC). However, endothelial sparklets are the result of the opening of a specific type of Ca^{2+}-permeable channels termed transient receptor potential (TRP) channels. The first endothelial TRP-sparklets to be identified were transient receptor potential vanilloid 4-sparklets [116]. These sparklets occured repetitively at the same site (between IEL holes or at the end of the cells), with a spatial spread averaging around 11 μm^2 [114]. Sparklets were shown to have an effect on a number of proteins localized within MEPs like IK and SK leading to membrane hyperpolarization that is transmitted onto vascular SMCs through gap junctions [114]. Additionally, TRPA1-sparklets were identified in rat cerebral arteries [117]. They were found to induce dilation of cerebral arteries through the activation of IK channels [118].

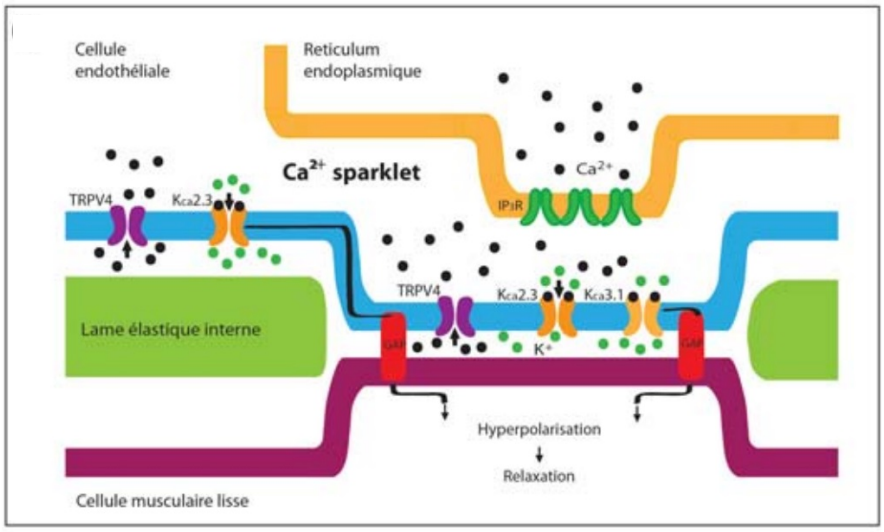

Figure 4 Calcium sparklets (Charbel et al., 2013)

Ca^{2+}: Calcium

Calcium pulsars

Ca^{2+} pulsars were first characterized in mouse mesenteric arteries [16]. They are generated following Ca^{2+} release from the ER after the activation of several clusters of IP3Rs. Pulsars occur in ECs under resting conditions and were found to be blocked following the inhibition of PLC [16]. Ca^{2+} pulsars are a major player in endothelial Ca^{2+} signalling. This type of signalling is initiated by the spontaneous activation of IP3Rs, and subsequent spatially restricted Ca^{2+} release from the ER, within MEPs. The regulatory mechanisms of Ca^{2+} pulsars remain to be further explored. Ca^{2+} pulsars described in mesenteric arteries possess an average area ~ 14-16 μm^2, and a duration ~ 250-270 ms.

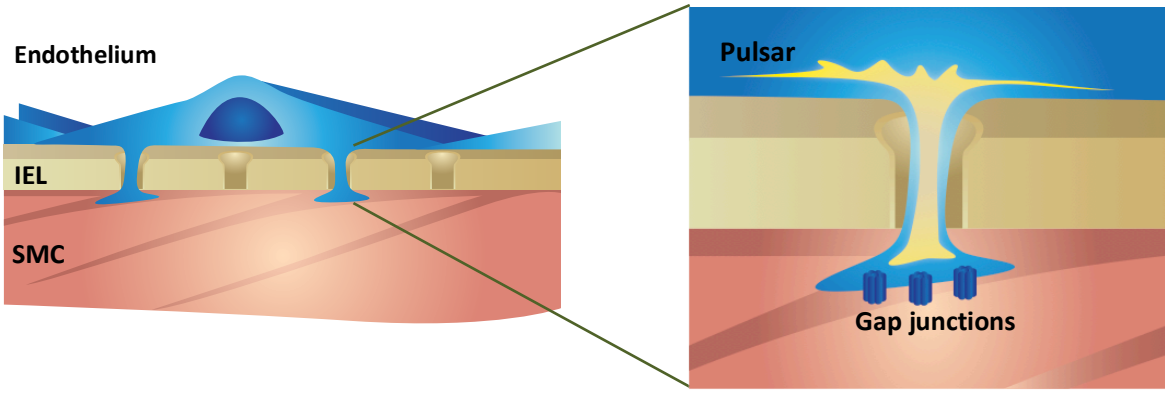

Figure 5 Endothelial calcium pulsars, adapted from Ledoux et al., 2008

Illustration of a Ca^{2+} pulsar occurring in an IEL hole. IEL: internal elastic lamina. SMC: smooth muscle cell.

Calcium wavelets

Similarly to other aforementioned local Ca^{2+} transients, Ca^{2+} wavelets are also initiated following the activation of IP_3Rs [119]. Wavelets are localized in proximity to MEP and play a role in myoendothelial feedback. Therefore, an initial vasoconstrictive stimulus that depolarizes vascular smooth muscle is followed by a Ca^{2+} response that includes the activation of endothelial vasorelaxing actors that include NOS, SK, and IK [119].

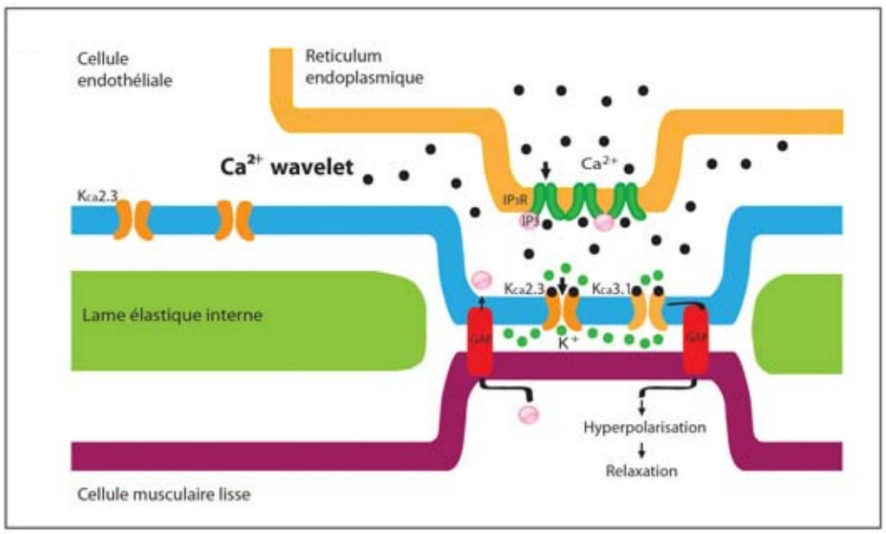

Figure 6 Calcium wavelets (Charbel et al., 2013)

Ca^{2+}: Calcium

The effect of localized Ca^{2+} signals on vascular tone often involves additional transmembrane ion channels, as well as regulatory proteins. In addition to their abundant expression in ECs and SMCs, Transient receptor potential channels have been previously associated with the regulation of vascular reactivity.

3. The transient receptor potential channels family

The transient receptor potential (TRP) family of channels are membrane proteins that mediate the transmembrane flux of cations. TRP channels were first identified in the drosophila visual system where a characterized mutation resulted in an altered response to light [120] [121]. Since then, TRP channels have been described in a large number of organisms such as C. elegans as well as in mammals [122] [123]. TRP channels are expressed in many tissues and cell types. They are involved in a variety of primordial cellular functions including but not limited to cell survival and development, sensory transduction, endocytosis and exocytosis, membrane potential change, and enzymatic activity.

3.1 Classification of TRP channels

There are six subfamilies of TRP that have been identified: TRPC (Canonic), TRPV (Vanilloid), TRPM (Melastatin), TRPP (Polycystine), TRPML (Mucolipine), and TRPA (Ankyrine), and an additional subfamily that has also been described: TRPN (nompC) [124] [125]. In mammals, 28 channels are currently known to belong to six of the seven sub-families (TRPN is absent) [126] [127]. These six subfamilies are divided into two groups based on sequence and topological differences. Group 1 channels include TRPC, TRPA, TRPM and TRPV families; while group 2 includes members of the TRPML and TRPP subfamilies [128]. In humans, approximately 27 genes form the family of TRP channels are described [129].

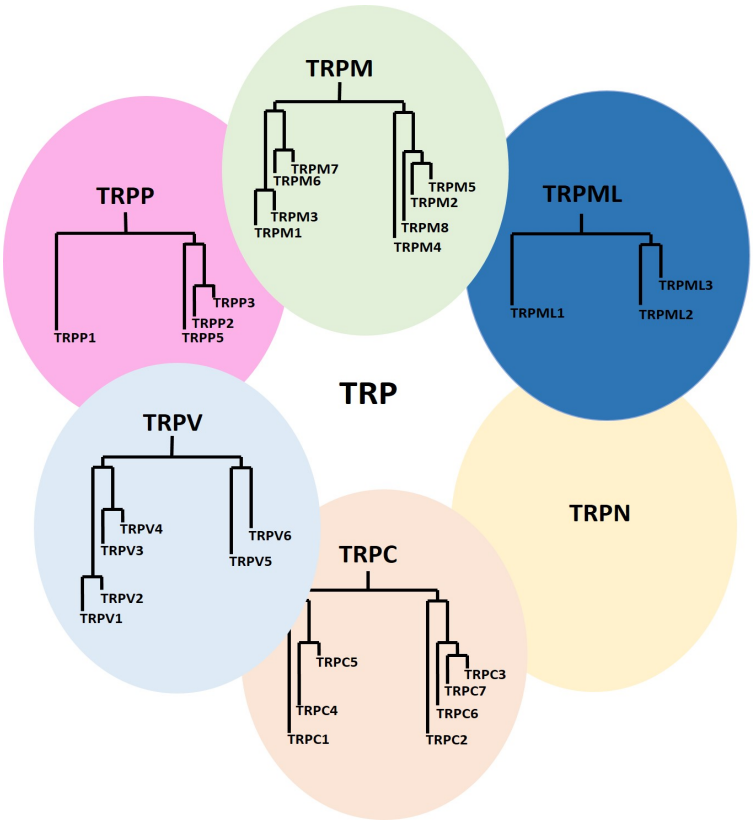

Figure 7 TRP channels family, modified from Nilius et al., 2007

3.2 Structure of TRP channels

All TRP proteins are composed of six transmembrane domains separated by hydrophilic loops. There is a small hydrophobic segment that participates in the formation of the pore between the fifth and the sixth domains [130] [131], as well as cytosolic carboxy and amino termini with multiple protein-protein interaction sites. TRP channels owe their nomenclature to a small well-conserved segment known as TRP, consisting of 23-25 amino acids. This segment was shown to be involved in the regulation of channel activity by certain lipids such as PIP_2 [132]. A functional TRP channel is formed by the association of four identical (homotetrameric channel) or different subunits (heterotetrameric channel) [133]. Finally, some protein domains, such as ankyrines, mainly involved in the anchoring of the channels to the cytoskeleton, are conserved in the N-terminal loop of the C and V families.

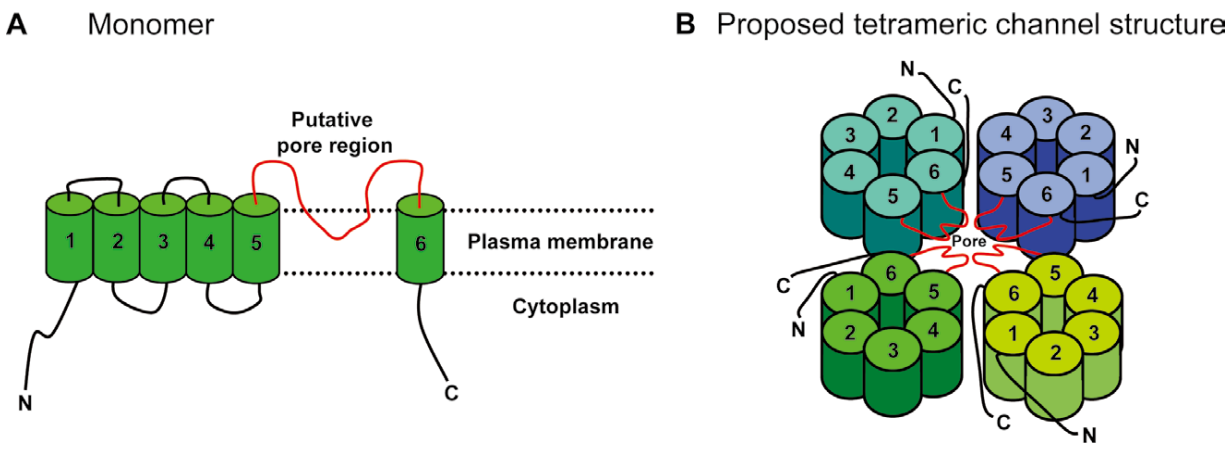

Figure 8 A: Structure of a TRP channel showing the 6 transmembrane domains and the pore region. B: Tetrameric structure of a TRP channel (Watanabe et al., 2009)

3.3 Activation of TRP channels

An important characteristic of TRP channels is their activation by a large number of stimuli allowing them to be involved in several cellular processes and pathological conditions [128]. TRP channels can be activated by exogenous stimuli such as mechanical forces, stretch, and thermal changes. Additionally, they can be activated by endogenous stimuli such as intracellular mediators, osmotic stress, Ca^{2+} concentration, and neurohormonal factors. They can equally be activated by membrane depolarization. For example, activation of the TRPC subfamily members has been shown to be dependent on phospholipase C (PLC), store depletion, conformational coupling, and exocytosis [134]. TRPV channels are activated by high temperatures, chemical compounds [135], PH changes, proinflammatory cytokines, and mechanical stretch (the TRPV family of proteins will be detailed in a later section). TRPA proteins can be activated by chemicals and environmental irritants as well as bradykinin and poly-unsaturated fatty acids [136].

3.4 The TRPV family

TRPV channels were named after the first member TRPV1 was identified due to its reactivity to the inflammatory vanilloid compound capsaicin [137]. The TRPV subfamily is comprised of six members (TRPV1-6).

3.4.1 Expression of TRPV channels

TRPV channels are expressed in a multitude of tissues and cell types. TRPV1-3 are highly expressed in the central nervous system (CNS), particularly in the vagal ganglia and dorsal root ganglia (DRG). TRPV4 is expressed in the kidney, lung, heart, liver, ECs, SMCs, and DRG [138]. TRPV5-6 are found in the intestines, pancreas and placenta. TRPV5 is also expressed in the kidneys [128].

3.4.2 Activation of TRPV channels

A noticeable feature of TRPV channels is their activation by temperature [139]; for example, TRPV1 and TRPV2 are activated by relatively high temperatures (> 43° C and > 52°C respectively) [137]. TRPV3 and TRPV4 activation is increased at lower temperatures (33-39°C and 27-34°C respectively) [134]. TRPV5 and TRPV6 are not affected by thermal variations. TRPV proteins can equally be activated by PLC, arachidonic acid, changes in extracellular osmocity, and mechanical stretch [140]. TRPV channels activity can be affected by additional stimuli such as chemicals, low PH, proinflammatory cytokines, bradykinin, nerve growth factor (NGF), and phosphatidylinositol-3-kinase (PI3K). For example, a low PH contributes to the activation of TRPV1 channels [137] [141] due to the presence of two main PH-sensing sites [142], while TRPV1 and TRPV2 channels can increase in expression and activity following an elevation in pre-inflammatory cytokines [143]. Furthermore, studies have found that the excitability of TRPV1 was upregulated following bradykinin release during airway inflammatory reaction [144]. Moreover, nerve growth factor (NGF) and phosphatidylinositol 3-kinase (PI3K) were both found to cause the activation of TRPV channels; in fact, NGF sensitizes pain-receptor neurons through increased trafficking of TRPV1 channels. This mechanism was found to involve PI3K interaction with TRPV1 [145].

Amongst all TRPV family members, TRPV4 channels' importance in the regulation of physiological processes has emerged due to their wide distribution, ability to be activated by a large range of stimuli, and their basal activity under normal conditions. Moreover, various pathologies have been attributed to the absence or abnormal functioning of these channels (the properties of TRPV4 channels as well as their role in physiological and pathological states will

be detailed in a later section of this thesis). Therefore, the further exploration of these channels is of high interest.

3.5 TRPV4 channels

The TRPV4 protein is a non-selective cation channel with preferential permeability to Ca^{2+} (5-10 times more permeable to Ca^{2+} than to Na^{+}), allowing its entry upon activation by a number of stimuli.

3.5.1 Structure of TRPV4: from the gene to the protein

The TRPV4 gene is located at the 12q23-q24.1 chromosomal region. It has 15 exons [146] [147]. TRPV4 was first cloned from the kidney, hypothalamus, and auditory epithelium. It was given a number of names like Osm-9-like TRP channel 4 (OTRPC4) [148], vanilloid receptor-related osmotically activated channel (VR-OAC) [146], and TRP12 [149]. The TRPV4 protein is an 871 amino acid protein that shares the same basic six transmembrane domains structure with the other TRP proteins, with its N and C terminals located on the cytoplasmic end [150]. A pore forming loop is located between the 5^{th} and the 6^{th} transmembrane helices. TRPV4 proteins contain six ankyrin motifs that are indispensable for their trafficking, and allow their interaction with other proteins [151]. A glycosylation site also influences trafficking of TRPV4 [152]. The NH_2 terminus seems to be required for the activation of TRPV4 by mechanical stress. In fact studies have shown that deletion of the ankyrin domain impairs the protein's mechanosensitivity [146]. The C-terminal region of TRPV4 can form bonds with CaM. The CaM-BD of TRPV4 is present at the C-terminal region [153]. TRPV4 can couple and form functional channels with all other TRPV subfamily members as well as different TRP channels like TRPC1 or TRPP2 [154].

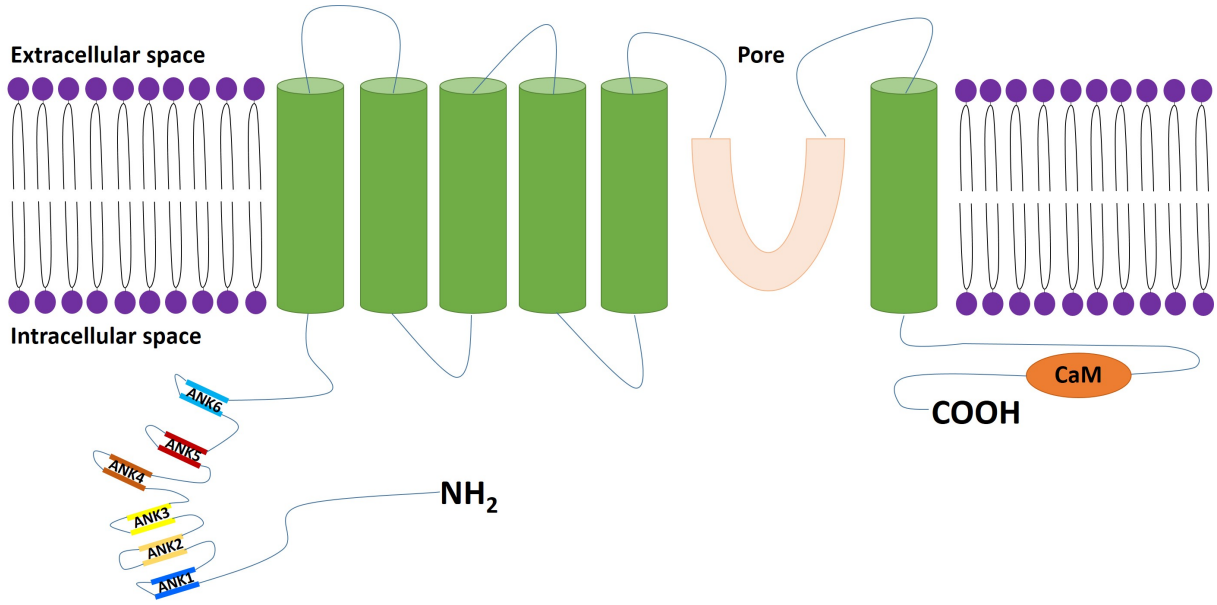

Figure 9 Schematic representation of TRPV4 protein, modified from Nilius et al., 2003

CaM: calmodulin

3.5.2 Permeability and selectivity of TRPV4

TRPV4 channels are non-selective channels, permeable to a variety of monovalent and divalent cations [155], with a higher affinity to Ca^{2+} [156] [157] [158] [153] [148]. Activation of TRPV4 under physiological conditions leads to an influx of Ca^{2+}, and activation of consequent Ca^{2+}-dependent signalling pathways. TRPV4 selectivity to Ca^{2+} is related to aspartate (Asp^{672}, Asp^{682}). Neutralization of those residues resulted in a marked reduction of TRPV4 Ca^{2+} selectivity [157]. Other mutations and factors have also been shown to affect the overall permeability of TRPV4 channels. For example, a mutation in the D682 residue leads to a decrease in the channel's permeability to Ca^{2+} and Mg^{2+}.

TRPV4 currents are outward rectifying with a slight inward rectifying current and a reversing potential close to 0 mV. Ca^{2+} and Mg^{2+} are responsible for these rectifications. Single channel conductance of TRPV4 is around 60pS for inward rectifying currents and 90 pS for outward

rectifying currents.

3.5.3 Regulation of TRPV4 activity

TRPV4 can be regulated by a number of stimuli ranging from physical activators like temperature, chemical activators like synthetic agonists, up to its modulation by different factors like Ca^{2+} or regulatory proteins.

Physical stimuli

TRPV4 can be activated by moderate temperatures (30-35°C) [159], which suggests that this channel could have basal activity in tissues. Thermal activation of TRPV4 could be mediated through phosphorylation [160]. Other studies have suggested that TRPV4 activation by temperature is an indirect mechanism that occurs via the production or enhancement of a heat-dependent ligand [161]. TRPV4 can also be activated by changes in extracellular osmolarity. A reduction in osmolarity stimulates increased Ca^{2+} influx in ECs [148]. Additionally, a loss of EC response to hypotonicity was observed in $TRPV4^{-/-}$ mice [162].
More importantly, TRPV4 channels can be activated by mechanical stimuli. Membrane stretch/shear stress, which may be a result of osmotic changes or physical stress applied on the cells, induces the activation of TRPV4 channels [163]. According to a number of findings, one mechanism through which shear stress activates TRPV4 happens via PLA_2. Mechanical stimuli are detected by membrane-bound PLA_2 triggering downstream production of arachidonic acid (AA), which is in turn metabolized by P450 epoxydases to epoxyeicosatrienoic acids (EETs) [164], which will activate TRPV4. Another mechanism of activation of TRPV4 by mechanical forces is a direct one through the recognition of mechanical forces by TRPV4 itself. This mechanism was suggested following the first evidence of the receptor incorporation into the cell membrane. An early study had demonstrated that mechanosensitivity of TRPV4 was dramatically impaired by a deletion of the N-terminal ARD, a domain responsible for the correct trafficking of TRPV4 and its anchoring to the cell membrane forming a mechanical link for stretch activation and gating [146] [150].
Interestingly, temperature seems to be a critical modulator of the activation parameters of other

stimuli. For example, activation of TRPV4 by shear stress and hypotonic swelling which is slow at room temperature is significantly faster once temperature is raised to body temperature (37°C).

Chemical stimuli

TRPV4 can be activated by a number of endogenous agonists like arachidonic acid metabolites like cytochrome P450 (CYP450) product EET [164]. Specific synthetic agonists to TRPV4 exist like 4α-phorbol-12,13-didecanoate (4α-PDD) [158], which interacts directly with the channel [165], and N-((1S)-1-3-hydroxypropanoyl)-1-piperazinyl]carbonyl}-3-methylbutyl)-1-benzothiophene-2-carboxamide (GSK1016790A) [166].

TRPV4 channels activity is inhibited by a number of molecules and compounds like ruthenium red in micromolar concentrations [114], as well as Gd^{3+} (micromolar concentrations ~ 100 μM) [146] and La^{3+} (micromolar concentrations ~ 100 μM) . In addition, specific TRPV4 antagonists exist including HC067047 (1 μM) [167].

Calcium regulation of TRPV4

Ca^{2+} is a highly important regulator of TRPV4 activity. In fact, intracellular Ca^{2+} concentration can either activate or inactivate the channel. A small increase in intracellular Ca^{2+} activates -TRPV4. However, high Ca^{2+} intracellular concentrations seem to lead to inactivation of the channel. Spontaneous TRPV4 activity was noticeably reduced in the absence of extracellular Ca^{2+}. In addition, activation of TRPV4 by 4α-phorbol esters or by hypotonic solutions is slower in the absence of Ca^{2+} [153]. Interestingly, a study by Watannabe et al., described different activation and current characteristics of TRPV4 according to Ca^{2+} concentrations. In fact, they have shown that in addition to TRPV4 dependence on extracellular Ca^{2+}, a higher Ca^{2+} concentration resulted in currents activating more rapidly while being smaller and turning off earlier. Furthermore, they have shown that in the continuous presence of a stimulus, TRPV4 currents are transient and decay to varying degrees following a current maximum. This decay being also Ca^{2+}-dependent [168].

Ca^{2+}- dependent modulation of TRPV4 is similar to all TRP channels in general. It is due to the binding of the Ca^{2+}- CaM complex to a CaM-binding domain (CaM-BD) present in the channels' intracellular sequence [153].

3.5.4 Physiological role of TRPV4 channels

Seeing that TRPV4 is widely expressed in tissues and cells; it has been implicated in a large range of physiological responses. TRPV4 channels are involved in systemic osmoregulation. In fact, TRPV4$^{-/-}$ mice exhibited defects in osmoregulation including diminished drinking and an elevated systemic osmotic pressure [169]. In addition, TRPV4 channels were involved in the nociceptive response of primary sensory neurons to hypotonic stimulation [170]. The mechanosensitive properties of TRPV4 channels were also shown to participate in hearing [171]. TRPV4 is also involved in thermosensation and thermoregulation. The activation of TRPV4 channels under physiological temperature led to a number of investigations around their role under normal conditions. In TRPV4$^{-/-}$ mice, altered responsiveness to heat was found via increases in tail withdrawal latency to moderately hot temperatures [172]. Additionally, TRPV4 channels expression on the vascular level makes them important modulators of vascular function.

3.5.5 TRPV4 regulation of vascular tone

TRPV4 channels are expressed on both ECs and SMCs. Noticeably, TRPV4 channels are highly expressed in ECs and SMCs of PAs, as well as in the aorta and cerebral arteries [173] [174]. A large number of studies have investigated the importance of TRPV4 channels in the regulation of vascular tone. Activation of endothelial TRPV4 channels causes endothelial Ca^{2+} levels increase and a consequent vasodilation [175]. A study by Earley et al., has shown that TRPV4 deficient mice exhibited higher than normal blood pressures [176]. TRPV4 was shown to participate in endothelium-dependent vasodilation through Ca^{2+} influx in resistance mesenteric arteries [114]. TRPV4-related vasodilation has also been shown to be mediated through Ca^{2+} - induced NO synthesis [175]. In fact, a study has shown decreased acetylcholine-induced NO production as well as significantly lowered EDHF-mediated vascular relaxation in TRPV4 knockout mice [177]. Additionally, selective inhibition of Ca^{2+}-activated K^+ channels (SKCa and IKCa) inhibited TRPV4-induced vasodilation [178].

In vascular SMCs, TRPV4 channels were shown to interact with a number of proteins consequently inducing vasodilation. Ca^{2+} entry following activation of SMCs-TRPV4 was shown to activate large conductance Ca^{2+}-activated K^+ channels ($K_{Ca}1.1$) leading to cellular hyperpolarization and vascular relaxation [173]. A study has shown that EETs in turn activate TRPV4 channels on SMCs and induce hyperpolarization in mesenteric arteries [176]. The EETs-TRPV4- $K_{Ca}1.1$ axis was described in several vascular beds [179] [180]. SMCs-TRPV4 was also shown to interact with TRPC1 resulting in SMC hyperpolarization and vascular relaxation [181]. Additionally, TRPV4 channels play a role in the contraction of pulmonary vascular SMCs through their interaction with RyR [182].

3.5.6 Pathological role of TRPV4

TRPV4 channels are involved in a number of pathologies. According to studies, TRPV4 channels are highly implicated in the progression of inflammatory bowel disease (IBD) [183] [184]. TRPV4 channels were found to play a role in the pain pathway (somatic and visceral) of IBD patients [185] [186]. TRPV4 impaired activity was shown to be responsible for altered pressure maintenance and abolished stretch sensing in C-fibers of the dorsal root ganglia [187] and retinal ganglion cells in mice [188]. TRPV4 were also shown to have pathological implications in hypoxia-induced cerebral pathologies [189]. TRPV4 channels were implicated in bladder disorders. In fact, it was demonstrated that TRPV4 was involved in cystitis-induced bladder dysfunction in mice [190]. A recent study has shown that a disruption in endothelial TRPV4 channels activation was observed in a mouse model of angiotensin II-induced hypertension [114]. In chronic hypoxic PH, TRPV4 channels were upregulated [191]. In addition, TRPV4 channels were shown to activate lung macrophages thus participating in ventilator-induced lung injury [192].

The wide distribution of TRPV4 channels within cellular types and tissues, the large number of stimuli that can activate them, as well as their undisputed involvement in the regulation of vascular function, make TRPV4 channels an important subject of study in a wide range of diseases. Additionally, as briefly mentioned in previous sections of this thesis, the involvement of TRPV4 in the pulmonary circulation and in PH leads us to investigate their participation in group II PH, the main focus of this thesis work. Can TRPV4 channels be therapeutic targets?

4 The pulmonary circulation in disease

4.1 Pulmonary hypertension

4.1.1 Historical background

The first classification of PH was in 1973 during the first meeting of the World Health Organization (WHO). PH was divided into two categories: 1) primary pulmonary hypertension and (2) secondary pulmonary hypertension when the underlying causes were known [1]. In 1998, during the Second Global Symposium in Pulmonary hypertension, a clinical classification of PH had been established based on clinical characteristics and therapeutic options, thus dividing PH into five groups: pulmonary arterial hypertension (group I-PAH), PH associated with left heart failure (group II-PH), PH associated with chronic disease and / or hypoxia (group III-PH), PH associated with chronic thromboembolic disease (group IV-PH), and PH due to multifactorial mechanisms (Group V-PH). During subsequent global meetings, this classification was subjected to several changes while keeping the five groups initially identified. During the fifth international symposium held in Nice, France in 2013, Modifications for Group I were proposed.

4.1.2 Groups of pulmonary hypertension

Table 1 summarizes the classification of the various groups of PH (2013).

The work of this thesis focuses exclusively on group II pulmonary hypertension. Therefore, a detailed description of other groups of PH is not included in this chapter of the introduction. However, a brief description of PAH pathophysiology and advancements in PAH treatments is included, because the treatments that are currently being applied or explored in group I-PH represent possible therapeutic avenues for group II-PH.

1. Pulmonary arterial hypertension
1.1 Idiopathic PAH
1.2 Heritable PAH
1.2.1 BMPR2
1.2.2 ALK-1, ENG, SMAD9, CAV1, KCNK3
1.2.3 Unknown
1.3 Drug and toxin induced
1.4 Associated with:
1.4.1 Connective tissue disease
1.4.2 HIV infection
1.4.3 Portal hypertension
1.4.4 Congenital heart diseases
1.4.5 Schistosomiasis
1' Pulmonary veno-occlusive disease and/or pulmonary capillary hemangiomatosis
1" Persistent pulmonary hypertension of the newborn (PPHN)
2. Pulmonary hypertension due to left heart disease
2.1 Left ventricular systolic dysfunction
2.2 Left ventricular diastolic dysfunction
2.3 Valvular disease
2.4 Congenital/acquired left heart inflow/outflow tract obstruction and congenital cardiomyopathies
3. Pulmonary hypertension due to lung diseases and/or hypoxia
3.1 Chronic obstructive pulmonary disease
3.2 Interstitial lung disease
3.3 Other pulmonary diseases with mixed restrictive and obstructive pattern
3.4 Sleep-disordered breathing
3.5 Alveolar hypoventilation disorders
3.6 Chronic exposure to high altitude
3.7 Developmental lung diseases
4. Chronic thromboembolic pulmonary hypertension (CTEPH)
5. Pulmonary hypertension with unclear multifactorial mechanisms
5.1 Hematologic disorders: chronic hemolytic anemia, myeloproliferative disorders, splenectomy
5.2 Systemic disorders: sarcoidosis, pulmonary histiocytosis, Lymphangioleiomyomatosis
5.3Metabolic disorders: glycogenstorage disease,Gaucher disease, thyroiddisorders
5.4 Others: tumoral obstruction, fibrosing mediastinitis, chronic renal failure, segmental PH

Table 1 Clinical classification of pulmonary hypertension, adapted from Simmoneau et al., 2013, (5th WSPH Nice 2013. Main modifications to the previous Dana Point classification)

4.1.3 Group II: pulmonary hypertension subsequent to left heart disease.

Left heart failure is the most common cause of PH [193]. It comprises the largest set of PH patients [194]. The presence of PH in heart failure signals the presence of a poor prognosis. Furthermore, no pharmaceutical treatments have yet been approved for the treatment of this specific group. Therefore, it is imperative to look deeper into the mechanisms of disease progression and aim to identify key molecules that play a role in PH-II progression.

In the clinical classification, group II-PH could be associated with left ventricular systolic dysfunction (PH associated with heart failure with reduced ejection fraction: HF_rEF), left ventricular diastolic dysfunction (PH associated with heart failure with preserved ejection fraction: HF_pEF), or valve disease.

Distinct Pathophysiological features of group II-PH:

When the ability of the LV to propel blood into the systemic circulation decreases, a resulting increase in blood volume at the end of systole induces a rise in pressure at the LV level. This elevation is transmitted backwards to the left atrium and reaches the pulmonary venous bed. At this stage group II-PH is said to be passive. The increase in pulmonary venous pressure reaches the pulmonary capillaries. However, if the increase in venous pressure persists, the alveolar-capillary membrane undergoes potentially irreversible remodelling. Pulmonary structural remodelling is accompanied by gas transfer impedance, which leads to a reduction in pulmonary diffusion capacity. In addition, the constant increase in pulmonary venous pressure may lead to pathological changes in the veins and pulmonary arteries, including muscularization of the arterioles, hypertrophy of the media and formation of neo-intima in distal PAs, leading to increased PVR.

Hemodynamic definition of group II-PH:

Group II-PH was initially distinguished from other groups by the presence of pulmonary venous hypertension. Over the years, different definitions of group II-PH have been used. The hemodynamic definition of group II-PH had three components: a pulmonary artery wedge pressure (PAWP), PVR, and a transpulmonary gradient (TPG), defined by (mean pulmonary arterial pressure (PAPm)- pulmonary capillary wedge pressure (PCWP)).

First, PH secondary to left heart disease was defined by an mPAP≥ 25 mm and a PAWP≥

15 mm. This definition evolved throughout the years to include PVR which indicated the difference between unfixed (pulmonary vascular resistance (PVR) < 6 WU (woods unit)) and fixed (PVR>6 WU) PH. Following that, transpulmonary gradient (TPG) was used to discriminate passive and mixed (out-of-proportion) PH. A ``Normal`` TPG (<12 mmHg) determined reversible PH-II, which does not represent any abnormality of the pulmonary arterial bed, while reactive PH-II is defined by a TPG ≥ 12 mmHg and high PVR [195]. Succeeding these definitions came an additional parameter known as the diastolic pressure gradient (DPG) [196], which is the difference between PAP and PAWP which was included in the updated PH definition of the European Society of Cardiology and the European Respiratory Society[2]. Post-capillary PH was therefore divided into isolated post-capillary (Ipc-PH) (DPG< 7 mmHg and/or PVR is ≤3 WU) and combined post-capillary and pre-capillary PH (Cpc-PH) (DPG ≥ 7 mmHg or the PVR is >3 WU).

4.2 Therapeutic strategies in pulmonary hypertension

Group I PAH is the group most concerned with therapeutic interventions with increasingly effective treatments of functional signs and survival of patients. These treatments mainly concern ET receptor antagonists, *PDE-5* inhibitors, PGI_2 analogs, Ca^{2+} channel blockers, and sGC stimulators [197] ([198] [199].

4.2.1 ET_R antagonists

ET-1 is a potent vasoconstrictor and a factor for proliferation of SMCs, thus contributing to the increase in pulmonary vascular tone and hypertrophy of the pulmonary arterial walls. There are high plasma levels of ET-1 in patients suffering from PAH. Bosentan is a non-selective blocker of the ET_A and ET_B. Bosentan has an antiproliferative action through the suppression of the overexpression of TRPC6 observed in the course of idiopathic PH. Sitaxentan is a selective inhibitor of ET_A and consequently vasoconstriction and proliferation of PAs. Ambrisentan is another ET-1 receptors inhibitor, poorly selective on ET_A receptors. Macitentan, a dual ET_R antagonist showed high binding affinity to both ET receptors, sustained receptor binding, and high tissue penetration in pre-clinical studies [200, 201]. Additionally, Macitentan and its active metabolite both have the advantage of a relatively long elimination half-life [202].

4.2.2 PDE-5 inhibitors

Inhibition of PDE-5 is responsible for an increase in the intracellular concentration of cGMP, resulting in relaxation of the pulmonary vascular smooth muscle and inhibition proliferation. Sildenafil is one of the most potent inhibitors of PDE-5 [203]. It limits the degradation of intracellular cGMP therefore increasing its availability and promoting the action of NO. Other phosphodiesterase inhibitors exist such as Tadalafil and Vardenafil. The therapeutic effect of those drugs has been validated in patients with PAH [204] [205].

4.2.3 PGI_2 analogues

PGI_2 is produced by ECs and produces smooth muscle relaxation and inhibition of platelet aggregation by increasing intracellular concentration of cAMP. Epoprostenol, is administered intravenously (IV) continuously by means of a pump connected to a catheter because of its short half-life (3 minutes). This treatment significantly reduces PAH symptoms by improving exercise capacity evaluated by the six-minute walk test and hemodynamic parameters. Optimal doses of Epoprostenol are between 22 and 45 ng/kg/min. Lower doses appear to be less effective, while higher doses may result in inappropriate elevation of cardiac output [206]. Epoprostenol remains the reference treatment in most severe cases. Treprostinil and Iloprost, are two PGI_2 analogs that can be proposed to patients suffering from PAH. Iloprost administered by inhalation is indicated for the treatment of idiopathic and familial PAH. Treprostinil may be administered continuously either by dermal route using a mini pump or intravenously. It is however available in inhaled and tablet forms. This treatment improves exercise ability and patients' hemodynamics. Beraprost, which is another prostacyclin analogue is administered orally.

4.2.4 Calcium channel blockers

Ca^{2+} is at the basis of pulmonary vascular remodeling in PH due to its participation in SMC constriction and proliferation. Briefly, in addition to Ca^{2+} increase in SMCs which causes vasoconstriction, Ca^{2+} is at the basis of activation of Ca^{2+}-dependent kinases, and several transcription factors including the transcription factor nuclear factor of activated T cells (NFAT). Additionally, Ca^{2+} exerts its effects through voltage-gated channels (L-type and T-type), which have been linked to SMC proliferation [207]. Since vasoconstriction and SMC hypertrophy are major contributors to the advancement of PH, vasodilators are used in its treatment. Ca^{2+} antagonists may oppose vasoconstriction, but they have no effect on pulmonary vascular

remodeling. These inhibitors are only effective on a minority of patients with PAH (10 to 20%). These patients are identified by a test of acute vasodilation induced by inhaled NO during right catheterization [208]. In these patients, high doses of diltiazem (240 to 720 mg/day), Nifedipine (120 to 240 mg/d) or Amlodipine (10 to 20 mg/d) are most often used, and lead to very satisfactory hemodynamics, as well as an excellent prognosis [209].

4.2.5 Soluble guanylate cyclase stimulators

The dysregulation in NO production and sGC activity, as well as cGMP degradation were demonstrated in PH. Soluble guanylate cyclase catalyses the synthesis of cGMP which leads to vasodilation, inhibition of SMC proliferation, as well as downstream vascular remodelling. sGC stimulators directly affect sGC; they increase the sensitivity of sGC to NO, and they directly stimulate the receptor to mimic the action of NO. In addition to their vasoactive properties, sGC stimulators like Riociguate have shown antifibrotic, antiproliferative, and anti-inflammatory effects in pre-clinical models [210].

4.2.6 Combination therapy

Due to the complex nature of PH pathogenesis as well as the multitude of factors and pathways involved in disease progression, combination therapy may be applied in cases of disease worsening. This type of therapy can be either applied sequentially (addition of a second treatment to initial monotherapy) or starting with more than one treatment for patients that have yet to receive any treatment [211] [212, 213] [214] . In PAH, ET levels are found to be increased [215], while NO and PGI2 levels are found to be decreased [216] [217]. Therefore, combination therapy was sought in group I-PAH and was performed in order to target multiple pathways that are involved in disease progression in parallel. According to the 5th world symposium on PH, it was recommended that combination therapy in group I- PAH targets at least one of the three main disease pathways: ET, NO, and PGI_2. In a recent study, the combined clinical and hemodynamic effects of Macitentan and Riociguate were evaluated as a first line treatment in patients with PAH [218]. This study reported positive results for the combination of both drugs. In another study using a human *ex-vivo* model, combination therapy using Vardenafil and Macitentan inhibited sequential constriction with ET1 and norepinephrine in PAs. This study concluded that when using the right doses, the combined effect of both drugs could surpass monotherapy [219]. Finally, in a

study on newborns with persistent PH, demonstrated that the combined use of Sildenafil and Bosentan was more advantageous that Sildenafil alone [220].

4.2.7 Other therapies in group I: pulmonary arterial hypertension

PAH can be idiopathic, hereditary, associated with the usage of certain medication or the ingestion of toxins (table 1). It can also be due to congenital heart diseases or it can be associated with other pathologies like an HIV infection. Despite the fact that group I-PH pathophysiological mechanisms are more extensively explored than group II-PH, the multifactorial nature of group I still represents challenges in the search for optimal therapeutic targets. PAH is characterized by extensive vascular remodelling involving ECs, SMCs, fibroblasts, and myofibroblasts exhibiting an exaggerated proliferative and anti-apoptotic phenotype. Recent advances in PAH therapy have been aimed at the common characteristics that pulmonary vascular cells in PAH have with cancer cells, and the targeting of proliferative pathways.

Briefly, endothelial damage occurs in PAH resulting from this multitude of factors (genetic mutations, toxins, autoimmune diseases, mechanical or hemodynamic stress, infectious diseases or inflammation). Whatever the root cause, endothelial damage is followed by an endothelial-mesenchymal transition due to the activation of certain transcription factors, resulting in an increased EC proliferation and the formation of pulmonary vascular lesions. Additionally, endothelial cells' damage leads to a decreased production of NO, PGI2, and EDHF while production of TXA2 is increased. The advancement of PAH is worsened following the infiltration of inflammatory cells and elevated levels of pro-inflammatory mediators (IL-1, IL-6, TNFα), which were found to correlate with bad clinical outcomes [221] [222] [223] [224]. Inflammatory mediators cause the accumulation of extracellular matrix components and are directly involved in the exaggerated proliferation of pulmonary vascular cells

Furthermore, several growth factors (example: fibroblast growth factor-2 (FGF2), and insulin-like growth factor 1 (IGF-1)) activate various signalling pathways involved in cell growth, proliferation and survival [225]. Some of the signalling pathways have been found to be activated in cancer cells [226]. Interestingly, cytokines that have been shown to be involved in PAH progression, notably IL-6 and PDGF, have also been shown to be

involved in cancer progression. Growth factors, which were shown to play an important role in pulmonary vascular remodelling, have equally been involved in cancer progression pathways. Based on the above mentioned findings, targeting those pathways can be an effective PH treatment [225] [227]. This cancer theory of PAH has occupied recent PAH studies.

Furthermore, pulmonary vascular cells in PAH were found to shift to a glycolytic metabolism as a response to hypoxia, ER stress, or inflammation. The metabolic theory of PAH states that similarly to cancer cells, pulmonary vascular cells in PH undergo metabolic adaptations. In response to various factors, mitochondria of PAH cells undergo fission (as opposed to healthy cells, in which mitochondria is constantly dividing and fusing to maintain function), and show a fragmented pattern (also observed in cancer cells).

In fact, mitochondrial malfunction was found to be at the basis of several changes observed in PVSMCs. More specifically, PASMCs were found to share a large number of molecular abnormalities with cancer cells [228] that were attributed to one common cause: the metabolic phenotype of PAH. Downstream implications include decreased proapoptotic mediators, increase in the availability of non-oxidized sugars, lipids, and amino acids for the building blocks of proliferating cells, and a potential effect on signals to the nucleus regulating epigenetic mechanisms. Therefore, one single therapy aimed at normalizing mitochondrial abnormality can have beneficial effects on a wide range of pathways that have been observed in PAH, like upregulated expression of growth factors and increased expression and activation of NFAT.

Recent and ongoing work is aimed at identifying new therapeutic targets for PAH, through the further exploration of the cancer and metabolic theories. Advancement in PAH treatment may represent hope for the discovery of a treatment of group II-PH.

4.3 Advancements and obstacles in group II-PH treatment

Clinically approved drugs in PAH were found to have deleterious consequences in PH-LHD [194]. A number of clinical trials found that intravenous or oral administration of vasodilators such as Milrinone and Epoprostenol increased mortality [229] [230]. Other studies using inhaled or systemic vasodilators such as NO or Iloprost have reported vasoconstriction during the

vasodilatory response in subjects with increased pulmonary pressure [231] [232] [233]. The underlying reason for the vasoconstrictive effect was attributed to a protective mechanism against fluid leak and edema formation [234].

The PDE-5 inhibitor Sildenafil has shown promise in the treatment of group II-PH. The effects of long-term oral administration of Sildenafil in animal models are reduced lung vascular resistance, lung vascular remodelling, and RV hypertrophy and dysfunction [235]. A few clinical studies have reported that acute Sildenafil administration lead to improved PH, PAP, and PVR [236] [237]. Chronic administration showed improved indexes of LV function and exercise capacity [238]. Nevertheless, these results are countered by clinical trials that have shown that Sildenafil administration failed to improve echocardiographic parameters and exercise capacity significantly, as well as diastolic function parameters and overall quality of life [239].

Prostaglandings have also been the subject of clinical studies for the treatment of group II-PH with conflicting results. On one hand, a few studies had shown that chronic infusion with Epoprostenol increased mortality [229]. On the other hand, following studies reported beneficial effects. A study conducted on an animal model of aortic banding showed that inhaled administration of Iloprost reduced PH without any detectable side effects [240]. Another study on CHF patients prior to heart transplantation showed that inhalation of prostacyclin induced pulmonary vasodilation and a decrease on PVR, PAP, and TPG [241].

Using ET-1 receptors antagonists for the treatment of group II-PH did not show any promise [242] [243] [244].

Clinical trials using Riociguat reported improved LV functional indexes and decreased PVR [245].

Existing clinical trials and studies on PH-LHD treatments have tested several classes of PAH-approved medication basing their studies on the theoretical benefits of the pharmacologic mechanism that each drug presents. However, until presently, these studies have lacked compelling evidence showing promise for those drugs in the handling of group II-PH. Concordantly, treatment of PH-LHD focused on optimizing the management of underlying heart failure.

The reasons behind conflicting evidence and diverge opinions regarding the efficacy of PAH drugs in PH-LDH are the high incidence of their detrimental side effects and a lacking clear link between disease stage and progression with its impact on the pulmonary vasculature (increase in pressure vs pulmonary vascular remodelling). Through the course of group II-PH progression, additional factors that may impact NO availability, ET expression, collagen deposition, and other

potential mechanisms involved in vascular dysfunction and remodelling need to be taken into consideration. There is also the added complexity of these patients being under standard heart failure therapy. Well characterized studies surrounding that subject are limited.

Therefore, an important step towards treating PH-LHD consists of proper determination of disease state and underlying vascular alterations. This step is crucial in animal model studies for the selection of animal groups as well as clinical studies for the assessment and randomisation of patients.

4.4 Animal models of pulmonary hypertension

A non-negligible number of animal models has been developed in the purpose of mimicking key clinical, hemodynamic, and histopathological features of human PH. PH can be induced following the injection of natural chemicals or synthetic components (eg: microspheres). Additionally, PH can be developed after exposing animals to certain external conditions like low pressures or low oxygen. Other methods of PH induction are surgical techniques. While PH induced following the injection of natural and synthetic components is mainly directed towards the study of histopathologic features of the disease, surgically induced PH has been used so far for the study of the increased blood flow and repercussions of hemodynamics of LV and RV dysfunction. However, in general, surgical methods require highly technical skills and are usually associated with high mortality rates. Some models are used to study more than one group of PH when they represent disease characteristics common to those groups, while others are specifically designed for one PH group.

4.4.1 Genetic animal models of PH

Genetic animal models of PH are used to study group I-PAH mainly. They include BMPR-2 knockout model [246], the vasoactive intestinal peptide knockout model ($VIP^{-/-}$) [247], the apolipoprotein-E knockout model ($ApoE^{-/-}$), the neprilysin knockout model [248], the interleukin-6 overexpression model [224], the angiopoietin-1 overexpression model [249], the serotonin transporter overexpression model, the S100A4/Mts-1 overexpression model [250], and the ET_B knockout model. Transgenic rats with ET_B-receptor deficiency present with an increased mPAP and PVR and diminished cardiac output (CO) after exposure to hypobaric hypoxia [251]. A lot of

work done using this model has contributed to the development of ET receptor antagonists like Bosentan as treatment for PH.

4.4.2 Single pathological insult models

The monocrotaline model

The monocrotaline (MCT) model is the most widely used model in the study of PH. Lalich and Merkow were the first to describe that oral ingestion on MCT induced progressive PH in rats. MCT is an alkaloid from the pyrolizidin family that can be found in the leaves and seeds of the plant Crotalaria spectabilis. MCT has toxic effects on the lungs and liver. After injection, MCT is metabolized in the liver by CYP-450 dependent enzymes into active metabolite MCT pyrrole [252]. This active metabolite is then transported in the blood stream until it reaches the pulmonary system. In some animals, the active form MCT pyrrole must be injected directly. Therefore, this component is very dependent on the animals' metabolic differences. In the MCT-induced PAH (group I) model, one single injection of MCT (sub-cutaneous or intraperitoneal) is sufficient to cause pulmonary edema as well as endothelial injury [253]. In MCT-induced PH murine models, changes in pulmonary vascular reactivity were observed [254]. Additionally, decreased activity of eNOS was observed, accompanied by overexpression of inflammatory cytokines [255]. Decreased expression of BMP-RII gene has been shown. This animal model is largely used due to its feasibility and reproducibility, as well as its high similarity with human PH.
MCT can be combined with another insult like a pneumonectomy causing more severe PH [256].

The chronic hypoxia-induced PH model

It was as early as the 1970s when researchers experimented the development of PH in animals exposed to chronic hypoxia. The chronic hypoxia model was induced in the following animals: guinea pig, mouse, rat, pig, and sheep. In this model exposure to hypoxic conditions through normal air at hypobaric pressure or to oxygen poor air at normal pressure results in pulmonary vasoconstriction, muscularization of non-muscular arterioles, increased media thickness and matrix deposition [257] [258] [259]. However, the response to hypoxia is different between different animal species. Nevertheless, this model is often used for the study of group I-PAH progression even though it is a model for group III-PH.

The schistosomiasis model

Schistosomiasis is caused by the parasites of the Trematoda class. These parasites penetrate the skin, invade the intestine, liver, and genito-urinary system and release their eggs in the urine or feces of the host, after which the eggs are secreted into water where they hatch and miracidiae infect the fresh water snail to facilitate their own transformation into cercardiae. After their release into the water again, they penetrate the host's skin. After penetration, the cercardiae are transformed into schistosomulae that are transported via the blood stream to the lungs where they induce granulomas. Patients with schistosomiasis were shown to develop a form of idiopathic PH. The schistosomiasis model was induced in female C57/BL6 mice that were injected with a Puerto Rican strain of S. mansoni. Injected mice were subjected to several post-injection periods (subacute and chronic). Only mice from the chronic study had a large lung egg content as well as significant pulmonary vascular remodelling and plexiform like lesions [260]. This model was further improved where mice were infected with S. mansoni cercariae and intravenously challenged with S. mansoni eggs by placing the mice's tails in a vial containing carcarciae for 30 minutes then re-injected intravenously with viable eggs after a period of fifty-five days. This technique resulted in PH dependent on the upregulation of interleukin-13, with pulmonary vascular remodeling [261]. The schistosomiasis model is mainly used for the study of idiopathic PH [262].

The fawn-hooded rat model

The fawn-hooded rat is an outbred strain developed from German brown, albino, and long Evan's rats. Fawn-hooded rats have underdeveloped lungs with a reduced number of alveoli, an inherited platelet disorder characterized by deficient serotonin uptake into platelets, an abnormality within chromosome-1 that disrupts the mitochondrial reactive oxygen species inducible factor alpha (HIF-1α)-k^+ channel pathway that plays a role in PH development [263].

The bleomycin model

Bleomycin is a chemotherapeutic antibiotic that has been used in animal models of pulmonary fibrosis [264]. The bleomycin model *(group III-PH)* has been induced in dogs, rats, mice, and rabbits. In addition to pulmonary fibrosis, bleomycin administration leads to lung inflammation and muscularization.

PH induced by pulmonary embolism

This model is used for the study of Group IV chronic thromboembolic PH. The repeated injection of synthetic microspheres such as Sephadex microspheres or blood clots or by air or fat embolism in this model induces chronic emboli. Specific vessel sizes are targeted via injection of microspheres of different diameter sizes. This model has been used with dogs, pigs, rats, and sheep, and has shown to lead to the development of moderate PH.

4.4.3 Multiple pathological insult models (group I-PAH)

The main advantage of multiple insult PH models is that they mimic more accurately human PH and exhibit a more severe form of the disease than single insult models.

The chronic hypoxia combined with SU-5416 model

This pre-clinical model was developed in 2011 by the group of Ciuclan [265]. Semaxinib (SU-5416) is a vascular endothelial growth factor 2 (VEGF-2) antagonist. Administration of SU-5416 initiates endothelial cell death, which leaves apoptosis resistant ECs with a high proliferative potential. Combination of hypoxia with a pharmacologic alteration in VEGF signalling resulted in severe PH in animals, with human-like vascular alterations that included neointima formation. Additionally, this model displays increased right ventricular hypertrophy (RVH) and right ventricular systolic pressure (RVSP) [266]. In fact, the presence of the hypoxic environment seemed to further increase proliferation of ECs. This model was induced in rats and mice. Therefore, this model has shown to mimic most accurately human PH than single stimuli models [267].

The chronic hypoxia combined with MCT model

In this particular model of PAH, a significantly increased mPAP is observed, accompanied by increased RVSP and RVH. Additionally, studies have shown increased levels of pro-inflammatory cytokines as demonstrated in PAH patients [221] [268] [269]. An extensive number of studies have successfully shown that combining hypoxia exposure with MCT injections generates a PAH model that is more relevant to an advanced stage in the pathogenesis of human severe PAH [270].

The MCT accompanied by a pneumonectomy model

Performing a pneumonectomy causes an increase in shear stress. Studies have found that when combined with pneumonectomy, MCT-injected animals (mainly rats and mice) develop substantial RVH, as well as plexiform-like lesions [271].

4.4.4 Models used for the study of group II- PH

Animal models used for the study of group II-PH are mainly animal models of heart failure. Very few of those models have been successfully used for the study of PH-LHD. Up until presently, there was no defined model for group II-PH offering determining characteristics of the presence of the disease.

Heart failure in animal models has been induced through aortic, pulmonary, or coronary artery banding or ligation, or aortocaval fistula. Studies have demonstrated that chronic transverse aortic constriction (TAC) induces LV dysfunction and causes increased left ventricular end diastolic pressure (LVEDP). Additionally, it leads to profound pulmonary fibrosis and remodelling, as well as lung vascular remodelling. This model also presented with RVH, increased right ventricular end diastolic pressure (RVEDP), and right atrial hypertrophy. A study demonstrated that TAC-induced increases in lung weights and RVH correlates with severity of LV failure [272]. The aortic banding model demonstrated that congestive heart failure in animals causes severe lung disease. The pulmonary artery banding (PAB) consists in a constriction of the pulmonary artery leading to increased afterload in the right ventricle (RV). The PAB induced PH model is mainly used to study the mechanisms of RV dysfunction which is highly important seeing that RV dysfunction has been shown to be the most important prognostic indicator of PH [273].

Surgical creation of left to right shunts in animals is performed to mimic PH associated with congenital heart diseases [274]. The creation of an aortopulmonary shunt in animals like piglets or lambs or rodents leads to the development of moderate PH with medial hypertrophy [275] [276]. Persistent pulmonary hypertension of the newborn (PPHN) has been induced in large animals like foetal lambs and ewes, which allows surgical in utero intervention [277]. This type of PH is induced following the constriction or closure of the ductus arteriosus causing an acute increase in in pulmonary blood flow or by creation of a diaphragmatic hernia [278]. After birth, animals have shown persistent PH. Evaluation of PH in those animals has revealed pathophysiological characteristics similar to those observed in human PH. Additionally, vascular structural alterations that consist of PASMCs proliferation in non-muscularized distal arteries, and

adventitial fibrosis in intra-acinar arteries are observed. Since PH has been recognized as a clinical complication of the metabolic syndrome [279], animals (mainly rats and mice) have been put on high fat diets to induce obesity, glucose intolerance, insulin resistance, hyperlipidemia and PH. A recent study was conducted in 2016 by Potus et al., where rats with HFpEF induced by supra-coronary aortic banding were subjected to a high fat diet and daily injections of olanzapine initiated two weeks after surgery to induce metabolic syndrome. This study introduced this particular model as a pre-clinical model for the study of PH-HFpEF by showing that those mice presented with decreased pulmonary artery acceleration time (PAAT), and tricuspid annular plane systolic excursion (TAPSE) accompanied by increased mPAP and RVSP. Additionally, a study performed the following year demonstrated the development of a metabolic syndrome mouse model with PH and HFpEF [279]. In this study, mice were subjected to 20 weeks of high fat diet thus inducing obesity, glucose intolerance, insulin resistance, hyperlipidemia, and PH. LV and RV indexes were evaluated, and the study validated the metabolic syndrome mouse model as a specific model for the study of PH associated with HFpEF.

In addition to surgical models, genetic models of heart failure can also be used in the study of PH-LHD. These models include cardiac muscle LIM knockout mice and the cardiomyocyte-specific TNF-α overexpressing mouse [280].

Animal models used for PH-LHD studies mostly rely on HF induction and subsequent monitoring of hemodynamic parameters. Many challenges are related to the development of a well-characterized validated model for PH-LHD. First, creation of these models is technically challenging and requires a lengthy post-operative period. Second, common guidelines for the determination of PH presence and stage are lacking, and therefore prevent proper usage and consequently cause wasting of these animals. Finally, there is a high cost and technical challenge related to assessment techniques and tests (catheterization and respiratory function tests), that limits the usage of small animals and its related advantages; Small animals are relatively inexpensive, have shorter gestational periods, can be genetically manipulated to target key molecules and pathways, and generate large data sets. Therefore, attention should be directed towards the development of PH-LHD-specific models or towards deeper evaluation of existing models and adequate assessment of PH stage and progression, in order to fully explore pathophysiological mechanisms and establish treatment strategies.

A sick pulmonary circulation is a deleterious outcome of heart disease. As mentioned in previous sections of this thesis introduction, a thorough investigation of pulmonary vascular mechanisms' alterations underlying the pathophysiological processes of group II-PH is of high importance, as it would aid in expanding investigations around PH-LHD therapies. Nevertheless, very few PH-LHD studies focused on assessing vascular remodelling and on studying the specific structural and functional pulmonary vascular changes that play part throughout the progression of PH-LHD. An in depth understanding of the changes in the pulmonary circulation underlying the progression of group II-PH is of high importance. The following section describes pulmonary capillary failure and arteriolar remodelling in LHD. Additionally, it highlights the critical role that endothelial dysfunction and Ca^{2+} dyshomeostasis play in pulmonary vascular reactivity alterations and consequent remodelling through the course of PH progression.

5 Lung capillary stress failure and arteriolar remodelling in pulmonary hypertension associated with left heart disease (Group 2 PH)

Nour R. Dayeh[a, b], Jonathan Ledoux[a, c], Jocelyn Dupuis[a, b, c]

[a]Research Center, Montreal Heart Institute, Montreal, QC, Canada
[b]Département de Médecine, Université de Montréal, Montréal, QC, Canada
[c]Département de Physiologie, Université de Montréal, Montréal, QC, Canada

Progress in Cardiovascular Diseases 2016 59, 11-21DOI: (10.1016/j.pcad.2016.05.002)

This review article was accepted on May 8th 2016 and published on May 16th 2016

Available online at www.s ciencedirect.com

ScienceDirect

www.onlinepcd .com

Progress in Cardiovascular Diseases

Lung Capillary Stress Failure and Arteriolar Remodelling in Pulmonary Hypertension Associated with Left Heart Disease (Group 2 PH)

Nour R. Dayeh[a, b], *Jonathan Ledoux*[a, c], *Jocelyn Dupuis*[a, b, c, *]

[a]*Research Center, Montreal Heart Institute, Montreal, QC, Canada* [b]*Département de Médecine, Université de Montréal, Montréal, QC, Canada* [c]*Département de Physiologie, Université de Montréal, Montréal, QC, Canada*

ARTICLE INFO

Keywords:

Pulmonary hypertension
Heart failure
Lung remodelling
Vascular endothelium
Pathophysiology

ABSTRACT

Left heart diseases (LHD) represent the most prevalent cause of pulmonary hypertension (PH), yet there are still no approved therapies that selectively target the pulmonary circulation in LHD. The increase in pulmonary capillary pressure due to LHD is a triggering event leading to physical and biological alterations of the pulmonary circulation. Acutely, mechanosensitive endothelial dysfunction and increased capillary permeability combined with reduced fluid resorption lead to the development of interstitial and alveolar oedema. From repeated cycles of such capillary stress failure, originate more profound changes with pulmonary endothelial dysfunction causing increased basal and reactive pulmonary vascular tone. This contributes to pulmonary vascular remodelling with increased arterial wall thickness, but most prominently, to alveolar wall remodelling characterized by myofibroblasts proliferation with collagen and interstitial matrix deposition. Although protective against acute pulmonary oedema, alveolar wall thickening becomes maladaptive and is responsible for the development of a restrictive lung syndrome and impaired gas exchanges contributing to shortness of breath and PH. Increasing awareness of these processes is unraveling novel pathophysiologic processes that could represent selective therapeutic targets. Thus, the roles of caveolins, of the intermediate myofilament nestin and of endothelial calcium dyshomeostasis were recently evaluated in pre-clinical models. The pathophysiology of PH due to LHD (group II PH) is distinctive from other groups of PH. Therefore, therapies targeting PH due to LHD must be evaluated in that context.

The most prevalent cause of pulmonary hypertension (PH) is left-sided heart disease (LHD), classified as group 2 PH. Although clinicians are well aware of the negative functional and vital prognostic impact of PH in heart failure with reduced ejection fraction (HFrEF) and heart failure with preserved ejection fraction (HFpEF), there currently are no approved therapies to selectively target and treat group 2 PH. A better understanding of the pathophysiologic processes leading to group 2 PH is imperative. We will review the current knowledge regarding the physical impact of LHD on the

Statement of Conflict of Interest: see page 18.

* Address reprint requests to Jocelyn Dupuis, MD, PhD, Research Center, Montreal Heart Institute, 5000 Bélanger est, Montreal, QC, Canada H1T 1C8.
E-mail address: dupuisj@me.com (J. Dupuis).

http://dx.doi.org/10.1016/j.pcad.2016.05.002

Abbreviations and Acronyms

EDHF = endothelial-derived hyperpolarizing factors

Cav-1 = caveolin-1

eNOS = endothelial nitric oxide synthase

HF = heart failure

HFrEF = heart failure with reduced ejection fraction

HFpEF = heart failure with preserved ejection fraction

IEL = internal elastic lamina

LHD = left-sided heart disease

NO = nitric oxide

PAH = pulmonary arterial hypertension

PH = pulmonary hypertension

PDGF = platelet-derived growth factor

PGI_2 = prostacyclin

ET-1 = endothelin-1

VEGF = vascular endothelium growth factor

VIP = vasoactive intestinal peptide

PDE_2 = phophodiesterase E_2

L-NAME = L-N^G-Nitroarginine methyl ester

TRPV4 = transient receptor potential vanilloid 4

fragile lung capillaries and the reactive biologic alterations leading to lung structural and arteriolar remodelling.

Functional structure of the pulmonary vasculature

The normal pulmonary vasculature, a low-pressure low-resistance system compared to the systemic circulation, is capable of accommodating large increases in blood flow with minimal elevation in pressure. Pulmonary arteries and arterioles are thin-walled compared their systemic counterparts. In addition to luminal diameter, the extent of contribution of the artery to pulmonary resistance is based on structural features, the cellular composition of each of the wall layers as well as fibrotic content.[1]

The tunica intima of the pulmonary vasculature at the alveolar capillary level is responsible for assuring optimal gas ex-change while limiting the flux of fluid and macromolecules to the alveolar and interstitial spaces. Pulmonary vascular endothelial cells share a number of markers with endothelial cells of other vascular beds, but differ in their morphology and express pulmonary-specific markers and proteins like angiotensin I converting enzyme (ACE) and human lung endothelial-cell-specific molecule-1 promoter (ESM-1),[2] due to their role as well as the low pressure and flow conditions within the pulmonary circulation.[3,4] Moreover, pulmonary endothelial cells differ between the macro and microcirculation of the lung in their shape, their mechanosensing properties, glycocalyx structure, caveolae density[5,6] as well as ion channel expression and function. For example, pulmonary microvascular endothelial cells express a number of calcium channels that are not found in extra-alveolar endothelial cells.[7]

The tunica media or smooth muscle layer of pulmonary arteries is also much thinner compared their systemic counterparts of similar luminal diameter. The degree of muscularization of the tunica media varies with pulmonary vessel diameter.[8] Additionally, the extent of elastic laminae thickness changes with vessel size: as arterial lumen diameter decreases down the pulmonary vascular tree, the elastic laminae become less prominent and are replaced by smooth muscle cells.[8] The internal elastic lamina (IEL) of arteries is studded with holes (fenestrations) that permit endothelial cell-smooth muscle cell communication. This communication is enabled by the presence of endothelial cell/smooth muscle cellular extensions through those fenestrations, termed myoendothelial projections. Studies on pulmonary arteries have reported modifications in IEL structure and composition, as well as changes in the number of gaps in the IEL in several cardiovascular diseases including PH.[9,10] Finally, the nature of endothelium-derived factors that control pulmonary vascular tone, as well as the extent of their relative contribution differ along the pulmonary vascular tree.

Endothelial control of the pulmonary circulation: Mechanisms of regulation of pulmonary vascular tone

Endothelial influence on pulmonary vascular function is inferred through mechanisms and substances with vasoconstrictor/vasodilator properties and modulating growth and proliferation of cells within the vessel wall. The pulmonary circulation has a low resting tone under normal conditions. Pulmonary vascular endothelial cells control tone through numerous pathways and molecules like nitric oxide (NO), endothelium-derived hyperpolarizing factor (EDHF), prostacyclin (PGI_2), endothelin-1 (ET-1) as well as many additional factors including platelet-derived growth factor (PDGF), vascular endothelium growth factor (VEGF), vasoactive intestinal pep-tide (VIP), urotensin, adrenomedullin and leukotrienes. In addition, the pulmonary vascular endothelium is an important site for metabolism and clearance of circulating mediators such as angiotensin-I, endothelin, serotonin, adrenomedullin, and many others through specific receptors, enzymes and transporters.[11–17] The pulmonary endothelium will therefore modulate local, but also systemic vascular biology. This review will restrict its focus to some of the pathways that may be more relevant to PH associated with LHD. It is generally recognized that endothelial dysfunction is a core abnormality contributing to all forms of PH, including group II PH. Current therapies approved for group I PH all target endothelial products or properties: prostacyclin and its analogs, PDE_2 inhibitors, endothelin receptor antagonists, soluble guanylate cyclase stimulators. One notable exception is calcium channel blockers, targeting the smooth muscle cell, that are very effective for the treatment of vasoreactive PH, a rare form of group I PH with a good prognosis. None of these PH therapies are however currently approved for PH due to LHD (group II PH).

Nitric oxide pathway

Extensive work has established the role of the NO pathway in background mechanisms preserving basal pulmonary vascular tone. Animal model studies showed involvement of NO in the maintenance of a lower basal pulmonary vascular tone.[18] By using nitric oxide synthase inhibitors such as L-NAME in

healthy humans, studies validated the participation of NO in resting pulmonary vasorelaxation.[19–22] These investigations revealed a prominent but partial role for NO in opposing increases in tone; a role that seems to be more pronounced in large conduit arteries compared to smaller resistance vessels. Basal constitutive expression of eNOS (NOSIII) in pulmonary vascular endothelium has been reported[23,24] and is essential for a sustained low pulmonary vascular pressure.[22]

Moreover, subcellular distribution of the enzyme appears critical to its activity. Indeed, Cav-1 binding to the calmodulin-binding site of eNOS leads to the enzyme uncoupling and incapacity to produce NO, therein located within caveolae.[25–27] As we will discuss later, caveolins seem to play a key role in the maintenance of pulmonary microcirculatory homeostasis.[28]

Prostacyclin (PGI_2)

PGI_2 is metabolized from arachidonic acid through the cyclooxygenase pathway (COX). Endothelial production and release of PGI_2 causes vasodilation of underlying smooth muscle cells by stimulating cyclic adenosine monophosphate (cAMP) formation. In the normal pulmonary circulation, PGI_2 was shown to be a contributor to basal pulmonary vascular tone in a number of animal studies.[29,30] Several types of prostanoid receptors, including the PGI_2 receptors (IP) that control pulmonary vascular tone have been identified in mice lungs.[31] Additionally, a number of human and animal studies demonstrated that stimulation of adenylate cyclase and the ensuing increase in smooth muscle cAMP levels lead to the opening of K^+ channels and pulmonary vasodilation.[32,33]

Endothelial-derived hyperpolarizing factors

EDHF consists of an amalgam of mechanisms (excluding NO and PGI_2) of endothelial origin leading to hyperpolarization of vascular smooth muscle cells. These mechanisms can involve either direct electrical coupling through myoendothelial communication or the release of factors that directly influence myocyte membrane potential such as K^+ clouds (spatially restricted accumulation of K^+ ions in the intercellular space). The nature of these mechanisms and factors and their respective contribution to the regulation of vascular tone varies with arterial diameter and the species studied. It consists in a wide range of proteins, molecules and mechanisms including small and intermediate calcium-activated potassium channels ($K_{Ca}2.x$ and $K_{Ca}3.1$), connexins, epoxyeicosatreionic acids (EETs; metabolites of arachidonic acid), hydrogen peroxide (H_2O_2), and C-type natriuretic peptide. Similarly to NO, the role of EDHF in the maintenance of low resting pulmonary vascular tone has been established.[34,35] Animal models aided in demonstrating the participation of EDHF in the regulation of pulmonary tone through cytochrome P450 metabolites or activation of small and intermediate Ca^{2+}-activated K^+ channels.[36–38] Unlike NO, the role of EDHF was found to be more pronounced in the pulmonary microcirculation compared to larger vessels.[39,40]

Endothelin (ET)

ET-1 is the predominant isoform of this potent vasoconstrictor and proliferator peptide produced by endothelial cells. ET receptors are present on both vascular endothelial (ET_B) and smooth muscle cells (ET_A and ET_B).[41] Stimulation of endothelial ET_B receptor causes pulmonary vasodilation while the smooth muscle ET_A and ET_B receptors promote vasoconstriction and proliferation.[42] The endothelial ET_B is responsible for clearance of circulating ET-1, suggesting that the lungs are a primary target of this peptide.[15] Furthermore, pulmonary artery smooth muscle ET receptors can form heterodimers, modifying their pharmacological response.[43,44] In healthy humans, endothelin influences pulmonary vasomotor tone in physiological states,[19,45,46] and its modulatory role is greatly increased in pathological conditions as discussed in later sections.

Endothelial dysfunction is a great contributor to pulmonary vascular tone alterations, and potentially to pulmonary vascular remodelling. An improved understanding of pulmonary vascular alterations that contribute to PH in LHD and how it differs from group I PH is required. Fig 1 summarizes the factors that contribute to the control of normal pulmonary vascular tone. The remaining of this review discusses pathological alterations of the pulmonary circulation of group II PH.

Lung capillary injury in LHD

Shortness of breath, the cardinal clinical symptom of HF, occurs when pulmonary capillary pressure increases due to LHD. Backward transmission of elevated left heart filling pressure to pulmonary veins is in turn transferred to pulmonary capillaries. Consequent alteration of the capillary hydrostatic/oncotic pressures balance promotes augmented passage of fluid across the alveolar-capillary barrier according to the Starling principle. This accumulation of fluid within the interstitial space and ultimately into alveoli is accompanied by a decreased clearance with eventual physical disruption of the alveolar-capillary barrier; a phenomenon termed capillary stress failure.[47,48] A recent study, suggested that increased intracellular calcium levels of lung microvascular endothelial cells causes endothelial retraction thus increasing capillary permeability and promoting oedema.[49] Indeed, pathological and pharmacological activation of calcium channels expressed in capillary endothelial cells was found to promote vascular leakage through alveolar-capillary membranes.[50–52] Resorption of alveolar fluid occurs through the amiloride-sensitive alveolar epithelium sodium channel (ENaC)[53] and lung sodium handling is impaired in human subjects after myocardial infarction,[54] further contributing to the development of alveolar oedema. Studies support an important role for activation of the Ca^{2+}-permeable transient receptor potential vanilloid 4 (TRPV4) channels in hydrostatic pulmonary edema.[52,55] Transgenic deletion of this mechano-sensitive channel appears to protect from hydrostatic pulmonary edema[56] and pharmacological blockade effectively prevents and treats pulmonary oedema in acute and chronic heart failure (HF) models.[55]

Repetitive and sustained elevations in pulmonary capillary pressure, resulting from recurrent retrograde increases in left ventricular pressure, will induce a series of injury-repair cycles to the capillary wall. Initiation of capillary remodelling, along with increased fluid clearance[57] is protective mechanisms against pulmonary oedema in patients with chronic HF.[58,59]

However, this reparative process impairs capillaries' diffusion efficiency and the associated gas exchange, thus further contributing to disease progression.[58] Studies on both animal models and humans have shown collagen deposition and alveolar septa thickening accompanied by cellular proliferation[58,60–65] that were associated with reduced alveolar capillary permeability and correlated with a diminished respiratory function in HF. Additionally, a study using an aortic banding-induced HF model demonstrated calcium handling-related cytoskeletal disorganization contributing to alveolar-capillary remodelling.[66]

Abnormal vascular reactivity in PH associated with LHD

Dysregulation of pulmonary vascular tone in PH has been established through a number of studies that mainly focused on NO-, ET-1-, PGI_2-, and EDHF-dependent pathways. Rat models of congestive heart failure showed an impaired NO-dependent vasodilator response in pulmonary arteries[67] and elevated sustained levels of ET-1 involved in alterations of vascular reactivity.[44,68,69]

Human patient studies revealed that endothelial dependent vasodilation was impaired due to deficient basal production of NO. These findings strongly suggested that the loss of NO-dependent vasodilation contributes to the development of PH.[23,67] The concomitant role of the endothelin system in the development of PH was previously reviewed in detail.[42,70] In a number of human HF studies, elevation in circulating levels of ET-1 was found[71,72] and correlated especially well with increased pulmonary artery pressure[73] and worse prognosis.[74] Accordingly, endothelin receptor antagonists selectively reduce pulmonary vascular resistance in HF.[75] Cross-talks between endothelin and NO systems occur as chronically increased ET levels reduce pulmonary vascular reactivity to NO.[41] However, other mechanisms are potentially involved in pulmonary vascular reactivity in HF including PGI_2- and EDHF-associated pathways. A potential role for EDHF in endothelium-dependent relaxation has been suggested from a number of animal models of HF.[76] In a canine model of pacing-induced HF, a disruption of receptor-mediated stimulation of adenylate cyclase was observed, along with a depressed dilatory response to arachidonic acid and PGI_2.[77] Intravenous administration of prostaglandin E1 in patients with mitral valve disease or congenital heart disease resulted in a significant fall in pulmonary arterial pressure.[78,79] Moreover, clinical studies on inhaled vasodilators like Epoprostenol or Iloprost (prostacyclin PGI_2 analogs) validated impaired PGI_2-associated endothelium-dependent vasodilation in group 2 PH.[80–82]

Remodelling process of small pulmonary arteries

Although less prominent than in other types of PH, lung vascular remodelling contributes to increased pulmonary vascular resistance (PVR) in PH due to LHD. A study by Delgado and colleagues conducted on a group of heart

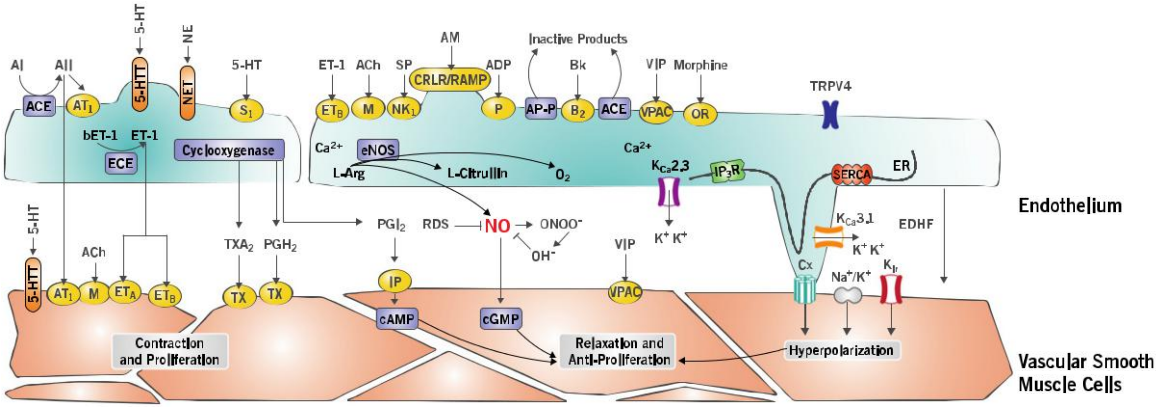

Fig 1 – Biologic functions of the endothelial and muscular layers of the pulmonary vasculature. Various mediators are produced, transformed or inactivated by the pulmonary vascular endothelial cells. Specific receptors and transporters are expressed by endothelial and vascular smooth muscle cells. Nitric oxide (NO); endothelium-derived hyperpolarizing factor (EDHF); prostacyclin (PGI2); angiotensin-converting enzyme (ACE); acetylcholine (Ach); angiotensin I (AI); angiotensin II (AII); angiotensin 1 receptor (AT1); bradykinin (Bk); cyclo-oxygenase (COX); endothelin-converting enzyme (ECE); endothelin A and B receptors (ETA, ETB); endothelin-1 (ET-1); L-arginine (L-Arg); prostaglandin H2 (PGH2); reactive oxygen species (ROS); serotoninergic receptor (S1); thromboxane receptor (TH); thrombin (Thr); thromboxane A2 (TXA2); serotonin (5-HT); opioid receptor (OR); calcitonin receptor-like receptor-receptor activity modifying protein (CRLR-RAMP); adrenomedullin (AM); neurokinin receptor (NK-1); substance P (SP); vasoactive intestinal peptide receptor (VPAC); vasoactive intestinal peptide (VIP); aminopeptidase P (AP-P); norepinephrine transporter (NET); norepinephrine (NE); serotonin transporter (5-HTT); prostacyclin receptor (IP); transient receptor potential vanilloid channel 4 (TRPV4); inositol triphosphate receptor (IP_3R); sarco/endoplasmic reticulum Ca^{2+}-ATPase (SERCA); endoplasmic reticulum (ER); small conductance calcium-activated potassium channel 3 (K_{Ca} 2.3); intermediate conductance calcium-activated potassium channel (K_{Ca} 3.1); connexin (Cx); inward rectifiying potassium channel (K_{ir}); sodium/potassium triphosphatase pump (Na^+/K^+).

transplantation recipients with preoperative chronic HF validated pulmonary vascular remodelling as a determining factor for the severity of PH in right ventricular failure after heart transplantation.[83] Intravascular ultrasound further documented pulmonary vascular remodelling in patients with PH subsequent to LHD. Pulmonary medial hypertrophy and smaller intraluminal diameter were reported to be more pronounced in lower lobes and to correlate with pulmonary artery pressure and elevated plasma ET-1 levels.[84] Preponderant alterations found in the lower lobes, more sensitive to gravitational forces, suggest the importance of chronically increased capillary hydrostatic pressures as an initiating event.[84] Although changes in the pulmonary vessels with medial hypertrophy contribute to PH due to LHD, these alterations appear milder than those found in group I PH. Indeed, tunica media thickening of small pulmonary arteries (50–200 μM diameter) from rats with systolic HF was only of 4–5%. In larger pulmonary arteries from the same models there was also medial hypertrophy with increased collagen and elastin content.[85] The uniqueness of group II PH remodelling therefore resides, at least partially, in the changes occurring in the alveolar vessels and pulmonary veins.

Endothelial dysfunction and calcium dyshomeostasis in PH associated with LHD

Both systemic and microvascular pulmonary endothelial dysfunction are present in HF and the former most likely impacts the latter. In a recent study by Farrero et al.[86] peripheral endothelial dysfunction was shown to directly correlate with PVR in patients with HFpEF. This work identified endothelial dysfunction and abnormal collagen metabolism as markers in identifying patients with HFpEF at risk of developing PH. Pulmonary arteries from rats with compensated systolic HF were characterized with an endothelial dysfunction from a reduced NO production (both basal and stimulated) and decreased eNOS expression.[85]

Variations in $[Ca2^{+}]_i$ are central to a multitude of cellular processes, including the genesis of various endothelial factors.[87] Endothelial $[Ca2^{+}]_i$ regulation is thus a highly dynamic requiring finely tuned processes that involve a broad range of molecules, receptors, calcium-permeable channels[36,88] and anchoring proteins. Intracellular endothelial calcium signalling should however be considered from a spatial perspective, with global and local calcium signalling. In regards to global calcium signalling, the well-established activation of G-protein coupled receptors leads to the mobilization of a G protein subunit and the production of inositol triphosphate (IP_3) through the action of phospholipase C (PLC). The ensuing activation of IP_3 receptors evokes calcium release from the endoplasmic reticulum (ER). Propagated activation of numerous neighbouring IP_3 receptors triggers a massive Ca^{2+} release in the cytoplasm, also causing ER depletion and activation of the store-operated calcium entry (SOCE) pathways, responsible of a sustained elevated cytosolic calcium level. This substantial increase in $[Ca2^{+}]_i$ non-selectively activates a myriad of pathways involved for example in the control of vascular tone (NO, PGI_2, and EDHF), and vascular remodelling. In a rat model of HFpEF through aortic banding, pulmonary endothelial calcium impairment was shown to be associated to cytoskeletal reorganization and disruption of normal endothelial function.[66] In addition, dysfunctional pulmonary arterial function and structure were linked to modified calcium-permeable channels.[89] For instance, intracellular calcium regulation through TRPV4 channels is involved in the vascular permeability response to increased pulmonary vascular pressure.[56] Accordingly, it was demonstrated that inhibition of PDE_5 constitutes a negative feedback loop that attenuates pressure-induced $[Ca2^{+}]_i$ increase within pulmonary capillaries.[90]

Local calcium signalling, on the other hand, consists of spontaneous and spatially restricted intracellular calcium oscillations. Several local calcium signals have been characterized, mainly based on their specific intracellular localization and kinetic. Spatial restriction of intracellular calcium dynamics confers significant benefits: specific modulation of calcium-sensitive signalling pathways within a defined intra-cellular region without affecting other cellular functions and in a highly efficient manner, on an energetic perspective. Spontaneous and propagating calcium increases in pulmonary microvascular cells termed calcium waves were reported.[91] Furthermore, pressure-induced calcium oscillations were studied in pulmonary capillaries.[92] Local endothelial calcium signalling in PH associated with LHD remains however to be characterized. Our team recently reported for the first time the presence of local endothelial calcium transients termed calcium pulsars in intact small pulmonary arteries using GCaMP-2 transgenic mice.[93] Interestingly, TRPV4 channels are major modulator of these calcium events. Exploring kinetic properties of those transients in the context of group 2 PH may unveil a significant role for those events in alterations of pulmonary vascular tone and/or a potential novel therapeutic avenue.

Lung alveolar wall remodelling: A central role for myofibroblasts

In HF, lung capillary injury and subsequent inflammation with activation of neurohumoral mediators cause the activation and proliferation of myofibroblats.[58,60–63] Myofibroblasts proliferate into the alveolar wall in response to lung injury and secrete collagen and interstitial matrix components protecting against development of pulmonary oedema. However this process can become maladaptive and trigger a restrictive lung syndrome that manifests through reduced compliance and impaired gas exchange. Fig 2 demonstrates examples of histologic findings in the lungs from a human subject with LHD and a mouse with LHD induced by coronary artery ligation. Similar histological changes are seen with obvious thickening of the alveolar septa resulting from myofibroblasts proliferation and collagen deposition. Further characterization of alveolar wall remodelling in rats with HF was performed by electron microscopy and showed myofibroblasts proliferation with collagen, elastin and reticulin deposition, thickening of basement membranes and increased formation of basement membrane-like material in the alveolar wall (Fig 3).[61] A number of studies using different animal models

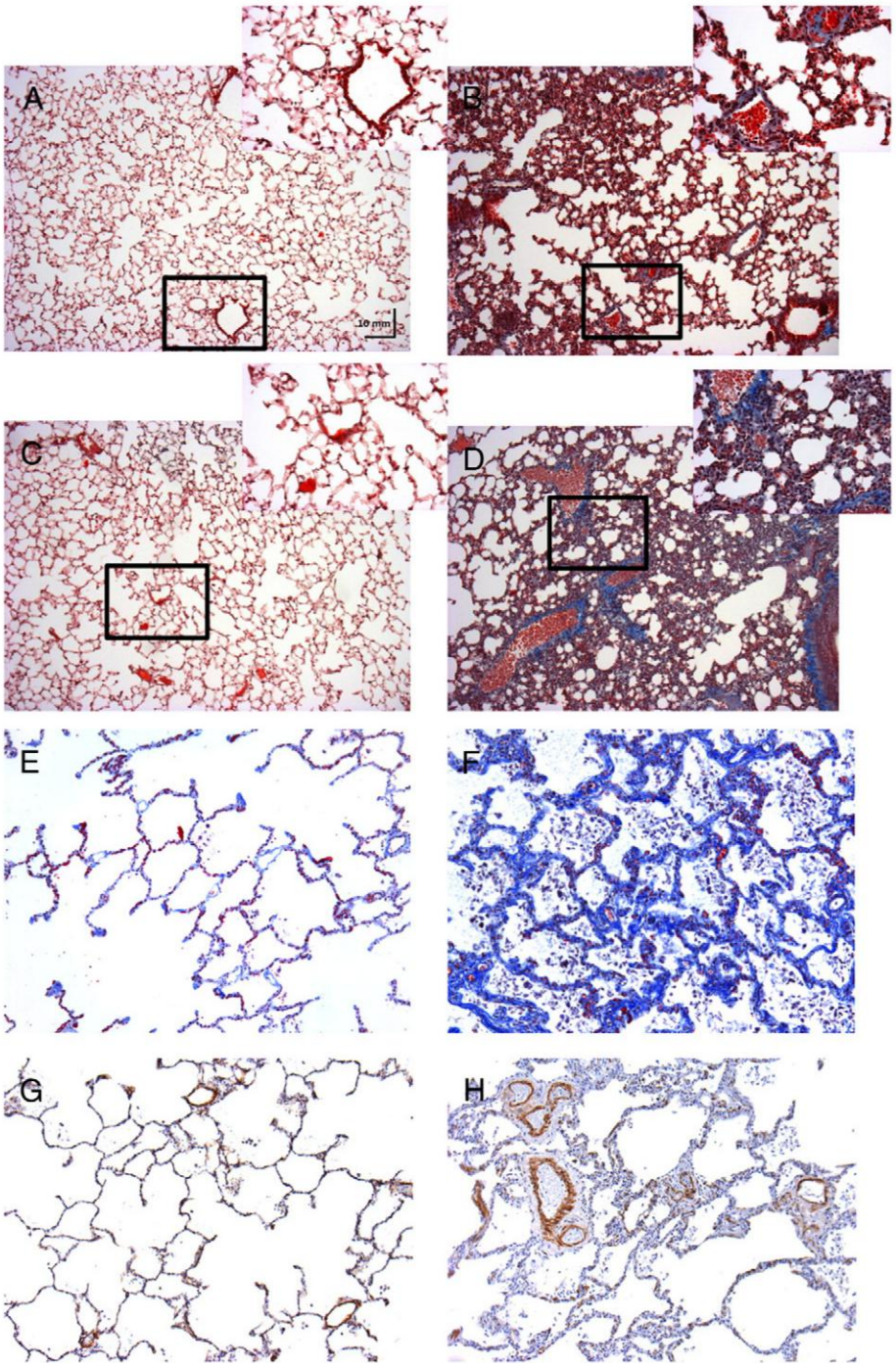

Fig 2 – Histologic examples of lung remodelling in animals and humans with LHD using with Masson's trichrome staining (A–F) and immunostaining for smooth muscle alpha-actin (G–H). Normal sham operated mice (A, C) are compared with mice with LHD 3 weeks after coronary artery ligation (B, D). There is important thickening of the alveolar septa in LHD with increased collagen content (blue) in alveolar and vessel walls. A human subject with LHD due to chronic ischemic cardiomyopathy (F) shows thickening of the alveolar wall with important collagen deposition compared to a subject without LHD (E). Compared to a control subject (G), immunostaining of smooth muscle alpha actin in a human subject with LHD due to aortic stenosis shows medial vascular hypertrophy and aveolar wall cells expressing the smooth muscles marker representing myofibroblasts (H).

of HF investigated the origin of proliferating myofibroblasts and revealed the contribution of bone marrow-derived progenitor cells,[94] as well as resident lung mesenchymal cells.[95] Amongst potentially relevant factors involved in pulmonary remodelling and myofibroblasts proliferation are reduced caveolins expression[28] and increased angiotensin-II levels.[61,96] Caveolin KO rats develop lung alveolar wall remodelling similar to that seen in LHD.[28] Angiotensin receptors are expressed in lung myofibroblasts and their activation

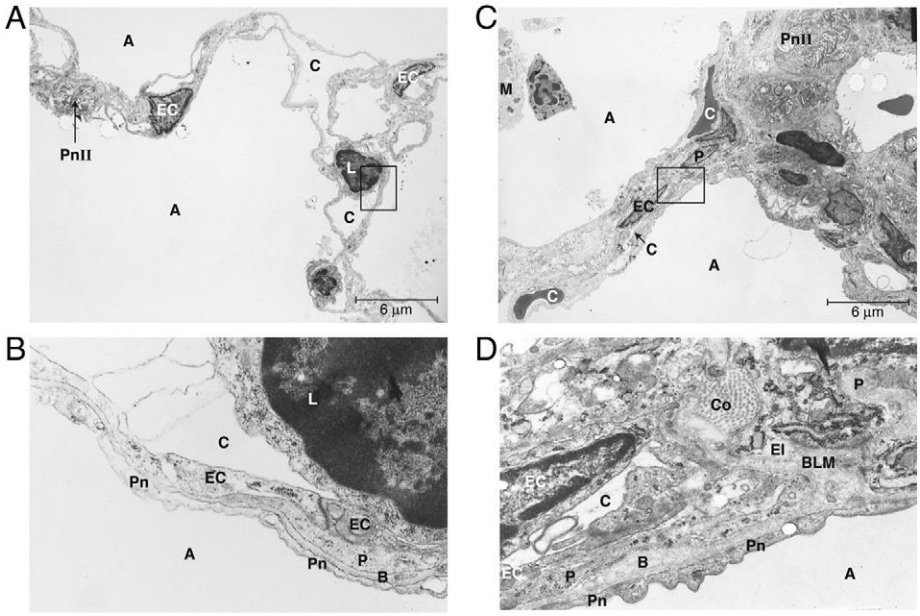

Fig 3 – Electron microscopy of lung sections from 2-week sham operated rats (a, b) and 2-week LHD rats induced by coronary artery ligation (c, d). (b) and (d) represent an 10X magnification of the squared region from picture (a) and (c) respectively. In the MI group there is thickening of the alveolar septum due to enlargement of the basal membrane, deposition of collagen and elastin and cellular proliferation. A, indicates alveoli; B, basal membrane; BLM, basal membrane-like material; C, capillaries; Co, collagen; EC, endothelial cells; El, elastin; L, lymphocyte; P, pericyte; Pn, type I pneumocyte; PnII, type II pneumocyte; M, macrophage. Reproduced with permission from Cardiovasc Res, 2003. 58(3): p. 621–31.

stimulates myofibroblast proliferation.[96] Moreover, the angiotensin receptor antagonist irbesartan efficiently prevented lung remodelling in rats with HFrEF.[61] More recently, increased expression of the intermediate filament protein nestin was reported in lung myofibroblasts in HFrEF, even preceding PH development.[97] Nestin expression also seems to play a role in endothelial/epithelial cell transition to a mesenchymal phenotype in the fibrotic PH lungs.[98]

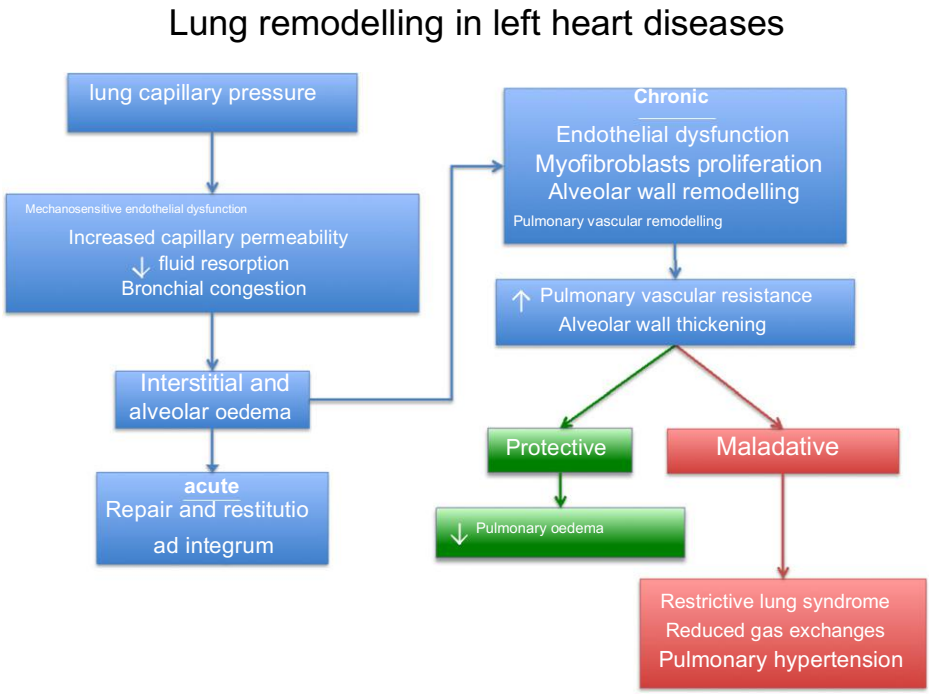

Fig 4 – Pathophysiology of lung vascular and structural remodelling associated with LHD.

Mechanistic studies were performed to evaluate pharmacological treatments efficiency in the reversal of adverse effects of HF on alveolar remodelling. For instance, PDE5 inhibition with Sildenafil showed promise in clinical studies as it improved exercise capacity and gas exchanges.[99,100] However, although many group I PH selective therapies including sildenafil were evaluated in HF, none had similar beneficial outcomes in group II PH. These previous studies were however not initially designed to specifically address group II PH and stratification was not established because study subjects were not stratified according to the presence of PH or the impact of lung remodelling. In contrast, very encouraging pre-clinical studies evaluating the effect of angiotensin receptor blockers[61] and atorvastatin[101] report an impressive reduction of lung structural remodelling and pulmonary hypertension associated with HF. Some PH specific therapies such as endothelin receptor antagonists however did not show benefit in pre-clinical models of systolic HF.[102] Fig 4 summarizes the pathophysiology of lung structural and vascular remodelling in LHD.

Conclusion

LHD directly physically impacts the pulmonary circulation through increased hydrostatic pressure with combined reduced alveolar resorption leading to pulmonary edema. Recurrent cycles of lung capillary injury and repair associated with pulmonary vascular endothelial dysfunction result in increased pulmonary vascular tone, pulmonary vascular remodelling and alveolar wall remodelling. Myofibroblasts proliferation, with concomitant deposition of collagen, plays a key role in alveolar wall thickening. This initially protective mechanism eventually leads to a restrictive lung syndrome and impaired gas exchange, further contributing to PH. Abnormal global and local pulmonary endothelial Ca^{+} signalling in HF requires better pathophysiological characterization. Substantial effort is currently being invested into unveiling the pathophysiological mechanisms underlying the development of PH in LHD. Extensive work is still needed but further elucidation of vascular changes and the herein mechanisms might significantly improve our capacity to reverse, limit the progression of the pathology or alleviate its symptoms.

Statement of conflict of interest

None of the authors have any conflicts of interests with regard to this publication.

Acknowledgements

The authors would like to thank Dr Martin Sirois and Marie-Élaine Clavet for the histology service provided on mouse lung sections.

REFERENCES

1. Wang Z, Chesler NC. Pulmonary vascular wall stiffness: An important contributor to the increased right ventricular afterload with pulmonary hypertension. Pulm Circ. 2011;1(2): 212-223.
2. Tsai JC, Zhang J, Minami T, et al. Cloning and characterization of the human lung endothelial-cell-specific molecule-1 promoter. J Vasc Res. 2002;39(2):148-159.
3. Aird WC. Mechanisms of endothelial cell heterogeneity in health and disease. Circ Res. 2006;98(2):159-162.
4. Aird WC. Phenotypic heterogeneity of the endothelium: I. Structure, function, and mechanisms. Circ Res. 2007;100(2): 158-173.
5. King J, Hamil T, Creighton J, et al. Structural and functional characteristics of lung macro- and microvascular endothelial cell phenotypes. Microvasc Res. 2004;67(2):139-151.
6. Zhou C, Chen H, King JA, et al. Alpha1G T-type calcium channel selectively regulates P-selectin surface expression in pulmonary capillary endothelium. Am J Phys Lung Cell Mol Phys. 2010;299(1):L86-L97.
7. Stevens T. Functional and molecular heterogeneity of pulmonary endothelial cells. Proc Am Thorac Soc. 2011;8(6): 453-457.
8. Townsley MI. Structure and composition of pulmonary arteries, capillaries, and veins. Compr Phys. 2012;2(1):675-709.
9. Aiello VD, Gutierrez PS, Chaves MJ, et al. Morphology of the internal elastic lamina in arteries from pulmonary hypertensive patients: a confocal laser microscopy study. Mod Pathol. 2003;16(5):411-416.
10. Lam CF, Peterson TE, Croatt AJ, et al. Functional adaptation and remodeling of pulmonary artery in flow-induced pulmonary hypertension. Am J Physiol Heart Circ Physiol. 2005;289(6):H2334-H2341.
11. Dupuis J, Goresky CA, Ryan JW, et al. Pulmonary angiotensin-converting enzyme substrate hydrolysis during exercise. J Appl Physiol. 1992;72(5):1868-1886.
12. Dupuis J, Goresky CA, Stewart DJ. Pulmonary removal and production of endothelin in the anesthetized dog. J Appl Physiol. 1994;76(2):694-700.
13. Dupuis J, Goresky CA, Fournier A. Pulmonary clearance of circulating endothelin-1 in dogs in vivo: exclusive role of ETB receptors. J Appl Physiol. 1996;81(4):1510-1515.
14. Dupuis J, Goresky CA, Rouleau JL, et al. Kinetics of pulmonary uptake of serotonin during exercise in dogs. J Appl Physiol. 1996;80(1):30-46.
15. Dupuis J, Stewart DJ, Cernacek P, et al. Human pulmonary circulation is an important site for both clearance and production of endothelin-1. Circulation. 1996;94(7):1578-1584.
16. Langleben D, Dupuis J, Langleben I, et al. Etiology-specific endothelin-1 clearance in human precapillary pulmonary hypertension. Chest. 2006;129(3):689-695.
17. Dupuis J, Caron A, Ruel N. Biodistribution, plasma kinetics and quantification of single-pass pulmonary clearance of adrenomedullin. Clin Sci (Lond). 2005;109(1):97-102.
18. Koizumi T, Gupta R, Banerjee M, et al. Changes in pulmonary vascular tone during exercise. Effects of nitric oxide (NO) synthase inhibition, L-arginine infusion, and NO inhalation. J Clin Invest. 1994;94(6):2275-2282.
19. Cooper CJ, Landzberg MJ, Anderson TJ, et al. Role of nitric oxide in the local regulation of pulmonary vascular resis-tance in humans. Circulation. 1996;93(2):266-271.
20. Stamler JS, Loh E, Roddy MA, et al. Nitric oxide regulates basal systemic and pulmonary vascular resistance in healthy humans. Circulation. 1994;89(5): 2035-2040.
21. Celermajer DS, Dollery C, Burch M, et al. Role of endothelium in the maintenance of low pulmonary vascular tone in normal children. Circulation. 1994;89(5):2041-2044.
22. Dinh-Xuan AT, Higenbottam TW, Clelland CA, et al. Impair-ment of endothelium-dependent pulmonary-artery relaxation in chronic obstructive lung disease. N Engl J Med. 1991;324(22):1539-1547.

23. Moraes DL, Colucci WS, Givertz MM. Secondary pulmonary hypertension in chronic heart failure: the role of the endothelium in pathophysiology and management. Circulation. 2000;102(14):1718-1723.
24. Kobzik L, Bredt DS, Lowenstein CJ, et al. Nitric oxide synthase in human and rat lung: immunocytochemical and histo-chemical localization. Am J Respir Cell Mol Biol. 1993;9(4): 371-377.
25. Grayson TH, Chadha PS, Bertrand PP, et al. Increased caveolae density and caveolin-1 expression accompany impaired NO-mediated vasorelaxation in diet-induced obesity. Histochem Cell Biol. 2013;139(2):309-321.
26. Feron O, Saldana F, Michel JB, et al. The endothelial nitric-oxide synthase-caveolin regulatory cycle. J Biol Chem. 1998;273(6):3125-3128.
27. Frank PG, Woodman SE, Park DS, et al. Caveolin, caveolae, and endothelial cell function. Arterioscler Thromb Vasc Biol. 2003;23(7):1161-1168.
28. Jasmin JF, Mercier I, Hnasko R, et al. Lung remodeling and pulmonary hypertension after myocardial infarction: path-ogenic role of reduced caveolin expression. Cardiovasc Res. 2004;63(4):747-755.

29. Frantz E, Soifer SJ, Clyman RI, et al. Bradykinin produces pulmonary vasodilation in fetal lambs: role of prostaglandin production. J Appl Phys (1985). 1989;67(4):1512-1517.
30. Gryglewski RJ, Chlopicki S, Uracz W, et al. Significance of endothelial prostacyclin and nitric oxide in peripheral and pulmonary circulation. Med Sci Monit. 2001;7(1):1-16.
31. Olschewski A, Olschewski H, Brau ME, et al. Basic electrical properties of in situ endothelial cells of small pulmonary arteries during postnatal development. Am J Respir Cell Mol Biol. 2001;25(3):285-290.
32. Schubert R, Serebryakov VN, Engel H, et al. Iloprost activates KCa channels of vascular smooth muscle cells: role of cAMP-dependent protein kinase. Am J Phys. 1996;271(4 Pt 1): C1203-C1211.

33. Jones RL, Qian Y, Wong HN, et al. Prostanoid action on the human pulmonary vascular system. Clin Exp Pharmacol Physiol. 1997;24(12):969-972.
34. Feletou M, Girard V, Canet E. Different involvement of nitric oxide in endothelium-dependent relaxation of porcine pulmonary artery and vein: influence of hypoxia. J Cardiovasc Pharmacol. 1995;25(4):665-673.

35. Hasunuma K, Yamaguchi T, Rodman DM, et al. Effects of inhibitors of EDRF and EDHF on vasoreactivity of perfused rat lungs. Am J Phys. 1991;260(2 Pt 1):L97-104.
36. Sukumaran SV, Singh TU, Parida S, et al. TRPV4 channel activation leads to endothelium-dependent relaxation mediated by nitric oxide and endothelium-derived hyperpolarizing factor in rat pulmonary artery. Pharmacol Res. 2013;78:18-27.

37. Karamsetty MR, Nakashima JM, Ou L, et al. EDHF contributes to strain-related differences in pulmonary arterial relaxation in rats. Am J Phys Lung Cell Mol Phys. 2001;280(3):L458-L464.
38. Fuloria M, Smith TK, Aschner JL. Role of 5,6-epoxyeicosatrienoic acid in the regulation of newborn piglet pulmonary vascular tone. Am J Phys Lung Cell Mol Phys. 2002;283(2):L383-L389.
39. Zou W, Yang Q, Yim AP, et al. Impaired endothelium-derived hyperpolarizing factor-mediated relaxation in porcine pul-monary microarteries after cold storage with Euro-Collins and University of Wisconsin solutions. J Thorac Cardiovasc Surg. 2003;126(1):208-215.

40. Zhang RZ, Yang Q, Yim AP, et al. Role of NO and EDHF-mediated endothelial function in the porcine pulmonary circulation: comparison between pulmonary artery and vein. Vasc Pharmacol. 2006;44(3):183-191.

41. Migneault A, Sauvageau S, Villeneuve L, et al. Chronically elevated endothelin levels reduce pulmonary vascular reactivity to nitric oxide. Am J Respir Crit Care Med. 2005;171(5):506-513.

42. Michel RP, Langleben D, Dupuis J. The endothelin system in pulmonary hypertension. Can J Physiol Pharmacol. 2003;81(6): 542-554.
43. Sauvageau S, Thorin E, Caron A, et al. Endothelin-1-Induced Pulmonary Vasoreactivity Is Regulated by ET(A) and ET(B) Receptor Interactions. J Vasc Res. 2007;44(5):375-381.
44. Sauvageau S, Thorin E, Caron A, et al. Evaluation of endothelin-1-induced pulmonary vasoconstriction following myocardial infarction. Exp Biol Med (Maywood). 2006;231(6): 840-846.

45. Johnson W, Nohria A, Garrett L, et al. Contribution of endothelin to pulmonary vascular tone under normoxic and hypoxic conditions. Am J Physiol Heart Circ Physiol. 2002;283(2): H568-H575.

46. Kourembanas S, McQuillan LP, Leung GK, et al. Nitric oxide regulates the expression of vasoconstrictors and growth factors by vascular endothelium under both normoxia and hypoxia. J Clin Invest. 1993;92(1):99-104.
47. West JB, Mathieu-Costello O. Vulnerability of pulmonary capillaries in heart disease. Circulation. 1995;92(3):622-631.
48. West JB, Tsukimoto K, Mathieu-Costello O, et al. Stress failure in pulmonary capillaries. J Appl Physiol (1985). 1991;70(4):1731-1742.
49. Goggel R, Uhlig S. The inositol trisphosphate pathway mediates platelet-activating-factor-induced pulmonary oedema. Eur Respir J. 2005;25(5):849-857.
50. Morty RE, Kuebler WM. TRPV4: an exciting new target to promote alveolocapillary barrier function. Am J Phys Lung Cell Mol Phys. 2014;307(11):L817-L821.
51. Hamanaka K, Jian MY, Weber DS, et al. TRPV4 initiates the acute calcium-dependent permeability increase during ventilator-induced lung injury in isolated mouse lungs. Am J Phys Lung Cell Mol Phys. 2007;293(4):L923-L932.
52. Alvarez DF, King JA, Weber D, et al. Transient receptor potential vanilloid 4-mediated disruption of the alveolar septal barrier: a novel mechanism of acute lung injury. Circ Res. 2006;99(9):988-995.

53. Hummler E, Planes C. Importance of ENaC-mediated sodium transport in alveolar fluid clearance using genetically-engineered mice. Cell Physiol Biochem. 2010;25(1): 63-70.

54. Guazzi M, Arena R, Guazzi MD. Evolving changes in lung interstitial fluid content after acute myocardial infarction: mechanisms and pathophysiological correlates. Am J Physiol Heart Circ Physiol. 2008;294(3):H1357-H1364.
55. Thorneloe KS, Cheung M, Bao W, et al. An orally active TRPV4 channel blocker prevents and resolves pulmonary edema induced by heart failure. Sci Transl Med. 2012;4(159):159ra148.
56. Jian MY, King JA, Al-Mehdi AB, et al. High vascular pressure-induced lung injury requires P450 epoxygenase-dependent activation of TRPV4. Am J Respir Cell Mol Biol. 2008;38(4):386-392.

57. Azzam ZS, Dumasius V, Saldias FJ, et al. Na,K-ATPase overexpression improves alveolar fluid clearance in a rat model of elevated left atrial pressure. Circulation. 2002;105(4): 497-501.

58. Azarbar S, Dupuis J. Lung capillary injury and repair in left heart disease: a new target for therapy? Clin Sci (Lond). 2014;127(2):65-76.

59. Dupuis J, Guazzi M. Pathophysiology and clinical relevance of pulmonary remodelling in pulmonary hypertension due to left heart diseases. Can J Cardiol. 2015;31(4):416-429.

60. Kapanci Y, Burgan S, Pietra GG, et al. Modulation of actin isoform expression in alveolar myofibroblasts (contractile interstitial cells) during pulmonary hypertension. Am J Pathol. 1990;136(4):881-889.

61. Jasmin JF, Calderone A, Leung TK, et al. Lung structural remodeling and pulmonary hypertension after myocardial infarction: complete reversal with irbesartan. Cardiovasc Res. 2003;58(3):621-631.

62. Kingsbury MP, Huang W, Donnelly JL, et al. Structural remodelling of lungs in chronic heart failure. Basic Res Cardiol. 2003;98(5):295-303.
63. Chen Y, Guo H, Xu D, et al. Left ventricular failure produces profound lung remodeling and pulmonary hypertension in mice: heart failure causes severe lung disease. Hypertension. 2012;59(6):1170-1178.

64. Townsley MI, Fu Z, Mathieu-Costello O, et al. Pulmonary microvascular permeability. Responses to high vascular pressure after induction of pacing-induced heart failure in dogs. Circ Res. 1995;77(2):317-325.
65. Townsley MI, Snell KS, Ivey CL, et al. Remodeling of lung interstitium but not resistance vessels in canine pacing-induced heart failure. J Appl Physiol. 1999;87(5):1823-1830.
66. Kerem A, Yin J, Kaestle SM, et al. Lung endothelial dysfunction in congestive heart failure: role of impaired Ca2 + signaling and cytoskeletal reorganization. Circ Res. 2010;106(6):1103-1116.

67. Ontkean M, Gay R, Greenberg B. Diminished endothelium-derived relaxing factor activity in an experimental model of chronic heart failure. Circ Res. 1991;69(4):1088-1096.

68. Staniloae C, Dupuis J, White M, et al. Reduced pulmonary clearance of endothelin in congestive heart failure: a marker of secondary pulmonary hypertension. J Card Fail. 2004;10(5): 427-432.

69. Lucas M, Jasmin JF, Dupuis J. Effect of ET(A) receptor antagonist on pulmonary hypertension and vascular reactivity in rats with congestive heart failure. Pulm Pharmacol Ther. 2001;14(4):307-314.
70. Dupuis J, Hoeper MM. Endothelin receptor antagonists in pulmonary arterial hypertension. Eur Respir J. 2008;31(2): 407-415.
71. McMurray JJ, Ray SG, Abdullah I, et al. Plasma endothelin in chronic heart failure. Circulation. 1992;85(4):1374-1379.
72. Wei CM, Lerman A, Rodeheffer RJ, et al. Endothelin in human congestive heart failure. Circulation. 1994;89(4):1580-1586.
73. Cody RJ, Haas GJ, Binkley PF, et al. Plasma endothelin correlates with the extent of pulmonary hypertension in patients with chronic congestive heart failure [published erratum appears in Circulation 1993 Mar;87(3):1064]. Circulation. 1992;85(2):504-509.

74. Pousset F, Isnard R, Lechat P, et al. Prognostic value of plasma endothelin-1 in patients with chronic heart failure. Eur Heart J. 1997;18(2):254-258.
75. Givertz MM, Colucci WS, LeJemtel TH, et al. Acute Endothelin A Receptor Blockade Causes Selective Pulmonary Vasodilation in Patients With Chronic Heart Failure. Circulation. 2000;101(25):2922-2927.

76. Baggia S, Perkins K, Greenberg B. Endothelium-dependent relaxation is not uniformly impaired in chronic heart failure. J Cardiovasc Pharmacol. 1997;29(3):389-396.
77. Mathew R, Wang J, Gewitz MH, et al. Congestive heart failure alters receptor-dependent cAMP-mediated relaxation of canine pulmonary arteries. Circulation. 1993;87(5):1722-1728.
78. Zhang CY, Ma ZS, Ma LL, et al. Effect of prostaglandin E1 inhalation on pulmonary hypertension following corrective surgery for congenital heart disease. Exp Clin Cardiol. 2013;18(1):13-16.
79. Szczeklik J, Dubiel JS, Mysik M, et al. Effects of prostaglandin E1 on pulmonary circulation in patients with pulmonary hypertension. Br Heart J. 1978;40(12):1397-1401.
80. Sablotzki A, Czeslick E, Schubert S, et al. Iloprost improves hemodynamics in patients with severe chronic cardiac failure and secondary pulmonary hypertension. Can J Anaesth. 2002;49(10):1076-1080.
81. Hache M, Denault A, Belisle S, et al. Inhaled epoprostenol (prostacyclin) and pulmonary hypertension before cardiac surgery. J Thorac Cardiovasc Surg. 2003;125(3):642-649.
82. Laflamme M, Perrault LP, Carrier M, et al. Preliminary experience with combined inhaled milrinone and prostacyclin in cardiac surgical patients with pulmonary hypertension. J Cardiothorac Vasc Anesth. 2015;29(1):38-45.
83. Delgado JF, Conde E, Sanchez V, et al. Pulmonary vascular remodeling in pulmonary hypertension due to chronic heart failure. Eur J Heart Fail. 2005;7(6):1011-1016.
84. Bressollette E, Dupuis J, Bonan R, et al. Intravascular ultra-sound assessment of pulmonary vascular disease in patients with pulmonary hypertension. Chest. 2001;120(3):809-815.
85. Driss AB, Devaux C, Henrion D, et al. Hemodynamic stresses induce endothelial dysfunction and remodeling of pulmonary artery in experimental compensated heart failure. Circulation. 2000;101(23):2764-2770.
86. Farrero M, Blanco I, Batlle M, et al. Pulmonary hypertension is related to peripheral endothelial dysfunction in heart failure with preserved ejection fraction. Circ Heart Fail. 2014;7(5):791-798.

87. Berridge MJ. Elementary and global aspects of calcium signalling. J Exp Biol. 1997;200(Pt 2):315-319.
88. Firth AL, Remillard CV, Platoshyn O, et al. Functional ion channels in human pulmonary artery smooth muscle cells: Voltage-dependent cation channels. Pulm Circ. 2011;1(1):48-71.
89. Jeffery TK, Morrell NW. Molecular and cellular basis of pulmonary vascular remodeling in pulmonary hypertension. Prog Cardiovasc Dis. 2002;45(3):173-202.
90. Yin J, Hoffmann J, Kaestle SM, et al. Negative-feedback loop attenuates hydrostatic lung edema via a cGMP-dependent regulation of transient receptor potential vanilloid 4. Circ Res. 2008;102(8):966-974.

91. Ying X, Minamiya Y, Fu C, et al. Ca2 + waves in lung capillary endothelium. Circ Res. 1996;79(4):898-908.
92. Kuebler WM, Ying X, Bhattacharya J. Pressure-induced endothelial Ca(2 +) oscillations in lung capillaries. Am J Phys Lung Cell Mol Phys. 2002;282(5):L917-L923.
93. Dayeh N, Safar S, Gillis M-A, et al. TRPV4-associated alterations of Ca2 + pulsars in a murine model of pulmonary hypertension secondary to heart failure (1090.11). FASEB J. 2014;28(1 Supplement).

94. Dupuis J, Prefontaine A, Villeneuve L, et al. Bone marrow-derived progenitor cells contribute to lung remodelling after myocardial infarction. Cardiovasc Pathol. 2007;16(6):321-328.

95. Powell DW, Mifflin RC, Valentich JD, et al. Myofibroblasts. I. Paracrine cells important in health and disease. Am J Phys. 1999;277(1 Pt 1):C1-C9.
96. Lefebvre F, Prefontaine A, Calderone A, et al. Modification of the pulmonary renin-angiotensin system and lung structur-al remodelling in congestive heart failure. Clin Sci (Lond). 2006;111(3):217-224.
97. Chabot A, Meus MA, Naud P, et al. Nestin is a marker of lung remodeling secondary to myocardial infarction and type I diabetes in the rat. J Cell Physiol. 2015;230(1):170-179.
98. Chabot A, Hertig V, Boscher E, et al. Endothelial and Epithelial Cell Transition to a Mesenchymal Phenotype Was Delineated by Nestin Expression. J Cell Physiol. 2015;231: 1407-1627. [Pages i–i].

99. Guazzi M, Vicenzi M, Arena R, et al. Pulmonary hypertension in heart failure with preserved ejection fraction: a target of phosphodiesterase-5 inhibition in a 1-year study. Circulation. 2011;124(2):164-174.

100. Guazzi M, Samaja M, Arena R, et al. Long-term use of sildenafil in the therapeutic management of heart failure. J Am Coll Cardiol. 2007;50(22):2136-2144.

101. Jiang BH, Tardif JC, Sauvageau S, et al. Beneficial effects of atorvastatin on lung structural remodeling and function in ischemic heart failure. J Card Fail. 2010;16(8):679-688.

102. Jiang BH, Tardif JC, Shi Y, et al. Bosentan does not improve pulmonary hypertension and lung remodeling in heart failure. Eur Respir J. 2011;37(3):578-586.

II. Chapter II Hypothesis and objectives of this thesis

The endothelium plays a major role in the local control of vascular tone. It has become clear that biomechanical and biochemical stimuli generated by blood flow regulate endothelial cells' function and the release of growth factors and vasoactive mediators. A right balance within endothelial vasoactive mediators is indispensable for the maintenance of a normal low pulmonary vascular tone [281]. Dysregulation of pulmonary vascular tone involves repercussions on all vascular layers. In PH, alterations in vasodilator substances induce abnormal proliferation, migration and hypertrophy of PVSMCs, as well as matrix protein deposition, resulting in vasoconstriction and remodelling of PAs. Increased PVR is due to a maintained vasoconstriction and remodelling of PAs. These various cell phenomena are associated with a dysregulation in endothelial Ca^{2+}. Therefore, the regulatory mechanisms of endothelial intracellular Ca^{2+} levels have a significant impact on vascular tone. Nevertheless, the role of Ca^{2+} homeostasis in PH remains to be elucidated.

Endothelial Ca^{2+} exerts its effects on SMCs through a highly dynamic process that requires fine-tuning, as well as a cross talk between ECs and SMCs. Bidirectional communication between both cell types is conferred by the presence of MEPs and a number of proteins [282]. This communication is controlled by a variety of feedback loops and pathways that regulate Ca^{2+} dynamics and vasoreactivity. These pathways are often disrupted in several cardiovascular diseases associated with altered vascular reactivity.

In this thesis, we shed light on the impact of local Ca^{2+} signalling in ECs. More specifically, we validated the importance of newly identified pulsar signalling within various vascular beds and explored the role of Ca^{2+} pulsars in PAs. Up until presently, the regulatory mechanisms of Ca^{2+} pulsars remained to be uncovered. The spatio-temporal characteristics of Ca^{2+} pulsars suggested that they could play a role in the control of pulmonary vascular tone, potentially involving more transmembrane ion channels, as well as regulatory proteins.

LHD is the most common cause of PH in humans. Since the development of PH in HF is initiated by a passive increase in pulmonary vascular pressure and further aggravated by an increased pulmonary vascular tone most likely attributed to endothelial

dysfunction [281], it is imperative to understand and unravel Ca^{2+} dyshomeostasis and related dysregulation underlying PH progression. An improved understanding of the changes in the pulmonary vasculature that contribute to PH-LHD is needed to reduce HF morbidity and mortality.

The goal of this thesis work was to elucidate the mechanistic modifications in pulmonary endothelial Ca^{2+} homeostasis involved in PH-LHD.

Thesis hypotheses

- The HFrEF mouse model induced by MI is a representative model for the study of group II-PH.
- Spontaneous endothelial Ca^{2+} pulsars occur in healthy non-stimulated pulmonary arteries.
- Ca^{2+} pulsars are preserved units amongst different vascular beds.
- TRPV4 channels play a role in the control of Ca^{2+} pulsars.
- Localized pulmonary endothelial Ca^{2+} signalling is altered in group II-PH.
- TRPV4 channels are responsible for altered pulsar activity in PH-HFrEF.

Objectives of this thesis

- To characterize the MI mouse model as the first animal model for the study of PH-LHD.
- To characterize spontaneous endothelial dynamics of Ca^{2+} in healthy pulmonary arteries.
- To accentuate the importance of Ca^{2+} pulsars by highlighting their presence and role in different vascular beds.
- To elucidate the role of TRPV4 channels in the control of Ca^{2+} pulsars.
- To evaluate the impact of PH-LHD on pulmonary localized endothelial Ca^{2+} signalling.
- To determine TRPV4-related alterations of Ca^{2+} pulsars in PH-LHD.

III. Chapter III: RESULTS

This thesis work sets a new foundation for the study of pulmonary vascular impairment in LHD, and focuses on endothelial function disruption, and the contribution of Ca^{2+} pulsars.

In order to fully understand endothelial mechanisms underlying the progression of PH-LHD to its non-reversible state, we sought to obtain a fully functional and highly representative animal model. Therefore, the first article presented in this section demonstrated the development of a murine model for the study of PH associated with HFrEF.

Since Ca^{2+} pulsars have been associated with cellular hyperpolarization and consequent vascular relaxation in mesenteric arteries, the study of these dynamics in other vascular beds, notably the pulmonary one was of high interest. Localized endothelial Ca^{2+} signalling was elucidated in the second article presented in this thesis. This study highlighted the regulatory importance of Ca^{2+} pulsars and legitimized pulsars as strongly conserved units within different vessel types.

The flow-driven nature of the pulmonary circulation makes it highly susceptible to the influence of endothelial dysfunction. Setting of specific criteria with threshold values for the determination of the presence of PH in HFrEF, along with the revelation of pulmonary pulsars aided us in our last study of endothelial dysfunction's part in vascular impairment observed in PH-LHD. The third article presented in this section investigated Ca^{2+} pulsars within the pulmonary endothelium and their contribution to the progression of this disease, and associated a new role for mechanosensitive TRPV4 channels in the alterations of endothelial Ca^{2+} dynamics underlying impaired vascular reactivity in group II-PH.

Echocardiographic validation of pulmonary hypertension due to heart failure with reduced ejection fraction in mice

Dayeh R. Nour[1,2], Tardif Jean-Claude[1,2], Shi Yanfen[1], Tanguay Mégane[2], §Ledoux Jonathan[1,2,3], §*Dupuis Jocelyn[1,2].

SCIENTIFIC REPORTS | (2018) 8:1363 | DOI:10.1038/s41598-018-19625-2

This article was accepted on January 5th 2018 and published on January 22nd 2018

Affiliations:
Research Center, Montreal Heart Institute, Quebec, Canada
[2] Departments of Medicine, [3] Pharmacology and Physiology, Université de Montréal, Quebec, Canada

§ Drs Ledoux and Dupuis share senior authorship.

*Corresponding author

Authors contributions:

Study design: ND, JD, JL

Experimentation: ND

Echocardiography performance and analysis: YS, JCT

Data collection and analysis: ND, MT, JL, JD

Manuscript redaction: ND, JD, JL

Critical review of manuscript: JCT, YS

Competing financial interests
The author(s) declare no competing financial interests.

SCIENTIFIC REPORTS

OPEN

Echocardiographic validation of pulmonary hypertension due to heart failure with reduced ejection fraction in mice

Received: 27 July 2017
Accepted: 5 January 2018
Published online: 22 January 2018

Nour R. Dayeh[1,2], Jean-Claude Tardif[1,2], Yanfen Shi[1], Mégane Tanguay[1], Jonathan Ledoux[1,2,3] & Jocelyn Dupuis[1,2]

Pulmonary hypertension (PH) associated with left heart diseases is the most prevalent cause of PH. The scarcity of studies exploring the pathophysiology and therapies of group II PH resides in the lack of validated small animal models with non-invasive determination of the presence and severity of PH. Heart failure (HF) was induced in mice by coronary artery ligation. Mice developed PH as evidenced by an elevated right ventricular (RV) systolic pressure and RV hypertrophy. Detailed non-invasive echocardiographic analysis on the left and right ventricles showed impaired left ventricular (LV) systolic and diastolic function. In addition, RV hypertrophy was confirmed by echo and accompanied by impaired function as well as increased pulmonary resistance. Correlation analysis validated the use of the LV wall-motion score index (WMSI) at a threshold value of ≥2.0 as a powerful and reliable indicator for the presence of PH and RV dysfunction. Echocardiography is an accurate non-invasive technique to diagnose PH in a HF mouse model. Moreover, an echocardiographic parameter of infarct size and LV function, the LV WMSI, reliably correlates with the presence of PH, RV hypertrophy and RV dysfunction and could be used to improve efficiency and design of pre-clinical studies.

The prognosis for left heart diseases in patients with preserved or reduced ejection fractions with associated pulmonary hypertension (PH) is very poor[1]. Additionally, PH associated with left heart diseases (LHD), classified as Group II PH, is the most prevalent form of PH[1], thus confirming the need for adequate therapeutic options. Group II PH is defined as a mean pulmonary arterial pressure ≥25 mmHg at rest associated with a pulmonary capillary wedge pressure >15 mmHg[2]. While potential therapeutic options have been suggested by clinical studies testing treatments for group I PH (PAH)[3–8], there is currently no approved treatment for group II PH. However, the pathophysiology of Group II PH is distinct from group I PH and few studies focused on group II PH using animal models[9–11]. The limited pre-clinical literature on Group II PH is in part due to the technical burden of the assessment of hemodynamic alterations.

Myocardial infarction is the most frequent cause of heart failure with reduced ejection fraction (HFrEF). The coronary artery ligation model is commonly used in animals to develop HFrEF with usual emphasis on the study of LV function. Few studies have however used that model to study group II PH. The development of PH in this model is essentially dependent on the severity of LV dysfunction that in turn will vary with infarct size, resulting in no or variable severity of PH. There has been no validation of proper diagnostic tools that can be utilized to non-invasively determine or predict the presence and severity of PH in those animals. Investigators usually use invasive hemodynamic evaluation with right heart catheterization to determine the presence of PH[9–11]. However, considering chamber size, right ventricular catheterization is a technically challenging invasive and usually terminal method. Alternatively, echocardiography is an attractive non-invasive method in the detection of pulmonary arterial hypertension (PAH) and right ventricular hypertrophy[12]. In humans, echocardiographic variables clinically used for the diagnosis of left heart failure, pulmonary hypertension and right heart function are well defined[13]. Surprisingly, corresponding characterization has yet to be performed in the mouse model of

[1]Research Center, Montreal Heart Institute, Quebec, Canada. [2]Department of Medicine, Université de Montréal, Quebec, Canada. [3]Department of Pharmacology and Physiology, Université de Montréal, Quebec, Canada. Jonathan Ledoux and Jocelyn Dupuis jointly supervised this work. Correspondence and requests for materials should be addressed to J.D. (email: dupuisj@me.com)

Abstract:

Pulmonary hypertension (PH) associated with left heart diseases is the most prevalent cause of PH. The scarcity of studies exploring the pathophysiology and therapies of group II PH resides in the lack of validated small animal models with non-invasive determination of the presence and severity of PH.

Heart failure (HF) was induced in mice by coronary artery ligation. Mice developed PH as evidenced by an elevated right ventricular (RV) systolic pressure and RV hypertrophy. Detailed non-invasive echocardiographic analysis on the left and right ventricles showed impaired left ventricular (LV) systolic and diastolic function. In addition, RV hypertrophy was confirmed by echo and accompanied by impaired function as well as increased pulmonary resistance. Correlation analysis validated the use of the LV wall-motion score index (WMSI) at a threshold value of ≥ 2.0 as a powerful and reliable indicator for the presence of PH and RV dysfunction.

Echocardiography is an accurate non-invasive technique to diagnose PH in a HF mouse model. Moreover, an echocardiographic parameter of infarct size and LV function, the LV WMSI, reliably correlates with the presence of PH, RV hypertrophy and RV dysfunction and could be used to improve efficiency and design of pre-clinical studies.

Introduction

The prognosis for left heart diseases in patients with preserved or reduced ejection fractions with associated pulmonary hypertension (PH) is very poor[1]. Additionally, PH associated with left heart diseases (LHD), classified as Group II PH, is the most prevalent form of PH[1], thus confirming the need for adequate therapeutic options. Group II PH is defined as a mean pulmonary arterial pressure ≥ 25 mmHg at rest associated with a pulmonary capillary wedge pressure > 15 mmHg[2]. While potential therapeutic options have been suggested by clinical studies testing treatments for group I PH (PAH)[3-8], there is currently no approved treatment for group II PH. However, the pathophysiology of Group II PH is distinct from group I PH and few studies focused on group II PH using animal models[9-22]. The limited pre-clinical literature on Group II PH is in part due to the technical burden of the assessment of hemodynamic alterations.

Myocardial infarction is the most frequent cause of heart failure with reduced ejection fraction (HFrEF). The coronary artery ligation model is commonly used in animals to develop HFrEF with usual emphasis on the study of LV function. Few studies have however used that model to study group II PH. The development of PH in this model is essentially dependant on the severity of LV dysfunction that in turn will vary with infarct size, resulting in no or variable severity of PH. There has been no validation of proper diagnostic tools that can be utilized to non-invasively determine or predict the presence and severity of PH in those animals. Investigators usually use invasive hemodynamic evaluation with right heart catheterization to determine the presence of PH[9-11]. However, considering chamber size, right ventricular catheterization is a technically challenging invasive and usually terminal method. Alternatively, echocardiography is an attractive non-invasive method in the detection of pulmonary arterial

hypertension (PAH) and right ventricular hypertrophy[23]. In humans, echocardiographic variables clinically used for the diagnosis of left heart failure, pulmonary hypertension and right heart function are well defined[24]. Surprisingly, corresponding characterization has yet to be performed in the mouse model of HFrEF induced by myocardial infarction despite the substantial advantages of echocardiography such as being non-invasive, allowing potential repetitive measurements to monitor progression of PH and identification of predictive PH severity in early stages of the disease.

The purpose of this study is to validate, through the use of echocardiography, the murine myocardial infarction HFrEF model for the study of WHO group II PH. In addition, we aimed to determine the possibility to use echocardiographic measurement of infarct size by the LV wall motion score index (WMSI) as a predictive parameter of the development of PH in this pre-clinical model.

Methods

The study was performed according to procedures approved by the ethics committee for animal research of the Montreal Heart Institute in accordance with the Canadian guidelines for the care of laboratory animals.

Surgical procedures:

A total of 67 mice aged 2 to 3 months (male and female, C57BL6 background, body weight 19-25 g) were used. Under anaesthesia, animals of the PH group (n=48) underwent thoracotomy followed by ligation of the left anterior descending coronary artery causing myocardial infarction (MI) as carried out previously in rats[9,15]. A post-MI survival rate of 50% due to early mortality

within the first week was noted (Supplemental Figure 1) and is consistent with other rodent models[25,26]. Animals of the sham group (n=19) underwent lateral thoracotomy without ligation of the coronary artery without any premature death.

Hemodynamic measurements and respiratory function tests:

Pulmonary and hemodynamic parameters were evaluated 4 weeks after surgery. Mice were anesthetized with xylazine (10 mg/kg) and ketamine (50 mg/kg). The trachea was isolated and connected to a ventilator (Flexivent, SCIREQ, Canada) to assess respiratory function. Measurement of hemodynamic parameters was performed using high-fidelity catheters (1.4 F) to measure intraventricular pressure (Millar Instruments, USA). Briefly, the catheter is inserted in the right carotid artery and advanced into the left ventricle (LV), or inserted in the right jugular vein and advanced into the right ventricle (RV) to monitor LV and RV hemodynamic parameters, respectively. Measurements were made on a polygraph (Powerlab, AD Instruments, USA).

Morphometric measurements of the heart and lungs:

Following pulmonary and hemodynamic evaluation, lungs and hearts were harvested and dissected. Right ventricular hypertrophy was assessed by the Fulton index (RV / (LV + septum) weight). Scars were dissected from the LV and weighed. Scar surface measurements were conducted by planimetry. To determine pulmonary structural remodelling, the wet lung (WL) weight and dry lung (DL) weight were measured and ratios WL / body weight (BW), and DL / BW were calculated. The left lung was perfused and fixed with optimal cutting temperature compound (OCT) and one lobe was removed and placed in cassettes left in formalin. Paraffin

embedded histological slides from lung tissue of MI and Sham mice were stained with Masson's trichrome and collagen deposition in the lungs was evaluated by histologic quantification.

Echocardiographic measurements:

All animals had complete echocardiographic data. Transthoracic echocardiography was performed prior to terminal assessment of cardiac and pulmonary functions using an i13L probe (10-14 MHz) and Vivid 7 Dimension ultrasound system (GE Healthcare, Norway), with mice being lightly sedated by 1.5-2% isofluorane. An average of 3 consecutive cardiac cycles was used for each measurement.

Two-dimensional echocardiography was used to visualize left ventricular (LV) wall segment's motion. 10 segments in short axis views (6 at level of papillary muscle and 4 at apex) were visualized for wall motion scoring. They were readably recorded in all mice scanned. For each myocardial segment, LV wall motion was scored as normal (1), hypokinesis (2), akinesis (3), dyskinesis (4), or aneurysmal (5). The LV Wall motion score index (WMSI) was calculated as sum of all scores / number of segments analysed. Thickness of LV anterior and posterior walls at end cardiac diastole (LVAWd, LVPWd), LV dimensions at end cardiac diastole and systole (LVDd, LVDs) were measured by M-mode echocardiography (M-mode). LV fractional shortening (FS), LV volumes at end cardiac diastole and systole (LVVd, LVVs) were determined and the LV ejection fraction computed from the Vivid 7 system software: FS = (LVDd-LVDs) / LVDd X 100%, EF = (LVVd-LVVs) / LVVd X 100%. LV mass was calculated using a formula recommended by Liao Y et al.[27] Time interval from mitral valve closure to opening (MVCO) was measured in trans-mitral flow by pulsed wave Doppler (PW). LV ejection time (LVET) was measured from the beginning to the ending of flow in LV outflow tract (LVOT) obtained also by

PW. LVOT flow was traced to obtain cardiac output (CO). LV global myocardial performance index (MPI global) was calculated as (MVCO-LVET)/LVET X 100%.

Right ventricular (RV) anterior wall thickness (RVAWd) and RV dimensions at end-diastole (RVDd) were measured by M-mode echocardiogram in parasternal long axis view at the level of aortic valve. Tricuspid annulus plane systolic excursion (TAPSE) was measured by M-mode. Pulmonary artery acceleration time (PAAT), and ejection time (PAET) were measured from pulmonary artery flow obtained by PW. Tricuspid annulus moving velocity in systole (S_R) was measured by tissue Doppler imaging.

The datasets generated during and/or analysed during the current study are available from the corresponding author on reasonable request.

Statistical analysis

Statistical analysis was performed using GraphPad Prism 7 software. Experimental groups were analyzed by ANOVA followed, when a significant group interaction was found, by multiple comparisons with Tukey's posthoc analysis. Values are presented as mean ± SE. WMSI correlations with hemodynamic and echocardiographic variables was obtained by linear regression analysis. Significant values were considered at $p < 0.05$.

Results

WMSI as a marker of LV dysfunction

From a hemodynamic standpoint, ischemia-induced LV dysfunction is characterized by an increased LV end-diastolic pressure (LVEDP) as well as impaired rates of ventricular contraction (+dP/dt) and relaxation (-dP/dt), leading to a reduced ejection fraction. Alteration of mouse LV function following coronary ligation was thus assessed by hemodynamic monitoring through intraventricular catheterization and echocardiography measurements. The hemodynamic parameters were analyzed with respect to WMSI values determined by echocardiography. LVEDP ($R^2 = 0.3234$; $p = 0.0270$) and LV ejection fraction ($R^2 = 0.6771$; $p < 0.0001$) correlated with WMSI (Figure 1A & B). Accordingly, WMSI values were found to correlate strongly with LV contractile ($R^2 = 0.5515$; $p = 0.0036$) and relaxation rates ($R^2 = 0.7212$; $p = 0.0002$) (Figure 1C & D).

WMSI and LV infarct sizes

Highest probability of developing PH was obtained in this investigation by focusing on mice with medium to large sized infarcts. Upon coronary ligation, myocardial scar surfaces ranged from 0 mm^2 (no scar) to 55 mm^2 as measured by pathologic planimetry. Furthermore, scar dimension and the associated dysfunctional LV were also sought non-invasively by correlation with WMSI.

Mice were sorted based on scar surface area and compared to WMSI values. WMSI and scar surface values correlated positively ($R^2 = 0.5204$; $p = 0.0011$) (Figure 2A). All mice with medium to large infarcts had WMSI values superior or equal to 2 (Figure 2B). Consequently, a WMSI threshold value of 2 was set for post-surgery identification of mice with significant infarct

surfaces and LV dysfunction and therefore at greater likelihood of developing PH and RV dysfunction.

Echocardiographic assessment of LV dysfunction and RV hypertrophy in mice with WMSI ≥ 2.0

In mice with WMSI values ≥ 2.0, in depth echocardiographic analysis revealed LV dysfunction (Figure 3). An increase in LV size was noted concomitantly with impaired LV systolic function and LV myocardial performance (MPI $_{Global}$). In addition, echocardiography revealed RV hypertrophy (end-diastolic anterior wall thickness ($RVAW_d$)) and dilation (end-diastolic dimension (RVD_d)) coinciding with impaired RV systolic function (tricuspid annulus plane systolic excursion (TAPSE)). Pulmonary hypertension was also evidenced by indicators of increased RV afterload with lower values of pulmonary artery acceleration time (PAAT), pulmonary artery ejection time (PAET), and PAAT/PAET (Table 1). Non-simultaneous measurements of PAAT at echo and of RVSP by hemodynamics were available for 15 animals and did not show correlation (R^2=0.11, p=0.23), emphasizing the technical limitations of hemodynamic measurements in small animals. Details of the wall motion abnormalities form all of the myocardial segments analyzed (10 per animal) is presented in supplemental table 1.

Hemodynamic and morphometric assessment of LV dysfunction and RV hypertrophy and pulmonary hypertension in mice with WMSI ≥ 2.0

As expected, a lower left ventricular systolic pressure (LVSP) was measured in mice following coronary ligation, as well as an increased left ventricular end diastolic pressure (LVEDP). LV

inotropy (+dP/dt) and lusitropy (-dP/dt) were reduced in MI mice with a WMSI ≥ 2.0. In contrast to their sham counterparts, development of PH was evidenced by an elevated right ventricular systolic pressure (RVSP) concomitantly with RV hypertrophy (RV weight/ (LV + septum) weight) (Table 2).

Mice respiratory function post-MI

Following hemodynamic recordings, respiratory function was assessed to evaluate the impact of MI on pulmonary capacity (Figure 4). Figure 4A and B illustrate the MI-induced pulmonary alveolar and vascular remodelling evidenced by collagen deposition, as well as cellular proliferation as seen previously in other animal models of myocardial infarction. According to previous work that had been done on a rat model of myocardial infarction, proliferating cells are composed principally of myofibroblasts[9,28]. Interestingly, and similar to the rat MI model, mice with MI and moderate to large infarcts did not display pulmonary oedema (Figure 4Ac). However, MI mice clearly developed a restrictive respiratory syndrome characterized by a decrease in lung compliance (Figure 4C) evidenced by a shift in the pressure-volume relationship compared to the sham group (Figure 5).

Correlation between WMSI and PH markers in mice with WMSI ≥ 2.0.

RV hypertrophy measured by the Fulton index correlated ($R^2 = 0.3156$; $p = 0.0293$) with WMSI (Figure 6A). Furthermore, TAPSE was inversely correlated with WMSI ($R^2 = 0.3067$; $p = 0.0171$) (Figure 6B). In addition, pulmonary arterial blood velocity and TAPSE values were significantly decreased in mice with large or medium infarcts when compared to sham animals

(Figure 6C and 6D). Moreover, ROC curves (Supplemental Figure 2) were constructed to determine the precision of WMSI to predict left ventricular dysfunction (LVEDP >10 mmHg) and right ventricular dysfunction (TAPSE < 1.0 mm) using mean values from the sham groups as cut-offs. The precision to predict both RV and LV dysfunction was good with areas under the ROC curves greater than 0.7 for both LVEDP and TAPSE. Accordingly, a WMSI of ≥2.0 predicts LV dysfunction with a sensitivity of 57%, a specificity of 86% and a likelihood ratio of 4.0. RV dysfunction is predicted with a sensitivity of 53%, a sensitivity of 83% and a likelihood ratio of 3.2.

Discussion

In this study, we demonstrated that mice with large surgically-induced MI develop pulmonary hypertension with lung remodeling and right ventricular dysfunction. We validated the use of echocardiography as non-invasive method of evaluating the severity of both LV and RV function in this small rodent model. More importantly, we validated the use of the WMSI as a reliable marker of infarct size that can be used to predict the development of PH and RV dysfunction.

There is a growing clinical necessity for specific therapies targeting PH associated with LHD (group II PH). The core of pre-clinical investigations resides in the use of a validated animal model for group II-PH that replicates human pathophysiology progression and phenotype. With the development of PH-selective therapies, evaluation of these drugs in properly phenotyped pre-clinical models of group II PH is warranted[29,30]. Myocardial infarct following coronary ligation is unequivocally the most clinically relevant model for group II-PH[11,14,15,31],

but assessment of actual PH and thus right ventricular dysfunction development essentially relies on hemodynamic measures using intraventricular catheters. However, in small rodents like mice, this approach is technically challenging due to the narrow right ventricle, even with expert hands and the smallest high-fidelity catheter available. Moreover, manipulations of weakened animals to introduce the catheter often result in blood loss and although less frequent, lethal hemorrhage. In the absence of RV function monitoring and the capacity to determine PH severity, planification of studies using these tissues becomes difficult. Furthermore, evaluation of novel therapies is impossible in the absence of adequate methods of assessing animals prior to therapeutic allocation. MI-induced PH is usually studied 4-5 weeks following surgery to allow development of PH, without tangible indications of the severity of MI and/or forthcoming PH until terminal hemodynamic assessment of cardiac function. Monitoring of disease progression to study potential treatments or therapeutic approaches is therefore needed.

These technical limitations and a substantial early post-surgical mortality rate are the main reasons the rare use of this model in mice despite growing needs for a better understanding of the mechanisms involved in the progression of the disease. The use of transgenic mice models for group II-PH investigation is desirable to accelerate knowledge acquisition. This study presents and validates in mice an approach commonly used in humans and larger animals to assess cardiac function and establish pulmonary hypertension. The lung histopathological changes found in mice are similar to those previously described in other models of chronic heart failure and in humans[28,32] and are characterized by an increase in dry lung weight with no significant pulmonary edema. Detailed histologic evaluations in rats and in man revealed that alveolar septa myofibroblasts proliferation is greatly responsible for the increased cellularity with collagen and interstitial matrix deposition[11,33,34]. Echocardiography has been previously

used in murine models of cardiomyopathy but not to validate PH in a mouse model of heart failure with reduced ejection fraction[35],[36-39]. Echocardiography is advantageous over cardiac catheterization, even in small animals like mice. This non-invasive technique is reproducible and can be repeated to monitor disease progression. Furthermore, we show that the WMSI is a reliable marker for infarct size and PH in mice. Correlation analysis of WMSI and LV dysfunction indicated a threshold WMSI of 2 for medium and large infarcts. Mice with WMSI $\geq$ 2.0 developed PH, RV dysfunction and lung remodelling with a restrictive respiratory physiology. Moreover, WMSI is shown to have good precision to predict both LV and RV dysfunction as assessed by LVEDP and TAPSE. Interestingly, WMSI correlates with infarct size and does not vary over time as shown previously[40]. Therefore, assessment of WMSI can be performed as early as 48 hr following coronary ligation and conservative prediction of the forthcoming PH severity can be made. This is a very important asset for early echocardiographic determination of PH. Since infarct size can be quite variable depending on surgical expertise, it allows to promptly discard animals with small or no infarcts that would not develop LV dysfunction and PH. More importantly, it would allow adequate randomization of animals to test and monitor impact of novel therapeutic approaches on PH evolution.

Animal groups were defined based on MI scar surface as an indicator of infarct severity. A close correlation was found between scar size and WMSI, where a WMSI of 2.0 and higher was associated with medium (20-30 mm^2) and large (>30 mm^2) infarcts. LV dysfunction was therefore associated with a threshold WMSI value of 2.0, revealing a minimal scar surface of 20 mm^2. Additionally, WMSI correlates with altered EF and LVEDP as well as LV inotropy and lusitropy. Although LV dysfunction is usually determined with classical intraventricular catheters, WMSI can be considered as a stand-alone reliable marker for LV dysfunction.

PH was determined by alteration of pulmonary artery blood flow, RV dysfunction and hypertrophy. Fulton's index and TAPSE values, respectively indicators of RV hypertrophy and function correlate with WMSI herein establishing the latter as a predictive marker of hypertrophied and dysfunctional RV and the consequent PH. RV function decline was also noted through PAAT and TAPSE in mice with medium to large infarcts. Since the WMSI is a measure of infarct size, its correlation with numerous severity parameters of both LV and RV function, many of them known to be co-linear isn't surprising. Other factors besides WMSI, such as the presence and severity of mitral regurgitation, will impact on the lung circulation and the development of PH. Nevertheless, a WMSI value of 2.0 and above appears as a reliable indicator and predictive marker for RV dysfunction, hypertrophy as well as the ensuing development of PH. The contrary however needs to be interpreted with caution and a WMSI < 2.0 was not associated with the absence of PH. Indeed, and despite the small sample size, some animals with WMSI < 2.0 had abnormal echocardiographic parameters suggestive of significant PH such as lower PAAT and higher RVAWd, and higher RVSP at cardiac catheterization.

The WSMI is a recognized measure of LV function. As expected, we found a strong inverse correlation between the WMSI and LVEF ($r = -0.822$, $p < 0.0001$). Previous human studies have validated the use of the WMSI after MI to predict adverse outcomes. In 144 patients after MI, a predischarge resting WMSI ≥ 1.50 was superior to LVEF $\leq 40\%$ to identify patients at risk of cardiac death, unstable angina, nonfatal reinfarction, and HF[41]. In 767 MI patients, WMSI was also an independent predictor of death and HF hospitalization, whereas LVEF was not[42]. Reasons for this discrepancy is unclear but could be explained by compensatory hyperkinesia of normal myocardial segments in the acute phase leading to LVEF overestimation. Furthermore, a comparative study of WMSI determined by cardiac ultrasound and LVEF

measured by the Simson's rule, to LVEF measured by magnetic resonance imaging in 111 patients found that Simpson's rule overestimated LVEF compared to CMR leading the authors to conclude that the WMSI was a simple, accurate and reliable alternative to the measurement of left ventricular function[43]. We choose the WMSI as a parameter of infarct size for its ease of measurement, its absence of variability in controls (value of 1) and its stability over time. Athought we did not petform a comparative analysis, the very good correlation of WMSI with LVEF however suggests that LVEF could also be used to predict future development of PH and RVH.

In summary investigations and pathophysiological understanding of group II-PH have been hindered by the lack of a validated pre-clinical murine model and protocol. We show that MI from coronary artery ligation is a robust and now validated mouse model of WHO group II PH, reproducing the most frequent aetiology of human PH, i.e. HFrEF consecutive to myocardial infarction [28]. Moreover, an indicator of infarct size through echocardiography, the WMSI is an accurate predictive marker of PH and ventricular dysfunction. Echocardiography in mice thus appears as a preferential method for the diagnosis and monitoring of group II PH over standard intraventricular catheterization.

Acknowledgement

The authors are grateful to Marc-Antoine Gillis and Emma Dedelis for their expert technical assistance.

This study was supported by the Fondation de l'Institut de Cardiologie de Montréal (JL), the Heart and Stroke Foundation of Canada (JL) and Fonds de Recherche du Québec – Santé (JL).

Parameters	Sham n = 19	MI (WMSI < 2) n = 7	p value WMSI < 2 vs sham	MI (WMSI ≥ 2) n = 18	p value (WMSI ≥ 2 vs sham)	p value WMSI < 2 vs WMSI ≥ 2
Left ventricular dimensions						
Anterior wall thickness at end diastole (LVAWd, mm)	0.72 ± 0.01	0.56 ± 0.05	n.s.	0.44 ± 0.06	<0.0001	n.s.
Posterior wall thickness at end diastole (LVPWd, mm)	0.7 ± 0.01	0.75 ± 0.01	n.s.	0.8 ± 0.03	<0.001	n.s.
Dimension at end diastole (LVDd, mm)	3.8 ± 0.06	4.5 ± 0.18	<0.05	5.2 ± 0.16	<0.0001	<0.05
Dimension at end systole (LVDs, mm)	2.35 ± 0.07	3.47 ± 0.18	<0.01	4.57 ± 0.2	<0.0001	<0.01
Volume at end diastole (LVVd, ml)	0.14 ± 0.006	0.23 ± 0.03	n.s.	0.36 ± 0.03	<0.0001	<0.05
Volume at end systole (LVVs, ml)	0.04 ± 0.003	0.11 ± 0.02	n.s.	0.26 ± 0.03	<0.0001	<0.01
Left ventricular function						
Wall motion score index (WMSI)	*1*	*1,55 ± 0.08*	<0.0001	*2.33 ± 0.08*	<0.0001	<0.0001
Ejection fraction (%)	74 ± 2	53 ± 3	<0.0001	31 ± 3	<0.0001	<0.0001
Cardiac output (ml/min)	12.4 ± 0.4	11.3 ± 0.7	n.s.	8.7 ± 0.6	<0.0001	<0.05
Fractional shortening (%)	38 ± 1	23 ± 2	<0.0001	13 ± 1	<0.0001	<0.01
Myocardial performance index (MPI, %)	47.52 ± 2.6	59.55 ± 7.8	n.s.	93.76 ± 5.3	<0.0001	<0.001
Left Atrial dimensions and function						
Left Atrial dimensions (mm)	2.32 ± 0.24	2.41 ± 0.25	n.s.	3.02 ± 0.4	<0.0001	<0.001
E/e'	35.2 ± 6.79	36.9 ± 5.1	n.s.	75.6 ± 1.65	<0.0001	<0.0001
Right ventricular dimensions and function						
Anterior wall thickness at end diastole (RVAWd, mm)	0.31 ± 0.01	0.38 ± 0.03	<0.05	0.38 ± 0.02	<0.01	n.s.
Dimension at end diastole (RVDd, mm)	1.74 ± 0.05	1.85 ± 0.06	n.s.	2.15 ± 0.1	<0.01	n.s.
Tricuspid annulus plane systolic excursion (TAPSE, mm)	1.06 ± 0.04	0.95 ± 0.04	n.s.	0.76 ± 0.04	<0.0001	n.s.
Lateral wall systolic contractility (S_R, cm/sec)	3.25 ± 0.25	3.04 ± 0.23	n.s.	2.1 ± 0.12	<0.001	<0.05
Pulmonary Artery						
Pulmonary artery acceleration time (PAAT, msec)	20.18 ± 0.76	16.75 ± 1.1	<0.05	15.62 ± 0.49	<0.0001	n.s.
Pulmonary artery ejection time (PAET, msec)	67.52 ± 2.09	63.17 ± 3.3	n.s.	60.31 ± 1.6	<0.05	n.s.
PAAT/PAET	0.3008 ± 0.01	0.27 ± 0.02	n.s.	0.26 ± 0.01	n.s.	n.s.

Table 1. Echocardiographic evaluation of ventricles in SHAM and MI mice. LVAWd: left ventricular anterior wall thickness in diastole, LVPWd: left ventricular posterior wall thickness in diastole, LVDd: left ventricular dimension in diastole, LVDs: left ventricular dimension in systole, LVVd: left ventricular volume in diastole, LVVs: left ventricular volume in systole, WMSI: wall motion score index, EF: ejection fraction, CO: cardiac output, FS: fractional shortening, MPI: myocardial performance index, RVAWd: right ventricular anterior wall thickness in diastole, RVDd: right ventricular dimension in diastole, TAPSE: tricuspid annular plane systolic excursion, S_R: lateral wall systolic contractility, PAAT: pulmonary artery acceleration time, PAET: pulmonary artery ejection time (SHAM n= 19; MI with WMSI≥2 n= 18). E/e': ratio of mitral peak velocity of early filling to early diastolic mitral annular velocity.

Parameters	Sham n = 9–10	MI(WMSI < 2) n = 3–5	p value (WMSI < 2 vs sham)	MI(WMSI ≥ 2) n = 12–15	p value (WMSI ≥ 2 vs sham)	p value (WMSI < 2 vs WMSI ≥ 2)
Scar						
Scar surface (mm^2)	NA	11.65 ± 6.4		26.51 ± 1.8		<0.001
Scar weight (mg)	NA	0.0096 ± 0.004		0.015 ± 0.001		<0.05
Left ventricle						
LV Weight (g)	0.06 ± 0.003	0.056 ± 0.009	n.s.	0.063 ± 0.005	n.s.	n.s.
(LV + septum) weight (g)	0.079 ± 0.004	0.082 ± 0.006	n.s.	0.09 ± 0.006	n.s.	n.s.
LV/BW	0.0026 ± 0.0002	0.0023 ± 0.0007	n.s.	0.0027 ± 0.0002	n.s.	n.s.
Systolic pressure (mmHg)	117 ± 10	103 ± 11	n.s.	93 ± 4	<0.05	n.s.
LVEDP (mmHg)	10 ± 2	9.8 ± 2	n.s.	18 ± 2	<0.05	n.s.
+dP/dt (mmHg/sec)	8476 ± 767	7568 ± 1149	n.s.	5649 ± 253	<0.01	n.s.
dP/dt (mmHg/sec)	−7591 ± 484	−6725 ± 832	n.s.	−4861 ± 289	<0.001	n.s.
Right ventricle						
RV Weight (g)	0.022 ± 0.0008	0.019 ± 0.002	n.s.	0.028 ± 0.003	n.s.	n.s.
RV/(LV + septum) weight (%)	15.27 ± 4.58	23.95 ± 4.9	n.s.	33.46 ± 3.7	<0.05	n.s.
RV/BW	0.00087 ± 0.00008	0.00077 ± 0.00007	n.s.	0.0013 ± 0.0001	<0.001	n.s.
Systolic pressure (mmHg)	24.32 ± 1.2	29.35 ± 0.4	n.s.	31.53 ± 3.2	<0.05	n.s.
RVEDP (mmHg)	5.06 ± 0.8	3.63 ± 0.6	n.s.	2.16 ± 0.5	<0.05	n.s.

Table 2. Morphometric and hemodynamic evaluation of ventricles in SHAM and MI mice. LVEDP: left ventricular end diastolic pressure, +dP/dt and −dP/dt: maximum and minimum rates of pressure change (indices of contractility and relaxation), RV: right ventricle, LV: left ventricle, RVEDP: right ventricular end diastolic pressure, BW: body weight.

Figures Legends

Figure 1: *Left ventricular function and Wall Motion Score Index*.

Correlation between Wall Motion Score Index (WMSI) and different left ventricular function parameters in mice following coronary ligation. Left ventricular function was assessed with left ventricular end diastolic pressure (LVEDP; panel **A**; n = 15), left ventricular ejection fraction (EF; panel **B**; n=25), left ventricular inotropy (+dP/dt; panel **C**; n = 13) and left ventricular lusitropy (-dP/dt; panel **D**; n = 13).

Figure 2: *Wall Motion Score Index and infarct size*.

A. Correlation between Wall Motion Score Index (WMSI) and the extent of infarct (scar surface) induced by coronary ligation in mice. **B.** WMSI correlation with scar surface illustrates that a WMSI ≥ 2.0 corresponds to a scar surface of ≥ 20 mm^2. n = 17.

Figure 3: *Echocardiographic and hemodynamic monitoring of cardiac function*.

Typical examples of cardiac function monitoring in mice without (**SHAM**, left column) or following coronary ligation (**MI**, right column). **LV-M mode**: M-mode echocardiographic recordings of left ventricular cycle. **LV, RV**: Intraventricular pressure measured in left (**LV**) and right (**RV**) ventricles with high-fidelity catheters. **TAPSE**: Echocardiographic assessment of tricuspid annular place systolic excursion (TAPSE). **PAAT**: Echocardiographic evaluation of pulmonary artery acceleration time (PAAT).

Figure 4: *Lung remodelling upon coronary ligation*.

A. Assessment of pulmonary oedema in mice without (**SHAM**, white) or with myocardial infarct (**MI**, black). Ratioed (**a**) wet lung and body weights (Sham n = 6; MI n = 15), (**b**) dry lung and body weights (Sham n = 6; MI n=11), and (**c**) wet and dry lung weights (Sham n = 5; MI n = 14). **Ba**. Typical examples of pulmonary structural remodelling in mice without (**SHAM**, white), or with medium (20-30 mm^2) or large (>30 mm^2) myocardial infarct (**MI**, black) revelaed by Masson trichrome stain (20X). **Bb**. Bar graph reporting collagen deposit in mice without (**SHAM**, white) and with myocardial infarct (**MI**, black) measured in experiments as in Ba. n = **C**. Bar graphs reporting respiratory function evaluation in mice without (**SHAM**, white) or with myocardial infarct (**MI**, black). **Ca**. Quasi-static compliance (Cst) **Cb**. Quasi-static elasticity (Est) **Cc**. Resistance (R). SHAM n = 7; MI n = 10.

* $p<0.05$, ** $p<0.01$ and *** $p<0.001$ vs SHAM.

Figure 5. Pulmonary pressure-volume curves after coronary ligation.

A. Typical example of pulmonary pressure-volume curves recorded from mice without (**SHAM**, black) and with myocardial infarct (**MI**, red). **B**. Bar graph reporting pulmonary capacity in mice without (**SHAM**, white) and with myocardial infarct (**MI**, black) calculated from experiments as in A using the Salazar-Knowles equation. **Ba**. Total inspiratory capacity (A) **Bb**. Difference between the total pulmonary capacity and the volume at zero pressure (B) **Bc**. Curvature parameter (K). SHAM n = 7; MI n = 10.

* $p<0.05$ vs SHAM.

Figure 6. *Right ventricle and pulmonary artery following myocardial infarct with a WMSI ≥ 2*.

A. Correlation of right ventricle hypertrophy with Wall Motion Score Index (WMSI) in mice following myocardial infarct. n = 15 **B**. Correlation between tricuspid annular place systolic excursion (TAPSE) in mice following myocardial infarct. n = 18 **C, D**. Bar graph illustrating the impact of left ventricular infarct on pulmonary artery acceleration time (PAAT, panel **C**) and tricuspid annular place systolic excursion (TAPSE, panel **D**) in mice with a WMSI ≥ 2. SHAM n = 19; MI n = 18.

*** $p<0.001$ vs Sham.

References

1. Guazzi, M. & Borlaug, B.A. Pulmonary hypertension due to left heart disease. *Circulation* **126**, 975-990 (2012).
2. Simonneau, G.*, et al.* Updated clinical classification of pulmonary hypertension. *J Am Coll Cardiol* **62**, D34-41 (2013).
3. Hache, M.*, et al.* Inhaled epoprostenol (prostacyclin) and pulmonary hypertension before cardiac surgery. *J Thorac Cardiovasc Surg* **125**, 642-649 (2003).
4. Laflamme, M.*, et al.* Preliminary experience with combined inhaled milrinone and prostacyclin in cardiac surgical patients with pulmonary hypertension. *J Cardiothorac Vasc Anesth* **29**, 38-45 (2015).
5. Guazzi, M., Samaja, M., Arena, R., Vicenzi, M. & Guazzi, M.D. Long-term use of sildenafil in the therapeutic management of heart failure. *J Am Coll Cardiol* **50**, 2136-2144 (2007).
6. Guazzi, M., Vicenzi, M., Arena, R. & Guazzi, M.D. Pulmonary hypertension in heart failure with preserved ejection fraction: a target of phosphodiesterase-5 inhibition in a 1-year study. *Circulation* **124**, 164-174 (2011).
7. Sablotzki, A.*, et al.* Iloprost improves hemodynamics in patients with severe chronic cardiac failure and secondary pulmonary hypertension. *Can J Anaesth* **49**, 1076-1080 (2002).
8. Guazzi, M., Tumminello, G., Reina, G., Vicenzi, M. & Guazzi, M.D. Atorvastatin therapy improves exercise oxygen uptake kinetics in post-myocardial infarction patients. *Eur J Clin Invest* **37**, 454-462 (2007).
9. Dupuis, J.*, et al.* Bone marrow-derived progenitor cells contribute to lung remodelling after myocardial infarction. *Cardiovasc Pathol* **16**, 321-328 (2007).
10. Jasmin, J.F., Calderone, A., Leung, T.K., Villeneuve, L. & Dupuis, J. Lung structural remodeling and pulmonary hypertension after myocardial infarction: complete reversal with irbesartan. *Cardiovasc Res* **58**, 621-631 (2003).
11. Jasmin, J.F.*, et al.* Lung remodeling and pulmonary hypertension after myocardial infarction: pathogenic role of reduced caveolin expression. *Cardiovasc Res* **63**, 747-755 (2004).
12. Lefebvre, F.*, et al.* Modification of the pulmonary renin-angiotensin system and lung structural remodelling in congestive heart failure. *Clin Sci (Lond)* **111**, 217-224 (2006).
13. Duran, J.M.*, et al.* Bone-derived stem cells repair the heart after myocardial infarction through transdifferentiation and paracrine signaling mechanisms. *Circ Res* **113**, 539-552 (2013).
14. Jiang, B.H.*, et al.* Beneficial effects of atorvastatin on lung structural remodeling and function in ischemic heart failure. *J Card Fail* **16**, 679-688 (2010).
15. Jiang, B.H., Tardif, J.C., Shi, Y. & Dupuis, J. Bosentan does not improve pulmonary hypertension and lung remodeling in heart failure. *Eur Respir J* **37**, 578-586 (2011).
16. Kemi, O.J., Haram, P.M., Hoydal, M.A., Wisloff, U. & Ellingsen, O. Exercise training and losartan improve endothelial function in heart failure rats by different mechanisms. *Scand Cardiovasc J* **47**, 160-167 (2013).
17. Kerem, A.*, et al.* Lung endothelial dysfunction in congestive heart failure: role of impaired Ca2+ signaling and cytoskeletal reorganization. *Circ Res* **106**, 1103-1116 (2010).
18. Rossoni, G.*, et al.* Sildenafil reduces L-NAME-induced severe hypertension and worsening of myocardial ischaemia-reperfusion damage in the rat. *Br J Pharmacol* **150**, 567-576 (2007).

19. Sauvageau, S., Thorin, E., Caron, A. & Dupuis, J. Evaluation of endothelin-1-induced pulmonary vasoconstriction following myocardial infarction. *Exp Biol Med (Maywood)* **231**, 840-846 (2006).
20. Yin, J.*, et al.* Sildenafil preserves lung endothelial function and prevents pulmonary vascular remodeling in a rat model of diastolic heart failure. *Circ Heart Fail* **4**, 198-206 (2011).
21. Ontkean, M., Gay, R. & Greenberg, B. Diminished endothelium-derived relaxing factor activity in an experimental model of chronic heart failure. *Circ Res* **69**, 1088-1096 (1991).
22. Morty, R.E. & Kuebler, W.M. TRPV4: an exciting new target to promote alveolocapillary barrier function. *Am J Physiol Lung Cell Mol Physiol* **307**, L817-821 (2014).
23. Bossone, E.*, et al.* Echocardiography in pulmonary arterial hypertension: from diagnosis to prognosis. *J Am Soc Echocardiogr* **26**, 1-14 (2013).
24. Rudski, L.G.*, et al.* Guidelines for the echocardiographic assessment of the right heart in adults: a report from the American Society of Echocardiography endorsed by the European Association of Echocardiography, a registered branch of the European Society of Cardiology, and the Canadian Society of Echocardiography. *J Am Soc Echocardiogr* **23**, 685-713; quiz 786-688 (2010).
25. Leenen, F.H. & Yuan, B. Mortality after coronary artery occlusion in different models of cardiac hypertrophy in rats. *Hypertension* **37**, 209-215 (2001).
26. Wollert, K.C., Studer, R., von Bulow, B. & Drexler, H. Survival after myocardial infarction in the rat. Role of tissue angiotensin-converting enzyme inhibition. *Circulation* **90**, 2457-2467 (1994).
27. Liao, Y.*, et al.* Echocardiographic assessment of LV hypertrophy and function in aortic-banded mice: necropsy validation. *Am J Physiol Heart Circ Physiol* **282**, H1703-1708 (2002).
28. Dupuis, J. & Guazzi, M. Pathophysiology and clinical relevance of pulmonary remodelling in pulmonary hypertension due to left heart diseases. *Can J Cardiol* **31**, 416-429 (2015).
29. Colvin, K.L. & Yeager, M.E. Animal Models of Pulmonary Hypertension: Matching Disease Mechanisms to Etiology of the Human Disease. *J Pulm Respir Med* **4**(2014).
30. Gomez-Arroyo, J.*, et al.* A brief overview of mouse models of pulmonary arterial hypertension: problems and prospects. *Am J Physiol Lung Cell Mol Physiol* **302**, L977-991 (2012).
31. Staniloae, C.*, et al.* Reduced pulmonary clearance of endothelin in congestive heart failure: a marker of secondary pulmonary hypertension. *J Card Fail* **10**, 427-432 (2004).
32. Azarbar, S. & Dupuis, J. Lung capillary injury and repair in left heart disease: a new target for therapy? *Clin Sci (Lond)* **127**, 65-76 (2014).
33. Kapanci, Y., Burgan, S., Pietra, G.G., Conne, B. & Gabbiani, G. Modulation of actin isoform expression in alveolar myofibroblasts (contractile interstitial cells) during pulmonary hypertension. *Am J Pathol* **136**, 881-889 (1990).
34. Gao, S., Ho, D., Vatner, D.E. & Vatner, S.F. Echocardiography in Mice. *Curr Protoc Mouse Biol* **1**, 71-83 (2011).
35. Odashima, M.*, et al.* Inhibition of endogenous Mst1 prevents apoptosis and cardiac dysfunction without affecting cardiac hypertrophy after myocardial infarction. *Circ Res* **100**, 1344-1352 (2007).

36. Depre, C.*, et al.* Activation of the cardiac proteasome during pressure overload promotes ventricular hypertrophy. *Circulation* **114**, 1821-1828 (2006).
37. Gelpi, R.J.*, et al.* Genetic inhibition of calcineurin induces diastolic dysfunction in mice with chronic pressure overload. *Am J Physiol Heart Circ Physiol* **297**, H1814-1819 (2009).
38. Guellich, A.*, et al.* Effects of cardiac overexpression of type 6 adenylyl cyclase affects on the response to chronic pressure overload. *Am J Physiol Heart Circ Physiol* **299**, H707-712 (2010).
39. Weinheimer, C.J., Lai, L., Kelly, D.P. & Kovacs, A. Novel mouse model of left ventricular pressure overload and infarction causing predictable ventricular remodelling and progression to heart failure. *Clin Exp Pharmacol Physiol* **42**, 33-40 (2015).

40. Carluccio, E.*, et al.* Usefulness of the severity and extent of wall motion abnormalities as prognostic markers of an adverse outcome after a first myocardial infarction treated with thrombolytic therapy. *Am J Cardiol* **85**, 411-415 (2000).
41. Moller, J.E.*, et al.* Wall motion score index and ejection fraction for risk stratification after acute myocardial infarction. *Am Heart J* **151**, 419-425 (2006).
42. Duncan, R.F.*, et al.* A study of the 16-Segment Regional Wall Motion Scoring Index and biplane Simpson's rule for the calculation of left ventricular ejection fraction: a comparison with cardiac magnetic resonance imaging. *Echocardiography* **28**, 597-604 (2011).

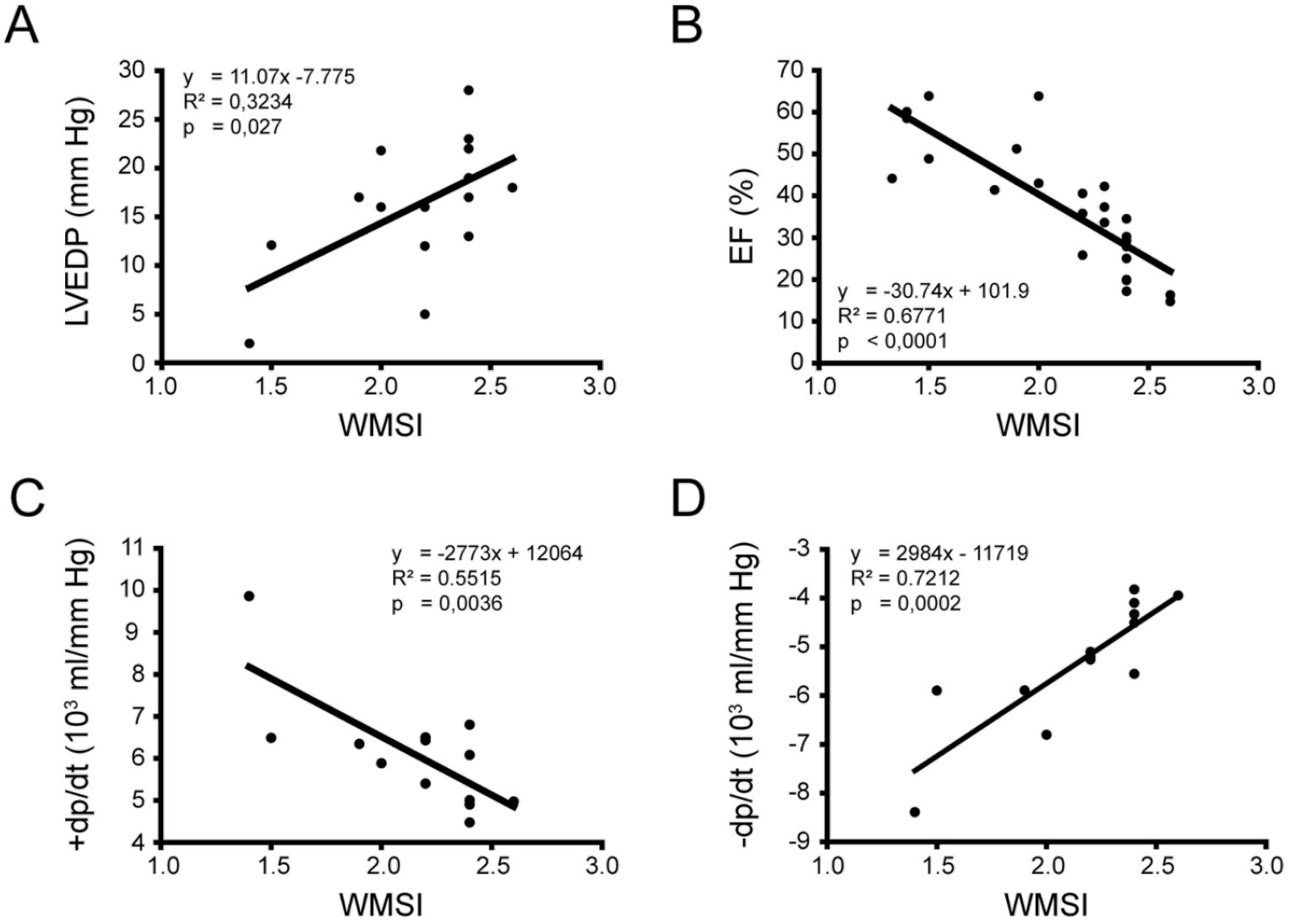
A
LVEDP (mm Hg)
y = 11.07x -7.775
R² = 0,3234
p = 0,027
WMSI
B
EF (%)
y = -30.74x + 101.9
R² = 0.6771
p < 0,0001
WMSI
C
+dp/dt (10³ ml/mm Hg)
y = -2773x + 12064
R² = 0.5515
p = 0,0036
WMSI
D
-dp/dt (10³ ml/mm Hg)
y = 2984x - 11719
R² = 0.7212
p = 0,0002
WMSI

A

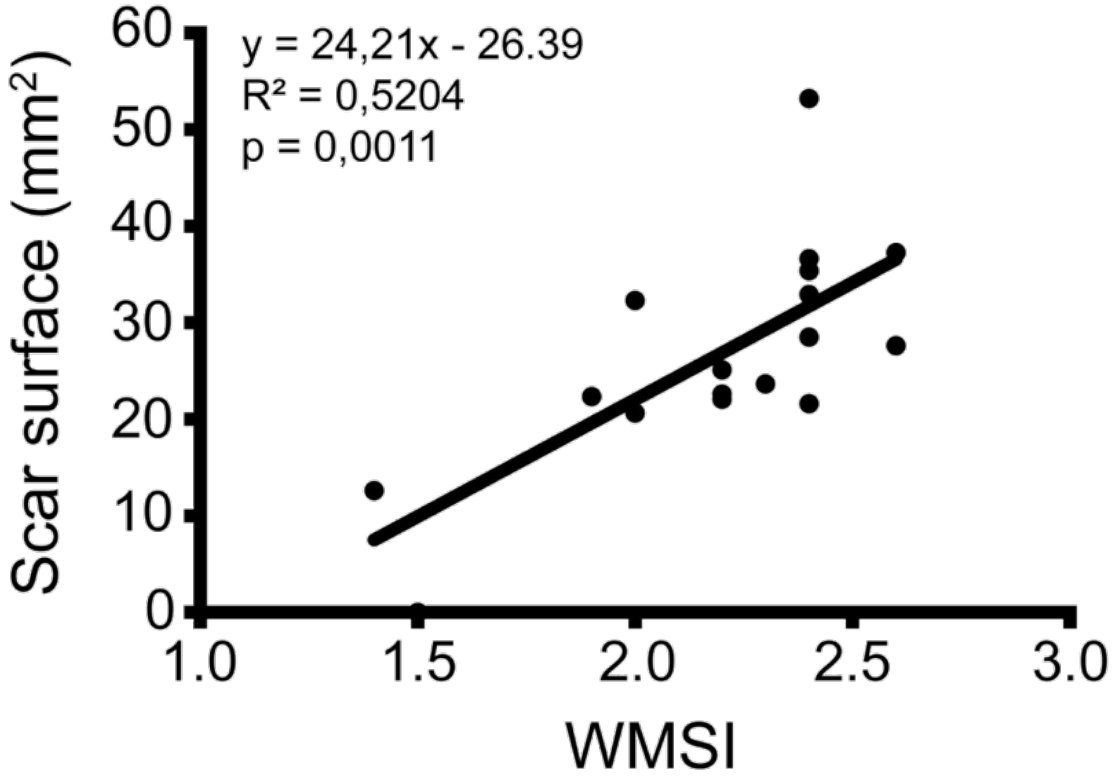
y = 24,21x - 26.39
R² = 0,5204
p = 0,0011
Scar surface (mm²)
60
50
40
30
20
10
0
1.0
1.5
2.0
2.5
3.0
WMSI

B

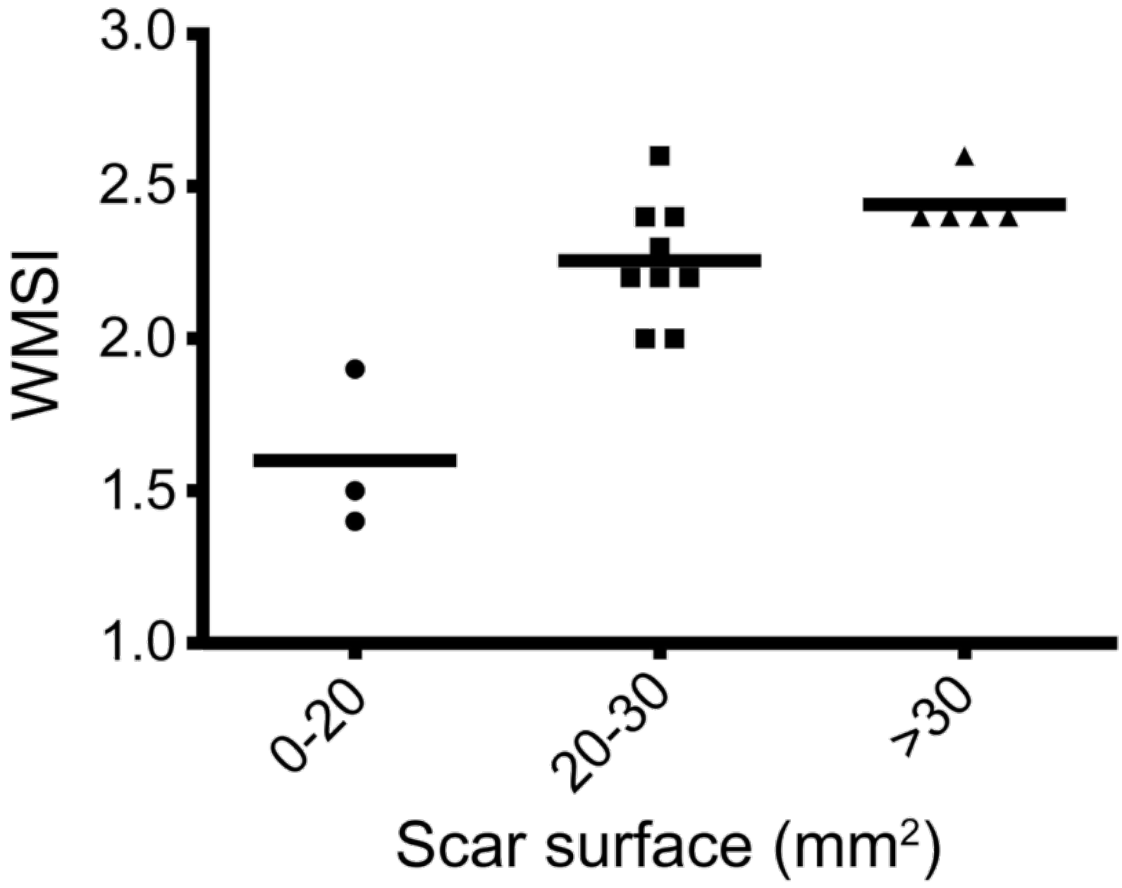
WMSI
3.0
2.5
2.0
1.5
1.0
0-20
20-30
>30
Scar surface (mm²)

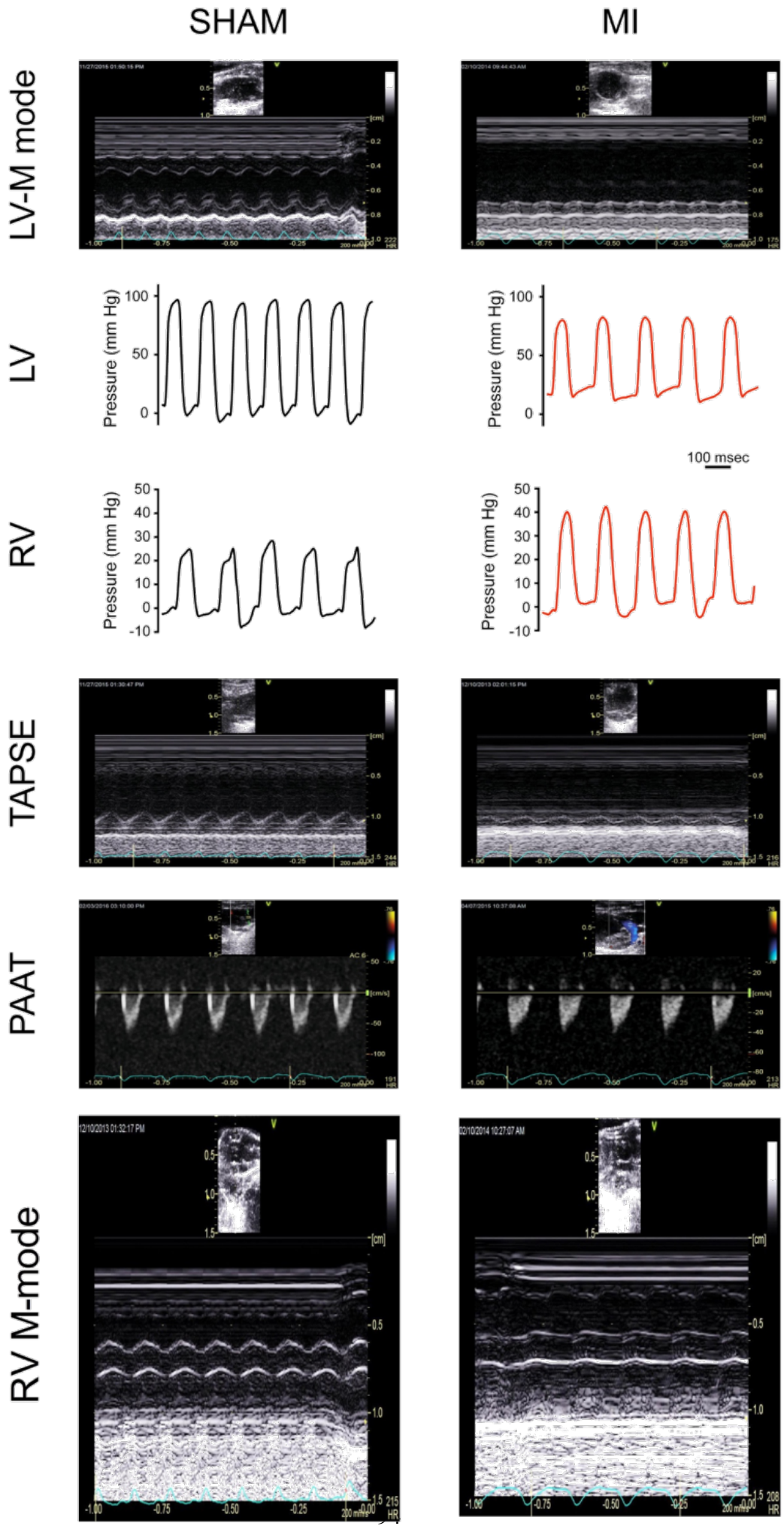
SHAM
MI
LV-M mode
LV
RV
TAPSE
PAAT
RV M-mode
Pressure (mm Hg)
100
50
0
50
40
30
20
10
0
-10
100 msec

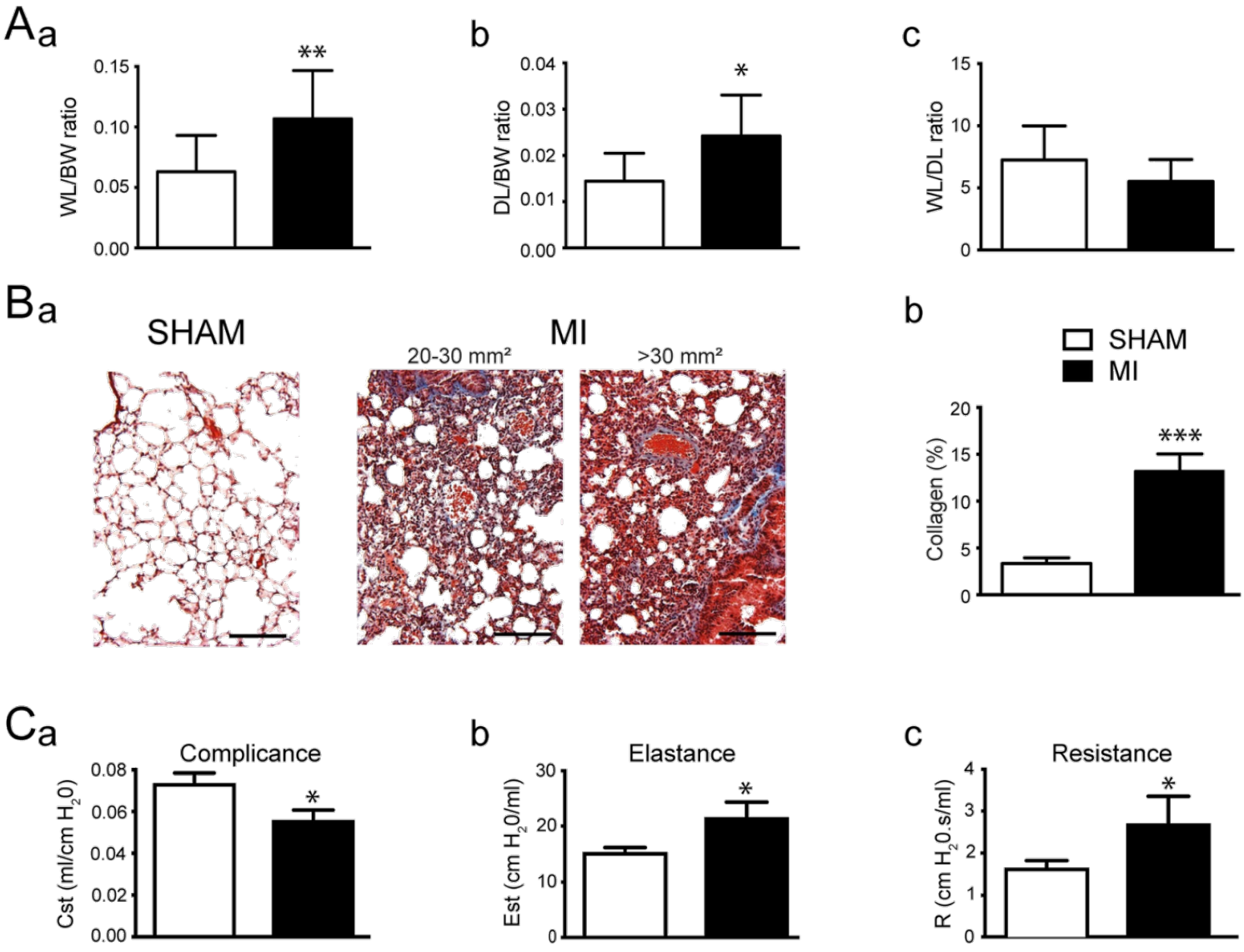
Aa
WL/BW ratio
0.15
0.10
0.05
0.00
**
b
DL/BW ratio
0.04
0.03
0.02
0.01
0.00
*
c
WL/DL ratio
15
10
5
0
Ba
SHAM
MI
20-30 mm²
>30 mm²
b
SHAM
MI
Collagen (%)
20
15
10
5
0
***
Ca
Complicance
Cst (ml/cm H2O)
0.08
0.06
0.04
0.02
0.00
*
b
Elastance
Est (cm H2O/ml)
30
20
10
0
*
c
Resistance
R (cm H2O.s/ml)
4
3
2
1
0
*

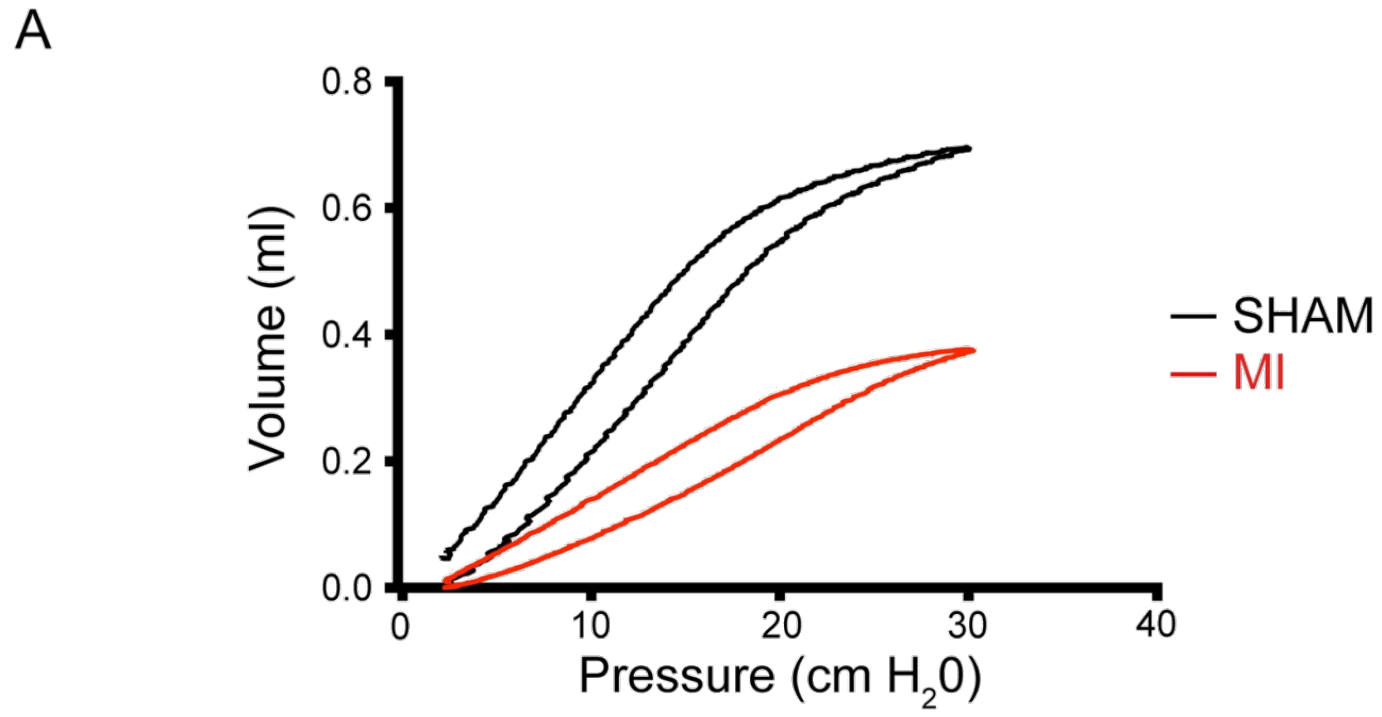
A
0.8
0.6
0.4
0.2
0.0
Volume (ml)
0
10
20
30
40
Pressure (cm H20)
SHAM
MI

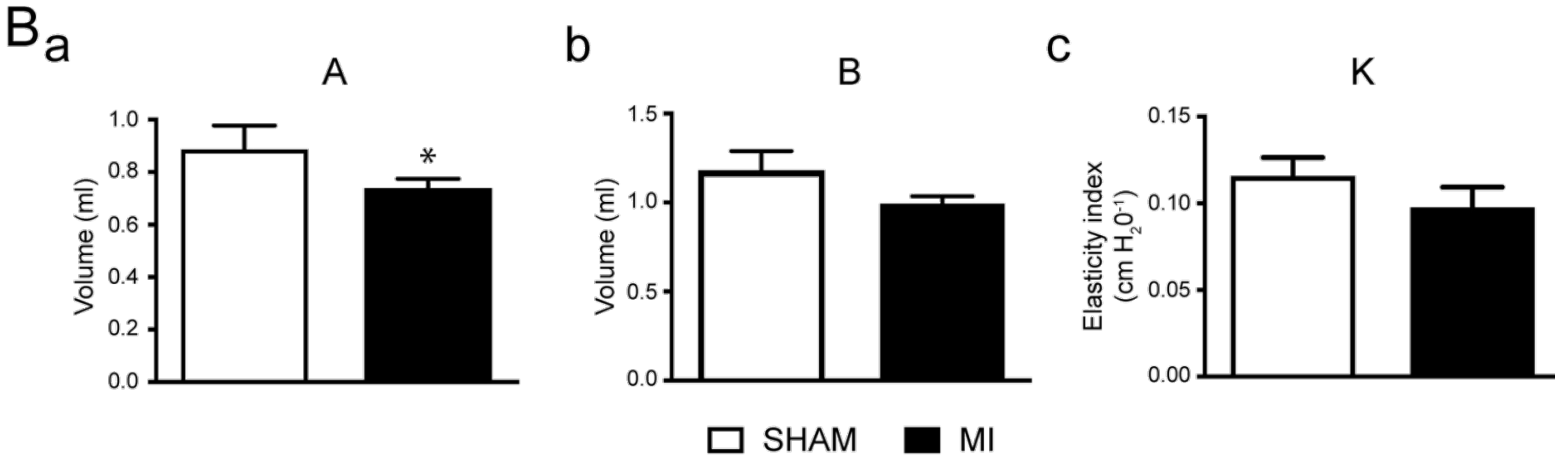
Ba
A
1.0
0.8
0.6
0.4
0.2
0.0
Volume (ml)
*
b
B
1.5
1.0
0.5
0.0
Volume (ml)
c
K
0.15
0.10
0.05
0.00
Elasticity index
(cm H20-1)
SHAM
MI

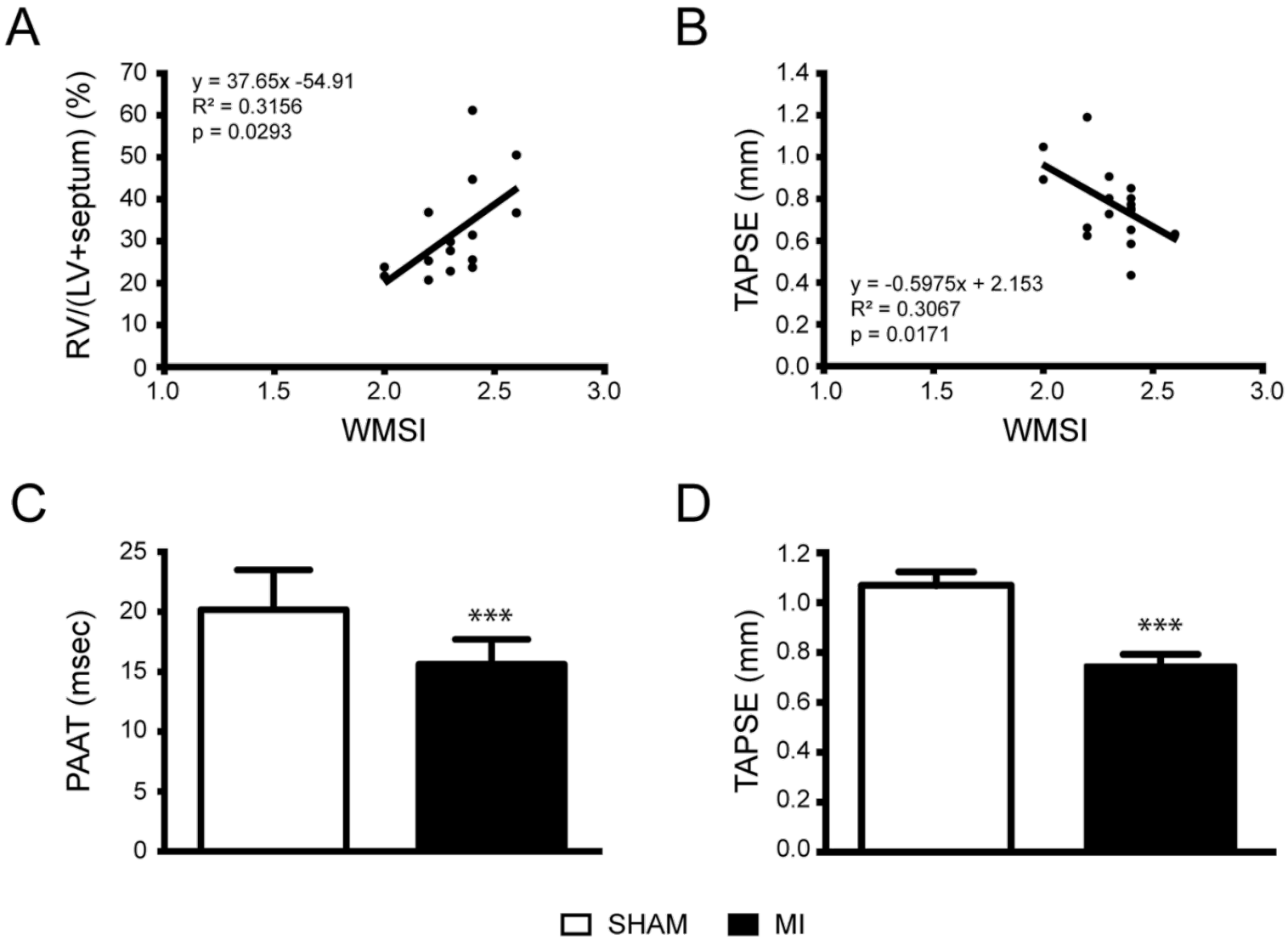
A
y = 37.65x -54.91
R² = 0.3156
p = 0.0293
RV/(LV+septum) (%)
WMSI
B
y = -0.5975x + 2.153
R² = 0.3067
p = 0.0171
TAPSE (mm)
WMSI
C
PAAT (msec)
***
D
TAPSE (mm)
***
SHAM
MI

Supplementary material

Echocardiographic validation of pulmonary hypertension due to heart failure with reduced ejection fraction in mice

Dayeh R. Nour[1,2], Tardif Jean-Claude[1,2], Shi Yanfen[1], Tanguay Mégane[2], §Ledoux Jonathan[1,2,3], §*Dupuis Jocelyn[1,2].

SCIENTIFIC REPORTS | (2018) 8:1363 | DOI:10.1038/s41598-018-19625-2

This article was accepted on January 5th 2018, and published on January 22nd 2018

Affiliations:

Research Center, Montreal Heart Institute, Quebec, Canada

Departments of Medicine, [3] Pharmacology and Physiology, Université de Montréal, Quebec, Canada

§ Drs Ledoux and Dupuis share senior authorship.

*Corresponding author

	Sham	*WMSI<2*	*WMSI≥2*
	N=19	*n=7*	*n=17*
Normal wall motion	*190/190*	*47/70*	*43.5/170*
Hypokinesis	*0/190*	*9.5/70*	*45.5/170*
Akinesis	*0/190*	*12.5/70*	*63.5/170*
Dyskinesis	*0/190*	*1/70*	*17.5/170*
Aneurysms	*0/190*	*0/70*	*0/170*

Suppl table 1. Grading of wall motion abnormalities in the study population. 10 segments were analyzed for each animal.

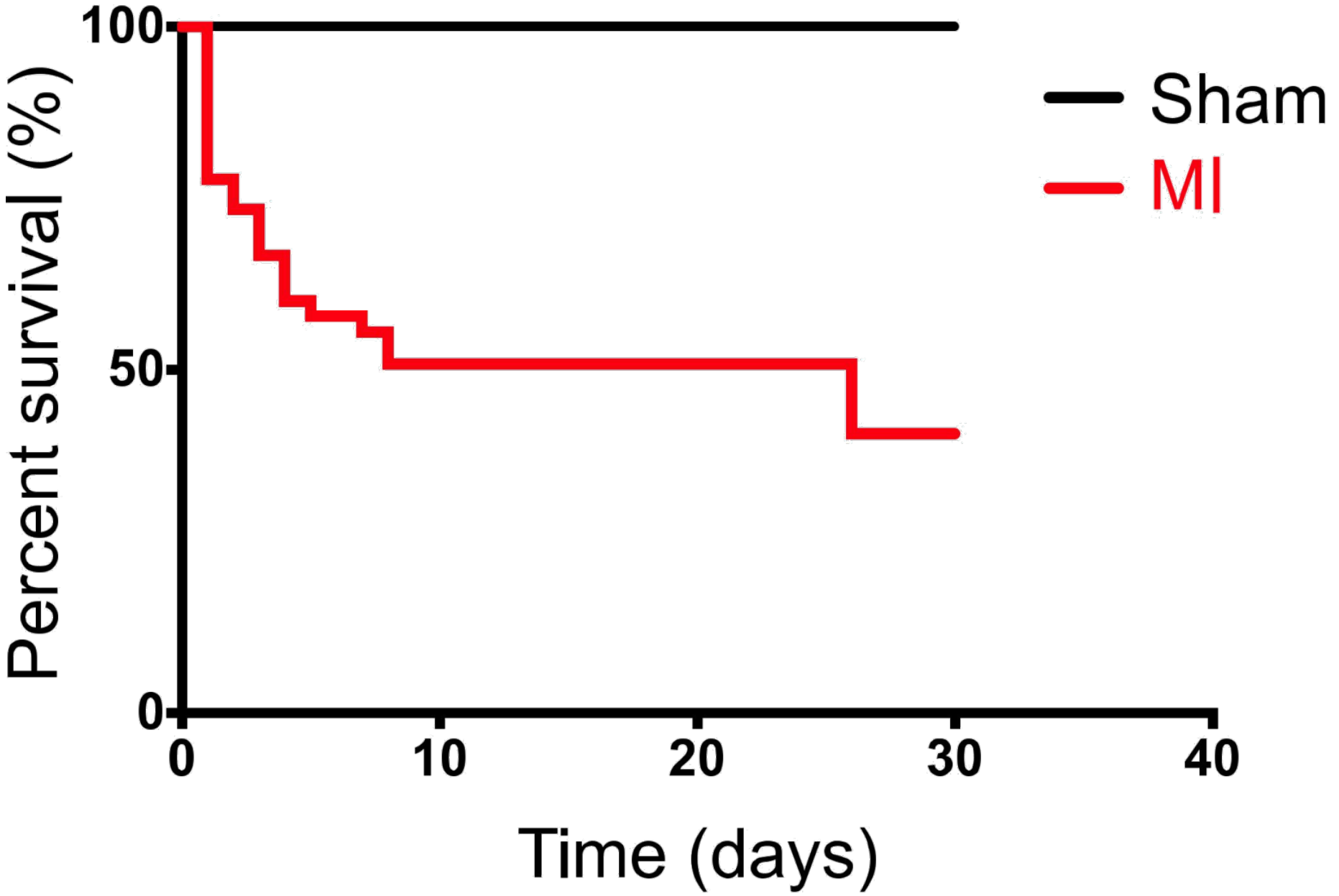
100
50
0
Percent survival (%)
0
10
20
30
40
Time (days)
Sham
MI

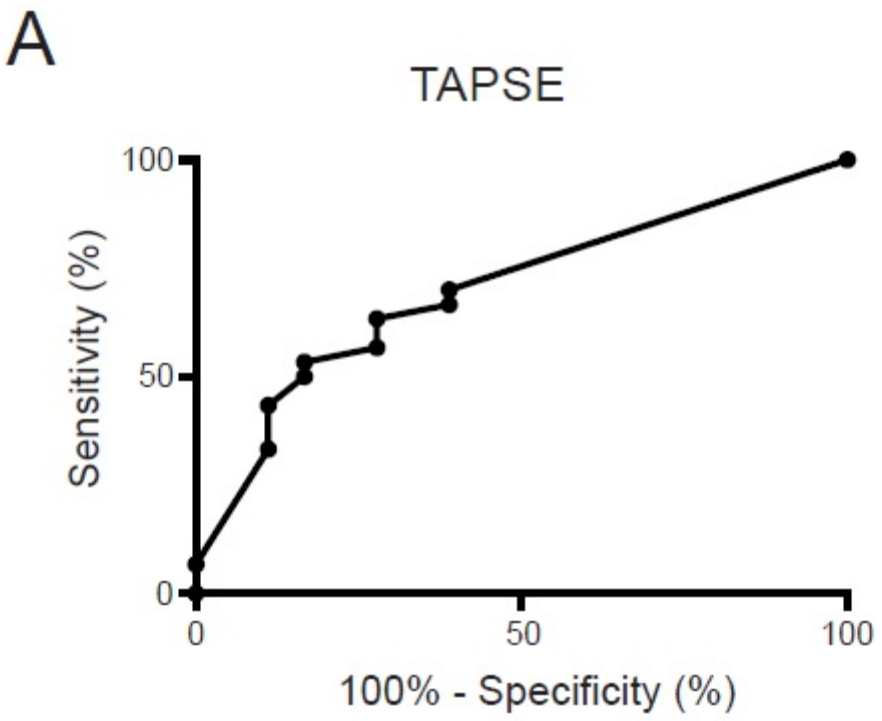
A
TAPSE
100
50
0
Sensitivity (%)
0
50
100
100% - Specificity (%)

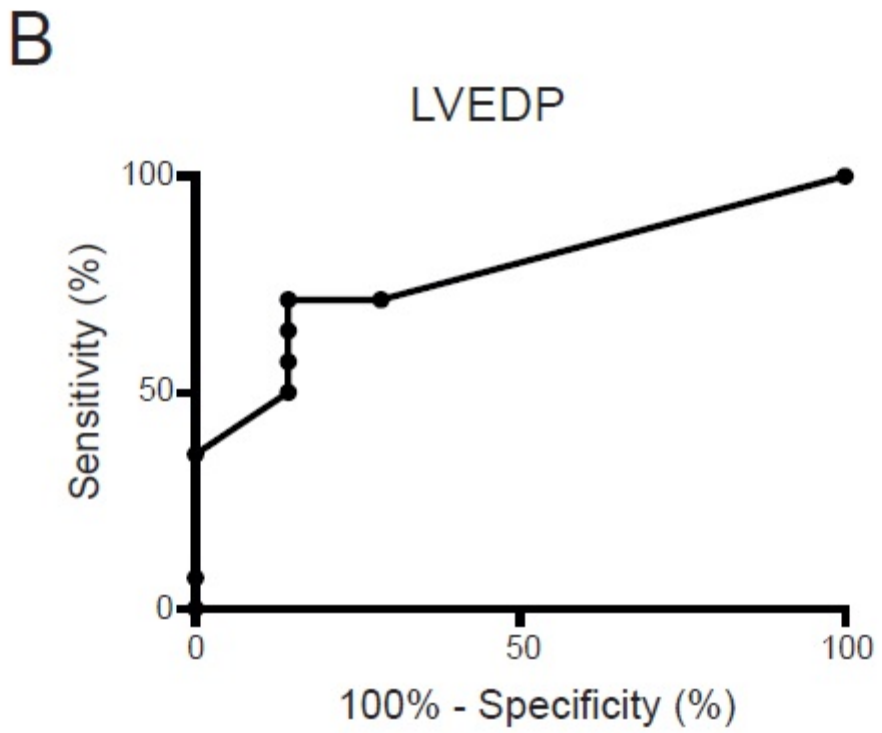
B
LVEDP
100
50
0
Sensitivity (%)
0
50
100
100% - Specificity (%)

Supplemental Figures Legends

Supplemental Figure 1: *Post MI survival curve*

Kaplan-Meir survival curve for mice following surgical procedure. Mice underwent thoracotomy without (SHAM, black, n= 19)) or with ligation of left anterior coronary artery (MI, red, n=48).

Supplemental Figure 2: *ROC curves with WMSI to predict type 2 pulmonary hypertension.*

ROC curves for TAPSE (**A**) and LVEDP (**B**) illustrating the efficiency of WMSI as an early indicator of type 2 pulmonary hypertension in mice. Area under the curve: TAPSE: 0.7009; LVEDP: 0.7755. TAPSE: n = 18 (CTRL) & 30 (PH); LVEDP: n = 7 (CTRL) & 14 (PH).

Localized endothelial Ca^{2+} signaling is strongly conserved amongst vascular beds

Chimène Charbel[1,2#], Nour R. Dayeh[1,3#], Alexandre Blanchette[1], Mark S. Taylor[6], Jocelyn Dupuis[1,3], Philippe Comtois[1,4,5], Jonathan Ledoux*[1-4]

This manuscript is in preparation to be submitted to AJP heart and circulatory physiology

*Corresponding author

[#]Authors equally contributed to this work

Short title: Conserved endothelial Ca^{2+} microdomains.

---

[1]Research Center, Montreal Heart Institute, Quebec, Canada. [2]Departments of Pharmacology, [3]Medicine, [4]Molecular and Integrative Physiology and [5]Institute of biomedical engineering, Université de Montréal, Quebec, Canada.

[6]Department of Physiology, University of South Alabama College of Medicine, Mobile, AL, USA Correspondence and requests for materials should be addressed to Jonathan Ledoux, Research Center, Montreal Heart Institute.

*Corresponding author: jonathan.ledoux@umontreal.ca

Authors' contributions:

Experimental design: CC, ND, JL

Experimentation: CC, ND

Data collection and analysis: CC, ND

Immunofluorescence data collection: AB

Immunofluorescence data quantification through the creation of an algorithm in Matlab (ATIFIsNI): PC

Final elaboration of the manuscript: CC, ND, JL, AB, JD, PC

Critical review of the manuscript: MT, JD

Abstract

Endothelial modulation of vascular tone is essentially dependent on intracellular Ca^{2+}. Recent advances suggest that endothelial Ca^{2+} microdomains, especially within myoendothelial projections, is important for endothelial-dependent hyperpolarization and vessel relaxation. Reports of different local Ca^{2+} dynamics, including Ca^{2+} pulsars, established their physiological relevance. However, vascular beds and their respective endothelium are specialized and adapted to their distinct environment. It is then unclear how local Ca^{2+} signals like Ca^{2+} pulsars differs throughout the vasculature. The characterization of Ca^{2+} pulsars and myoendothelial projections, site of these Ca^{2+} events was then sought in mesenteric, coronary and pulmonary resistance arteries. Fenestration of the internal elastic lamina, indicator of potential myoendothelial projections location was different between arterial beds with coronary arteries having the most fenestrated lamina. Accordingly, coronary arteries presented the highest density of myoendothelial projections as evidenced by calnexin immunostaining, whilst pulmonary arteries showed the lowest myoendothelial projection density. Endothelial Ca^{2+} pulsars from all three vascular beds were practically identical in regards to kinetics, suggesting that Ca^{2+} pulsars are highly conserved amongst resistance arteries. However, the frequency of Ca^{2+} pulsars appeared significantly different between the arteries. Mesenteric endothelium is the most active with the highest individual pulsars frequency and number of active sites. Interestingly, all vascular beds tested had a similar response to Ca^{2+} pulsar stimulation through smooth muscle α1-adrenergic agonist phenylephrine. This study establishes Ca^{2+} pulsars as a fundamental Ca^{2+} signal highly conserved throughout the vasculature. However, structural elements of the vessel wall, such as myoendothelial projections might be responsible for distinct incidence of Ca^{2+} pulsars.

Introduction

Endothelial Ca^{2+} signaling is a central component of endothelial functions, including the regulation of vascular tone. Seminal work showed that stimulation of vascular preparations with endothelial agonists such as bradykinin or ATP is associated with a significant rise of cytoplasmic Ca^{2+} accompanied with a vasorelaxation (11, 12). Basically, all regulatory pathways originating from the endothelium are activated or modulated to some extent by intracellular Ca2+. Indeed, production of nitric oxide by endothelial nitric oxide synthase (NOS3) is sensitive to intracellular Ca2+. Generation of arachidonic acid metabolites is also dependent on intracellular Ca2+ levels, since phospholipase A_2 (PLA_2) is modulated by Ca^{2+}. Likewise, endothelium-derived hyperpolarizing factor (EDHF), an amalgam of various mechanisms requires an increase in intracellular Ca^{2+} levels.

Characterization of vessel wall ultra-structures provided evidence of endothelial cells (ECs) polarity and architecture suggesting intracellular organization promoting subcellular Ca^{2+} microdomains. Although Ca^{2+}-activated K^+ channels (K_{Ca}) have been shown to be involved in endothelial-dependent regulation of vascular tone (15, 20), distinct role for ion channels subtypes in this process was suggested by a differential localization of $K_{Ca}2.3$ and $K_{Ca}3.1$ (14). $K_{Ca}3.1$ channels localization within myoendothelial projection (MEPs) allow their activation by Ca^{2+} pulsars and transmission of the hyperpolarization to the underlying smooth muscle (7, 10). Indeed, MEPs are endothelial projections through internal elastic lamina (IEL) fenestrations and making close contact with the underlying smooth muscle cells. The reported endothelium-smooth muscle bi-directional communications through gap junctions occurs within MEPs. Additionally, enrichment of enzymes responsible for endothelial

functions such as NOS3, IP3 receptors and CaMKII was shown in MEPs (3, 4, 6, 18, 21).

Arterial beds inherently differ in their environment, which enforce specific adaptation to fully achieve their functions, as to regulate optimal blood delivery and pressure to the supplied organ. Indeed, we recently reported differences in phospholipase C (PLC) expression pattern amongst arterial beds (2). Intracellular Ca^{2+} dynamics essentially rely on PLC production of IP3 to stimulate Ca^{2+} release from the endoplasmic reticulum (ER), suggesting differential Ca^{2+} signaling throughout the vasculature. Moreover, compelling evidence shows that Ca^{2+} microdomains are determined by important multiprotein complexes (3, 16, 17, 19) and may vary between vascular beds. Resistance arteries from three considerably different vascular beds were thus studied, first from a structural perspective and then on their respective intracellular Ca^{2+} dynamics. Mice coronary (CA), mesenteric (MA) and pulmonary arteries (PA) were compared through their MEPs characteristics and their ER-dependent localized Ca^{2+} signals. All arterial preparations evaluated showed distinctive internal elastic lamina structure and the associated MEPs. Whilst Ca^{2+} waves were similar, Ca^{2+} pulsar, a spatially restricted endothelial Ca^{2+} signal was significantly different in basal condition (in the absence of stimulation) with mesenteric endothelium being the most active. However, kinetics for Ca^{2+} pulsars were similar in all three arterial types, suggesting that Ca^{2+} pulsar consist of an elementary Ca^{2+} signal highly conserved throughout the vascular tree. Specific stimulation of Ca^{2+} pulsars with acute exposure to phenylephrine (PE) increased Ca^{2+} pulsars frequency in all vessels without modifying intrinsic kinetics. This study provides the first comparative evidence of spatially restricted Ca2+ signaling amongst arterial beds. The data from this study

strongly suggests that Ca^{2+} pulsars might represent a fundamental Ca^{2+} signal despite different environmental constraints.

Material & Methods

Tissue preparation.

Animal procedures used in this study were in accordance with the institutional guidelines and were approved by the Research Center of the Montreal Heart Institute Animal Deontology Committee. Mesenteric arteries (MA) (3rd and 4th order diameters ≈ 60-100 μm), pulmonary arteries (PA) (3rd order diameters ≈ 60-100 μm) and coronary arteries (CA) (2nd and 3rd order diameters ≈ 100-180 μm) were isolated from 3-4 months old male C57BL/6 mice. Arteries were dissected and cleaned of connective and adipose tissue prior their mounting on a Sylgard block (cut lengthwise, endothelium facing up) in cooled HEPES solution (134 mM NaCl, 6 mM KCl, 10 mM glucose, 10 mM Hepes, 1 mM MgCl2, 2 mM CaCl2, pH 7.4). Every set of experiments was performed on 3 to 5 arteries from a minimum of 2 mice.

Immunohistochemistry.

Acute stimulation of Ca^{2+} pulsars was made on mounted arteries incubated with phenylephrine (PE; 10 μM, 15 minutes). Then, all arteries were fixed with 4% paraformaldehyde (20 minutes) before permeabilization and blocking simultaneously with 0.2% Triton X-100 and 4% normal donkey serum, respectively. Arteries were incubated overnight at 4˚C with the primary antibody against calnexin, an endoplasmic reticulum membrane marker (rabbit Calnexin, Abcam Cat. No. ab22595). Tissues were incubated with fluorescent secondary antibody (donkey anti-rabbit Alexafluor 647, Invitrogen, ex/em: 647/670 nm) for 1 hour at room temperature. After several washes, arteries were mounted on a FluoroDish with 4% Dabco (1/10 glycerol). Internal elastic

lamina (IEL) autofluorescence was measured at ex/em 488/520 nm, where nuclear staining with DAPI at 405/460 nm. Z-stacks images (0.25 μm increments) were acquired using a Zeiss LSM 510 system confocal microscope (63X oil objective, numerical aperture of 1.4) and deconvolved using the Maximum Likelihood estimation algorithm and the appropriate experimentally determined Point Spread Function (PSF) with Huygens Professional software 3.6 (Scientific Volume Imaging, Netherlands). Images were then analysed with zen 2009 light software. Staining for calnexin within myoendothelial projections (MEP), represented as perforations in the IEL, was quantified with a custom-designed ATIFIsNI algorithm, created in Matlab v7.0.1 (The Mathworks inc., MA).

Endothelial Ca^{2+} high-speed confocal imaging

Ca^{2+} pulsars imaging was assessed in MA, PA and CA loaded with Fluo-4 (10 μM, 45 min at 37˚C) at 37°C in a physiological salt solution (PSS; 119 mM NaCl, 4.7 mM KCl, 24 mM NaHCO3, 1.2 mM KH2PO4, 1.2 mM MgCl2, 11 mM Glucose and 1.5 mM CaCl2). High-speed confocal imaging (≈15 frames/sec) at ex/em 488/510 was performed using an Andor Revolution confocal system (Andor Technology) with an iXon EMCCD camera on an upright Nikon microscope and a 60X, water-dipping objective (NA 1.0). Images were also acquired after specific stimulation of Ca^{2+} pulsars with PE. Recorded Fluo-4 fluorescence with Andor iQ 2.8 software (Andor Technology) was then analyzed offline using SparkAn software (A. Bonev, UVM) by measuring the fluorescence intensity (F) relative to baseline (F_0). Analysis of Ca^{2+} pulsars fractional fluorescence (F/F_0) was performed using a 5 × 5 pixel box region of interest (ROI) positioned at the peak pulsar amplitude.

Statistical analysis.

Statistical analyses were performed using GraphPad Prism 5 software. Data from unpaired t-test were presented as mean ± SEM. Significant values were considered at $p<0.05$.

Results

Endothelium-smooth muscle interface

The IEL is the only structure between vascular endothelium and the underlying smooth muscle cells. Taking advantage of its autofluorescent properties, mapping of IEL from mice mesenteric (MA), pulmonary (PA) and coronary arteries (CA) was performed using scanning confocal microscopy. IEL fenestrations from the three arterial types are qualitatively different (Figure 1A). Analysis with ATIFIsNI, custom-designed image analysis algorithm, provided further metrics in regards to IEL coverage in arteries. Incidence of IEL fenestrations as well as the total area covered by IEL fenestrations was found to be two-fold greater in CA than in PA and MA (Figure 1Ba & b). Interestingly, this higher fenestrated area in CA is not associated with larger individual fenestrations, as mean surface of IEL fenestrations is not significantly different from PA. However, MA has prominent IEL fenestrations, significantly larger than their corresponding structures in PA and CA (2.9 ± 0.1 vs. 2.1 ± 0.1 and 2.46 ± 0.1 μm^2, for MA, PA and CA, respectively) (Figure 1Bc). Myoendothelial projections can only occur within IEL fenestrations. However, holes in IEL do not necessarily guarantee the presence of MEPs at this exact location. Calnexin, an ER-restricted Ca^{2+} binding protein was then used as a surrogate to elucidate the presence of ER, and thence cytoplasmic protrusion within IEL fenestrations. Calnexin fluorescence was analyzed using deconvolved z-stacks of images (Figure 2Ab) with ATIFIsNI. As expected from the IEL fenestrations data, CA appears to have the highest incidence and surface

covered by MEPs (Figure 2Ba & b). Interestingly, mesenteric arteries show the highest efficiency ratio with 65% of IEL fenestrations marked with calnexin fluorescence compared to 32% and 39% for pulmonary and coronary arteries, respectively (Figure 2Bc). However, despite significant variations in IEL fenestration size, surface covered by individual MEPs is similar in all three arterial types (Figure 2Bd).

Basal Ca^{2+} dynamics in arterial endothelium

MEP and IEL fenestration being essential to ER-based endothelial localized Ca^{2+} dynamics, characterization of basal endothelial Ca^{2+} signaling was then sought. Intracellular Ca^{2+} dynamics were recorded in Fluo-4 loaded endothelium in situ as previously (10) from MA, CA and PA. Ca^{2+} waves were similar in all preparations, with very few occurrences over the recording period. Spatially restricted Ca^{2+} increase near IEL fenestrations was identified in all three preparations. Amplitude and kinetics of the Ca^{2+} signals recorded (Table 1) as well as their location are in accordance with the previously described Ca^{2+} pulsars in mesenteric arteries (10). All kinetic parameters evaluated were similar in all three preparations (Table 1). Although the area covered by individual Ca^{2+} pulsars was similar in MA and PA, Ca^{2+} pulsar spreading was significantly smaller in CA. Besides spreading, fundamental properties of Ca^{2+} pulsars in CA and PA matches those in MA, suggesting that a singular type of event was detected in all three vessel types. Pulmonary arteries were however different from mesenteric or coronary arteries in respect to occurrence of Ca2+ pulsars. Although similar populations of Ca^{2+} pulsar active sites were detected in CA and MA, active sites were twice less numerous in PA (12 ± 2 vs. 22 ± 3 and 22 ± 3 for PA, MA and CA, respectively) (Figure 3Ac). In resting conditions (i.e. in the absence of any stimulation), the mean frequency of individual Ca^{2+} pulsar sites was also significantly lower in PA compared to MA and CA (Figure 3Ab). Accordingly, total Ca^{2+} pulsar frequency,

representing the number of Ca^{2+} pulsars recorded within the entire field of view per second, is approximately three- and two-fold higher in MA and CA than in PA (Figure 3Aa).

Smooth muscle-dependent stimulation of Ca^{2+} pulsars

Endothelium-smooth muscle bi-directional communication occurs through MEPs. Myocyte modulation of endothelial Ca^{2+} signaling has been reported following stimulation of α1-adrenergic receptors with phenylephrine (PE) (1, 3). Based on the IEL-MEPs data described above, vascular bed differences in smooth muscle-dependent stimulation of Ca^{2+} pulsars were investigated. Acute exposure of MA to PE (10 μM) significantly increased total Ca^{2+} pulsars frequency in the endothelium (Figure 3Ba), as previously reported (3). A significant increase in total Ca^{2+} pulsar frequency was also observed in CA (203 ± 31% of control) and PA (251 ± 29% of control). Although frequency of PE-induced Ca^{2+} pulsar seems higher in PA, no statistical differences were found between arterial preparations. Similarly, firing rate of individual Ca^{2+} pulsar sites from all arteries were increased by PE (Figure 3Bb); with a slightly more prominent, although not statistically significant, increase in PA. Interestingly, PE exposure recruited about 25-50% de novo sites in all three arteries (144 ± 5%, 149 ± 15% and 127 ± 5% of control for MA, PA and CA, respectively) (Figure 3Bc). Moreover, application of PE did not alter the intrinsic characteristics of Ca^{2+} pulsars as no differences were found in amplitude or kinetics parameters of Ca^{2+} pulsars (Table 2).

Discussion

Endothelial intracellular Ca^{2+} level is critical to vascular tone modulation and a growing body of evidence suggests that Ca^{2+} microdomains are key players in endothelial functions. Building on previous reports of endothelial Ca^{2+} oscillations (7), Ca^{2+} pulsars, a spontaneous IP3R-dependent Ca^{2+} release event uniquely positioned at MEPs were first characterized in mesenteric endothelium from mouse (10). This oscillatory Ca^{2+} signal was shown to hyperpolarize membrane through activation of $K_{Ca}3.1$ channels. These Ca^{2+}- activated K^+ channels, strategically positioned within MEPs are involved in EDHF response. Ca^{2+} pulsars also stimulate nitric oxide production within MEPs (3, 4). In rat cremaster arterioles, Ca^{2+} wavelets were shown to be similar to Ca^{2+} pulsars with respect to the localization but the area covered by the transient Ca^{2+} signal is significantly larger (22). In addition to spontaneous Ca^{2+} release from ER stores, non-propagating Ca^{2+} influx through TRP channels was also identified in endothelium, TRP-sparklets, analogously to Ca^{2+} influx through Cav2.1 channels described in myocytes. So far, two TRP channels have been shown to contribute to local Ca^{2+} influx in endothelial cells, TRPV4 and TRPA1, respectively named TRPV4-sparklets (16, 17) and TRPA1-sparklets (13, 19). Noteworthy, TRPA1-sparklets are specific to the cerebral vasculature (13, 19), strengthening the concept of vascular bed differences in Ca^{2+} microdomains.

Within the skeletal microcirculation, structural differences have been reported according to the arterial diameter (8). IEL overlay of the endothelium-smooth muscle interface was different between large and small arteries. Differences were also noted between skeletal and mesenteric arteries. Accordingly, significant differences were found between the arterial preparations evaluated in this study. Indeed, coronary

circulation has the smallest IEL coverage, and accordingly the highest IEL fenestrations count and total fenestration surface.

On the other hand, pulmonary and mesenteric arteries were similar in number of IEL fenestrations. Interestingly, mesenteric arteries are the one with the largest individual fenestrae. IEL fenestration is a relatively slow process requiring enzymes such as metalloproteinase, and part of the blood vessel wall remodeling. This process can be accelerated in response to several stimuli or by a modification of the arterial environment. For example, aging has been shown to increase fenestrae size and incidence (23) as well as hypercholesterolemia (9). However, in the current study, all vessels were collected from healthy and age-matched animals. Therefore, aging or pathophysiological status would not explain the observed discrepancy between arterial wall anatomies. MEPs, as evidenced by the use of calnexin as surrogate for ER, were also different amongst arteries regardless of similar individual MEP surface. Calnexin, an ER-sequestered protein will help identify IEL fenestrations containing ER, which are assumed to be a cellular projection. However, MEP without ER can be present within an IEL fenestration and would not be detected in the experimental design used. In accordance with the IEL fenestration data, MEP incidence and coverage was found to be larger in coronary arteries. However, the role of such high MEP density in coronary circulation remains to be determined. Interestingly, mesenteric arteries showed the highest MEP-to-IEL fenestration incidental index. Alteration in these relative differences between arterial beds would be expected in pathophysiological conditions. For example, pulmonary hypertension or atherosclerosis are associated with vessel wall remodeling and would result in modification in MEP and IEL fenestrations. These pathophysiological conditions are also associated with progressive endothelial dysfunction. Such loss of endothelial capacity to regulate vascular hemostasis

correlates with Ca^{2+} dyshomeostasis. Ca^{2+} pulsars are spontaneous ER Ca^{2+} release events through endothelial IP3R located at MEPs. The amplitude as well as kinetics parameters of the Ca^{2+} signal are similar in mesenteric, coronary and pulmonary arteries. Moreover, stimulation of Ca^{2+} pulsars via smooth muscle α1-adrenergic receptors with PE had no effect on these parameters. This suggests that Ca^{2+} pulsars are fundamental Ca^{2+} events originating from the ER. It also suggests that the different components regulating Ca^{2+} homeostasis (SERCA pumps, etc.) are similar in these subcellular compartments. On the other hand, populations of active Ca^{2+} pulsar sites are significantly different between arteries in resting conditions. Pulmonary arteries showed significantly smaller population of Ca^{2+} pulsars sites and reduced global Ca^{2+} pulsar frequency. This correlates with a lower MEP occurrence, providing fewer anatomical structures essential to Ca^{2+} pulsars. Recent computational modeling suggests that high incidence of myoendothelial communications is not necessary to achieve optimal effect (5) suggesting that similar endothelial modulation of arterial tone can be obtained with fewer MEPs. However, this subcellular configuration could not explain the lower unitary Ca^{2+} pulsar frequency. This difference in Ca^{2+} pulsars found in pulmonary arteries might be due to experimental conditions. Indeed, given that the pulmonary vasculature is a low resistance/high flow system and that endothelial intracellular Ca^{2+} dynamics are sensitive to shear stress, one would expect that resting conditions for pulmonary vasculature would require higher flow. Therefore, resting Ca^{2+} pulsars dynamics might be similar to coronary or mesenteric endothelium in more physiological conditions. However, in order to compare endothelial Ca^{2+} dynamics with minimal variability in the experimental conditions, all arterial preparations were exposed to the same experimental conditions of flow, temperature and pressure. Further work will be required to establish the impact of flow/shear stress on Ca^{2+} pulsars,

especially in arteries exposed to high flow such as pulmonary arteries or intermittent perfusion like coronary arteries.

Specific stimulation of Ca^{2+} pulsars through smooth muscle α-adrenergic receptors was similar in all arterial beds tested. This is an unexpected finding, especially considering distinct MEP densities in pulmonary or coronary arteries. Indeed, less MEPs found in pulmonary arteries would have been expected to result in a lower PE potency to recruit de novo Ca^{2+} pulsar sites. However, MEPs identification was limited by the use of a ER marker in immunohistochemistry and confocal microscopy. Presence of ER within IEL fenestrations strongly suggests a correlated endothelial/myocyte protrusion, described as MEPs. However, the presence of MEP within IEL fenestrae does not guarantee direct heterocellular communications. Smooth muscle stimulation of Ca^{2+} pulsar requires a direct communication with the endothelium through gap junctions as carbenoxolone, a connexin inhibitor abolish PE-induced stimulation of Ca^{2+} pulsars.

This study establishes that Ca^{2+} pulsars are elementary Ca^{2+} release events highly conserved amongst arteriolar endothelium from different vascular beds. Moreover, MEPs and IEL fenestrations are essential to Ca^{2+} pulsars occurrence and incidence as these anatomical structures correlate with greater populations of Ca^{2+} pulsar sites and unitary frequency. These results suggest that in pathological conditions requiring stronger endothelial modulation of smooth muscle tone, enhanced MEPs and thus Ca^{2+} pulsars might represent an interesting therapeutic avenue.

Acknowledgements

This work was supported by CIHR (J.L.), FRQS (J.L.) and Heart & Stroke Foundation of Canada (J.L.) and through scholarships by FICM (C.C.), Université de Montréal (C.C., N.R.D.). The authors are thankful to Delphine Béziau and Fanny Toussaint for critical review of the manuscript.

Table 1. Basal Ca^{2+} pulsars kinetics in endothelium from mesenteric, pulmonary and coronary arteries

Ca^{2+} pulsar parameter	Mesenteric arteries	Pulmonary arteries	Coronary arteries
Amplitude (F/F_o)	1.30± 0.02	1.30± 0.07	1.33± 0.03
Rise (ms)	363 ± 9	332 ± 53	378 ± 38
Duration (ms)	443 ± 31	445 ± 48	417 ± 35
$t_{1/2}$ (ms)	227 ± 11	249 ± 5	215 ± 12

Kinetic parameters of Ca^{2+} pulsars in Fluo-4 loaded endothelium from mesenteric, pulmonary and coronary arteries in the absence of stimulation. Ca^{2+} pulsars parameters are characterized in terms of peak amplitude measured as F/F_o, rise time measured as upstroke time required for 10-90% of peak amplitude, duration measured as the time between 50% of the signal before and after the peak and half-time decay ($t_{1/2}$) measured as time between the peak and 50% of its amplitude.

Table 2. Effect of phenylephrine on Ca^{2+} pulsars kinetics in endothelium from mesenteric, pulmonary and coronary arteries

Ca^{2+} pulsar parameter	% of control		
	Mesenteric arteries	Pulmonary arteries	Coronary arteries
Amplitude	100 ± 4	98 ± 4	97 ± 1
Rise	101 ± 5	129 ± 17	98 ± 8
Duration	104 ± 4	115 ± 8	114 ± 11
$t_{1/2}$	102 ± 2	99 ± 2	109 ± 6

Kinetic parameters of Ca^{2+} pulsars in Fluo-4 loaded endothelium from mesenteric, pulmonary and coronary arteries in the presence of phenylephrine, a α_1-adrenergic agonist (10 μM). Ca^{2+} pulsars parameters are expressed as % of the values recorded in control conditions, i.e. in the absence of stimulation or agonist. Ca^{2+} pulsars are characterized in terms of peak amplitude measured as F/F_o, rise time measured as upstroke time required for 10-90% of peak amplitude, duration measured as the time between 50% of the signal before and after the peak and half-time decay ($t_{1/2}$) measured as time between the peak and 50% of its amplitude.

Figure Legends

Figure 1. *Internal elastic lamina fenestration of mesenteric, pulmonary and coronary arteries from mice*

A. Typical image of autofluorescent fenestrated internal elastic laminae (IEL, green) from mesenteric (MA), pulmonary (PA) and coronary (CA) arteries. Bar = 10 µm **B.** Bar graph summarizing IEL fenestration metrics in mesenteric (MA, white, n=6), pulmonary (PA, green, n=7) and coronary (CA, blue, n=9) arteries. *$p < 0.05$

Figure 2. *Myoendothelial projections within IEL fenestrations of mesenteric, pulmonary and coronary arteries*

Aa. Typical images of immunostaining for calnexin (red), a protein sequestered in the endoplasmic reticulum at a focal plane corresponding to the IEL (green) in mesenteric (MA), pulmonary (PA) and coronary (CA) arteries. Bar = 10 µm **Ab.** Cropped views from z-stacks of images as in (a) showing calnexin staining throughout IEL fenestrations. **Ba-d**. Bar graphs reporting calnexin densities analysis within IEL fenestrations from mesenteric (MA, white, n=6), pulmonary (PA, green, n=7) and coronary (CA, blue, n=9) arteries. *$p < 0.05$

Figure 3. *Comparative endothelial Ca^{2+} pulsar activities in freshly isolated mesenteric, pulmonary and coronary arteries in resting conditions and in the presence of phenylephrine.*

A. Basal Ca^{2+} pulsar activity monitored with high-speed confocal imaging in mesenteric (MA, white, n=5), pulmonary (PA, green, n=4) and coronary (CA, blue, n=5) arteries and expressed as **(a)** global Ca^{2+} pulsar frequency, **(b)** individual Ca^{2+} pulsar frequency per site and **(c)** number of active Ca^{2+} pulsar sites in the absence of stimulation. *$p < 0.05$ **B.** Endothelial Ca^{2+} pulsars stimulation by phenylephrine in mesenteric (MA, white, n=5), pulmonary (PA, green, n=4) and coronary (CA, blue, n=5) arteries and expressed as % of change from control (absence of stimulation) of **(a)** global Ca^{2+} pulsar frequency, **(b)** individual Ca^{2+} pulsar frequency per site and **(c)** number of active Ca^{2+} pulsar sites. *$p < 0.05$

References

1. **Bagher P**, **Beleznai T**, **Kansui Y**, **Mitchell R**, **Garland CJ**, **Dora KA**. Low intravascular pressure activates endothelial cell TRPV4 channels, local Ca2+ events, and IKCa channels, reducing arteriolar tone. *Proceedings of the National Academy of Sciences* 109: 18174–18179, 2012.

2. **Béziau DM**, **Toussaint F**, **Blanchette A**, **Dayeh NR**, **Charbel C**, **Tardif J-C**, **Dupuis J**, **Ledoux J**. Expression of Phosphoinositide-Specific Phospholipase C Isoforms in Native Endothelial Cells. *PLoS ONE* 10: e0123769, 2015.

3. **Charbel C**, **Toussaint F**, **Béziau DM**, **Gillis M-A**, **Blanchette A**, **Mamarbachi M**, **Bousette N**, **Comtois P**, **Ledoux J**, **ledoux**. Functional activation of endothelial CaMKII by Ca^{2+} microdomains. *Proceedings of the National Academy of Sciences*.

4. **Charbel C**, **Toussaint F**, **Gillis M-A**, **Blanchette A**, **Comtois P**, **Ledoux J**. New insights on endothelial Ca^{2+} microdomains and CaMKII in Angiotensin II-induced hypertension. *Hypertension*.

5. **Hald BO**, **Jacobsen JCB**, **SANDOW SL**, **Holstein Rathlou NH**, **Welsh DG**. Less is more: minimal expression of myoendothelial gap junctions optimizes cell-cell communication in virtual arterioles. *The Journal of Physiology* 592: 3243–3255, 2014.

6. **Isakson BE**. Localized expression of an Ins(1,4,5)P3 receptor at the myoendothelial junction selectively regulates heterocellular Ca2+ communication. *Journal of Cell Science* 121: 3664–3673, 2008.

7. **Kansui Y**, **Garland CJ**, **Dora KA**. Enhanced spontaneous Ca2+ events in endothelial cells reflect signalling through myoendothelial gap junctions in pressurized mesenteric arteries. *Cell Calcium* 44: 135–146, 2008.

8. **Kirby BS**, **Bruhl A**, **Sullivan MN**, **Francis M**, **Dinenno FA**, **Earley S**. Robust internal elastic lamina fenestration in skeletal muscle arteries. *PLoS ONE* 8: e54849, 2013.

9. **Kwon HM**, **Sangiorgi G**, **Spagnoli LG**, **Miyauchi K**, **Holmes DR**, **Schwartz RS**, **Lerman A**. Experimental hypercholesterolemia induces ultrastructural changes in the internal elastic lamina of porcine coronary arteries. *Atherosclerosis* 139: 283–289, 1998.

10. **Ledoux J**, **Taylor MS**, **Bonev AD**, **Hannah RM**, **Solodushko V**, **Shui B**, **Tallini Y**, **Kotlikoff MI**, **Nelson MT**. Functional architecture of inositol 1,4,5-trisphosphate signaling in restricted spaces of myoendothelial projections. *Proceedings of the National Academy of Sciences* 105: 9627–9632, 2008.

11. **Lückhoff A**, **Busse R**. Increased free calcium in endothelial cells under stimulation with adenine nucleotides. *J Cell Physiol* 126: 414–420, 1986.

12. **Morgan-Boyd R**, **Stewart JM**, **Vavrek RJ**, **Hassid A**. Effects of bradykinin and angiotensin II on intracellular Ca2+ dynamics in endothelial cells. *Am J Physiol* 253: C588–98, 1987.

13. **Qian X**, **Francis M**, **Solodushko V**, **Earley S**, **Taylor MS**. Recruitment of dynamic endothelial Ca2+ signals by the TRPA1 channel activator AITC in rat cerebral arteries. *Microcirculation* 20: 138–148, 2013.

14. **SANDOW SL**, **Neylon CB**, **Chen MX**, **Garland CJ**. Spatial separation of endothelial small- and intermediate-conductance calcium-activated potassium channels (KCa) and connexins: possible relationship to vasodilator function? *Journal of Anatomy* 209: 689–698, 2006.

15. **Si H**. Impaired Endothelium-Derived Hyperpolarizing Factor-Mediated Dilations and Increased Blood Pressure in Mice Deficient of the Intermediate-Conductance Ca2+-Activated K+ Channel. *Circulation Research* 99: 537–544, 2006.

16. **Sonkusare SK**, **Bonev AD**, **Ledoux J**, **Liedtke W**, **Kotlikoff MI**, **Heppner TJ**, **Hill-Eubanks DC**, **Nelson MT**. Elementary Ca2+ Signals Through Endothelial TRPV4 Channels Regulate Vascular Function. *Science* 336: 597–601, 2012.

17. **Sonkusare SK**, **Dalsgaard T**, **Bonev AD**, **Hill-Eubanks DC**, **Kotlikoff MI**, **Scott JD**, **Santana LF**, **Nelson MT**. AKAP150-dependent cooperative TRPV4 channel gating is central to endothelium-dependent vasodilation and is disrupted in hypertension. *Science Signaling* 7: ra66–ra66, 2014.

18. **Straub AC**, **Billaud M**, **Johnstone SR**, **Best AK**, **Yemen S**, **Dwyer ST**, **Looft-Wilson R**, **Lysiak JJ**, **Gaston B**, **Palmer L**, **Isakson BE**. Compartmentalized connexin 43 s-nitrosylation/denitrosylation regulates heterocellular communication in the vessel wall. *Arteriosclerosis, Thrombosis, and Vascular Biology* 31: 399–407, 2011.

19. **Sullivan MN**, **Gonzales AL**, **Pires PW**, **Bruhl A**, **Leo MD**, **Li W**, **Oulidi A**, **Boop FA**, **Feng Y**, **Jaggar JH**, **Welsh DG**, **Earley S**. Localized TRPA1 channel Ca2+ signals stimulated by reactive oxygen species promote cerebral artery dilation. *Science Signaling* 8: ra2–ra2, 2015.

20. **Taylor MS**. Altered Expression of Small-Conductance Ca2+-Activated K+ (SK3) Channels Modulates Arterial Tone and Blood Pressure. *Circulation Research* 93: 124–131, 2003.

21. **Toussaint F**, **Charbel C**, **Blanchette A**, **Ledoux J**. CaMKII regulates intracellular Ca^{2+} dynamics in native endothelial cells. *Cell Calcium*.

22. **Tran CHT**, **Kurjiaka D**, **Welsh DG**. Emerging trend in second messenger communication and myoendothelial feedback. *Front Physio* 5, 2014.

23. **Wong LC**, **Langille BL**. Developmental remodeling of the internal elastic lamina of rabbit arteries: effect of blood flow. *Circulation Research* 78: 799–805, 1996.

Figure 1

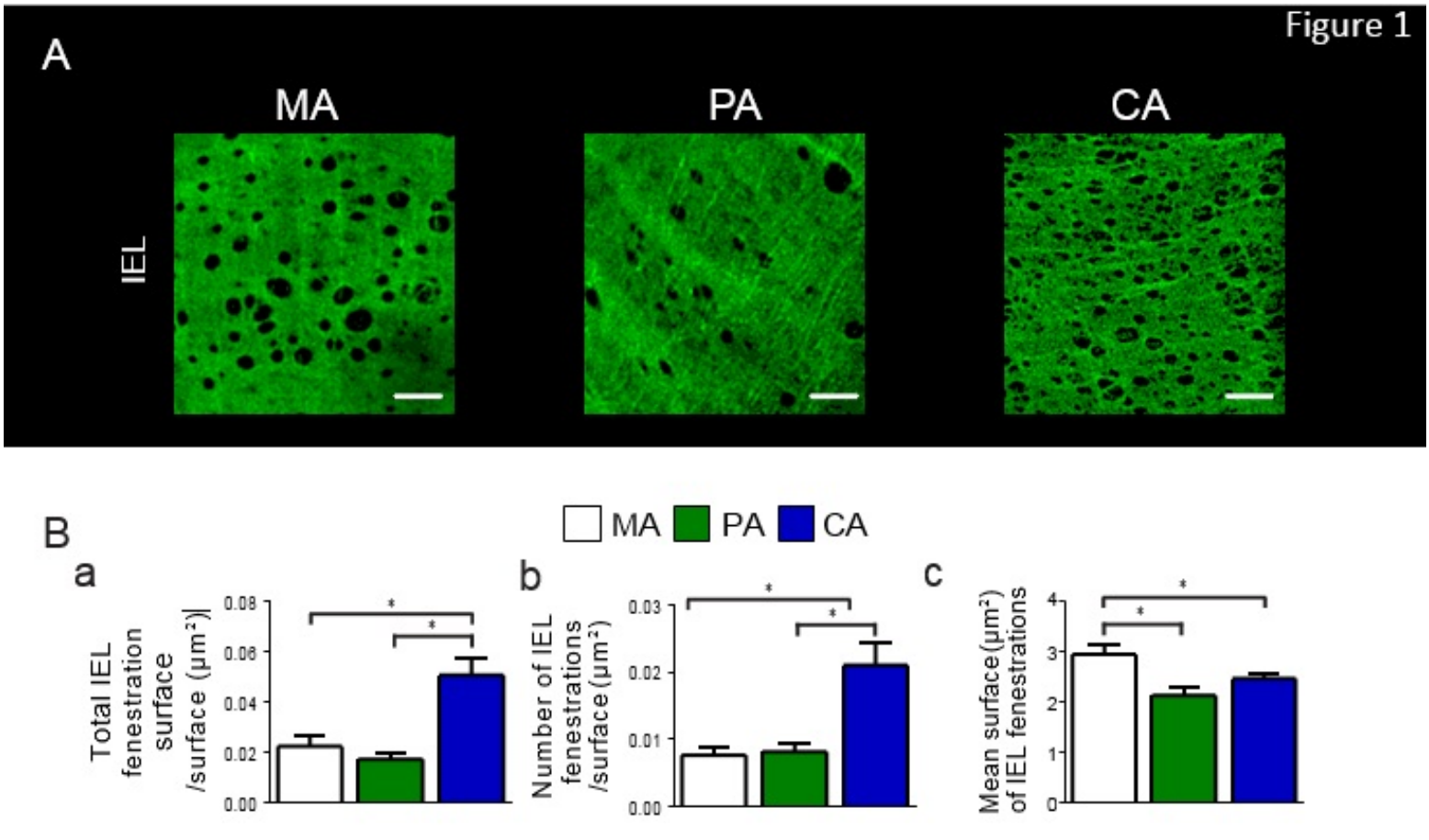
A
MA
PA
CA
IEL
B
MA
PA
CA
a
Total IEL fenestration surface /surface (µm²)
0.08
0.06
0.04
0.02
0.00
b
Number of IEL fenestrations /surface (µm²)
0.03
0.02
0.01
0.00
c
Mean surface (µm²) of IEL fenestrations
4
3
2
1
0
*

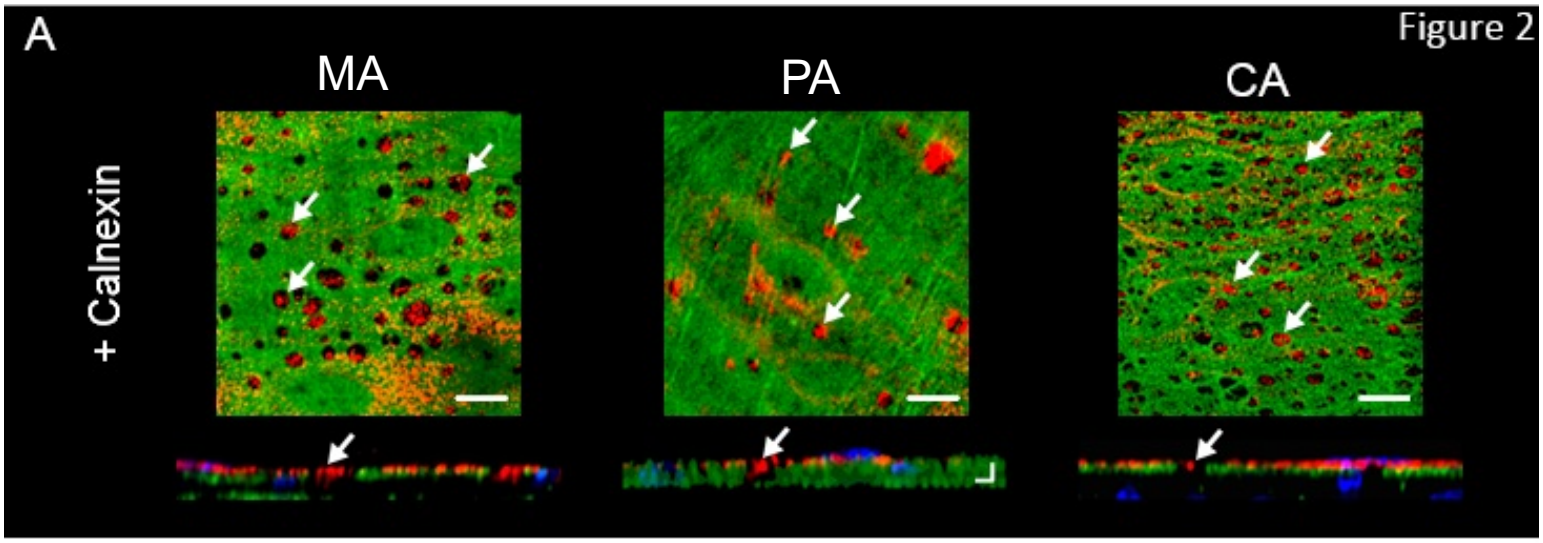
A
Figure 2
MA
PA
CA
+ Calnexin

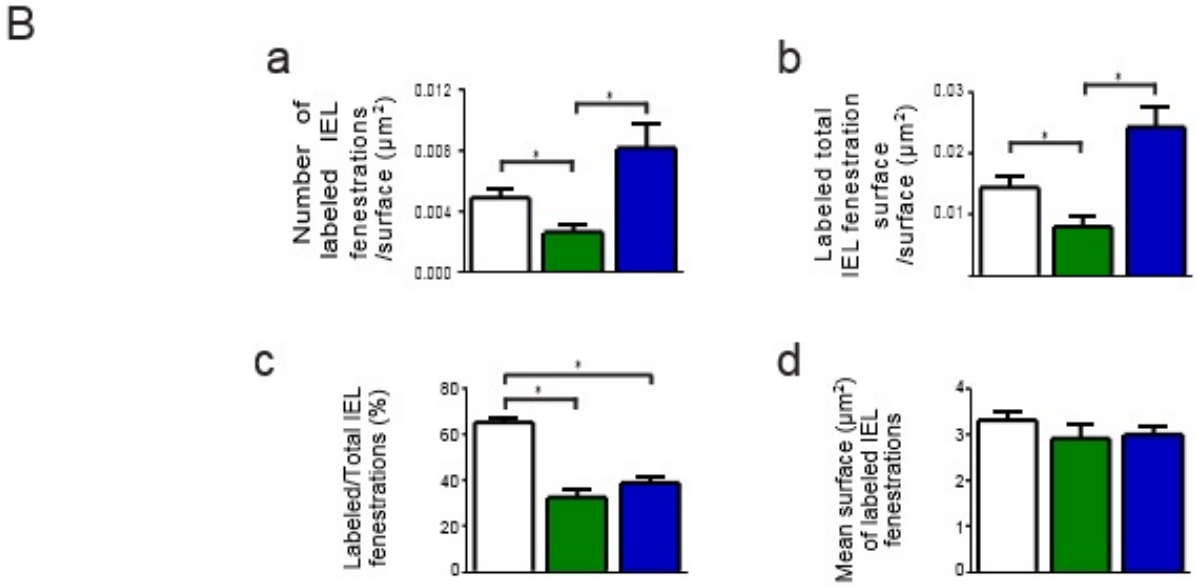
B
a
Number of labeled IEL fenestrations /surface (µm²)
0.012
0.008
0.004
0.000
b
Labeled total IEL fenestration surface /surface (µm²)
0.03
0.02
0.01
c
Labeled/Total IEL fenestrations (%)
80
60
40
20
0
d
Mean surface (µm²) of labeled IEL fenestrations
4
3
2
1
0

Figure 3

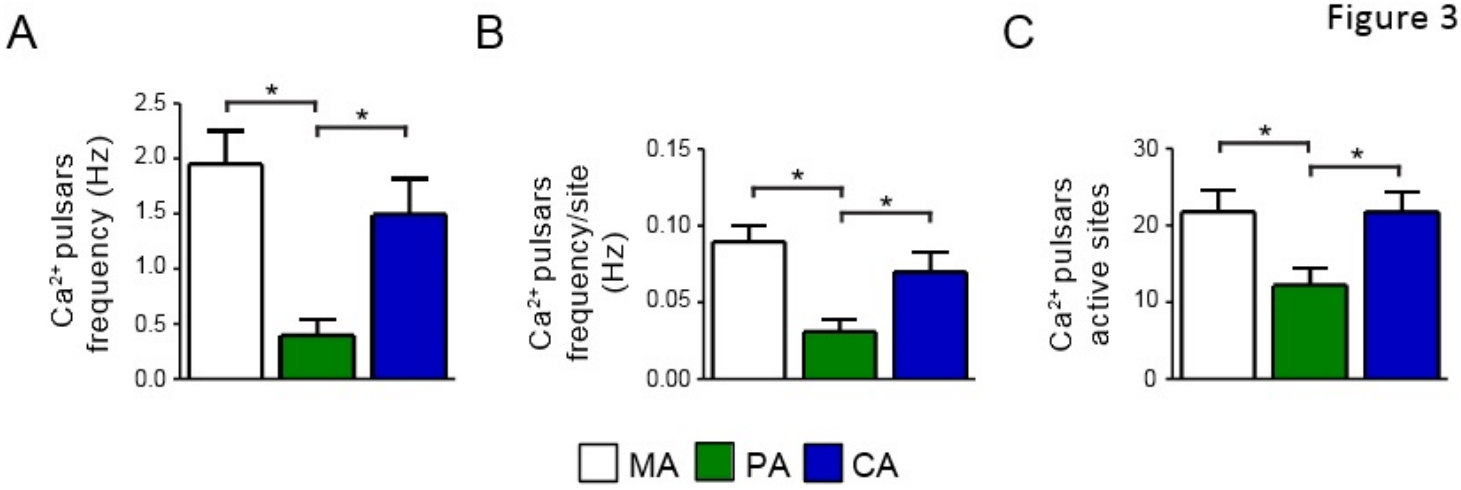
A
B
C
Ca2+ pulsars frequency (Hz)
Ca2+ pulsars frequency/site (Hz)
Ca2+ pulsars active sites
MA
PA
CA

+ PE

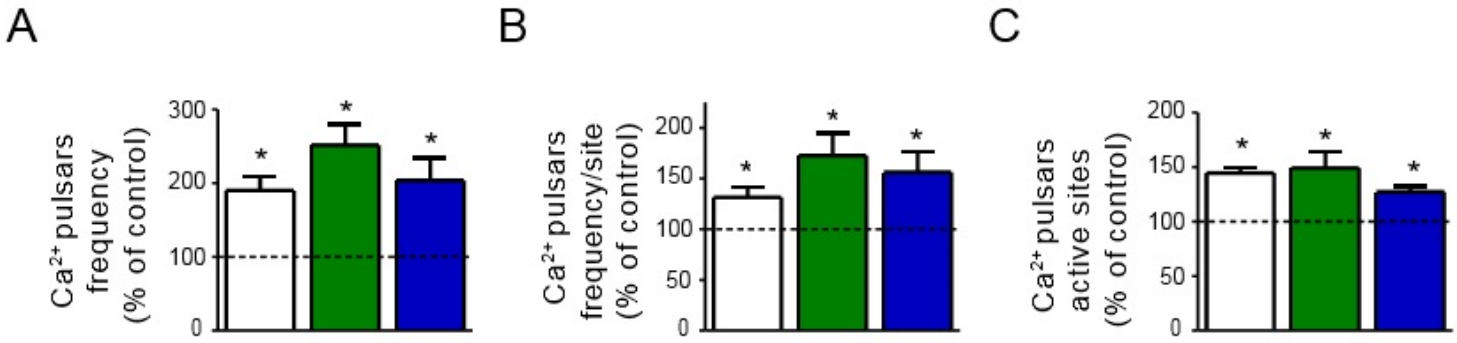
A
B
C
Ca2+ pulsars frequency (% of control)
Ca2+ pulsars frequency/site (% of control)
Ca2+ pulsars active sites (% of control)

Involvement of endothelial TRPV4 in alterations of calcium pulsars in pulmonary hypertension associated with left heart failure

Dayeh R. Nour[1,2], Shi Yanfen[1], Tardif Jean-Claude[1,2], Ledoux Jonathan[1,2,3], *Dupuis Jocelyn[1,2].

This manuscript is in preparation

Affiliations:

[1] Research Center, Montreal Heart Institute, Quebec, Canada
[2] Departments of Medicine and [3] Physiology, Université de Montréal, Quebec, Canada

*Corresponding author

Authors' contributions:

Experimental design: ND, JL, JD

Experimentation: ND

Data collection and analysis: ND

Echocardiography performance and analysis: YS, JCT

Manuscript writing: ND

Final revision of the manuscript: ND, JL, JD

Abstract:

Background- Pulmonary hypertension (PH)-associated pathophysiological mechanisms underlying pulmonary vascular alterations in left heart disease (LHD) are poorly explored. A better understanding of the cellular and molecular mechanisms is needed for the development of effective therapies.

Methods and results- We utilized our previously developed mouse model of PH-LHD in GCaMP-2 mice expressing an endothelial fluorescent Ca^{2+} biosensor. We isolated small pulmonary arteries (PAs) of circa 60-100 μM diameter in order to study Ca^{2+} pulsars using real time confocal microscopy. We identified Ca^{2+} pulsars in non-stimulated pulmonary endothelium and studied their dynamic properties, kinetics, and spatial spread in the setting of PH. PAs from control, sham and PH mice were exposed to endothelial (acetylcholine) and smooth muscle (phenylephrine) stimulation in order to assess vascular reactivity. In order to determine the participation of TRPV4 channels in the regulation of Ca^{2+} pulsars, we performed western blot, PCR and immunohistochemistry for TRPV4 expression in lung tissue as well as isolated PAs and exposed PAs from all three groups of mice to HC067047, a specific TRPV4 inhibitor, and GSK1016790A, a specific TRPV4 agonist. Unlike the control and sham groups, endothelial and smooth muscle stimulation did not seem to elicit responses in the PH group. Incubation of unstimulated PAs with HC067047 did not affect pulsar activity showing that TRPV4 did not exert basal influence on pulsars. Nevertheless, a subsequent addition of GSK1016790A inhibited any increase in local activity. Additionally, exposing PAs to GSK1016790A caused a rise in pulsar activity, as well as an induction of new sites in the control and sham groups. However, the agonist had little to no effect in PH-LHD.

Conclusion- Ca^{2+} pulsars activity is altered in group II-PH. Deregulated TRPV4 signaling may contribute to PH-related vascular response alterations. This work offers an innovative approach to study PH-LHD and enhances our understanding of Ca^{2+} dyshomeostasis occurring in a clinically relevant model.

Introduction

Heart failure is the most frequent cause of pulmonary hypertension (PH) (group II) [1]. Group II-PH ultimately leads to right ventricular hypertrophy and is associated with high morbidity and mortality. Alterations in vasodilatory responses lead to the increased pulmonary vascular pressure (PVP) observed in PH [2], resulting in an elevated vascular tone and consequent vascular remodelling [3]. Endothelial dysfunction is an initiator of vascular dysregulations [4,5,6] and is associated with alterations in calcium (Ca^{2+}) homeostasis [7,8].

Ca^{2+} dynamics have recently been the subject of investigations in the context of heart diseases and related complications. Amongst a number of different types of Ca^{2+} dynamics, several local oscillatory events have been identified. Ca^{2+} pulsars are local endothelial Ca^{2+} signals whose activity is finely regulated by IP_3 and Ca^{2+} [9]. In mesenteric arteries, Ca^{2+} pulsars were shown to induce endothelium-dependent relaxation of vascular smooth muscle cells [9]. Up until now, the regulatory mechanisms of Ca^{2+} pulsars remain to be uncovered. The spatio-temporal characteristics of these dynamics suggest that they could play a role in the control of pulmonary vascular tone, potentially involving more transmembrane ion channels, as well as regulatory proteins. Transient receptor potential vanilloid 4 (TRPV4) channels are non-selective mechanosensitive cation channels broadly expressed in a number of tissues [10]. Activation of TRPV4 channels allows Ca^{2+} entry into the cell [11]. In pulmonary artery smooth muscle cells, activation of TRPV4 leads to contraction [12]. TRPV4 deficient mice present unusual phenotypes including compromised vascular endothelial function [13]. TRPV4 is implicated in permeability increase during lung injury and blocking of TRPV4 prevents heart failure-induced pulmonary edema [14,

15,16,17]. Endothelial TRPV4 potential channelopathy in group II-PH is yet to be confirmed.

Endothelial Ca^{2+}- related pathophysiological mechanisms modulating pulmonary vascular tone and leading to the development of group II-PH are poorly defined. This study aimed to identify and characterize alterations of pulmonary endothelial Ca^{2+} pulsars in a mouse model of PH-LHD and to reveal the implication of TRPV4 channels in their deregulation.

Materials and methods:

The animal study was performed according to procedures approved by the ethics committee for animal research of the Montreal Heart Institute.

Development of the animal model:

Surgical procedures

In total 24 GCAMP-2 mice that express a Ca^{2+} biosensor exclusive to the endothelium (body weight 21-23 g) were used in this study. The PH group consisted of 12 mice that had underwent lateral thoracotomy followed by ligation of the left anterior descending coronary artery causing myocardial infarction (MI). The sham group underwent the same procedure without ligation of the artery.

Control group

The control group consisted of 15 GCaMP-2 mice that did not receive any surgical intervention.

Assessment of the presence of PH

We had previously validated the use of echocardiography as a non-invasive method in the determination of the presence of PH. In this study, mice that have developed PH were chosen according to parameters we had previously described [18] (supplemental table 1 and supplemental figure 1).

High-speed confocal imaging:

Small pulmonary arteries were isolated and cut longitudinally and pinned on a silicone block in an *en face* preparation exposing endothelial cells. Ca^{2+} activity was recorded using a Revolution Andor confocal system (Andor Technology). Images were acquired at ≈15 frames/sec (ex/em 488/510) using Andor iQ 2.8 software (Andor Technology) with an iXon EMCCD camera on an upright Nikon microscope and a 60X, water-dipping objective (NA 1.0). All experiments were performed at 37°C in a physiological salt solution (PSS; 119 mM NaCl, 4.7 mM KCl, 24 mM $NaHCO_3$, 1.2 mM KH_2PO_4, 1.2 mM $MgCl_2$, 11 mM Glucose and 1.5 mM $CaCl_2$). Endothelial Ca^{2+} imaging was performed on pulmonary arteries taken from control mice, Sham mice, and mice with PH.

Confocal imaging analysis of the preparations was carried out using SparkAn software (A. Bonev, UVM) by measuring the fluorescence intensity (F) relative to baseline (F_0). Analysis of Ca^{2+} pulsars fractional fluorescence (F/F_0) was performed using a 5 × 5 pixel box region of interest (ROI) positioned at the peak pulsar amplitude.

Every set of experiments (compound added) was performed on 4 to 5 arteries from a minimum of 2 mice.

Immunohistochemistry:

Pulmonary artery preparations were cut open and mounted endothelium facing up on silicone blocks, fixed with 4% formaldehyde for 20 minutes, permeabilized with 0.2 % Triton X-100, blocked with 4% NDS and incubated with rabbit polyclonal primary antibody (anti-TRPV4, ab39260, Abcam, USA) overnight at 4ºC. Arteries were washed and incubated with florescent secondary anti-goat antibody (Alexa Fluor 555 Life Technologies) for 1 hour at room temperature. Immunofluorescence was detected using a Zeiss LSM 510 system confocal microscope. Auto fluorescence of the internal elastic lamina was assessed at excitation and emission wavelengths 488 nm and 520 nm and DAPI staining at excitation and emission wavelengths 405 nm and 460 nm.

Western blot analysis:

Lung tissue lysates were collected from sham and PH mice. Protein extraction was performed and samples were concentrated using Amicon Ultra-0.5 centrifugal filter devices with a cutoff value of 10K (Millipore, USA). Protein concentration was determined according to standard protocol using the Lowry assay, and bovine serum albumin (BSA) as the standard. Detection of TRPV4 was performed using Rabbit polyclonal primary antibody (anti-TRPV4, ab39260, Abcam, USA).

Polymerase chain reaction:

Total RNA from lung tissue as well as isolated PAs was extracted using RNeasy Micro kits (Qiagen). RNA purity and concentration were assessed using a Nanodrop spectrophotometer, followed by reverse transcription using iScript kits (Bio-Rad, California, USA) according to the manufacturer's instructions. TRPV4 primers, as shown in the present table were used. Following denaturation at 94°C, 45 cycles of DNA amplification were performed using Taq DNA polymerase (Invitrogen,

California, USA) at 94°C for 45 sec, 55°C for 30 sec and 72°C for 90 sec. A final extension step was performed for 10 min at 72°C. Electrophoresis of amplicons on 3% ethidium bromide stained agarose gels was carried out. PCR product sizes were estimated using the Gene ruler low range DNA ladder (Thermoscientific, Massachusetts, USA) and compared to theoretical amplicon size.

TRPV4	
Forward (5' - 3')	ATGAGATGCTGGCTGTAGAGC
Reverse (5' - 3')	GAGGTCATCACGCTCTTCACA

Table 1: TRPV4 primers

Statistical analysis.

Statistical analysis was performed using GraphPad Prism 7 software. Significant values from t-tests are presented as mean± SE and were considered at $p<0.05$. For grouped analysis ANOVA test was performed, followed, when a significant group interaction was found, by multiple comparisons with Tukey's posthoc analysis.

Results:

Characterization of spontaneous Ca^{2+} pulsars in the pulmonary endothelium

Ca^{2+} transients, similar to those previously described in mesenteric arteries, were found in non-stimulated pulmonary endothelium. We have compared the characteristics of these events (localization throughout endothelial cells, amplitude, duration, half time of decay $t_{1/2,}$ and spread), and found that those events are similar to Ca^{2+} pulsars previously characterized in third order mesenteric arteries (Figure 1A and 1B). In fact, pulmonary pulsars are located in proximity to IEL holes ($2.88 \pm 0.11\ \mu m$), and have an average amplitude of 1.26 ± 0.009, a rise time of $302 \pm 15\ ms$, a duration of 397 ± 17

ms, $t_{1/2}$ of *206 ± 10 ms*, an average frequency of *0.023 ± 0.003*, and an average spatial spread of *15.64 ± 1.5 μm^2* (table 2).

Ca^{2+} pulsars response to endothelial and smooth muscle cell stimulation in control PAs

Following the addition of acetylcholine (10 μM), a significant increase in total frequency was observed accompanied by the appearance of newly active pulsar sites (Figure 1C). No changes were seen in amplitude, rise time, duration, and $T_{1/2}$ following the application of acetylcholine (supplemental table 2).

Adding phenylephrine (10 μM) led to a significant increase in total pulsars frequency per field. A significant increase in the number of sites was observed as well (Figure 1C). No changes in amplitude, rise time, duration, and $T_{1/2}$ were observed (supplemental table 3).

Effect of TRPV4 on Ca^{2+} pulsars activity in control PAs

TRPV4 protein is expressed in lung tissue as well as in isolated small PAs on the protein and mRNA level (Figure 2A). Additionally, immunofluorescence analysis demonstrates TRPV4 expression in ECs of isolated PAs in co-localization with holes of the IEL (Figure 2B). Immunofluorescence staining for Calnexin, a protein found in the endoplasmic reticulum demonstrates its presence in IEL holes through which MEPs pass (Figure 2B).

Activation of TRPV4 with the synthetic agonist GSK1016790A (10 nM and 100 nM) led to a dose-dependent increase in the total frequency and frequency per site of Ca^{2+} pulsars, with the recruitment of new active sites (Figure 2C). No changes were observed in the amplitude, rise time, or durations of these Ca^{2+} events.

Basal pulsars activity in non-stimulated PAs from sham and PH mice

Basal pulsars activity was found to be higher in PAs of PH mice compared to the sham group. Analysis of pulsars characteristics and kinetics revealed that Ca^{2+} transients in PAs of PH mice had higher frequencies, frequencies per sites, compared to pulsars from sham PAs (Figure 3A). When compared to non-stimulated PA from control mice that had not received a thoracotomy, pulsars from sham and PH PAs displayed similar amplitudes and spread values. However, pulsars of PH arteries had longer duration (table 3).

Ca^{2+} pulsars response to stimulation in PAs from sham and PH mice

Addition of acetylcholine (10μM) in sham PAs, lead to an increase in the total frequency of pulsars. This effect was not significant in PAs from mice with PH. Recruitment of new sites was significant in the sham group following the addition of acetylcholine unlike the effect observed in the PH group (figure 3C). The addition of acetylcholine did not seem to have an effect on amplitude, duration, rise time, and $T_{1/2}$ of pulsars in either group (supplemental table 4).

Following the addition of phenylephrine (10μM), a significant increase in total pulsar frequency was observed accompanied by a significant increase in the frequency per site and an elevation in the number of pulsar sites in the sham group. This effect was not observed in PAs from the PH group (figure 3C). PAs from both groups did not display alterations in pulsars amplitude and kinetics following the addition of phenylephrine. (supplemental table 5).

Effect of TRPV4 activation on Ca^{2+} pulsars activity in PAs from sham and PH mice

Western blot analysis demonstrated the expression of TRPV4 proteins within lungs of sham and PH mice with a higher tissue expression in the PH group. Additionally, immunofluorescence analysis showed the expression of TRPV4 in the lungs as well as pulmonary endothelium within proximity and around IEL holes of sham and PH mice. The presence of MEPs through calnexin staining was also shown in arteries of both groups (figure 4A and 4B).

Following the addition of TRPV4 agonist GSK1016790A (10 nM and 100 nM), a dose-dependent increase in total frequency per field was observed in PAs from the sham group. This increase was accompanied by the appearance of new pulsar sites and an elevation in pulsars' spread area. This effect was not observed in PAs from the PH group. Additionally, addition of GSK1016790A lead to the recruitment of new sites in PAs from the sham group; an effect that was not observed in PAs of the PH group (figure 4C). No changes in the amplitude, rise time, duration, and $t_{1/2}$ of pulsars was observed in either group following stimulation with the TRPV4 agonist (supplemental table 6).

Effect of TRPV4 on basal Ca^{2+} pulsars activity in PAs from sham and PH mice

The incubation of unstimulated PAs with TRPV4 specific inhibitor HC067047 did not affect pulsar characteristics. Nevertheless, addition of GSK1016790A at 10 nM following incubation of PAs with HC067047 inhibited any increase in pulsars activity as well as the appearance of new pulsar sites in both groups (figure 5).

Discussion

Localized Ca^{2+} has the advantage of modulating Ca^{2+} sensitive signaling pathways in defined regions of the cell without affecting other cellular functions. Spontaneous Ca^{2+} transients within endothelial cells have been proposed to be involved in endothelial control of vascular relaxation through their participation in endothelium-derived hyperpolarization [9] [19] and were suggested to exert their effect on Ca^{2+}-activated K^+ channels (K_{Ca}) [20, 21]. Additionally, TRPV4 channels have been linked to endothelium-dependent vasodilatory responses [19] and are therefore implicated in the regulation of vascular tone [22].

In this study, we have addressed the question of whether pulmonary Ca^{2+} pulsars are influenced by TRPV4 activation and explored TRPV4-related pulsar deregulation in PH associated with heart failure with reduced ejection fraction (HFrEF). Our results demonstrate that Ca^{2+} pulsars within the intact pulmonary endothelium are increased upon endothelial and smooth muscle stimulation. Additionally, we show that stimulation of PAs with the TRPV4 channel agonist GSK1016790A, led to a noticeable increase in pulsar activity accompanied by the appearing of new pulsar sites. We then sought to evaluate pulsar activity in the setting of PH-LHD; in non-stimulated PAs, mice with PH presented with a noticeable higher local Ca^{2+} activity that can be attributed to a protective mechanism involving local transients including pulsars previously described in other vascular beds [23, 24]. However, PAs from mice with PH presented with decreased pulsar responses to both endothelial and smooth muscle stimulation, thus showing endothelial dysfunction and deregulation in vascular reactivity. The absence of Ca^{2+} pulsars' response to smooth muscle α-adrenergic receptors stimulation in arteries from the PH-LHD group could suggest that these arteries present with disturbed endothelial-smooth muscle communication through

myoendothelial projections. We have shown calnexin staining through immunofluorescence. Calnexin, a protein found in the endoplasmic reticulum is an indicator of the presence of myoendothelial projections. However, due to technical limitations, we were unable to compare the presence of projections between both groups. Nevertheless, is it imperative that myoendothelial projections density through calnexin staining, be evaluated and compared.

We have demonstrated an elevated TRPV4 protein expression within lung tissue of mice with PH-LHD. This finding is in concordance with other studies that have indicated upregulated TRPV4 pulmonary expression in the context of LHD associated with myofibroblasts differentiation and pulmonary fibrosis [25]. However, the significantly diminished responsiveness of TRPV4 channels to stimulation by GSK1016790A in PH arteries clearly underlines a role for those channels in the initiation and/or progression of pulmonary vascular reactivity alterations. Application of the TRPV4 specific inhibitor HC067047 demonstrated that TRPV4 channels did not exert a basal effect on pulsars and completely abolished pulsars increase following the addition of GSK1016790A. Consistent with our findings, previous studies have shown that the lung endothelial Ca^{2+} response to hydrostatic stress was mediated by activation of TRPV4 and abolished in the setting of congestive heart failure. Additionally, forgoing work had shown that in congestive heart failure activation of TRPV4 in lung capillaries with the specific agonist 4α-PDD, did not elicit an increase in Ca^{2+} responses [8]. This observation was associated with decreased TRPV4 expression within ECs.

Here, we show new evidence that endothelial TRPV4 unresponsiveness in PH-LHD can exhibit through Ca^{2+} pulsars. However, further evaluation of TRPV4 pulmonary endothelial expression in PH-LHD is indeed required.

A sustained pulmonary pressure elevation accompanied by Ca^{2+}

dyshomeostasis, ultimately leads to consequent vascular tone alterations and increased vascular resistance. In this study, TRPV4 channels are shown to be influencers of pulmonary vascular tone through their effect of Ca^{2+} pulsars. This effect can manifest through a potential subsequent influence on K_{Ca} channels. In fact, disturbed endothelium-dependent hyperpolarization through K_{Ca} channels was found to lead to hypertension [26]. Additionally, TRPV4-related Ca^{2+} entry was found to activate K_{Ca} [27]. Further investigation around that area in the context of PH-LHD is indeed needed.

Our current results suggest that in group II-PH, TRPV4 channel-related pulsar malfunction is associated with endothelial dysfunction potentially negatively influencing the exertion of its effects on endothelial hyperpolarization through K_{Ca} channels. Additionally, our findings suggest a potential alteration in myoendothelial communication that needs to be further investigated. The fine-tuning of pulsars pathway seems to be altered in the setting of PH-LHD.

Ca^{2+} pulsar parameter	Value
Amplitude, F/F0	1.26 ± 0.009
Rise time, ms	302 ± 15
Duration, ms	397 ± 17
t1/2, ms	206 ± 10
Frequency, Hz	0.023 ± 0.003
Spread area, µm²	15.64 ± 1.5
Distance from IEL holes, µm	2.8 ± 0.11

Table 2. Characterization of pulmonary Ca^{2+} pulsars parameters and kinetics in non-stimulated murine pulmonary arteries in terms of peak amplitude, rise time as measured during 10 –90% of the signal, duration as measured from 50% of the signal before and after the peak, half-life of decay ($t_{1/2}$), and spread (n=6 arteries).

Ca^{2+} pulsar parameter	SHAM	PH	p value
Amplitude, F/F0	1.21 ± 0.004	1.21 ± 0.003	ns
Rise time, ms	295 ± 10	330 ± 10	ns
Duration, ms	395 ± 9	422 ± 7	< 0.05
t1/2, ms	207 ± 6	216 ± 5	ns
Spread area, µm²	14.89 ± 1	14.34 ± 1.6	ns

Table 3. Basal pulsars' kinetics and descriptive parameters in non-stimulated pulmonary arteries of sham and PH mice in terms of peak amplitude, rise time as measured during 10 –90% of the signal, duration as measured from 50% of the signal before and after the peak, half-life of decay ($t_{1/2}$), and spread. Comparison of both groups was done through unpaired t-test (n=20 arteries).

References

1. Simonneau, G., et al., *Updated clinical classification of pulmonary hypertension.* J Am Coll Cardiol, 2013. **62**(25 Suppl): p. D34-41.
2. Guazzi, M. and B.A. Borlaug, *Pulmonary hypertension due to left heart disease.* Circulation, 2012. **126**(8): p. 975-90.
3. Delgado, J.F., et al., *Pulmonary vascular remodeling in pulmonary hypertension due to chronic heart failure.* Eur J Heart Fail, 2005. **7**(6): p. 1011-6.
4. Sandoo, A., et al., *The endothelium and its role in regulating vascular tone.* Open Cardiovasc Med J, 2010. **4**: p. 302-12.
5. Moraes, D.L., W.S. Colucci, and M.M. Givertz, *Secondary pulmonary hypertension in chronic heart failure: the role of the endothelium in pathophysiology and management.* Circulation, 2000. **102**(14): p. 1718-23.
6. Rajendran, P., et al., *The vascular endothelium and human diseases.* Int J Biol Sci, 2013. **9**(10): p. 1057-69.
7. House, S.J., et al., *The non-excitable smooth muscle: calcium signaling and phenotypic switching during vascular disease.* Pflugers Arch, 2008. **456**(5): p. 769-85.
8. Kerem, A., et al., *Lung endothelial dysfunction in congestive heart failure: role of impaired Ca2+ signaling and cytoskeletal reorganization.* Circ Res, 2010. **106**(6): p. 1103-16.
9. Ledoux, J., et al., *Functional architecture of inositol 1,4,5-trisphosphate signaling in restricted spaces of myoendothelial projections.* Proc Natl Acad Sci U S A, 2008. **105**(28): p. 9627-32.
10. Vriens, J., et al., *Cell swelling, heat, and chemical agonists use distinct pathways for the activation of the cation channel TRPV4.* Proc Natl Acad Sci U S A, 2004. **101**(1): p. 396-401.
11. Nilius, B., et al., *TRPV4 calcium entry channel: a paradigm for gating diversity.* Am J Physiol Cell Physiol, 2004. **286**(2): p. C195-205.
12. Ducret, T., et al., *Serotonin-induced activation of TRPV4-like current in rat intrapulmonary arterial smooth muscle cells.* Cell Calcium, 2008. **43**(4): p. 315-23.
13. Nilius, B. and T. Voets, *The puzzle of TRPV4 channelopathies.* EMBO Rep, 2013. **14**(2): p. 152-63.
14. Thorneloe, K.S., et al., *An orally active TRPV4 channel blocker prevents and resolves pulmonary edema induced by heart failure.* Sci Transl Med, 2012. **4**(159): p. 159ra148.
15. Alvarez, D.F., J.A. King, and M.I. Townsley, *Resistance to store depletion-induced endothelial injury in rat lung after chronic heart failure.* Am J Respir Crit Care Med, 2005. **172**(9): p. 1153-60.
16. Alvarez, D.F., et al., *Transient receptor potential vanilloid 4-mediated disruption of the alveolar septal barrier: a novel mechanism of acute lung injury.* Circ Res, 2006. **99**(9): p. 988-95.
17. Hamanaka, K., et al., *TRPV4 initiates the acute calcium-dependent permeability increase during ventilator-induced lung injury in isolated mouse lungs.* Am J Physiol Lung Cell Mol Physiol, 2007. **293**(4): p. L923-32.
18. Dayeh, N.R., et al., *Echocardiographic validation of pulmonary hypertension due to heart failure with reduced ejection fraction in mice.* Sci Rep, 2018. **8**(1): p. 1363.
19. Hill-Eubanks, D.C., et al., *Vascular TRP channels: performing under pressure and going with the flow.* Physiology (Bethesda), 2014. **29**(5): p. 343-60.

20. Sonkusare, S.K., et al., *Elementary Ca2+ signals through endothelial TRPV4 channels regulate vascular function.* Science, 2012. **336**(6081): p. 597-601.
21. Bagher, P., et al., *Low intravascular pressure activates endothelial cell TRPV4 channels, local Ca2+ events, and IKCa channels, reducing arteriolar tone.* Proc Natl Acad Sci U S A, 2012. **109**(44): p. 18174-9.
22. Filosa, J.A., X. Yao, and G. Rath, *TRPV4 and the regulation of vascular tone.* J Cardiovasc Pharmacol, 2013. **61**(2): p. 113-9.
23. Nausch, L.W., et al., *Sympathetic nerve stimulation induces local endothelial Ca2+ signals to oppose vasoconstriction of mouse mesenteric arteries.* Am J Physiol Heart Circ Physiol, 2012. **302**(3): p. H594-602.
24. Tran, C.H., et al., *Endothelial Ca2+ wavelets and the induction of myoendothelial feedback.* Am J Physiol Cell Physiol, 2012. **302**(8): p. C1226-42.
25. Rahaman, S.O., et al., *TRPV4 mediates myofibroblast differentiation and pulmonary fibrosis in mice.* J Clin Invest, 2014. **124**(12): p. 5225-38.
26. Brahler, S., et al., *Genetic deficit of SK3 and IK1 channels disrupts the endothelium-derived hyperpolarizing factor vasodilator pathway and causes hypertension.* Circulation, 2009. **119**(17): p. 2323-32.
27. Sukumaran, S.V., et al., *TRPV4 channel activation leads to endothelium-dependent relaxation mediated by nitric oxide and endothelium-derived hyperpolarizing factor in rat pulmonary artery.* Pharmacol Res, 2013. **78**: p. 18-27.

Figure legends

Figure 1. A) Average of 10 images of a field of endothelial cells (EC) of a pulmonary artery showing Ca^{2+} pulsars initiation sites (coloured squares) (scale bar: 10 μm). B) Representative Ca^{2+} pulsar depicted by an increase in fluorescence over time emerging within an internal elastic lamina hole. C) Pulmonary arteries' pulsars response to A) endothelial and B) smooth muscle stimulation (acetylcholine n=4 arteries; phenylephrine n=4 arteries) represented as percentage change *p< 0.05 ***p< 0.001. D) Representative plots showing one pulsar in a non-stimulated PA as well as after the addition of acetylcholine and phenylephrine.

Figure 2. A) Western blot analysis showing the presence of TRPV4 at the protein level in lung tissue and isolated pulmonary arteries, and PCR product illustrating the mRNA expression of TRPV4 in isolated Pulmonary arteries, B) Immunofluorescence showing pulmonary endothelial TRPV4 expression co-localizing with IEL holes (scale: 10 μm) (white arrows point at IEL holes and corresponding TRPV4 protein), and calnexin staining within IEL holes in 2D as well as orthogonal view (white arrows point at IEL holes and corresponding calnexin protein). C) Dose-dependent effect of TRPV4 activation by specific agonist GSK106790A (10nM and 100nM) on Ca^{2+} pulsars in terms of total frequency, frequency per site, and number of sites (n=5 arteries represented as percentage change *p< 0.05, and representative time plots illustrating Dose-dependent effect of TRPV4 activation by specific agonist GSK106790A (10nM and 100nM) on Ca^{2+} pulsars kinetics: control (non-stimulated), GSK1016790A 10nM and 100 nM.

Figure 3. A) Evaluation of basal Ca^{2+} pulsars activity in non-stimulated PA from sham mice and mice with PH in terms of total frequency (Hz), frequency per site, number of sites, and spatial spread (Sham group n=20 arteries; PH group n=20 arteries; control group n=6 arteries) represented as percent change **p< 0.01 ***p< 0.001. B) Representative time plot illustrating Ca^{2+} pulsars kinetics in unstimulated PA from a sham mouse and a mouse with PH-LHD. C) Sham and PH pulmonary arteries' pulsars response to endothelial and smooth muscle stimulation in terms of total frequency, frequency per site, and number of sites (acetylcholine: sham group n=5 arteries PH-LHD group n=4 arteries) (phenylephrine: sham group n=4 arteries; PH-LHD group n=4 arteries) represented as percentage change *p< 0.05 (ns=non-significant).

Figure 4. A) Western blot analysis showing the expression of TRPV4 at the protein level in lung tissue of sham mice and mice with PH-LHD, B) Immunofluorescence showing TRPV4 expression in lungs of sham and PH-LHD mice, B) Immunofluorescence showing pulmonary endothelial TRPV4 expression co-localizing with IEL holes of sham and PH arteries and calnexin expression within IEL holes (scale: 10 μm). C) Effect of TRPV4 activation by specific agonist GSK106790A (10nM and 100nM) on pulsars' activity in sham and PH arteries in terms of total frequency, frequency per site, and number of sites (sham group n=4 arteries PH-LHD group n=4 arteries) represented as percentage change *p< 0.05 ***p< 0.001 (ns=non-significant).

Figure 5. Effect of TRPV4 inhibition with HC067047 (10 μM) on pulsars' activity in sham and PH arteries in terms of total frequency, frequency per site, and number of

sites (sham group n=4 arteries PH-LHD group n=4 arteries) represented as percentage change (ns=non-significant).

Figure 1

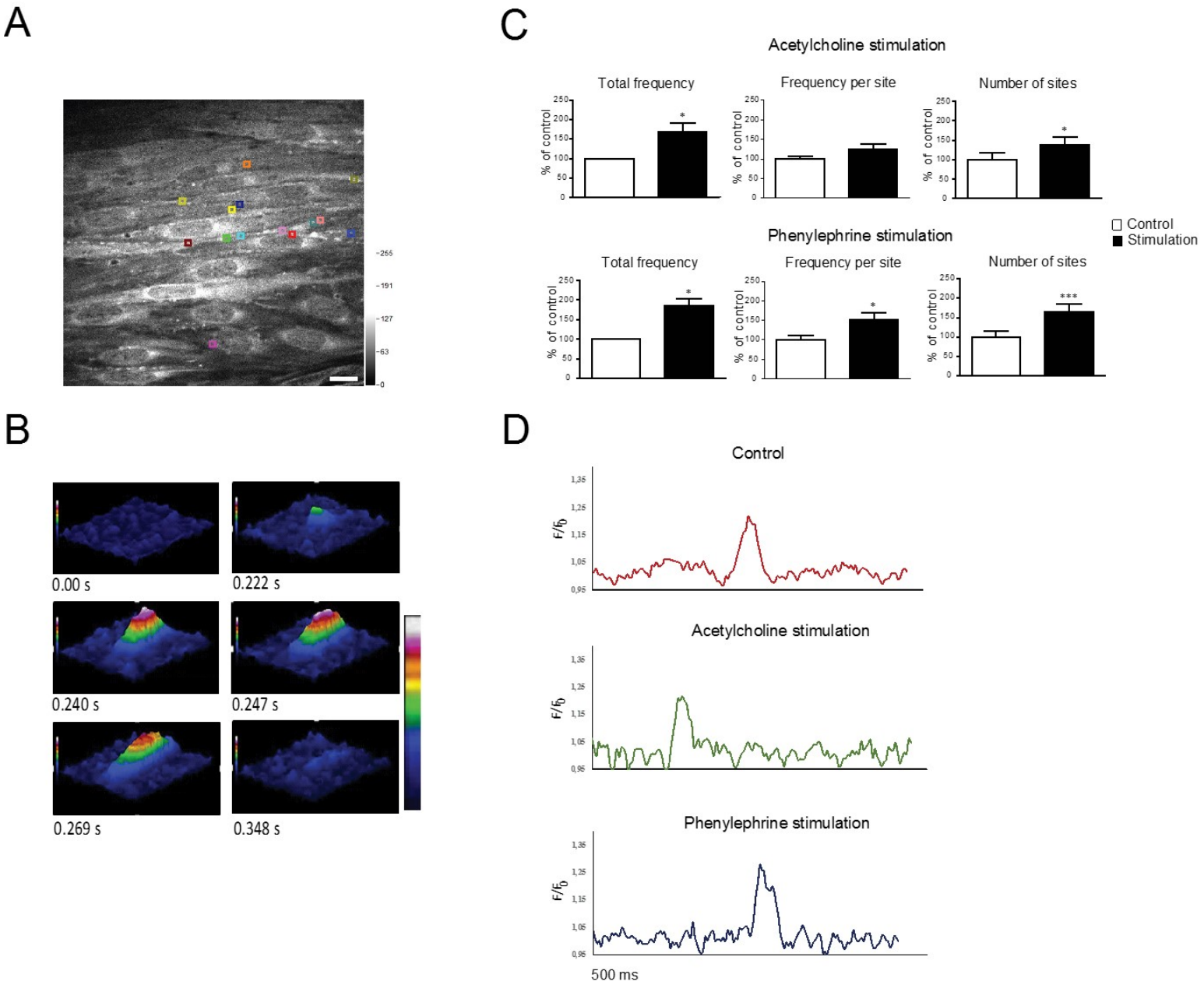
A
255
191
127
63
0
B
0.00 s
0.222 s
0.240 s
0.247 s
0.269 s
0.348 s
C
Acetylcholine stimulation
Total frequency
Frequency per site
Number of sites
% of control
Phenylephrine stimulation
Control
Stimulation
D
Control
Acetylcholine stimulation
Phenylephrine stimulation
F/F0
500 ms

Figure 2

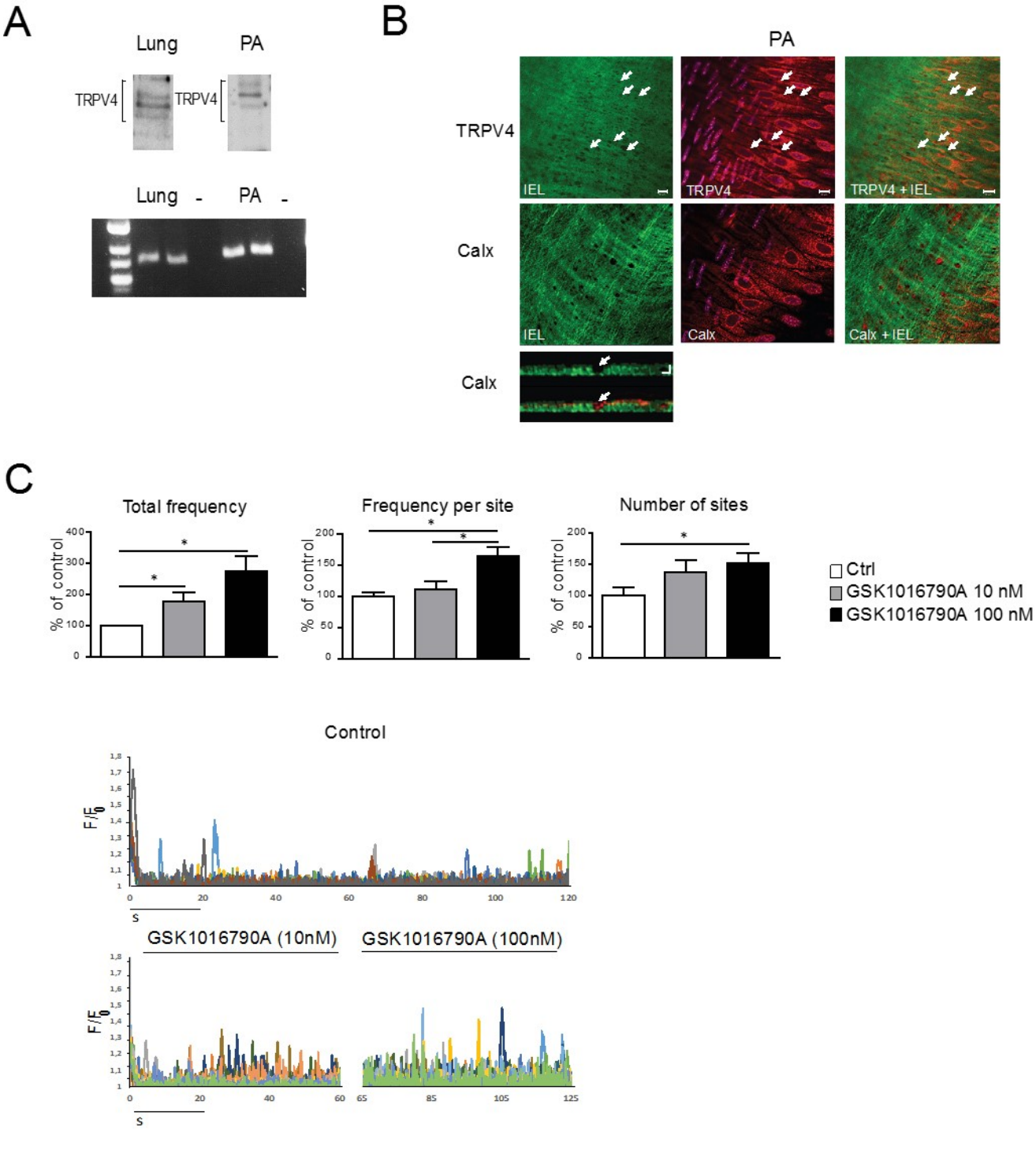
A
Lung
PA
TRPV4
TRPV4
Lung - PA -
B
PA
TRPV4
IEL
TRPV4
TRPV4 + IEL
Calx
IEL
Calx
Calx + IEL
Calx
C
Total frequency
Frequency per site
Number of sites
% of control
Ctrl
GSK1016790A 10 nM
GSK1016790A 100 nM
Control
F/F0
s
GSK1016790A (10nM)
GSK1016790A (100nM)

Figure 3

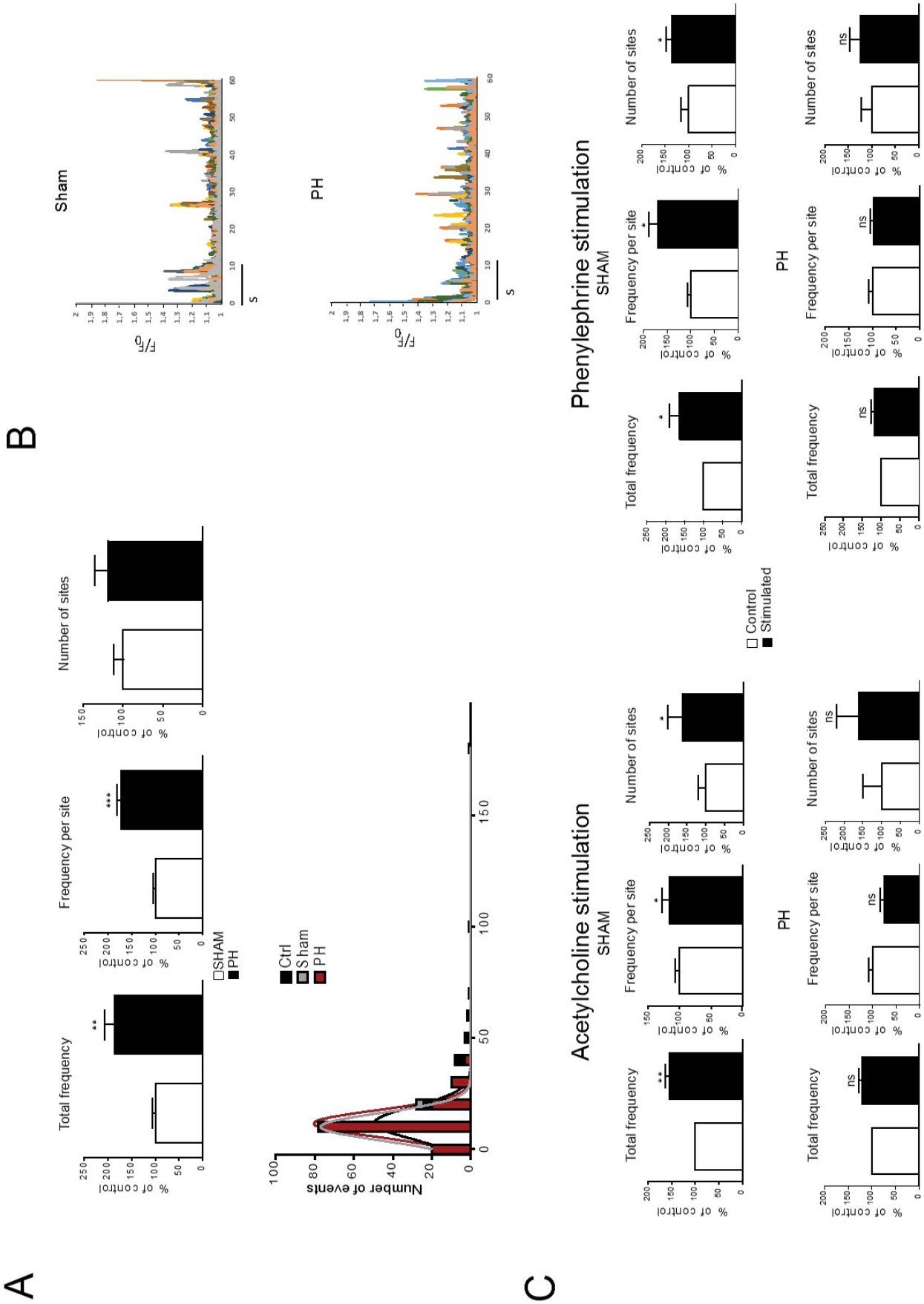
A
B
C
Total frequency
Frequency per site
Number of sites
% of control
SHAM
PH
Ctrl
Sham
PH
Number of events
Sham
PH
F/F0
s
Phenylephrine stimulation
Acetylcholine stimulation
Control
Stimulated
ns

Figure 4

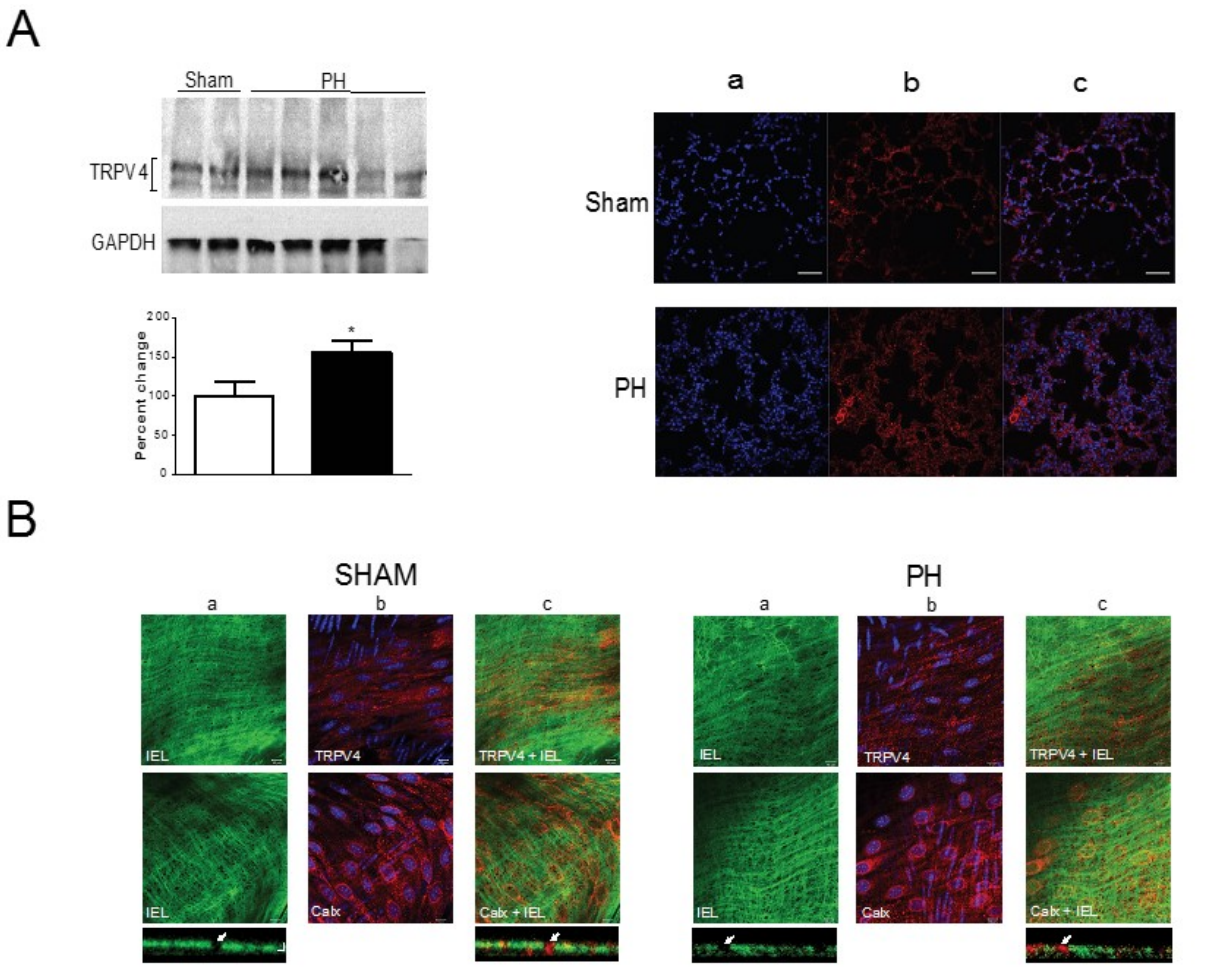
A
Sham
PH
TRPV4
GAPDH
Percent change
a
b
c
Sham
PH
B
SHAM
PH
IEL
TRPV4
TRPV4 + IEL
Calx
Calx + IEL
C
SHAM
Total frequency
Frequency per site
Number of sites
Pulsars spread
% of control
Ctrl
GSK1016790A 10 nM
GSK1016790A 100 nM
PH
ns

Figure 5

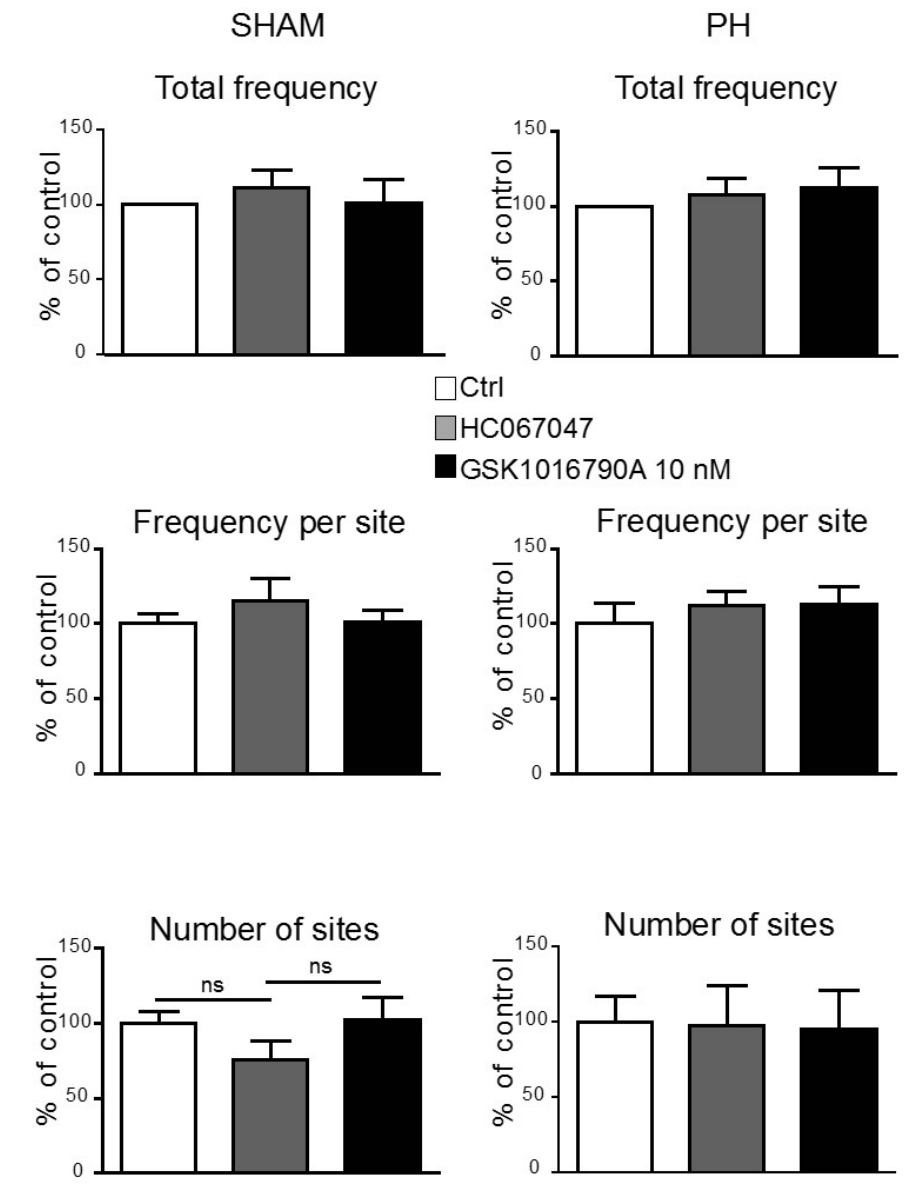
SHAM
PH
Total frequency
Total frequency
% of control
150
100
50
0
Ctrl
HC067047
GSK1016790A 10 nM
Frequency per site
Frequency per site
Number of sites
Number of sites
ns
ns

Supplementary material

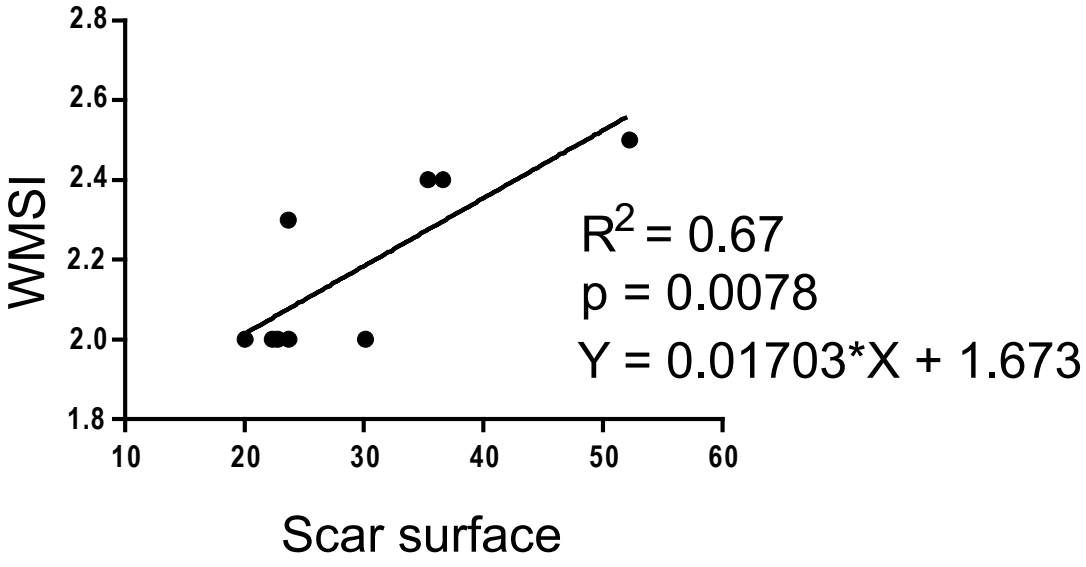

Figure 1. Correlation between scar surface measurements and WMSI measurements.

Mouse	SHAM				PH			
	LV		RV		LV		RV	
	Scar surface	WMSI	*PAAT*	*TAPSE*	*Scar surface*	*WMSI*	*PAAT*	*TAPSE*
1	0	1	NA	NA	23.67	2.3	20.697	0.803
2	0	1	31.142	1.484	36.62	2.4	17.429	0.754
3	0	NA	NA	NA	35.38	2.4	14.171	0.624
4	0	NA	NA	NA	22.35	2	17.098	1.049
5	0	1	18.922	1.046	30.15	2	15.291	NA
6	0	1	15.859	1.071	20.05	2	NA	NA
7	0	1	17.301	0.841	22.1	NA	NA	NA
8	0	1	16.148	0.824	52.23	2.5	10.381	0.668
9	0	1	23.7	1.013	NA	2	12.918	0.521
10	0	1	18.349	0.882	23.7	2	18.635	0.458
11	0	1	17.202	1.176	22.8	2	17.775	0.795
12	0	NA	NA	NA	20.91	NA	NA	NA
Average	**0**	**1**	**19.83 ± 1.8**	**1.042**	**28.91 ± 3**	**2.16 ± 0.04**	**16.04 ± 1.06**	**0.709 ± 0.07**

Suppl table 1.

Ca^{2+} pulsar parameter	Control	ACh	p value
Amplitude, F/F0	1.21 ± 0.01	1.23 ± 0.008	ns
Rise time, ms	316 ± 20	321 ± 10	ns
Duration, ms	417 ± 20	436 ± 8	ns
t1/2, ms	230 ± 20	228 ± 7	ns

Suppl table 2.

Ca^{2+} pulsar parameter	Control	PE	p value
Amplitude, F/F0	1.25 ± 0.02	1.23 ± 0.007	ns
Rise time, ms	300 ± 20	321 ± 10	ns
Duration, ms	442 ± 20	441 ± 9	ns
t1/2, ms	232 ± 10	228 ± 7	ns

Suppl table 3.

Ca^{2+} pulsar parameter	SHAM			PH		
	Control	**Ach**	**p value**	**Control**	**ACh**	**p value**
Amplitude, F/F0	1.22 ± 0.009	1.21 ± 0.004	ns	1.21 ± 0.009	1.21 ± 0.007	ns
Rise time, ms	290 ± 30	311 ± 20	ns	342 ± 20	387 ± 30	ns
Duration, ms	416 ± 20	419 ± 10	ns	449 ± 10	446 ± 8	ns
t1/2, ms	217 ± 10	201 ± 10	ns	236 ± 8	233 ± 6	ns

Suppl table 4.

Ca^{2+} pulsar parameter	SHAM			PH		
	Control	**PE**	**p value**	**Control**	**PE**	**p value**
Amplitude, F/F0	1.2 ± 0.006	1.2 ± 0.004	ns	1.23 ± 0.008	1.25 ± 0.01	ns
Rise time, ms	305 ± 30	295 ± 10	ns	344 ± 10	371 ± 20	ns
Duration, ms	416 ± 10	406 ± 10	ns	468 ± 7	471 ± 7	ns
t1/2, ms	223 ± 10	213 ± 8	ns	267 ± 10	254 ± 7	ns

Suppl table 5.

Ca^{2+} pulsar parameter	SHAM			PH		
	Control	**GSK 10nM**	**GSK 100nM**	**Control**	**GSK 10nM**	**GSK 100nM**
Amplitude, F/F0	1.22 ± 0.02	1.2 ± 0.006	1.21 ± 0.005	1.2 ± 0.005	1.21 ± 0.005	1.25 ± 0.01
Rise time, ms	325 ± 20	289 ± 10	372 ± 20	344 ± 17	324 ± 14	330 ± 15
Duration, ms	387 ± 9	379 ± 8	420 ± 10	426 ± 10	436 ± 8	405 ± 10
t1/2, ms	207 ± 8	198 ± 6	219 ± 6	211 ± 8	226 ± 6	198 ± 7

Suppl table 6.

Supplemental Figure Legends

Supplemental figure 1. Correlation between scar surface measurements and WMSI measurements. WMSI correlations with scar surface measurements was obtained by linear regression analysis (n=9 mice).

Supplemental table 1. Selection criteria of mice with pulmonary hypertension (PH). LV: left ventricle, Rv: right ventricle, WMSI: wall motion score index, PAAT: pulmonary artery acceleration time, TAPSE: tricuspid annular plane systolic excursion (sham n=12, PH n=12 mice).

Supplemental table 2. Pulsars' kinetics and descriptive parameters following stimulation of pulmonary arteries with ACh in terms of peak amplitude, rise time as measured during 10 –90% of the signal, duration as measured from 50% of the signal before and after the peak, and half-life of decay ($t_{1/2}$) (n=5 arteries) (unpaired t-test).

Supplemental table 3. Pulsars' kinetics and descriptive parameters following stimulation of pulmonary arteries with PE in terms of peak amplitude, rise time as measured during 10 –90% of the signal, duration as measured from 50% of the signal before and after the peak, and half-life of decay ($t_{1/2}$) (n=4 arteries) (unpaired t-test).

Supplemental table 4. Pulsars' kinetics and descriptive parameters following stimulation of Sham and PH pulmonary arteries with ACh in terms of peak amplitude, rise time as measured during 10 –90% of the signal, duration as measured from 50% of the signal before and after the peak, and half-life of decay ($t_{1/2}$) (sham n=5, PH-LHD n=4 arteries) (unpaired t-test).

Supplemental table 5. Pulsars' kinetics and descriptive parameters following stimulation of Sham and PH pulmonary arteries with PE in terms of peak amplitude, rise time as measured during 10 –90% of the signal, duration as measured from 50% of the signal before and after the peak, and half-life of decay ($t_{1/2}$) (sham n=4, PH-LHD n=4 arteries) (unpaired t-test).

Supplemental table 6. Pulsars' kinetics and descriptive parameters following stimulation of Sham and PH pulmonary arteries with GSK1016790A in terms of peak amplitude, rise time as measured during 10 –90% of the signal, duration as measured from 50% of the signal before and after the peak, and half-life of decay ($t_{1/2}$) (sham n=4, PH-LHD n=4 arteries). Comparison of all three conditions (ctrl- GSK 10 nM- GSK 100 nM) was done by ANOVA followed by a comparison of ctrl vs GSK 10 nM, ctrl vs GSK 100 nM, and GSK 10 nM vs GSK 100 nM in both sham and PH-LHD groups by unpaired t-test, which was non-significant.

IV. Chapter IV: DISCUSSION

Significant advances have been made for the treatment of HF. Nevertheless, the morbidity and mortality among patients with advanced HF, who have developed PH remains high. A progressive increase in mPAP and in PVR, are important markers that signal progression of the disease and its poor outcome. Vascular tone deregulations observed in PH precede vascular remodelling and are therefore a highly contributing factor to PH development. In fact, abnormal vascular reactivity in HF has been reported in a number of studies involving animal models as well as human patients. Various vascular beds have displayed endothelial dysfunction and vascular remodelling in HF including the pulmonary vascular system [283] [284] [285]. Nevertheless, investigations around pulmonary endothelial dysfunction in the context of PH in HFrEF remain scarce.

In this thesis, we proposed a new viewpoint to study vascular impairment in PH-LHD.

First, we properly characterized an adequate animal model for the study of the pathophysiological mechanisms of PH-LHD. Second, we identified, for the first time, a new form of local Ca^{2+} signalling within the pulmonary endothelium termed Ca^{2+} pulsars and shed light on their unique restricted localization in proximity to IEL holes. We have validated furthermore the importance of pulsar-dependent signalling by demonstrating that Ca^{2+} pulsars' characteristics and kinetics were preserved regardless of the nature and type of vascular bed. Finally, we have demonstrated that Ca^{2+} pulsars deregulation is present group II-PH. In addition to that, we associated a new role for mechano-sensitive TRPV4 channels in alterations of pulsars and their effect on pulmonary vascular tone in the context of PH-LHD.

Heart failure and pulmonary hypertension

Development of a model for PH-LHD

Using a pre-clinical animal model in any project requires a robust and cost-effective way to determine whether there is any merit to extensively testing a particular hypothesis. The study of PH-LHD was hampered by the lack of a representative model for the disease, despite the existence of animal models of HF. Furthermore, notwithstanding the fact that the MI model was the primary model utilized for group II-PH investigations, accurate assessment of disease onset was absent. Moreover, the MI model had been narrowly executed in large animals. The main reason behind these

limitations is the lack of proper diagnostic tools that can be used to accurately assess disease presence and progression, and that can be applied on small animals with technical ease. In this thesis work, we have associated, for the first time, an animal model properly characterized for the study of PH in HFrEF.

In concordance with what was previously shown in rat models [286] [287], we had demonstrated through our hemodynamic and morphometric measurements, as well as respiratory function tests, that our MI mouse model is functional for the study of PH in mice. Mice developed left heart failure and right ventricular dysfunction and presented with right ventricular hypertrophy. This was accompanied by pulmonary remodelling without the presence of pulmonary oedema. Additionally, mice had restrictive pulmonary syndrome represented by a decrease in quasi-static compliance, an increased pulmonary resistance and a shift in the pressure-volume curve. We aimed at correlating our hemodynamic findings with echocardiography data that we obtained from sham and MI mice, days prior to their sacrifice. The purpose of this investigation was to use echocardiography as a reliable method to identify the presence of PH within those mice. Echocardiography analysis presents the advantage of being non-invasive, as well as giving the opportunity to perform several measurements during the course of progression of PH if needed [288]. We have indeed shown that echocardiography performed almost 4 weeks after MI surgery correlates with our catheterization results and our morphometric measurements. We have also demonstrated that mice with MI have a dysfunctional left ventricle and a hypertrophied right ventricle.

Setting specific parameters and cutoff values

The results of our first study clearly established that the myocardial infarction through coronary artery ligation model led to the development of PH. We have demonstrated that the presence of PH can easily be determined through non-invasive echocardiography. Moreover, we have established the specific parameter WMSI with a clear cutoff value of 2 for the determination of the presence of PH. We have shown that mice with a WMSI value of ≥ 2 presented with decreased pulmonary artery acceleration time (PAAT) as well as a lower tricuspid annular plane systolic excursion (TAPSE), two indispensable predictors of the presence of PH.

The importance of setting this parameter will aid in future PH-LHD studies as it will set for the first time, common guidelines for the selection of animals that have

developed PH following MI surgery and will therefore facilitate the study of certain aspects of the disease all while being aware of all the potential surrounding contributing factors and mechanisms. Additionally, our choice of mice presents a number of advantages including the avoidance of high costs associated with the use of large animals, and the possibility of using transgenic mice.

The pulmonary endothelium in heart failure

Calcium pulsars are present in the pulmonary endothelium

Earlier studies have exposed a variety of spatially and temporally restricted endothelial Ca^{2+} transients [289, 290] [16] . These Ca^{2+} dynamics are primarily involved in the control of vascular relaxation. For instance, Ca^{2+} transients have been associated with the activation of eNOS and the subsequent production of NO [291]. Additionally, localized Ca^{2+} increases can lead to the activation of small and intermediate Ca^{2+}-activated K^+ channels [292] [293] leading to endothelium-derived hyperpolarization of vascular SMCs [294]. Furthermore, endothelial Ca^{2+} increases can lead to PLA_2-mediated production of AA metabolites like PGI_2 and EETs [295].

In this thesis, we focused our attention on localized endothelial Ca^{2+} signalling because it presents the advantage of selectively modulating Ca^{2+} sensitive signalling pathways in defined regions of the cell without affecting other cellular functions. Therefore, we aimed to investigate the presence of Ca^{2+} pulsars within the pulmonary endothelium. We have successfully identified, for the first time the presence of this new form of local Ca^{2+} dynamics in pulmonary endothelial cells, exclusively present within sites of MEPs. We further explored and confirmed the nature of these localized endothelial Ca^{2+} events and evaluated their kinetics as well as their source thus showing high similarity with previously identified mesenteric pulsars [16].

The integrity of pulsars

In the second article presented in this thesis, we sought out to evaluate characteristics and kinetics of Ca^{2+} pulsars as well as related vascular structures in three different vascular beds: coronary, mesenteric, and pulmonary. We have shown in the first place that the number of IEL fenestrations was different amongst all three beds, coronary arteries having the highest number of fenestrations where MEPs can be potentially present. We evaluated the percentage of MEPs occupied by fenestrations

and found that the highest ratio of MEPs to fenestrations was present within mesenteric arteries. PAs seemed to present with the lowest number of fenestrations as well as percentage of MEPs occupancy. Non-stimulated arteries presented with differences in the number of active pulsar sites as well as global pulsar frequency per vascular bed. The number of active sites in each vascular type correlated with the number of MEPs, PAs having the lowest number of MEPs concordantly with the lowest pulsar activity reflected by the number of active sites.

However, previous evidence had shown that optimal vasoactive effect does not necessarily require high incidence of myoendothelial communication [296]. Secondly, we have established that Ca^{2+} pulsars preserved their fundamental characteristics and kinetics amongst all three vascular beds. Stimulation of Ca^{2+} pulsars *via* smooth muscle α_1-adrenergic receptors with PE had no effect on these parameters. Therefore, we have demonstrated through this study that Ca^{2+} pulsars are preserved functional units amongst all three vascular beds. This important finding establishes Ca^{2+} pulsars as elemental actors in the regulation of vascular tone through their previously determined involvement in endothelial-derived hyperpolarization. Linking endothelial pulsars in the pulmonary and coronary beds to endothelial-derived hyperpolarization through Ca^{2+}-activated K^+ channels remains to be confirmed. However, as mentioned previously in this section, earlier evidence supports this hypothesis and associates local endothelial Ca^{2+} dynamics to the activation of these channels.

In regards to baseline global frequency of pulsars in the non-stimulated pulmonary endothelium, which we demonstrated to be lowest amongst all three beds, one must give importance to the influence of the distinct nature of the pulmonary vasculature. We have conducted our experiments on cut open preparations using similar flow in all three vascular beds. More elaborately, the pulmonary circulation is a high flow system, which did not coincide with our experimental conditions. Our technique clearly presented a limitation in terms of how closely our pulmonary arterial preparations mimicked the physiological condition. However, this suggests that our findings could have more impact in the physiological setting.

TRPV4 and pulmonary pulsars: location, location, location

A number of studies have underlined the importance of TRPV4 in the regulation of vascular tone and have connected it to endothelium-dependent vasodilatory responses [180]. Interestingly, TRPV4 dilatory effects have been associated with the activity of local Ca^{2+} dynamics. In fact, a role for TRPV4 has been previously linked with increased sparklet activity [114] [297], leading to vascular dilation. Nevertheless, a similar mechanism has not been shown in the pulmonary vasculature. Therefore, in this thesis work we proposed that TRPV4 channels have an indirect effect on vascular tone through their induction of Ca^{2+} pulsars. We have shown that TRPV4 protein is expressed in lung tissue as well as in isolated PAs. We have equally shown TRPV4 mRNA expression in PAs and have demonstrated that endothelial TRPV4 channels were indeed located around and within MEPs. Following the application of the TRPV4 specific channel agonist GSK1016790A, there was an increase in Ca^{2+} pulsars occurrence frequency. These findings enabled us to demonstrate that TRPV4 channels stimulate pulsar activity.

Interestingly, the restricted localization of pulsars within MEPs and the cellular expression of TRPV4 channels leads us to focus our attention on the impact of MEP-bound TRPV4 only. Seeing that TRPV4 channels were found to increase sparklet activity in vascular endothelial cells [114], we can associate both mechanisms and raise the question of whether TRPV4 activation of Ca^{2+} pulsars happens indirectly via increased sparklet activity. In fact, sparklets are restricted increases in Ca^{2+} following its direct entry via TRPV4 channels upon their activation. Studies conducted on TRPV4-induced sparklet activity have clearly specified that these Ca^{2+} dynamics are membrane-delimited and occur along the plasma membrane [114, 298]. However, these studies specified that it only takes a few activated MEP-bound TRPV4 channels to induce maximal dilation in resistance arteries. These findings are in concordance with our work that attempted to emphasize the key role that the strategic localization of TRPV4 channels can play in their effect on vascular function. Following these findings, we can propose the TRPV4-sparklet-pulsar activation cascade; cooperation between both types of events is of high probability and has never been shown in the pulmonary vascular bed. In fact, sparklets may solicit Ca^{2+} store release events. Any potential impairment of this mechanism could be a contributor to pulmonary endothelial dysfunction and changes in vascular tone. Seeing that sparklets are low amplitude signals and that their visualization requires Ca^{2+} store depletion, our imaging analysis

technique as well as our experimental conditions did not permit their visualisation in our preparations. The versatility of local transients' types, the individuality of each vascular bed, as well as the possibilities of cooperativity amongst different local transients direct us to question the predominance of pulsar signalling in the pulmonary vasculature.

TRPV4 activation leads to Ca^{2+} entry into the cell, which could activate NO dependent mechanisms, PGI_2, as well as EDHF [299]. However, studies have shown that in smaller arteries EDHF component plays a much bigger role in vascular relaxation [43]. Additionally, TRPV4 has been shown to be involved in EDHF [114]. In this thesis, we aimed at demonstrating evidence for the participation of TRPV4 channels in endothelium dependent hyperpolarization through its induction of Ca^{2+} pulsars. We hypothesized a link between TRPV4 - associated pulsar activity within MEPs to activation of small (K_{Ca} 2.3) and intermediate (K_{Ca} 3.1) Ca^{2+}-activated K^+ channels (SK, IK), and hyperpolarization of vascular SMCs. Therefore, it is crucial to delineate pulmonary endothelium-dependent pathways activated through TRPV4 channels and explore the contribution of EDHF to the relaxant TRPV4-mediated response. Following this hypothesis, and considering the different localizations of SK and IK channels, is the following question: would TRPV4-pulsar stimulation activate one or both types of channels? The answer to that question will be conditioned by further exploration of already shown TRPV4-IK coupling and pulmonary endothelial localization of both channel types.

Impact of PH-LHD on localized endothelial Ca^{2+} signalling.

Through the third article presented in this thesis, we aimed to uncover any possible modifications in pulsar activity in mice with PH-LHD, and to expose underlying TRPV4-related dysfunction.

1) Pulsar activity is disturbed in PH-LHD

This study enabled us to discover that in non-stimulated PAs, basal pulsar activity was higher in PH mice when compared to the sham group. This unexpected finding led us to investigate whether potentially existing basal TRPV4 activity could be influencing pulsar activity. We therefore sought to evaluate pulsar stir following the incubation of non-stimulated PAs with the TRPV4 specific inhibitor HC067047. Results revealed that TRPV4 channels did not have basal pulsar influence in either

group. Nevertheless, high pulsar activity in PAs of hypertensive mice suggests a potential protective mechanism against increased vascular pressure. In fact, in the presence of an elevated pressure and PH, a preventive mechanism that regulates blood flow and pressure by promoting vasodilation through increased pulsar activity can be activated. This potentiality is supported by existing evidence of EC-SMC gap junctional communication [300], as well as previous work that has indicated that in the presence of elevated intraluminal pressure or flow shear stress, an opposing mechanism is triggered; EC-SMC communication leads to a myoendothelial feedback response following SMC depolarization. This is followed by an increased endothelial Ca^{2+} concentration and the consequent effect of vasodilatory pathways. A number of studies have confirmed that this aforementioned feedback involves the generation of Ca^{2+} wavelets and/or Ca^{2+} pulsars within or near endothelial projections, both clearly and as mentioned throughout this thesis, spatially and temporally restricted events [301] [119]. Furthermore, earlier work has demonstrated increased local Ca^{2+} oscillatory activity within the pulmonary endothelium following increases in pressure [302]. Moreover, our deductions regarding the prospective protective role of pulsars allow us to formulate a probability that adds an advantage to the restricted nature of these transients. The protective potentiality of pulmonary pulsars could carry an additional lead related to their confined nature; in fact, these relatively small increases in Ca^{2+} could avoid otherwise deleterious intracellular endothelial Ca^{2+} increases in response to pressure rises.

2) TRPV4-related pulsars dysfunction in PH-LHD

We have found that activation of TRPV4 following the addition of GSK1016790A did not lead to increased pulsar activity in PH arteries when compared to PAs of the sham group. This finding, along with our above-mentioned deductions led us to hypothesize the following: in the setting of PH, TRPV4-affiliated pulsars' defect is an associated factor to endothelial dysfunction and resulting variations in pulmonary vascular reactivity and pressure. We have clearly demonstrated pulsars' deregulation and shed light on the endothelial response's tuning effect of pulsars.

The significance of our results concerning TRPV4 malfunction can be discussed on the following levels. First, our results involving the absence of PH arteries' response to stimulation with PE raises the question of whether the setting of PH-LHD exerts negative consequence on the presence of MEPs. In other words, could PH pulmonary

arteries have less MEPs? This hypothesis would indeed clarify one of the reasons contributing to decreased vascular response. Further analysis is admittedly needed. Second, and considering that TRPV4 itself could be affected in PH, it is noteworthy to mention that within the axis of TRPV4 activation and its following consequences, lies a number of factors and regulatory proteins that remain to be examined. In fact, according to the literature, the dominant pathway for activation of TRPV4 by mechanical stimuli is the PLA_2-Cytochrome P450 axis. It has been established that shear stress activates phospholipase A_2, which causes the formation of AA from membrane phospholipids. AA is then transformed through the action of the enzyme cytochrome p-450 into EETs. In this context, EETs activation of TRPV4 can be suggested in our model, and impaired production of EETs and/or EETs-TRPV4 interaction could constitute potential reasons affecting the activity of TRPV4. Furthermore, recognition of mechanical stress by TRPV4 is in fact related to its N-terminal domain, which suggests that structural changes affecting this domain could be influencing the channel's ability to detect pressure increases. More recent data reveals that phosphorylation by PKC plays an important role in TRPV4 activation. That relationship has even been shown to mediate increased vascular permeability in lung injury [303], which in our case could represent a potential reason for TRPV4 unresponsiveness. On a different but not unrelated note, AKAP150 scaffolding proteins have been shown to influence the activity of several types of ion channels [304-306] [307]. These mentioned findings were taken all together in a study by the group of Merkado who revealed an interaction between AKAP150 proteins and TRPV4 channels in vascular smooth muscle cells. In this study, TRPV4 interaction with AKAP-150 releases PKC from the complex, thus allowing PKC to phosphorylate TRPV4 channels, forming a feedback system that opposes vasoconstriction in smooth muscle cells [308]. These studies can easily direct our attention towards a strong implication for AKAP150 proteins in TRPV4 channel activity. The validity of this idea is further supported by another elegant study by the group of Sonkursare. This study reveals an AKAP150-PKC-TRPV4 axis similar to the aforementioned work, within endothelial cells. More specifically, the authors show that muscarinic activation of TRPV4 is dependent on PKC and the PKC anchoring protein AKAP150 located within MEPs, thus suggesting that only TRPV4 within MEPs is activated [115]. On one hand, it is known that PKC can directly phosphorylate TRPV4. On the other hand, evidence shows that shear stress-induced activation of TRPV4 requires PKC sensitization of the channel [309, 310].

Based on this evidence we can suggest that in the setting of PH-LHD, impairment in TRPV4 activity could be due to a disruption of the localization of AKAP150 proteins within MEPs. This modification could be at the base of alterations of vascular tone. Although an AKAP150-PKC-TRPV4 axis has been demonstrated in mesenteric arteries, neither such relation nor its participation is vascular tone alterations in PH-LHD has been revealed.

Indeed, several pathways present as candidates for the activation of TRPV4. Supplementary possibilities could explain TRPV4-related pulsar dysregulation including decreased TRPV4 expression within MEPs. In fact, despite the fact that our results do not include TRPV4 expression in isolated PAs and in isolated pulmonary ECs, we can argue that the possibility of TRPV4 decreased expression cannot be dismissed.

Limitations and future directions

The work presented in this thesis laid a new foundation in the studies of pulmonary endothelial dysfunction in HFrEF. Our studies led to a number of novel findings: We have developed a mouse model and have validated that this HF model is indeed adequate for the study of group II-PH. We have identified, for the first time, a new form of local Ca^{2+} signalling within the pulmonary endothelium and shed light on the undeniable fact that the finely tuned nature of pulsars can exert influence on the regulation of endothelial responses. Additionally, we demonstrated that this form of signalling is altered in PH-LHD. Furthermore, we have revealed a new role for mechano-sensitive TRPV4 channels in alterations of Ca^{2+} pulsars and discussed their effect on pulmonary vascular tone. A similar direct mechanism has not been shown in pulmonary vasculature. Nevertheless, in this thesis work we demonstrated that TRPV4 channels have an indirect effect on vascular tone through their induction of pulsars. Any potential impairment of this process could be associated with pulmonary endothelial dysfunction and changes in vascular tone. We therefore propose a new mechanism that could play a role in the vascular pathophysiology of PH associated with LHD.

Our approach offers a novel angle for future studies of group II-PH. However, as in any research project, our findings only mark the beginning of a long road that can gradually unveil substantial evidence incriminating TRPV4 and local Ca^{2+} signalling in the progression of PH in LHD. Future supportive work complementing our findings

should be aimed at addressing the following notions; first, it is imperative to explore the molecular mechanisms upstream of TRPV4 activation and investigate any potential dysregulations. Second, measuring vascular contraction is useful for evaluating the physiological response of an artery under normal or pathological conditions, such as in PH. Quantifiable assessment of endothelial dysfunction is in the inability of the artery to dilate in response to a stimulus. Our technique did not permit us to assess pulsar activity simultaneously with diameter measurements. In order to further confirm the new role we have attributed in this thesis for endothelial TRPV4 channels in pulmonary vascular relaxation, future experiments should be conducted on pulmonary reactivity. Third, supplementary inspection of pulmonary IK and SK function in PH-LHD should be of interest. In fact, K_{Ca} channels were found to exert positive feedback on local Ca^{2+} dynamics [311]. However, endothelial stimulation is needed to observe these effects. Furthermore, impaired endothelium-dependent hyperpolarization involving both IK and SK channels was shown to provoque hypertension [312]. Moreover, previous work reported that TRPV4 channels were primary targets of K_{Ca} feedback through local Ca^{2+} transients [311] and that and that K_{Ca} – transient's effect required TRPV4-mediated Ca^{2+} entry. These findings can be aligned with our TRPV4 data leading to hypothesize that K_{Ca} could act as amplifiers of the endothelial response through their positive influence on pulsars requiring Ca^{2+} influx through TRPV4 thereby further expanding the spatial/temporal range of Ca^{2+} signals. Despite the fact that TRPV4-related vascular relaxation in PAs was shown to be related via both NO and K_{Ca} pathways [299], the dominance of EDHF has been demonstrated in small arteries [313, 314].

Fourth, throughout this thesis, we had the chance to conduct some preliminary experiments investigating the presence of pulsars-like Ca^{2+} transients in human pulmonary microvascular endothelial cells. We were able to mimic to a certain limit endothelial/smooth muscle cells interactions by co-culturing both cell types (human pulmonary microvascular endothelial cells and human pulmonary vascular smooth muscle cells) in a setting allowing the formation of MEPs. The optimization of this technique was done thanks to the efforts of Fanny Toussaint and Alexandre Blanchette from Dr. Ledoux's Laboratory. We were successful at demonstrating the presence of human pulmonary pulsars within our co-culture preparations (figure 10). We then sought to test whether TRPV4 channels would have the same effect we had uncovered in murine arteries within human cell preparations. We were equally successful at demonstrating that similar interactions were occurring in human endothelial cells

(figure 11).

Figures and tables:

A

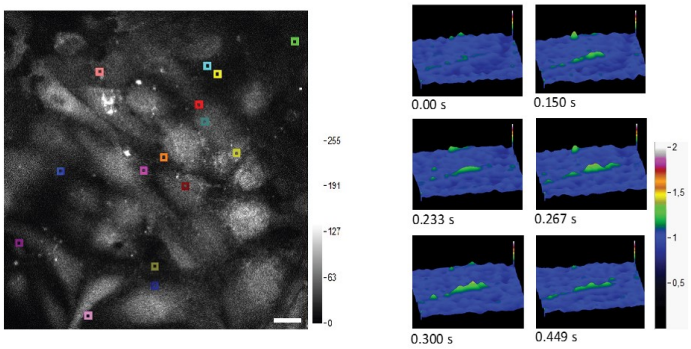

C

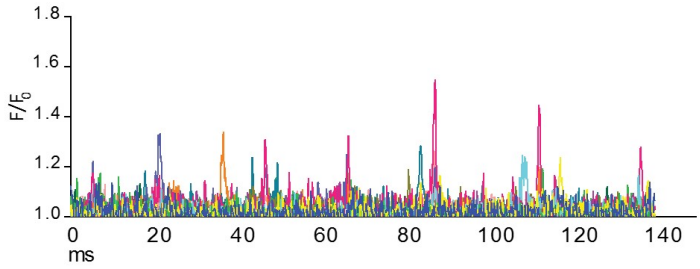

Figure 10 Human endothelial pulsars

A) Human Ca^{2+} pulsar represented by an increase in fluorescence over time emerging within one of those holes. B) Representative Ca^{2+} pulsar depicted by an increase in fluorescence over time emerging within an internal elastic lamina hole. C) Representative time plot illustrating Ca^{2+} pulsars kinetics in human pulmonary microvascular endothelial cells.

Ca^{2+} pulsar parameter	Human pulsars	Murine pulsars
Amplitude, F/F0	1.22 ± 0.01	1.26 ± 0.009
Rise time, ms	499 ± 42	302 ± 15
Duration, ms	540 ± 22	397 ± 17
t1/2, ms	274 ± 22	206 ± 10
Frequency, Hz	0.017 ± 0.002	0.023 ± 0.003
Spread area, µm²	18.67 ± 1.9	15.64 ± 1.5

Table 2 Basal pulsars' kinetics and descriptive parameters in non-stimulated pulmonary arteries control mice and human pulmonary miscrovascular endothelial cells.

Basal pulsars' representation in terms of peak amplitude, rise time as measured during 10 –90% of the signal, duration as measured from 50% of the signal before and after the peak, half-life of decay ($t_{1/2}$), and spread.

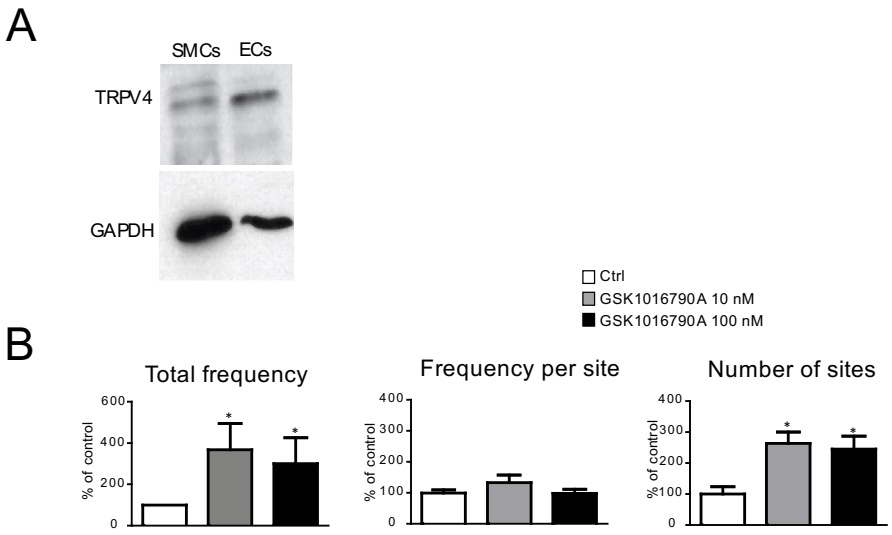

Figure 3 Human TRPV4 expression and activation

A) Western blot analysis showing the expression of TRPV4 at the protein level in co-cultured human pulmonary microvascular smooth muscle cells and human pulmonary microvascular endothelial cells. B) Dose-dependent effect of TRPV4 activation by specific agonist GSK106790A (10nM et 100nM) on human Ca^{2+} pulsars in terms of total frequency (Hz), frequency per site (Hz), and number of sites (n=3 arteries) *p< 0.05 (ANOVA).

These important preliminary findings put our entire work in a clinical context,

emphasize the significance of exploring endothelial pulsars and their related pathways, and pave the way to a long yet to be explored territory in PH-LHD research.

Conclusion

Our studies offer an innovative approach to the study of pulmonary hypertension in left heart failure and enhances our understanding of endothelial Ca^{2+} dyshomeostasis occurring in a clinically relevant model of pulmonary hypertension. Our findings open the door to identifying a potential new therapeutic target for the treatment or prevention of pulmonary arterial hypertension due to left heart failure in humans.

Original contribution to the literature

- Characterization and validation of the myocardial infarction mouse model as a pathological model for the study of PH associated with HFrEF
- Determination of specific echocardiographic parameters and threshold values for the assessment of the presence of PH in mice
- Characterization of the presence of Ca^{2+} pulsars in the pulmonary endothelium
- Association of a role for endothelial TRPV4 channels in the control of Ca^{2+} pulsars
- Show of evidence of pulsar activity deregulation in PH-LHD
- Demonstration of TRPV4 unresponsiveness to stimulation and decreased pulsar activity in PH-LHD

Bibliography

1. Simonneau, G., et al., *Updated clinical classification of pulmonary hypertension.* J Am Coll Cardiol, 2013. **62**(25 Suppl): p. D34-41.
2. Galie, N., et al., *2015 ESC/ERS Guidelines for the diagnosis and treatment of pulmonary hypertension: The Joint Task Force for the Diagnosis and Treatment of Pulmonary Hypertension of the European Society of Cardiology (ESC) and the European Respiratory Society (ERS): Endorsed by: Association for European Paediatric and Congenital Cardiology (AEPC), International Society for Heart and Lung Transplantation (ISHLT).* Eur Heart J, 2016. **37**(1): p. 67-119.
3. Griese, M., *Pulmonary surfactant in health and human lung diseases: state of the art.* Eur Respir J, 1999. **13**(6): p. 1455-76.
4. Lammers, S., et al., *Mechanics and function of the pulmonary vasculature: implications for pulmonary vascular disease and right ventricular function.* Compr Physiol, 2012. **2**(1): p. 295-319.
5. Kilner, P.J., *Pulmonary resistance in cardiovascular context.* Int J Cardiol, 2004. **97 Suppl 1**: p. 3-6.
6. Townsley, M.I., *Structure and composition of pulmonary arteries, capillaries, and veins.* Compr Physiol, 2012. **2**(1): p. 675-709.
7. Tsai, J.C., et al., *Cloning and characterization of the human lung endothelial-cell-specific molecule-1 promoter.* J Vasc Res, 2002. **39**(2): p. 148-59.
8. Block, E.R., *Pulmonary endothelial cell pathobiology: implications for acute lung injury.* Am J Med Sci, 1992. **304**(2): p. 136-44.
9. Rajendran, P., et al., *The vascular endothelium and human diseases.* Int J Biol Sci, 2013. **9**(10): p. 1057-69.
10. Klagsbrun, M. and S. Dluz, *Smooth muscle cell and endothelial cell growth factors.* Trends Cardiovasc Med, 1993. **3**(6): p. 213-7.
11. Botney, M.D., et al., *Active collagen synthesis by pulmonary arteries in human primary pulmonary hypertension.* Am J Pathol, 1993. **143**(1): p. 121-9.
12. Rabinovitch, M., et al., *Pulmonary artery endothelial abnormalities in patients with congenital heart defects and pulmonary hypertension. A correlation of light with scanning electron microscopy and transmission electron microscopy.* Lab Invest, 1986. **55**(6): p. 632-53.
13. Sandow, S.L., D.J. Gzik, and R.M. Lee, *Arterial internal elastic lamina holes: relationship to function?* J Anat, 2009. **214**(2): p. 258-66.
14. Aiello, V.D., et al., *Morphology of the internal elastic lamina in arteries from pulmonary hypertensive patients: a confocal laser microscopy study.* Mod Pathol, 2003. **16**(5): p. 411-6.
15. Kirby, B.S., et al., *Robust internal elastic lamina fenestration in skeletal muscle arteries.* PLoS One, 2013. **8**(1): p. e54849.
16. Ledoux, J., et al., *Functional architecture of inositol 1,4,5-trisphosphate signaling in restricted spaces of myoendothelial projections.* Proc Natl Acad Sci U S A, 2008. **105**(28): p. 9627-32.
17. Sandow, S.L., et al., *What's where and why at a vascular myoendothelial microdomain signalling complex.* Clin Exp Pharmacol Physiol, 2009. **36**(1): p. 67-76.
18. Masuda, H., et al., *Adaptive remodeling of internal elastic lamina and endothelial lining during flow-induced arterial enlargement.* Arterioscler Thromb Vasc Biol, 1999. **19**(10): p. 2298-307.

19. Gunst, S.J. and J.J. Fredberg, *The first three minutes: smooth muscle contraction, cytoskeletal events, and soft glasses.* J Appl Physiol (1985), 2003. **95**(1): p. 413-25.
20. Kuriyama, H., et al., *Factors modifying contraction-relaxation cycle in vascular smooth muscles.* Am J Physiol, 1982. **243**(5): p. H641-62.
21. Stenmark, K.R., et al., *Role of the adventitia in pulmonary vascular remodeling.* Physiology (Bethesda), 2006. **21**: p. 134-45.
22. Michel, R.P., F. Hu, and B.O. Meyrick, *Myoendothelial junctional complexes in postobstructive pulmonary vasculopathy: a quantitative electron microscopic study.* Exp Lung Res, 1995. **21**(3): p. 437-52.
23. Wagenvoort, C.A., *Morphologic changes in intrapulmonary veins.* Hum Pathol, 1970. **1**(2): p. 205-13.
24. Aharinejad, S., et al., *Scanning and transmission electron microscopy of venous sphincters in the rat lung.* Anat Rec, 1992. **233**(4): p. 555-68.
25. Schraufnagel, D.E. and K.R. Patel, *Sphincters in pulmonary veins. An anatomic study in rats.* Am Rev Respir Dis, 1990. **141**(3): p. 721-6.
26. Gao, Y. and J.U. Raj, *Role of veins in regulation of pulmonary circulation.* Am J Physiol Lung Cell Mol Physiol, 2005. **288**(2): p. L213-26.
27. Matsuki, T. and T. Ohhashi, *Endothelium and mechanical responses of isolated monkey pulmonary veins to histamine.* Am J Physiol, 1990. **259**(4 Pt 2): p. H1032-7.
28. Raj, J.U. and J. Anderson, *Pulmonary venous responses to thromboxane A2 analogue and atrial natriuretic peptide in lambs.* Circ Res, 1990. **66**(2): p. 496-502.
29. Baile, E.M., *The anatomy and physiology of the bronchial circulation.* J Aerosol Med, 1996. **9**(1): p. 1-6.
30. Walker, C.M., et al., *Bronchial arteries: anatomy, function, hypertrophy, and anomalies.* Radiographics, 2015. **35**(1): p. 32-49.
31. Celermajer, D.S., et al., *Role of endothelium in the maintenance of low pulmonary vascular tone in normal children.* Circulation, 1994. **89**(5): p. 2041-4.
32. Dinh-Xuan, A.T., *Endothelial modulation of pulmonary vascular tone.* Eur Respir J, 1992. **5**(6): p. 757-62.
33. Dawson, C.A., *Role of pulmonary vasomotion in physiology of the lung.* Physiol Rev, 1984. **64**(2): p. 544-616.
34. Kubota, E., et al., *Autonomic innervation of pulmonary artery: evidence for a nonadrenergic noncholinergic inhibitory system.* Exp Lung Res, 1988. **14**(3): p. 349-58.
35. Gordon, J.B., et al., *Pulmonary vascular responses during acute and sustained respiratory alkalosis or acidosis in intact newborn piglets.* Pediatr Res, 1999. **46**(6): p. 735-41.
36. Naeije, R. and N. Chesler, *Pulmonary circulation at exercise.* Compr Physiol, 2012. **2**(1): p. 711-41.
37. Swiston, J.R., S.R. Johnson, and J.T. Granton, *Factors that prognosticate mortality in idiopathic pulmonary arterial hypertension: a systematic review of the literature.* Respir Med, 2010. **104**(11): p. 1588-607.
38. McLaughlin, V.V., et al., *ACCF/AHA 2009 expert consensus document on pulmonary hypertension: a report of the American College of Cardiology Foundation Task Force on Expert Consensus Documents and the American Heart Association: developed in collaboration with the American College of*

Chest Physicians, American Thoracic Society, Inc., and the Pulmonary Hypertension Association. Circulation, 2009. **119**(16): p. 2250-94.
39. Rossaint, R., et al., *Inhaled nitric oxide: its effects on pulmonary circulation and airway smooth muscle cells.* Eur Heart J, 1993. **14 Suppl I**: p. 133-40.
40. Dias-Junior, C.A., S.B. Cau, and J.E. Tanus-Santos, *[Role of nitric oxide in the control of the pulmonary circulation: physiological, pathophysiological, and therapeutic implications].* J Bras Pneumol, 2008. **34**(6): p. 412-9.
41. Moncada, S. and E.A. Higgs, *The discovery of nitric oxide and its role in vascular biology.* Br J Pharmacol, 2006. **147 Suppl 1**: p. S193-201.
42. Feletou, M. and P.M. Vanhoutte, *Endothelium-derived hyperpolarizing factor: where are we now?* Arterioscler Thromb Vasc Biol, 2006. **26**(6): p. 1215-25.
43. Feletou, M., in *The Endothelium: Part 2: EDHF-Mediated Responses "The Classical Pathway"*. 2011: San Rafael (CA).
44. Busse, R., et al., *EDHF: bringing the concepts together.* Trends Pharmacol Sci, 2002. **23**(8): p. 374-80.
45. Feletou, M. and P.M. Vanhoutte, *EDHF: an update.* Clin Sci (Lond), 2009. **117**(4): p. 139-55.
46. White, S.R., et al., *Epithelial modulation of airway smooth muscle response to endothelin-1.* Am Rev Respir Dis, 1991. **144**(2): p. 373-8.
47. Imai, T., et al., *Induction of endothelin-1 gene by angiotensin and vasopressin in endothelial cells.* Hypertension, 1992. **19**(6 Pt 2): p. 753-7.
48. Yoshizumi, M., et al., *Hemodynamic shear stress stimulates endothelin production by cultured endothelial cells.* Biochem Biophys Res Commun, 1989. **161**(2): p. 859-64.
49. Montani, D., et al., *Endothelin-1/endothelin-3 ratio: a potential prognostic factor of pulmonary arterial hypertension.* Chest, 2007. **131**(1): p. 101-8.
50. Spiropoulos, K., et al., *Endothelin-1 levels in the pathophysiology of chronic obstructive pulmonary disease and bronchial asthma.* Respir Med, 2003. **97**(8): p. 983-9.
51. Muller, D.N., et al., *Vascular angiotensin-converting enzyme expression regulates local angiotensin II.* Hypertension, 1997. **29**(1 Pt 1): p. 98-104.
52. Abenhaim, L., et al., *Appetite-suppressant drugs and the risk of primary pulmonary hypertension. International Primary Pulmonary Hypertension Study Group.* N Engl J Med, 1996. **335**(9): p. 609-16.
53. Kramer, M.S. and D.A. Lane, *Aminorex, dexfenfluramine, and primary pulmonary hypertension.* J Clin Epidemiol, 1998. **51**(4): p. 361-4.
54. Rieg, A.D., et al., *Cardiovascular agents affect the tone of pulmonary arteries and veins in precision-cut lung slices.* PLoS One, 2011. **6**(12): p. e29698.
55. Arrigoni, F.I., et al., *Newborn intrapulmonary veins are more reactive than arteries in normal and hypertensive piglets.* Am J Physiol, 1999. **277**(5 Pt 1): p. L887-92.
56. Back, M., et al., *Modulation of vascular tone and reactivity by nitric oxide in porcine pulmonary arteries and veins.* Acta Physiol Scand, 2002. **174**(1): p. 9-15.
57. Bina, S., et al., *Factors contributing to differences in the regulation of cGMP in isolated porcine pulmonary vessels.* Eur J Pharmacol, 1998. **351**(2): p. 253-60.
58. Okogbule-Wonodi, A.C., et al., *Phosphodiesterase activity in intrapulmonary arteries and veins of perinatal lambs.* Mol Genet Metab, 1998. **65**(3): p. 229-37.

59. Brink, C., et al., *Effects and specific binding sites of endothelin in human lung preparations.* Pulm Pharmacol, 1991. **4**(1): p. 54-9.
60. Aharinejad, S., et al., *Endothelin-1 focally constricts pulmonary veins in rats.* J Thorac Cardiovasc Surg, 1995. **110**(1): p. 148-56.
61. Toga, H., B.O. Ibe, and J.U. Raj, *In vitro responses of ovine intrapulmonary arteries and veins to endothelin-1.* Am J Physiol, 1992. **263**(1 Pt 1): p. L15-21.
62. Wang, Y. and F. Coceani, *Isolated pulmonary resistance vessels from fetal lambs. Contractile behavior and responses to indomethacin and endothelin-1.* Circ Res, 1992. **71**(2): p. 320-30.
63. Kemp, B.K., J.J. Smolich, and T.M. Cocks, *Evidence for specific regional patterns of responses to different vasoconstrictors and vasodilators in sheep isolated pulmonary arteries and veins.* Br J Pharmacol, 1997. **121**(3): p. 441-50.
64. Miller, D.S., et al., *Role of arachidonic acid metabolites in hypoxic contractions of isolated porcine pulmonary artery and vein.* Exp Lung Res, 1989. **15**(2): p. 213-22.
65. Walch, L., et al., *Prostanoid EP(1)- and TP-receptors involved in the contraction of human pulmonary veins.* Br J Pharmacol, 2001. **134**(8): p. 1671-8.
66. House, S.J., et al., *The non-excitable smooth muscle: calcium signaling and phenotypic switching during vascular disease.* Pflugers Arch, 2008. **456**(5): p. 769-85.
67. Hill, C.E., J.K. Phillips, and S.L. Sandow, *Heterogeneous control of blood flow amongst different vascular beds.* Med Res Rev, 2001. **21**(1): p. 1-60.
68. Alzayady, K.J., et al., *Functional inositol 1,4,5-trisphosphate receptors assembled from concatenated homo- and heteromeric subunits.* J Biol Chem, 2013. **288**(41): p. 29772-84.
69. Thrower, E.C., R.E. Hagar, and B.E. Ehrlich, *Regulation of Ins(1,4,5)P3 receptor isoforms by endogenous modulators.* Trends Pharmacol Sci, 2001. **22**(11): p. 580-6.
70. Mikoshiba, K., *IP3 receptor/Ca2+ channel: from discovery to new signaling concepts.* J Neurochem, 2007. **102**(5): p. 1426-46.
71. Mikoshiba, K., *The IP3 receptor/Ca2+ channel and its cellular function.* Biochem Soc Symp, 2007(74): p. 9-22.
72. Finch, E.A., T.J. Turner, and S.M. Goldin, *Calcium as a coagonist of inositol 1,4,5-trisphosphate-induced calcium release.* Science, 1991. **252**(5004): p. 443-6.
73. Marchant, J.S. and C.W. Taylor, *Cooperative activation of IP3 receptors by sequential binding of IP3 and Ca2+ safeguards against spontaneous activity.* Curr Biol, 1997. **7**(7): p. 510-8.
74. Iino, M., *Biphasic Ca2+ dependence of inositol 1,4,5-trisphosphate-induced Ca release in smooth muscle cells of the guinea pig taenia caeci.* J Gen Physiol, 1990. **95**(6): p. 1103-22.
75. Franzini-Armstrong, C., *Studies of the triad. II. Penetration of tracers into the junctional gap.* J Cell Biol, 1971. **49**(1): p. 196-203.
76. Kushnir, A. and A.R. Marks, *The ryanodine receptor in cardiac physiology and disease.* Adv Pharmacol, 2010. **59**: p. 1-30.
77. Inui, M., A. Saito, and S. Fleischer, *Isolation of the ryanodine receptor from cardiac sarcoplasmic reticulum and identity with the feet structures.* J Biol Chem, 1987. **262**(32): p. 15637-42.

78. Bhat, M.B., et al., *Functional calcium release channel formed by the carboxyl-terminal portion of ryanodine receptor.* Biophys J, 1997. **73**(3): p. 1329-36.
79. Yang, X.R., et al., *Multiple ryanodine receptor subtypes and heterogeneous ryanodine receptor-gated Ca2+ stores in pulmonary arterial smooth muscle cells.* Am J Physiol Lung Cell Mol Physiol, 2005. **289**(2): p. L338-48.
80. Zheng, Y.M., et al., *Heterogeneous gene expression and functional activity of ryanodine receptors in resistance and conduit pulmonary as well as mesenteric artery smooth muscle cells.* J Vasc Res, 2008. **45**(6): p. 469-79.
81. Tripathy, A. and G. Meissner, *Sarcoplasmic reticulum lumenal Ca2+ has access to cytosolic activation and inactivation sites of skeletal muscle Ca2+ release channel.* Biophys J, 1996. **70**(6): p. 2600-15.
82. Steele, D.S. and A.M. Duke, *Defective Mg2+ regulation of RyR1 as a causal factor in malignant hyperthermia.* Arch Biochem Biophys, 2007. **458**(1): p. 57-64.
83. Laver, D.R., G.K. Lenz, and G.D. Lamb, *Regulation of the calcium release channel from rabbit skeletal muscle by the nucleotides ATP, AMP, IMP and adenosine.* J Physiol, 2001. **537**(Pt 3): p. 763-78.
84. Tripathy, A., et al., *Calmodulin activation and inhibition of skeletal muscle Ca2+ release channel (ryanodine receptor).* Biophys J, 1995. **69**(1): p. 106-19.
85. Rodriguez, P., M.S. Bhogal, and J. Colyer, *Stoichiometric phosphorylation of cardiac ryanodine receptor on serine 2809 by calmodulin-dependent kinase II and protein kinase A.* J Biol Chem, 2003. **278**(40): p. 38593-600.
86. Wehrens, X.H., et al., *Ca2+/calmodulin-dependent protein kinase II phosphorylation regulates the cardiac ryanodine receptor.* Circ Res, 2004. **94**(6): p. e61-70.
87. Brini, M. and E. Carafoli, *Calcium pumps in health and disease.* Physiol Rev, 2009. **89**(4): p. 1341-78.
88. Meldolesi, J. and T. Pozzan, *The endoplasmic reticulum Ca2+ store: a view from the lumen.* Trends Biochem Sci, 1998. **23**(1): p. 10-4.
89. Clark, J.H., et al., *Identification of functionally segregated sarcoplasmic reticulum calcium stores in pulmonary arterial smooth muscle.* J Biol Chem, 2010. **285**(18): p. 13542-9.
90. Prieto-Lloret, J. and P.I. Aaronson, *Intracellular remodelling of Ca2+ stores in pulmonary hypertension.* Cardiovasc Res, 2014. **103**(2): p. 189-91.
91. Balint, Z., et al., *Double-stranded RNA attenuates the barrier function of human pulmonary artery endothelial cells.* PLoS One, 2014. **8**(6): p. e63776.
92. Nicoll, D.A., et al., *A new topological model of the cardiac sarcolemmal Na+-Ca2+ exchanger.* J Biol Chem, 1999. **274**(2): p. 910-7.
93. Shigekawa, M., et al., *Probing ion binding sites in the Na+/Ca2+ exchanger.* Ann N Y Acad Sci, 2002. **976**: p. 19-30.
94. Rinne, A., K. Banach, and L.A. Blatter, *Regulation of nuclear factor of activated T cells (NFAT) in vascular endothelial cells.* J Mol Cell Cardiol, 2009. **47**(3): p. 400-10.
95. McCord, A.M., J. Cuevas, and B.E. Anderson, *Bartonella-induced endothelial cell proliferation is mediated by release of calcium from intracellular stores.* DNA Cell Biol, 2007. **26**(9): p. 657-63.
96. Yiu, A.J., et al., *Melamine induces Ca(2+)-sensing receptor activation and elicits apoptosis in proximal tubular cells.* Am J Physiol Cell Physiol, 2017. **313**(1): p. C27-C41.

97. Otun, H., et al., *Interactions between inositol trisphosphate and Ca2+ dependent Ca2+ release mechanisms on the endoplasmic reticulum of permeabilised bovine aortic endothelial cells.* Cell Calcium, 1996. **19**(4): p. 315-25.
98. Berridge, M.J., *Elementary and global aspects of calcium signalling.* J Physiol, 1997. **499 (Pt 2)**: p. 291-306.
99. Amberg, G.C. and M.F. Navedo, *Calcium dynamics in vascular smooth muscle.* Microcirculation, 2013. **20**(4): p. 281-9.
100. Parker, I., J. Choi, and Y. Yao, *Elementary events of InsP3-induced Ca2+ liberation in Xenopus oocytes: hot spots, puffs and blips.* Cell Calcium, 1996. **20**(2): p. 105-21.
101. Bootman, M., et al., *Imaging the hierarchical Ca2+ signalling system in HeLa cells.* J Physiol, 1997. **499 (Pt 2)**: p. 307-14.
102. Huser, J. and L.A. Blatter, *Elementary events of agonist-induced Ca2+ release in vascular endothelial cells.* Am J Physiol, 1997. **273**(5 Pt 1): p. C1775-82.
103. Burdyga, T., et al., *A new technique for simultaneous and in situ measurements of Ca2+ signals in arteriolar smooth muscle and endothelial cells.* Cell Calcium, 2003. **34**(1): p. 27-33.
104. Foskett, J.K., et al., *Inositol trisphosphate receptor Ca2+ release channels.* Physiol Rev, 2007. **87**(2): p. 593-658.
105. Yao, Y., J. Choi, and I. Parker, *Quantal puffs of intracellular Ca2+ evoked by inositol trisphosphate in Xenopus oocytes.* J Physiol, 1995. **482 (Pt 3)**: p. 533-53.
106. Thomas, D., et al., *Microscopic properties of elementary Ca2+ release sites in non-excitable cells.* Curr Biol, 2000. **10**(1): p. 8-15.
107. Bootman, M.D., *Hormone-evoked subcellular Ca2+ signals in HeLa cells.* Cell Calcium, 1996. **20**(2): p. 97-104.
108. Marchant, J., N. Callamaras, and I. Parker, *Initiation of IP(3)-mediated Ca(2+) waves in Xenopus oocytes.* EMBO J, 1999. **18**(19): p. 5285-99.
109. Cheng, H., W.J. Lederer, and M.B. Cannell, *Calcium sparks: elementary events underlying excitation-contraction coupling in heart muscle.* Science, 1993. **262**(5134): p. 740-4.
110. Wegner, F., et al., *Elementary Ca2+ release events in mammalian skeletal muscle: effects of the anaesthetic drug thiopental.* J Muscle Res Cell Motil, 2006. **27**(5-7): p. 315-26.
111. Benham, C.D. and T.B. Bolton, *Spontaneous transient outward currents in single visceral and vascular smooth muscle cells of the rabbit.* J Physiol, 1986. **381**: p. 385-406.
112. Jaggar, J.H., et al., *Calcium sparks in smooth muscle.* Am J Physiol Cell Physiol, 2000. **278**(2): p. C235-56.
113. Perez, G.J., A.D. Bonev, and M.T. Nelson, *Micromolar Ca(2+) from sparks activates Ca(2+)-sensitive K(+) channels in rat cerebral artery smooth muscle.* Am J Physiol Cell Physiol, 2001. **281**(6): p. C1769-75.
114. Sonkusare, S.K., et al., *Elementary Ca2+ signals through endothelial TRPV4 channels regulate vascular function.* Science, 2012. **336**(6081): p. 597-601.
115. Sonkusare, S.K., et al., *AKAP150-dependent cooperative TRPV4 channel gating is central to endothelium-dependent vasodilation and is disrupted in hypertension.* Sci Signal, 2014. **7**(333): p. ra66.
116. Santana, L.F. and M.F. Navedo, *Molecular and biophysical mechanisms of Ca2+ sparklets in smooth muscle.* J Mol Cell Cardiol, 2009. **47**(4): p. 436-44.

117. Earley, S., A.L. Gonzales, and R. Crnich, *Endothelium-dependent cerebral artery dilation mediated by TRPA1 and Ca2+-Activated K+ channels.* Circ Res, 2009. **104**(8): p. 987-94.
118. Sullivan, M.N., et al., *Localized TRPA1 channel Ca2+ signals stimulated by reactive oxygen species promote cerebral artery dilation.* Sci Signal, 2015. **8**(358): p. ra2.
119. Tran, C.H., et al., *Endothelial Ca2+ wavelets and the induction of myoendothelial feedback.* Am J Physiol Cell Physiol, 2012. **302**(8): p. C1226-42.
120. Montell, C. and G.M. Rubin, *Molecular characterization of the Drosophila trp locus: a putative integral membrane protein required for phototransduction.* Neuron, 1989. **2**(4): p. 1313-23.
121. Clapham, D.E., *Signal transduction. Hot and cold TRP ion channels.* Science, 2002. **295**(5563): p. 2228-9.
122. Clapham, D.E., L.W. Runnels, and C. Strubing, *The TRP ion channel family.* Nat Rev Neurosci, 2001. **2**(6): p. 387-96.
123. Montell, C., *Physiology, phylogeny, and functions of the TRP superfamily of cation channels.* Sci STKE, 2001. **2001**(90): p. re1.
124. Moran, M.M., et al., *Transient receptor potential channels as therapeutic targets.* Nat Rev Drug Discov, 2011. **10**(8): p. 601-20.
125. Fernandez, R.A., et al., *Pathogenic role of store-operated and receptor-operated ca(2+) channels in pulmonary arterial hypertension.* J Signal Transduct, 2012. **2012**: p. 951497.
126. Banner, K.H., F. Igney, and C. Poll, *TRP channels: emerging targets for respiratory disease.* Pharmacol Ther, 2011. **130**(3): p. 371-84.
127. Flockerzi, V., *An introduction on TRP channels.* Handb Exp Pharmacol, 2007(179): p. 1-19.
128. Venkatachalam, K. and C. Montell, *TRP channels.* Annu Rev Biochem, 2007. **76**: p. 387-417.
129. Pan, Z., H. Yang, and P.S. Reinach, *Transient receptor potential (TRP) gene superfamily encoding cation channels.* Hum Genomics, 2011. **5**(2): p. 108-16.
130. Ramsey, I.S., M. Delling, and D.E. Clapham, *An introduction to TRP channels.* Annu Rev Physiol, 2006. **68**: p. 619-47.
131. Owsianik, G., et al., *Structure-function relationship of the TRP channel superfamily.* Rev Physiol Biochem Pharmacol, 2006. **156**: p. 61-90.
132. Rohacs, T., et al., *PI(4,5)P2 regulates the activation and desensitization of TRPM8 channels through the TRP domain.* Nat Neurosci, 2005. **8**(5): p. 626-34.
133. Watanabe, H., *Pathological role of TRP channels in cardiovascular and respiratory diseases.* Nihon Yakurigaku Zasshi, 2009. **134**(3): p. 127-30.
134. Montell, C., *The TRP superfamily of cation channels.* Sci STKE, 2005. **2005**(272): p. re3.
135. Zygmunt, P.M., et al., *Vanilloid receptors on sensory nerves mediate the vasodilator action of anandamide.* Nature, 1999. **400**(6743): p. 452-7.
136. Bandell, M., et al., *Noxious cold ion channel TRPA1 is activated by pungent compounds and bradykinin.* Neuron, 2004. **41**(6): p. 849-57.
137. Caterina, M.J., et al., *The capsaicin receptor: a heat-activated ion channel in the pain pathway.* Nature, 1997. **389**(6653): p. 816-24.
138. Plant, T.D. and R. Strotmann, *TRPV4: A Multifunctional Nonselective Cation Channel with Complex Regulation*, in *TRP Ion Channel Function in Sensory*

Transduction and Cellular Signaling Cascades, W.B. Liedtke and S. Heller, Editors. 2007: Boca Raton (FL).
139. Caterina, M.J., et al., *A capsaicin-receptor homologue with a high threshold for noxious heat.* Nature, 1999. **398**(6726): p. 436-41.
140. Xu, H., et al., *Oregano, thyme and clove-derived flavors and skin sensitizers activate specific TRP channels.* Nat Neurosci, 2006. **9**(5): p. 628-35.
141. Tominaga, M., et al., *The cloned capsaicin receptor integrates multiple pain-producing stimuli.* Neuron, 1998. **21**(3): p. 531-43.
142. Jordt, S.E., M. Tominaga, and D. Julius, *Acid potentiation of the capsaicin receptor determined by a key extracellular site.* Proc Natl Acad Sci U S A, 2000. **97**(14): p. 8134-9.
143. Boltana, S., et al., *The expression of TRPV channels, prostaglandin E2 and pro-inflammatory cytokines during behavioural fever in fish.* Brain Behav Immun, 2018. **71**: p. 169-181.
144. Jia, Y. and L.Y. Lee, *Role of TRPV receptors in respiratory diseases.* Biochim Biophys Acta, 2007. **1772**(8): p. 915-27.
145. Stratiievska, A., et al., *Reciprocal regulation among TRPV1 channels and phosphoinositide 3-kinase in response to nerve growth factor.* Elife, 2018. **7**.
146. Liedtke, W., et al., *Vanilloid receptor-related osmotically activated channel (VR-OAC), a candidate vertebrate osmoreceptor.* Cell, 2000. **103**(3): p. 525-35.
147. Delany, N.S., et al., *Identification and characterization of a novel human vanilloid receptor-like protein, VRL-2.* Physiol Genomics, 2001. **4**(3): p. 165-74.
148. Strotmann, R., et al., *OTRPC4, a nonselective cation channel that confers sensitivity to extracellular osmolarity.* Nat Cell Biol, 2000. **2**(10): p. 695-702.
149. Wissenbach, U., et al., *Trp12, a novel Trp related protein from kidney.* FEBS Lett, 2000. **485**(2-3): p. 127-34.
150. Everaerts, W., B. Nilius, and G. Owsianik, *The vanilloid transient receptor potential channel TRPV4: from structure to disease.* Prog Biophys Mol Biol, 2010. **103**(1): p. 2-17.
151. Arniges, M., et al., *Human TRPV4 channel splice variants revealed a key role of ankyrin domains in multimerization and trafficking.* J Biol Chem, 2006. **281**(3): p. 1580-6.
152. Xu, H., et al., *Glycosylation of the osmoresponsive transient receptor potential channel TRPV4 on Asn-651 influences membrane trafficking.* Am J Physiol Renal Physiol, 2006. **290**(5): p. F1103-9.
153. Strotmann, R., G. Schultz, and T.D. Plant, *Ca2+-dependent potentiation of the nonselective cation channel TRPV4 is mediated by a C-terminal calmodulin binding site.* J Biol Chem, 2003. **278**(29): p. 26541-9.
154. Ma, X., et al., *Functional role of vanilloid transient receptor potential 4-canonical transient receptor potential 1 complex in flow-induced Ca2+ influx.* Arterioscler Thromb Vasc Biol, 2010. **30**(4): p. 851-8.
155. Liedtke, W., *Transient receptor potential vanilloid channels functioning in transduction of osmotic stimuli.* J Endocrinol, 2006. **191**(3): p. 515-23.
156. Nilius, B., et al., *Differential activation of the volume-sensitive cation channel TRP12 (OTRPC4) and volume-regulated anion currents in HEK-293 cells.* Pflugers Arch, 2001. **443**(2): p. 227-33.
157. Voets, T., et al., *Molecular determinants of permeation through the cation channel TRPV4.* J Biol Chem, 2002. **277**(37): p. 33704-10.

158. Watanabe, H., et al., *Activation of TRPV4 channels (hVRL-2/mTRP12) by phorbol derivatives.* J Biol Chem, 2002. **277**(16): p. 13569-77.
159. Watanabe, H., et al., *Heat-evoked activation of TRPV4 channels in a HEK293 cell expression system and in native mouse aorta endothelial cells.* J Biol Chem, 2002. **277**(49): p. 47044-51.
160. Wegierski, T., et al., *Tyrosine phosphorylation modulates the activity of TRPV4 in response to defined stimuli.* J Biol Chem, 2009. **284**(5): p. 2923-33.
161. Nilius, B., H. Watanabe, and J. Vriens, *The TRPV4 channel: structure-function relationship and promiscuous gating behaviour.* Pflugers Arch, 2003. **446**(3): p. 298-303.
162. Vriens, J., et al., *Modulation of the Ca2 permeable cation channel TRPV4 by cytochrome P450 epoxygenases in vascular endothelium.* Circ Res, 2005. **97**(9): p. 908-15.
163. Jin, M., J. Berrout, and R.G. O'Neil, *Regulation of TRP Channels by Osmomechanical Stress*, in *TRP Channels*, M.X. Zhu, Editor. 2011: Boca Raton (FL).
164. Watanabe, H., et al., *Anandamide and arachidonic acid use epoxyeicosatrienoic acids to activate TRPV4 channels.* Nature, 2003. **424**(6947): p. 434-8.
165. Vriens, J., et al., *Cell swelling, heat, and chemical agonists use distinct pathways for the activation of the cation channel TRPV4.* Proc Natl Acad Sci U S A, 2004. **101**(1): p. 396-401.
166. Jin, M., et al., *Determinants of TRPV4 activity following selective activation by small molecule agonist GSK1016790A.* PLoS One, 2011. **6**(2): p. e16713.
167. Dong, Q., et al., *Blockage of transient receptor potential vanilloid 4 alleviates myocardial ischemia/reperfusion injury in mice.* Sci Rep, 2017. **7**: p. 42678.
168. Watanabe, H., et al., *Modulation of TRPV4 gating by intra- and extracellular Ca2+.* Cell Calcium, 2003. **33**(5-6): p. 489-95.
169. Liedtke, W. and J.M. Friedman, *Abnormal osmotic regulation in trpv4-/- mice.* Proc Natl Acad Sci U S A, 2003. **100**(23): p. 13698-703.
170. Alessandri-Haber, N., et al., *Hypotonicity induces TRPV4-mediated nociception in rat.* Neuron, 2003. **39**(3): p. 497-511.
171. Tabuchi, K., et al., *Hearing impairment in TRPV4 knockout mice.* Neurosci Lett, 2005. **382**(3): p. 304-8.
172. Lee, H. and M.J. Caterina, *TRPV channels as thermosensory receptors in epithelial cells.* Pflugers Arch, 2005. **451**(1): p. 160-7.
173. Earley, S., et al., *TRPV4 forms a novel Ca2+ signaling complex with ryanodine receptors and BKCa channels.* Circ Res, 2005. **97**(12): p. 1270-9.
174. Yang, X.R., et al., *Functional expression of transient receptor potential melastatin- and vanilloid-related channels in pulmonary arterial and aortic smooth muscle.* Am J Physiol Lung Cell Mol Physiol, 2006. **290**(6): p. L1267-76.
175. Mendoza, S.A., et al., *TRPV4-mediated endothelial Ca2+ influx and vasodilation in response to shear stress.* Am J Physiol Heart Circ Physiol, 2010. **298**(2): p. H466-76.
176. Earley, S., et al., *TRPV4-dependent dilation of peripheral resistance arteries influences arterial pressure.* Am J Physiol Heart Circ Physiol, 2009. **297**(3): p. H1096-102.
177. Zhang, D.X., et al., *Transient receptor potential vanilloid type 4-deficient mice exhibit impaired endothelium-dependent relaxation induced by acetylcholine in vitro and in vivo.* Hypertension, 2009. **53**(3): p. 532-8.

178. Kohler, R. and J. Hoyer, *Role of TRPV4 in the Mechanotransduction of Shear Stress in Endothelial Cells*, in *TRP Ion Channel Function in Sensory Transduction and Cellular Signaling Cascades*, W.B. Liedtke and S. Heller, Editors. 2007: Boca Raton (FL).
179. Feletou, M., *Calcium-activated potassium channels and endothelial dysfunction: therapeutic options?* Br J Pharmacol, 2009. **156**(4): p. 545-62.
180. Filosa, J.A., X. Yao, and G. Rath, *TRPV4 and the regulation of vascular tone.* J Cardiovasc Pharmacol, 2013. **61**(2): p. 113-9.
181. Kwan, H.Y., et al., *TRPC1 associates with BK(Ca) channel to form a signal complex in vascular smooth muscle cells.* Circ Res, 2009. **104**(5): p. 670-8.
182. Dahan, D., et al., *Implication of the ryanodine receptor in TRPV4-induced calcium response in pulmonary arterial smooth muscle cells from normoxic and chronically hypoxic rats.* Am J Physiol Lung Cell Mol Physiol, 2012. **303**(9): p. L824-33.
183. D'Aldebert, E., et al., *Transient receptor potential vanilloid 4 activated inflammatory signals by intestinal epithelial cells and colitis in mice.* Gastroenterology, 2011. **140**(1): p. 275-85.
184. Fichna, J., et al., *Transient receptor potential vanilloid 4 blockade protects against experimental colitis in mice: a new strategy for inflammatory bowel diseases treatment?* Neurogastroenterol Motil, 2012. **24**(11): p. e557-60.
185. Cenac, N., et al., *Transient receptor potential vanilloid-4 has a major role in visceral hypersensitivity symptoms.* Gastroenterology, 2008. **135**(3): p. 937-46, 946 e1-2.
186. Holzer, P., *Transient receptor potential (TRP) channels as drug targets for diseases of the digestive system.* Pharmacol Ther, 2011. **131**(1): p. 142-70.
187. Suzuki, M., et al., *Impaired pressure sensation in mice lacking TRPV4.* J Biol Chem, 2003. **278**(25): p. 22664-8.
188. Ryskamp, D.A., et al., *The polymodal ion channel transient receptor potential vanilloid 4 modulates calcium flux, spiking rate, and apoptosis of mouse retinal ganglion cells.* J Neurosci, 2011. **31**(19): p. 7089-101.
189. Butenko, O., et al., *The increased activity of TRPV4 channel in the astrocytes of the adult rat hippocampus after cerebral hypoxia/ischemia.* PLoS One, 2012. **7**(6): p. e39959.
190. Everaerts, W., et al., *Inhibition of the cation channel TRPV4 improves bladder function in mice and rats with cyclophosphamide-induced cystitis.* Proc Natl Acad Sci U S A, 2010. **107**(44): p. 19084-9.
191. Yang, X.R., et al., *Upregulation of osmo-mechanosensitive TRPV4 channel facilitates chronic hypoxia-induced myogenic tone and pulmonary hypertension.* Am J Physiol Lung Cell Mol Physiol, 2012. **302**(6): p. L555-68.
192. Hamanaka, K., et al., *TRPV4 channels augment macrophage activation and ventilator-induced lung injury.* Am J Physiol Lung Cell Mol Physiol, 2010. **299**(3): p. L353-62.
193. Simonneau, G., et al., *Updated clinical classification of pulmonary hypertension.* J Am Coll Cardiol, 2009. **54**(1 Suppl): p. S43-54.
194. Breitling, S., et al., *The pathophysiology of pulmonary hypertension in left heart disease.* Am J Physiol Lung Cell Mol Physiol, 2015. **309**(9): p. L924-41.
195. Adir, Y. and O. Amir, *Pulmonary hypertension associated with left heart disease.* Semin Respir Crit Care Med, 2013. **34**(5): p. 665-80.

196. Gerges, C., et al., *Diastolic pulmonary vascular pressure gradient: a predictor of prognosis in "out-of-proportion" pulmonary hypertension.* Chest, 2013. **143**(3): p. 758-766.
197. Humbert, M., O. Sitbon, and G. Simonneau, *Treatment of pulmonary arterial hypertension.* N Engl J Med, 2004. **351**(14): p. 1425-36.
198. Galie, N. and A. Branzi, *Pulmonary arterial hypertension: therapeutic algorithm.* Ital Heart J, 2005. **6**(10): p. 856-60.
199. Galie, N., et al., *Sildenafil citrate therapy for pulmonary arterial hypertension.* N Engl J Med, 2005. **353**(20): p. 2148-57.
200. Iglarz, M., et al., *Comparison of Macitentan and Bosentan on Right Ventricular Remodeling in a Rat Model of Non-vasoreactive Pulmonary Hypertension.* J Cardiovasc Pharmacol, 2015. **66**(5): p. 457-67.
201. Iglarz, M., et al., *Pharmacology of macitentan, an orally active tissue-targeting dual endothelin receptor antagonist.* J Pharmacol Exp Ther, 2008. **327**(3): p. 736-45.
202. Bruderer, S., et al., *Absorption, distribution, metabolism, and excretion of macitentan, a dual endothelin receptor antagonist, in humans.* Xenobiotica, 2012. **42**(9): p. 901-10.
203. Pauvert, O., et al., *Effect of sildenafil on cyclic nucleotide phosphodiesterase activity, vascular tone and calcium signaling in rat pulmonary artery.* Br J Pharmacol, 2003. **139**(3): p. 513-22.
204. Michelakis, E.D., et al., *Long-term treatment with oral sildenafil is safe and improves functional capacity and hemodynamics in patients with pulmonary arterial hypertension.* Circulation, 2003. **108**(17): p. 2066-9.
205. Singh, T.S., et al., *Tadalafil in the management of severe pulmonary artery hypertension.* Indian Heart J, 2006. **58**(1): p. 52-3.
206. Rich, S. and V.V. McLaughlin, *The effects of chronic prostacyclin therapy on cardiac output and symptoms in primary pulmonary hypertension.* J Am Coll Cardiol, 1999. **34**(4): p. 1184-7.
207. Kuga, T., et al., *Cell cycle--dependent expression of L- and T-type Ca2+ currents in rat aortic smooth muscle cells in primary culture.* Circ Res, 1996. **79**(1): p. 14-9.
208. Sitbon, O., et al., *Inhaled nitric oxide as a screening agent for safely identifying responders to oral calcium-channel blockers in primary pulmonary hypertension.* Eur Respir J, 1998. **12**(2): p. 265-70.
209. Sitbon, O., et al., *Long-term response to calcium channel blockers in idiopathic pulmonary arterial hypertension.* Circulation, 2005. **111**(23): p. 3105-11.
210. Humbert, M., et al., *Riociguat for the treatment of pulmonary arterial hypertension associated with connective tissue disease: results from PATENT-1 and PATENT-2.* Ann Rheum Dis, 2017. **76**(2): p. 422-426.
211. Lajoie, A.C., et al., *Combination therapy versus monotherapy for pulmonary arterial hypertension: a meta-analysis.* Lancet Respir Med, 2016. **4**(4): p. 291-305.
212. Hoeper, M.M., et al., *Combining inhaled iloprost with bosentan in patients with idiopathic pulmonary arterial hypertension.* Eur Respir J, 2006. **28**(4): p. 691-4.
213. Humbert, M., et al., *Combination of bosentan with epoprostenol in pulmonary arterial hypertension: BREATHE-2.* Eur Respir J, 2004. **24**(3): p. 353-9.
214. Schermuly, R.T., et al., *Urodilatin, a natriuretic peptide stimulating particulate guanylate cyclase, and the phosphodiesterase 5 inhibitor dipyridamole*

attenuate experimental pulmonary hypertension: synergism upon coapplication. Am J Respir Cell Mol Biol, 2001. **25**(2): p. 219-25.
215. Giaid, A., et al., *Expression of endothelin-1 in the lungs of patients with pulmonary hypertension.* N Engl J Med, 1993. **328**(24): p. 1732-9.
216. Christman, B.W., et al., *An imbalance between the excretion of thromboxane and prostacyclin metabolites in pulmonary hypertension.* N Engl J Med, 1992. **327**(2): p. 70-5.
217. Giaid, A. and D. Saleh, *Reduced expression of endothelial nitric oxide synthase in the lungs of patients with pulmonary hypertension.* N Engl J Med, 1995. **333**(4): p. 214-21.
218. Sulica, R., et al., *Clinical and hemodynamic benefit of macitentan and riociguat upfront combination in patients with pulmonary arterial hypertension.* Pulm Circ, 2019. **9**(1): p. 2045894019826944.
219. Hoenicka, M., et al., *Combination Therapy of Pulmonary Arterial Hypertension with Vardenafil and Macitentan Assessed in a Human Ex Vivo Model.* Cardiovasc Drugs Ther, 2019.
220. Fatima, N., et al., *Comparison Of The Efficacy Of Sildenafil Alone Versus Sildenafil Plus Bosentan In Newborns With Persistent Pulmonary Hypertension.* J Ayub Med Coll Abbottabad, 2018. **30**(3): p. 333-336.
221. Humbert, M., et al., *Increased interleukin-1 and interleukin-6 serum concentrations in severe primary pulmonary hypertension.* Am J Respir Crit Care Med, 1995. **151**(5): p. 1628-31.
222. Selimovic, N., et al., *Growth factors and interleukin-6 across the lung circulation in pulmonary hypertension.* Eur Respir J, 2009. **34**(3): p. 662-8.
223. Savale, L., et al., *Impact of interleukin-6 on hypoxia-induced pulmonary hypertension and lung inflammation in mice.* Respir Res, 2009. **10**: p. 6.
224. Steiner, M.K., et al., *Interleukin-6 overexpression induces pulmonary hypertension.* Circ Res, 2009. **104**(2): p. 236-44, 28p following 244.
225. Paulin, R., et al., *Signal transducers and activators of transcription-3/pim1 axis plays a critical role in the pathogenesis of human pulmonary arterial hypertension.* Circulation, 2011. **123**(11): p. 1205-15.
226. Yu, H., et al., *Revisiting STAT3 signalling in cancer: new and unexpected biological functions.* Nat Rev Cancer, 2014. **14**(11): p. 736-46.
227. Tuder, R.M., et al., *Expression of angiogenesis-related molecules in plexiform lesions in severe pulmonary hypertension: evidence for a process of disordered angiogenesis.* J Pathol, 2001. **195**(3): p. 367-74.
228. Paulin, R. and E.D. Michelakis, *The metabolic theory of pulmonary arterial hypertension.* Circ Res, 2014. **115**(1): p. 148-64.
229. Califf, R.M., et al., *A randomized controlled trial of epoprostenol therapy for severe congestive heart failure: The Flolan International Randomized Survival Trial (FIRST).* Am Heart J, 1997. **134**(1): p. 44-54.
230. Packer, M., et al., *Effect of oral milrinone on mortality in severe chronic heart failure. The PROMISE Study Research Group.* N Engl J Med, 1991. **325**(21): p. 1468-75.
231. Bueltmann, M., et al., *Inhaled milrinone attenuates experimental acute lung injury.* Intensive Care Med, 2009. **35**(1): p. 171-8.
232. Hentschel, T., et al., *Inhalation of the phosphodiesterase-3 inhibitor milrinone attenuates pulmonary hypertension in a rat model of congestive heart failure.* Anesthesiology, 2007. **106**(1): p. 124-31.

233. Sablotzki, A., et al., *Iloprost improves hemodynamics in patients with severe chronic cardiac failure and secondary pulmonary hypertension.* Can J Anaesth, 2002. **49**(10): p. 1076-80.
234. Olschewski, H., et al., *Physiologic basis for the treatment of pulmonary hypertension.* J Lab Clin Med, 2001. **138**(5): p. 287-97.
235. Yin, J., et al., *Sildenafil preserves lung endothelial function and prevents pulmonary vascular remodeling in a rat model of diastolic heart failure.* Circ Heart Fail, 2011. **4**(2): p. 198-206.
236. Lewis, G.D., et al., *Sildenafil improves exercise capacity and quality of life in patients with systolic heart failure and secondary pulmonary hypertension.* Circulation, 2007. **116**(14): p. 1555-62.
237. Guazzi, M., et al., *The effects of phosphodiesterase-5 inhibition with sildenafil on pulmonary hemodynamics and diffusion capacity, exercise ventilatory efficiency, and oxygen uptake kinetics in chronic heart failure.* J Am Coll Cardiol, 2004. **44**(12): p. 2339-48.
238. Guazzi, M., et al., *PDE5 inhibition with sildenafil improves left ventricular diastolic function, cardiac geometry, and clinical status in patients with stable systolic heart failure: results of a 1-year, prospective, randomized, placebo-controlled study.* Circ Heart Fail, 2011. **4**(1): p. 8-17.
239. Redfield, M.M., et al., *Effect of phosphodiesterase-5 inhibition on exercise capacity and clinical status in heart failure with preserved ejection fraction: a randomized clinical trial.* JAMA, 2013. **309**(12): p. 1268-77.
240. Yin, N., et al., *Inhaled nitric oxide versus aerosolized iloprost for the treatment of pulmonary hypertension with left heart disease.* Crit Care Med, 2009. **37**(3): p. 980-6.
241. Haraldsson, A., et al., *Comparison of inhaled nitric oxide and inhaled aerosolized prostacyclin in the evaluation of heart transplant candidates with elevated pulmonary vascular resistance.* Chest, 1998. **114**(3): p. 780-6.
242. Anand, I., et al., *Long-term effects of darusentan on left-ventricular remodelling and clinical outcomes in the EndothelinA Receptor Antagonist Trial in Heart Failure (EARTH): randomised, double-blind, placebo-controlled trial.* Lancet, 2004. **364**(9431): p. 347-54.
243. Kalra, P.R., J.C. Moon, and A.J. Coats, *Do results of the ENABLE (Endothelin Antagonist Bosentan for Lowering Cardiac Events in Heart Failure) study spell the end for non-selective endothelin antagonism in heart failure?* Int J Cardiol, 2002. **85**(2-3): p. 195-7.
244. Mylona, P. and J.G. Cleland, *Update of REACH-1 and MERIT-HF clinical trials in heart failure. Cardio.net Editorial Team.* Eur J Heart Fail, 1999. **1**(2): p. 197-200.
245. Bonderman, D., et al., *Riociguat for patients with pulmonary hypertension caused by systolic left ventricular dysfunction: a phase IIb double-blind, randomized, placebo-controlled, dose-ranging hemodynamic study.* Circulation, 2013. **128**(5): p. 502-11.
246. Soubrier, F., et al., *Genetics and genomics of pulmonary arterial hypertension.* J Am Coll Cardiol, 2013. **62**(25 Suppl): p. D13-21.
247. Said, S.I., et al., *Moderate pulmonary arterial hypertension in male mice lacking the vasoactive intestinal peptide gene.* Circulation, 2007. **115**(10): p. 1260-8.

248. Dempsey, E.C., et al., *Neprilysin null mice develop exaggerated pulmonary vascular remodeling in response to chronic hypoxia.* Am J Pathol, 2009. **174**(3): p. 782-96.
249. Chu, D., et al., *A new animal model for pulmonary hypertension based on the overexpression of a single gene, angiopoietin-1.* Ann Thorac Surg, 2004. **77**(2): p. 449-56; discussion 456-7.
250. Greenway, S., et al., *S100A4/Mts1 produces murine pulmonary artery changes resembling plexogenic arteriopathy and is increased in human plexogenic arteriopathy.* Am J Pathol, 2004. **164**(1): p. 253-62.
251. Das, M., et al., *A process-based review of mouse models of pulmonary hypertension.* Pulm Circ, 2012. **2**(4): p. 415-33.
252. Estep, J.E., et al., *[14C]monocrotaline kinetics and metabolism in the rat.* Drug Metab Dispos, 1991. **19**(1): p. 135-9.
253. Campian, M.E., et al., *How valid are animal models to evaluate treatments for pulmonary hypertension?* Naunyn Schmiedebergs Arch Pharmacol, 2006. **373**(6): p. 391-400.
254. Wang, H.L., et al., *5-HT1B receptor augmented 5-HT vasoconstrictor response of pulmonary artery in monocrotaline-induced pulmonary hypertensive rats.* Acta Pharmacol Sin, 2001. **22**(3): p. 269-73.
255. Naeije, R. and L. Dewachter, *[Animal models of pulmonary arterial hypertension].* Rev Mal Respir, 2007. **24**(4 Pt 1): p. 481-96.
256. Okada, M., et al., *Omentopexy for anastomotic dehiscence after tracheal sleeve pneumonectomy.* Thorac Cardiovasc Surg, 1997. **45**(3): p. 144-5.
257. Steudel, W., et al., *Sustained pulmonary hypertension and right ventricular hypertrophy after chronic hypoxia in mice with congenital deficiency of nitric oxide synthase 3.* J Clin Invest, 1998. **101**(11): p. 2468-77.
258. Janssens, S.P., et al., *Polycythemia and vascular remodeling in chronic hypoxic pulmonary hypertension in guinea pigs.* J Appl Physiol (1985), 1991. **71**(6): p. 2218-23.
259. Stenmark, K.R., et al., *Animal models of pulmonary arterial hypertension: the hope for etiological discovery and pharmacological cure.* Am J Physiol Lung Cell Mol Physiol, 2009. **297**(6): p. L1013-32.
260. Graham, B.B., et al., *Schistosomiasis-associated pulmonary hypertension: pulmonary vascular disease: the global perspective.* Chest, 2010. **137**(6 Suppl): p. 20S-29S.
261. Graham, B.B., et al., *Schistosomiasis-induced experimental pulmonary hypertension: role of interleukin-13 signaling.* Am J Pathol, 2010. **177**(3): p. 1549-61.
262. Papamatheakis, D.G., et al., *Schistosomiasis-associated pulmonary hypertension.* Pulm Circ, 2014. **4**(4): p. 596-611.
263. Muramatsu, M., *[Fawn-Hooded Rat; an animal model of development of pulmonary hypertension].* Nihon Rinsho, 2001. **59**(6): p. 1070-5.
264. Jarman, E.R., et al., *A translational preclinical model of interstitial pulmonary fibrosis and pulmonary hypertension: mechanistic pathways driving disease pathophysiology.* Physiol Rep, 2014. **2**(9).
265. Ciuclan, L., et al., *A novel murine model of severe pulmonary arterial hypertension.* Am J Respir Crit Care Med, 2011. **184**(10): p. 1171-82.
266. Taraseviciene-Stewart, L., et al., *Inhibition of the VEGF receptor 2 combined with chronic hypoxia causes cell death-dependent pulmonary endothelial cell*

proliferation and severe pulmonary hypertension. FASEB J, 2001. **15**(2): p. 427-38.
267. Taichman, D.B. and J. Mandel, *Epidemiology of pulmonary arterial hypertension.* Clin Chest Med, 2013. **34**(4): p. 619-37.
268. Cracowski, J.L., et al., *Proinflammatory cytokine levels are linked to death in pulmonary arterial hypertension.* Eur Respir J, 2014. **43**(3): p. 915-7.
269. Soon, E., et al., *Elevated levels of inflammatory cytokines predict survival in idiopathic and familial pulmonary arterial hypertension.* Circulation, 2010. **122**(9): p. 920-7.
270. Coste, F., et al., *Chronic hypoxia aggravates monocrotaline-induced pulmonary arterial hypertension: a rodent relevant model to the human severe form of the disease.* Respir Res, 2017. **18**(1): p. 47.
271. Okada, K., et al., *Pulmonary hemodynamics modify the rat pulmonary artery response to injury. A neointimal model of pulmonary hypertension.* Am J Pathol, 1997. **151**(4): p. 1019-25.
272. Chen, Y., et al., *Left ventricular failure produces profound lung remodeling and pulmonary hypertension in mice: heart failure causes severe lung disease.* Hypertension, 2012. **59**(6): p. 1170-8.
273. Hirata, M., et al., *Novel Model of Pulmonary Artery Banding Leading to Right Heart Failure in Rats.* Biomed Res Int, 2015. **2015**: p. 753210.
274. Linardi, D., et al., *Ventricular and pulmonary vascular remodeling induced by pulmonary overflow in a chronic model of pretricuspid shunt.* J Thorac Cardiovasc Surg, 2014. **148**(6): p. 2609-17.
275. Reddy, V.M., et al., *In utero placement of aortopulmonary shunts. A model of postnatal pulmonary hypertension with increased pulmonary blood flow in lambs.* Circulation, 1995. **92**(3): p. 606-13.
276. Dupuis, J. and N. Weissmann, *Animal Models of Pulmonary Hypertension*, in *Textbook of Pulmonary Vascular Disease*, J.X.J. Yuan, et al., Editors. 2011, Springer US: Boston, MA. p. 453-458.
277. Ford, W.D., et al., *Pulmonary hypertension in lambs with congenital diaphragmatic hernia: vasodilator prostaglandins, isoprenaline, and tolazoline.* J Pediatr Surg, 1990. **25**(5): p. 487-91.
278. van Loenhout, R.B., et al., *Congenital diaphragmatic hernia: comparison of animal models and relevance to the human situation.* Neonatology, 2009. **96**(3): p. 137-49.
279. Meng, Q., et al., *Development of a Mouse Model of Metabolic Syndrome, Pulmonary Hypertension, and Heart Failure with Preserved Ejection Fraction.* Am J Respir Cell Mol Biol, 2017. **56**(4): p. 497-505.
280. Patten, R.D. and M.R. Hall-Porter, *Small animal models of heart failure: development of novel therapies, past and present.* Circ Heart Fail, 2009. **2**(2): p. 138-44.
281. Budhiraja, R., R.M. Tuder, and P.M. Hassoun, *Endothelial dysfunction in pulmonary hypertension.* Circulation, 2004. **109**(2): p. 159-65.
282. Sandow, S.L., et al., *Myoendothelial contacts, gap junctions, and microdomains: anatomical links to function?* Microcirculation, 2012. **19**(5): p. 403-15.
283. Farrero, M., et al., *Pulmonary hypertension is related to peripheral endothelial dysfunction in heart failure with preserved ejection fraction.* Circ Heart Fail, 2014. **7**(5): p. 791-8.

284. Fayyaz, A.U., et al., *Global Pulmonary Vascular Remodeling in Pulmonary Hypertension Associated With Heart Failure and Preserved or Reduced Ejection Fraction.* Circulation, 2018. **137**(17): p. 1796-1810.
285. Gevaert, A.B., et al., *Targeting Endothelial Function to Treat Heart Failure with Preserved Ejection Fraction: The Promise of Exercise Training.* Oxid Med Cell Longev, 2017. **2017**: p. 4865756.
286. Jasmin, J.F., et al., *Lung structural remodeling and pulmonary hypertension after myocardial infarction: complete reversal with irbesartan.* Cardiovasc Res, 2003. **58**(3): p. 621-31.
287. Jasmin, J.F., et al., *Lung remodeling and pulmonary hypertension after myocardial infarction: pathogenic role of reduced caveolin expression.* Cardiovasc Res, 2004. **63**(4): p. 747-55.
288. Howard, L.S., et al., *Echocardiographic assessment of pulmonary hypertension: standard operating procedure.* Eur Respir Rev, 2012. **21**(125): p. 239-48.
289. Duza, T. and I.H. Sarelius, *Localized transient increases in endothelial cell Ca2+ in arterioles in situ: implications for coordination of vascular function.* Am J Physiol Heart Circ Physiol, 2004. **286**(6): p. H2322-31.
290. Kansui, Y., C.J. Garland, and K.A. Dora, *Enhanced spontaneous Ca2+ events in endothelial cells reflect signalling through myoendothelial gap junctions in pressurized mesenteric arteries.* Cell Calcium, 2008. **44**(2): p. 135-46.
291. Busse, R. and A. Mulsch, *Calcium-dependent nitric oxide synthesis in endothelial cytosol is mediated by calmodulin.* FEBS Lett, 1990. **265**(1-2): p. 133-6.
292. Crane, G.J., et al., *Small- and intermediate-conductance calcium-activated K+ channels provide different facets of endothelium-dependent hyperpolarization in rat mesenteric artery.* J Physiol, 2003. **553**(Pt 1): p. 183-9.
293. Ledoux, J., A.D. Bonev, and M.T. Nelson, *Ca2+-activated K+ channels in murine endothelial cells: block by intracellular calcium and magnesium.* J Gen Physiol, 2008. **131**(2): p. 125-35.
294. Feletou, M. and P.M. Vanhoutte, *Endothelium-dependent hyperpolarization of vascular smooth muscle cells.* Acta Pharmacol Sin, 2000. **21**(1): p. 1-18.
295. Campbell, W.B. and I. Fleming, *Epoxyeicosatrienoic acids and endothelium-dependent responses.* Pflugers Arch, 2010. **459**(6): p. 881-95.
296. Hald, B.O., et al., *Less is more: minimal expression of myoendothelial gap junctions optimizes cell-cell communication in virtual arterioles.* J Physiol, 2014. **592**(15): p. 3243-55.
297. Bagher, P., et al., *Low intravascular pressure activates endothelial cell TRPV4 channels, local Ca2+ events, and IKCa channels, reducing arteriolar tone.* Proc Natl Acad Sci U S A, 2012. **109**(44): p. 18174-9.
298. Demuro, A. and I. Parker, *Imaging the activity and localization of single voltage-gated Ca(2+) channels by total internal reflection fluorescence microscopy.* Biophys J, 2004. **86**(5): p. 3250-9.
299. Sukumaran, S.V., et al., *TRPV4 channel activation leads to endothelium-dependent relaxation mediated by nitric oxide and endothelium-derived hyperpolarizing factor in rat pulmonary artery.* Pharmacol Res, 2013. **78**: p. 18-27.
300. Lamboley, M., et al., *Evidence for signaling via gap junctions from smooth muscle to endothelial cells in rat mesenteric arteries: possible implication of a second messenger.* Cell Calcium, 2005. **37**(4): p. 311-20.

301. Nausch, L.W., et al., *Sympathetic nerve stimulation induces local endothelial Ca2+ signals to oppose vasoconstriction of mouse mesenteric arteries.* Am J Physiol Heart Circ Physiol, 2012. **302**(3): p. H594-602.
302. Kuebler, W.M., X. Ying, and J. Bhattacharya, *Pressure-induced endothelial Ca(2+) oscillations in lung capillaries.* Am J Physiol Lung Cell Mol Physiol, 2002. **282**(5): p. L917-23.
303. Hamanaka, K., et al., *TRPV4 initiates the acute calcium-dependent permeability increase during ventilator-induced lung injury in isolated mouse lungs.* Am J Physiol Lung Cell Mol Physiol, 2007. **293**(4): p. L923-32.
304. Jeske, N.A., et al., *A-kinase anchoring protein 150 mediates transient receptor potential family V type 1 sensitivity to phosphatidylinositol-4,5-bisphosphate.* J Neurosci, 2011. **31**(23): p. 8681-8.
305. Bengrine, A., J. Li, and M.S. Awayda, *The A-kinase anchoring protein 15 regulates feedback inhibition of the epithelial Na+ channel.* FASEB J, 2007. **21**(4): p. 1189-201.
306. Sekiguchi, F., et al., *AKAP-dependent sensitization of Ca(v) 3.2 channels via the EP(4) receptor/cAMP pathway mediates PGE(2) -induced mechanical hyperalgesia.* Br J Pharmacol, 2013. **168**(3): p. 734-45.
307. Navedo, M.F., et al., *AKAP150 is required for stuttering persistent Ca2+ sparklets and angiotensin II-induced hypertension.* Circ Res, 2008. **102**(2): p. e1-e11.
308. Mercado, J., et al., *Local control of TRPV4 channels by AKAP150-targeted PKC in arterial smooth muscle.* J Gen Physiol, 2014. **143**(5): p. 559-75.
309. Fan, H.C., X. Zhang, and P.A. McNaughton, *Activation of the TRPV4 ion channel is enhanced by phosphorylation.* J Biol Chem, 2009. **284**(41): p. 27884-91.
310. Mamenko, M., et al., *Discrete control of TRPV4 channel function in the distal nephron by protein kinases A and C.* J Biol Chem, 2013. **288**(28): p. 20306-14.
311. Qian, X., et al., *Positive feedback regulation of agonist-stimulated endothelial Ca2+ dynamics by KCa3.1 channels in mouse mesenteric arteries.* Arterioscler Thromb Vasc Biol, 2014. **34**(1): p. 127-35.
312. Brahler, S., et al., *Genetic deficit of SK3 and IK1 channels disrupts the endothelium-derived hyperpolarizing factor vasodilator pathway and causes hypertension.* Circulation, 2009. **119**(17): p. 2323-32.
313. Garland, C.J., et al., *Endothelium-dependent hyperpolarization: a role in the control of vascular tone.* Trends Pharmacol Sci, 1995. **16**(1): p. 23-30.
314. Tomioka, H., et al., *Relaxation in different-sized rat blood vessels mediated by endothelium-derived hyperpolarizing factor: importance of processes mediating precontractions.* J Vasc Res, 1999. **36**(4): p. 311-20.

Annexe: Expression of phosphoinositide specific phospholipase C isoforms in native endothelial cells

PLOS | ONE

RESEARCH ARTICLE

Expression of Phosphoinositide-Specific Phospholipase C Isoforms in Native Endothelial Cells

Delphine M. Béziau[1,2], Fanny Toussaint[1,2], Alexandre Blanchette[1], Nour R. Dayeh[1,4], Chimène Charbel[1,3], Jean-Claude Tardif[1,4], Jocelyn Dupuis[1,4], Jonathan Ledoux[1,2,3,4]*

[1]Research Center, Montreal Heart Institute, Montreal, Qc, Canada, [2] Department of Molecular and Integrative Physiology, Université de Montréal, Montreal, Qc, Canada, [3] Department of Pharmacology, Université de Montréal, Montreal, Qc, Canada, 4 Department of Medicine, Université de Montréal, Montreal, Qc, Canada

2. jonathan.ledoux@umontreal.ca

Citation: Béziau DM, Toussaint F, Blanchette A, Dayeh NR, Charbel C, Tardif J-C, et al. (2015) Expression of Phosphoinositide-Specific Phospholipase C Isoforms in Native Endothelial Cells. PLoS ONE 10(4): e0123769. doi:10.1371/ journal.pone.0123769

Academic Editor: Mohamed Trebak, Penn State Hershey College of Medicine, UNITED STATES

Received: December 4, 2014

Accepted: February 25, 2015

Published: April 13, 2015

Data Availability Statement: All relevant data are within the paper.

Funding: This study was support through studentship and salary grants: Université de Montréal Fanny Toussaint, Nour R. Dayeh; Société Québécois d'Hypertension Artérielle (SQHA) - Delphine M. Béziau and Fanny Toussaint; Fonds de Recherche du Québec - Santé (FRQS) - Jonathan Ledoux; Canadian Institutes of Health Research (CIHR) - Jonathan Ledoux; The Canada Foundation for Innovation (CFI) - Jonathan Ledoux; Heart and Stroke Foundation of Canada (HSFC) - Jonathan

Abstract

Phospholipase C (PLC) comprises a superfamily of enzymes that play a key role in a wide array of intracellular signalling pathways, including protein kinase C and intracellular calci-um. Thirteen different mammalian PLC isoforms have been identified and classified into 6 families (PLC-β, γ, δ, ε, ζ and η) based on their biochemical properties. Although the expres-sion of PLC isoforms is tissue-specific, concomitant expression of different PLC has been reported, suggesting that PLC family is involved in multiple cellular functions. Despite their critical role, the PLC isoforms expressed in native endothelial cells (ECs) remains undeter-mined. A conventional PCR approach was initially used to elucidate the mRNA expression pattern of PLC isoforms in 3 distinct murine vascular beds: mesenteric (MA), pulmonary (PA) and middle cerebral arteries (MCA). mRNA encoding for most PLC isoforms was de-tected in MA, MCA and PA with the exception of η2 and β2 (only expressed in PA), δ4 (only expressed in MCA), η1 (expressed in all but MA) and ζ (not detected in any vascular beds tested). The endothelial-specific PLC expression was then sought in freshly isolated ECs. Interestingly, the PLC expression profile appears to differ across the investigated arterial beds. While mRNA for 8 of the 13 PLC isoforms was detected in ECs from MA, two addition-al PLC isoforms were detected in ECs from PA and MCA. Co-expression of multiple PLC isoforms in ECs suggests an elaborate network of signalling pathways: PLC isoforms may contribute to the complexity or diversity of signalling by their selective localization in cellular microdomains. However in situ immunofluorescence revealed a homogeneous distribution for all PLC isoforms probed (β3, γ2 and δ1) in intact endothelium. Although PLC isoforms play a crucial role in endothelial signal transduction, subcellular localization alone does not appear to be sufficient to determine the role of PLC in the signalling microdomains found in the native endothelium.

Ledoux. The funders had no role in study design, data collection and analysis, decision to publish, or preparation of the manuscript.

Competing Interests: The authors declare that no competing interests exist.

Introduction

Vascular endothelium, a thin-cell monolayer lining blood vessels walls, is ideally positioned to detect and transduce biochemical and physical information. Endothelial cells (ECs) are essen-tial regulators of vascular tone, cellular adhesion and vascular smooth muscle cell (SMC) pro-liferation. The wide variety of stimuli sensed by ECs necessitates an intricate web of intracellular signalling components, including phosphoinositide-signalling involving phospho-lipases C (PLC) as main players.

PLC are calcium (Ca^{2+})-dependent phosphodiesterases that hydrolyze phosphatidyl-inosi-tol bisphosphate (PIP_2) into 1,2-diacylglycerol (DAG) plus inositol trisphosphate (IP_3) [1,2]. Once generated, IP_3 quickly diffuses in the cytoplasm and activates IP_3 receptors (IP_3R) located on the endoplasmic reticulum (ER) membrane, evoking a rapid release of Ca^{2+} into the cyto-plasm. PLC can also regulate several cellular functions through DAG production, via activation of protein kinase C [3] and through modulation of PIP_2 levels [4]. To date, a total of 13 mam-malian PLC isoforms have been identified and classified into 6 families: β(1–4), γ(1–2), δ (1,3,4), ε, z and η(1–2) [5]. The PLC families possess distinct mechanisms of activation. For ex-ample, PLCβ isoforms are activated by Gα and Gβ/γ subunits of heterotrimeric G proteins whereas PLCγ isoforms are activated by tyrosine kinase receptors and PLCε can be activated by both [5]. PLC isoforms can also be distinguished by their molecular weights, Ca^{2+}-sensitivity and subcellular localization: together, these suggest that each isoform might have a specific role in the modulation of physiological responses and this is further supported by several studies using knockout animal models [5–8]. For example, PLCε-null mice display abnormal develop-ment of the aortic and pulmonary valves [9]. The absence of PLCβ2 expression leads to de-creased intracellular calcium release and superoxide production in neutrophils [10]. These studies strengthened the notion that each PLC isoform has a specific and complementary role in physiology.

Downstream of PLC activation, IP_3R-dependent Ca^{2+} release is a key player in endothelial function. Indeed, these endothelial intracellular Ca^{2+} dynamics play a major role in the genera-tion of vasoregulatory signals [11–14]. Although highly dynamic, endothelial Ca^{2+} is finely tuned, as expected for a process with a significant functional impact. An increasing body of evi-dence suggests that spatially restricted Ca^{2+} signals are essential regulators of endothelial func-tion. Of the endothelial local Ca^{2+} signals characterized, Ca^{2+} pulsars are spontaneous IP_3R-dependent Ca^{2+} release events that occur within the myoendothelial projection (MEP) [11]. Although our current knowledge regarding the regulation of spatially-localized Ca^{2+} signalling in the endothelium is limited, the involvement of IP_3/IP_3Rs indicate a role for PLCs in the control of Ca^{2+} signals such as pulsars. A better understanding of the expression and subcellular locali-zation of PLCs in native ECs is necessary.

Cell-specific expression of individual PLCs is believed to be involved in modulating particu-lar functions. Roles for PLC β3 [15], γ1 [16] and δ [17] have been reported in ECs and the ex-pression of PLC isoforms was recently examined in human umbilical vein endothelial cells (HUVECs) [18]. However, placing ECs in culture results in phenotypic changes [19], including the loss of MEP and Ca^{2+} pulsars, suggesting that the regulatory pathways might be altered as well. Hence, the expression profile of PLCs and the associated signalling pathways may differ between HUVECs and native ECs. Endothelium is a specialized tissue whose functions vary de-pending on the vascular bed, suggesting that PLC expression might also vary from one vascular bed to the other [20–22]. Therefore, it is crucial to determine the expression and subcellular distribution of PLC isoforms in native ECs from different vascular beds. In this study, we deter-mined the expression of PLC isoforms in murine ECs freshly isolated from mesenteric (MAECs), pulmonary (PAECs) and middle cerebral arteries (MCAECs).

Materials and Methods

Tissue preparation

All animal manipulations were performed in accordance with the Canadian Council on Ani-mal Care guidelines. The Montreal Heart Institute Animal Research Ethics Committee ap-proved all animal studies (Protocol number: 2011-33-01). Resistance arteries: (3rd or 4th order MA, PA and MCA) were isolated from 3–4 months old C57BL/6 mice. Prior to experimenta-tion, arteries were carefully cleaned of adipose and connective tissue in cooled HEPES solution.

Molecular biology

Total RNA from MA, PA and MCA was extracted using RNeasy Micro kits (Qiagen). As con-trol, total RNA was isolated from brain and testis using RNeasy Lipid tissue Mini Kit (Qiagen) and from blood using QIAmp RNA blood Mini kit (Qiagen). The purity and concentration of RNA were assessed using a Nanodrop spectrophotometer. Next, reverse transcription was per-formed using iScript kits (Bio-Rad) according to manufacturer's instructions. Primers (Table 1) and 5 ng of cDNA were used for PCR amplification in a final volume of 25 μl. Following dena-turation at 94°C, 45 cycles of DNA amplification were performed using Taq DNA polymerase (Invitrogen) at 94°C for 45 sec, 55°C for 30 sec and 72°C for 90 sec. A final extension step was performed for 10 min at 72°C. Electrophoresis of amplicons on 3% ethidium bromide stained agarose gels was carried out. PCR product sizes were estimated using the Gene ruler low range DNA ladder (Thermoscientific) and compared to theoretical amplicon size (n 3, Table 1).

For quantitative real-time PCR (qPCR), ECs were freshly isolated from MA, PA and MCA as previously described by Socha et al [23]. Cell dissociation was performed in a tube contain-ing 137 mM NaCl, 5.6 mM KCl, 1 mM $MgCl_2$, 10mM HEPES, 10 mM glucose, 2 mM $CaCl_2$, 1.0 mg/ml DTT, 0.1% BSA and with enzymes 0.62mg/ml (MAECs) or 0.31mg/ml (PAECs and MCAECs) papain (Sigma, P4762), 1.5mg/ml (MAECs) or 0.75mg/ml (PAECs and MCAECs) collagenase (Sigma, C8051). Arterial segments were incubated in digestion solution for 25 min at 37°C followed by a triple wash in enzyme-free solution and then gently triturated. SMC-de-prived EC tubes were visually identified with a Zeiss Axiovert A1 microscope and individually

Table 1. List of primer couples for PLC isoforms.

Gene	Forward (5' ! 3')	Reverse (5' ! 3')	Amplicon size
PLCβ1	CTGAGCGGAGAAGAAAATGG	ACACAGCGACATCCAGACAG	185
PLCβ2	TCAACCCTGTTCTATTGCCCC	CGGAGGATAACAGGAGAGGC	240
PLCβ3	AACTAGCCGCTCTCATTGGG	ACTGAGGGAGGAGCTAGTGG	176
PLCβ4	GGAAGTGCCCTCTTTCTTGC	GCCTTCACTCTTCCACGTCA	130
PLCγ1	AGATCCGTGAAGTTGCCCAG	TCAGCCTTGGTTTCCGGAAA	193
PLCγ2	GATCATGGAGACTCGGCAGG	GACAAACTGGGTGCCGTAGA	181
PLCδ1	GCAAGATCATCGACCGCTC	CGTAGCTGTCATCCACCTGT	165
PLCδ3	GACAGCAGCACCAAAAGGC	CGTGAGCGGATCTTGAGGAG	113
	CAGCAACTGACCCGAGTGTA	CTCAGGGTCAAAGGTGGTGT	222
PLCδ4	TTCAATCCTGAGAGGCCAAT	TCCACTTTGGGGAGTTGTTG	86
PLCε	GGAGCCAACGTCTGTCTGAA	GAGTTTGGGAGCTGTGTGGA	118
PLCζ	AGACTTCCTGCTTTCGGACA	TGTCGGTTCCTATCCTCTCG	137
PLCη1	CCGCAGAAAAGTCAGGCAAA	AGCTCCTCCACAGTCAGGT	171
	AGTAGGGCAGTGGGTTGAAG	TACACAAACTCCGTGGCAGC	199
PLCη2	CGGCAGAGGGTGAAACAGAT	CTCGGCGGGTAGACATCATC	109
	TGTTCATGTGGCTGTCAGTG	GACTTGGCTTCTGGCTTTTG	194

doi:10.1371/journal.pone.0123769.t001

collected with patch micropipettes to ensure the purity of the isolated ECs. ECs mRNA was ex-tracted and purified (RNeasy Plus micro kit, Qiagen) before amplification using Message-BOOSTER Whole Transcriptome cDNA synthesis kit for qPCR (Epicentre Biotechnologies). Reverse transcription was performed using iScript kit (Bio-Rad) according to the manufactur-er's instructions. The purity of the isolated ECs was further assessed by qPCR analysis of the relative abundance of endothelial specific (CD31) and SMCs specific (SM22) mRNA (CD31/ SM22 ratio) in MAECs, PAECs and MCAECs (S1 Fig). qPCR was performed using a Strata-gene MX3005 system using iTaq fast Syber Green with ROX (Bio-Rad) and are normalized to cyclophilin A expression.

Immunocytochemistry

MA were cut longitudinally, and pinned (endothelium en face) on a Sylgard block. Arteries were fixed with 4% paraformaldehyde, permeabilized with 0.2% Triton X-100 then blocked with 4% normal donkey serum. Following overnight incubation at 4°C with primary antibodies (1:500; PLCβ3 Abcam #ab52199; PLCδ1 Abcam #ab154610; PLCγ2 Abcam #ab18983) in 0.1% Triton X-100, arteries were incubated for 1h with an Alexa Fluor 555-conjugated donkey anti-rabbit secondary antibody (Invitrogen). DAPI was applied to stain nuclei prior mounting for confocal imaging. Autofluorescence of the internal elastic lamina was also acquired. Fluores-cence emissions were detected using a Zeiss LSM 510 confocal microscope (63X oil objective/1.4, ex: 405 nm, 488 nm and 543 nm). All images were deconvolved with Huygens professional software using experimentally determined point spread functions (PSFs) and reconstructed with Zen 2009 Light Edition.

Western blotting

Protein extraction from MA was carried out by tissue immersion in ice-cooled acetone, 10% trichloroacetic acid and 10 mM dithiothreitol (DTT). Tissue was then lyophilized, disrupted and heated at 95°C for 10 minutes in SDS-gel sample buffer (60 mM Tris-HCl, pH 6.8, 2% SDS, 10% glycerol, 0.01% bromophenol blue, 0.1 M DTT) [24,25]. Finally, proteins were ex-tracted by continuously mixing samples in SDS-gel sample buffer overnight at 4°C. Proteins were separated by SDS-PAGE on 7.5% acrylamide gels and transferred to nitrocellulose mem-branes (Bio-Rad). Membranes were blocked using 5% fat-free dry milk and then incubated with primary antibodies (1:1000; PLCβ3 Abcam #ab52199; PLCδ1 Abcam #ab154610; PLCγ2 Abcam #ab18983) for 1 hour at room temperature. Membranes were then washed and incubat-ed with HRP-conjugated goat anti-rabbit secondary antibody (Jackson ImmunoResearch) for 1 hour at room temperature. Immunoreactive bands were revealed by enhanced chemilumines-cence (Western Lightning Plus, PerkinElmer).

Statistical analysis

Data are presented as means ± SEM. One-way ANOVA with Turkey's multiple comparisons test was used to compare the means; $P<0.05$ was considered significant.

Results

mRNA expression of PLC isoforms

Expression of PLC isoforms was initially determined in freshly isolated arteries from 3 different vascular beds: MA, PA and MCA (Figs 1–4, panels A). While mRNA for 8 of the 13 PLC iso-forms were detected in MA, 10 were found in MCA and 11 in PA. As shown in Fig 1A, PLCβ1, β3 and β4 mRNA was detected in all vascular beds studied. Interestingly, PLCβ2 was only

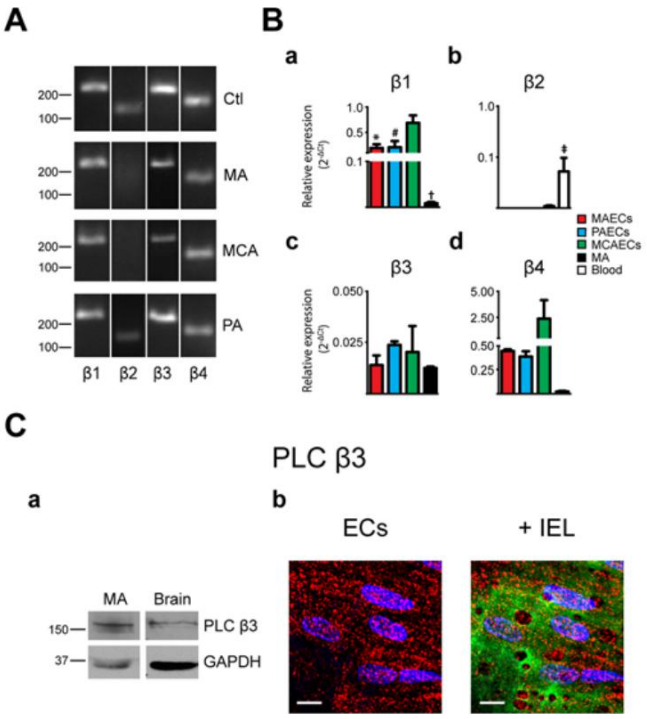

Fig 1. Characterization of phospholipase C β isoforms in native arteries. A. The presence of mRNA for phospholipase C (PLC) β isoforms was determined in mesenteric arteries (MA), pulmonary arteries (PA) and middle cerebral arteries (MCA) by PCR. Typical agarose gel electrophoresis of the PCR products showed the expression profile in different vascular beds. Brain and blood were used as positive control tissues. n = 3. B. Quantitative real time PCR analysis of mRNA expression levels of PLCβ isoforms in MA and freshly isolated endothelial cells (ECs) from MA, PA and MCA. Bar graphs show the expression profile of PLCβ1 (a), β2 (b), β3 (c) and β4 (d) isoforms in MAECs, PAECs, MCAECs, MA and blood as control for β2. n = 3. * P<0.05 between MAECs and MCAECs; # P<0.05 between PAECs and MCAECs; † P<0.05 between MCAECs and MAs; ‡ P<0.05 between control tissue and MA. C. (a) Representative immunoblots of murine MA and brain that were obtained using the primary antibody anti-PLC β3 (Abcam #ab52199). GAPDH was used as reference protein. Relevant molecular weight markers are indicated on the left. n = 3. (b) Intracellular distribution of PLCβ3 immunoreactivity in ECs. (Left) Typical image showing labelling of PLC β3 in red and nuclei in blue; scale = 10 μm. (Right) Labelling of PLC β3 (red) overlay with internal elastic lamina (IEL; green) where voids correspond to potential myoendothelial projections; nucleus in blue; scale = 10 μm; n = 4.

doi:10.1371/journal.pone.0123769.g001

detected in PA. PLCγ and ε isoforms were expressed in all arteries tested (Figs 2A and 4A). While PLCδ1 and δ3 were in all tested arteries, only MCA express δ4 (Fig 3A). PLC z was only detected in testis, our positive control, with no noticeable expression in arteries (Fig 4A). The PLCη family had a distinct expression pattern, as shown in Fig 4A. PLCη1 was found in MCA and PA but not in MA, whilst η2 was detected only in PA. Data from PCR experiments are summarized in Table 2. However, these expression profiles represent mRNA from all cells found in the arterial wall, including both endothelium and vascular SMCs. Assessment of en-dothelial-specific PLC expression requires isolation of mRNA from preparations of ECs.

Endothelial PLC expression was quantified in freshly isolated MAECs, PAECs and MCAECs by qPCR. The purity of EC isolations was assessed by determining the expression ratio of EC vs. SMC markers (CD31 and SM22, respectively; S1 Fig) in both isolated arteries and corresponding EC preparations. This assessment confirmed that EC samples used were highly enriched in ECs. The relative expression of PLC isoforms in MAECs, PAECs and MCAECs as well as in MA was then determined (Figs 1–4, panels B). PCR and qPCR yielded

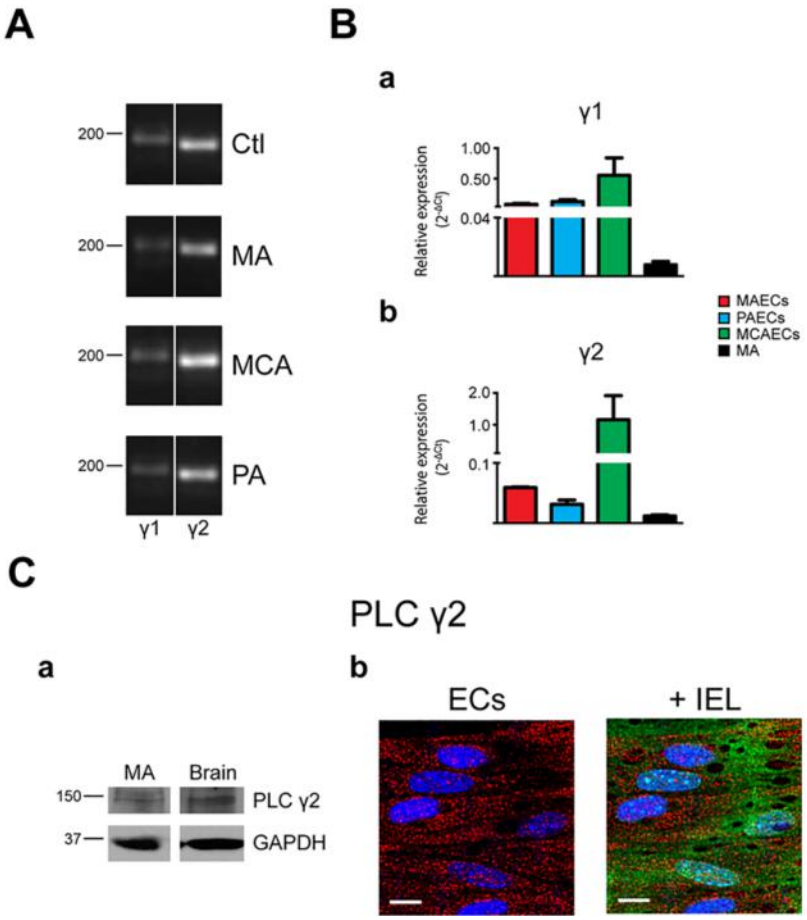

Fig 2. Characterization of phospholipase C γ isoforms in native arteries. A. The presence or mRNA for phospholipase C (PLC) γ isoforms was determined in mesenteric arteries (MA), pulmonary arteries (PA) and middle cerebral arteries (MCA) by PCR. Typical agarose gel electrophoresis of the PCR products showed the expression profile in the different vascular beds and brain was used as control tissue. n = 3. B. Quantitative real time PCR analysis of mRNA expression levels of PLCγ isoforms in MA and freshly isolated endothelial cells (ECs) from MA, PA and MCA. Bar graphs show the expression profile of PLCγ1 (a) and γ2 (b) isoforms in MAECs, PAECs, MCAECs and MA. n = 3. C. (a) Representative immunoblots of murine MA and brain that were analyzed using the primary antibody anti-PLC γ2 (Abcam #ab18983). GAPDH was used as reference protein. Relevant molecular weight markers are indicated on the left. n = 3. (b) Intracellular distribution of PLCγ2 immunoreactivity in ECs. (Left) Typical image showing labelling of PLCγ2 in red and nuclei in blue; scale = 10 μm. (Right) Labelling of PLCγ2 (red) overlay with internal elastic lamina (IEL; green) where voids correspond to potential myoendothelial projections; nucleus in blue; scale = 10 μm; n = 4.

doi:10.1371/journal.pone.0123769.g002

similar expression profiles for PLC mRNA in MA with the exception of PLCβ2 and η1, which were only detected using the more sensitive qPCR. Therefore, mRNA encoding for nine PLC isoforms was detected in MA by qPCR. An almost identical PLC profile was observed in MAECs, with the exception that PLCη2 was undetectable in MAECs (Fig 4B). From a vascular bed point of view, slight differences were found between MAECs, PAECs and MCAECs. ECs from all arteries tested expressed at least 8 of the 13 PLC isoforms: β(1,3,4), γ(1–2), δ(1,3) and ε. Additionally, PAECs and MCAECs expressed PLCη1, whereas MAECs did not. In accor-dance with our findings in whole arterial preparations, PLC δ4 mRNA was only detected in MCAECs and PLCη2 was only detected in PAECs. These results are summarized in Table 2.

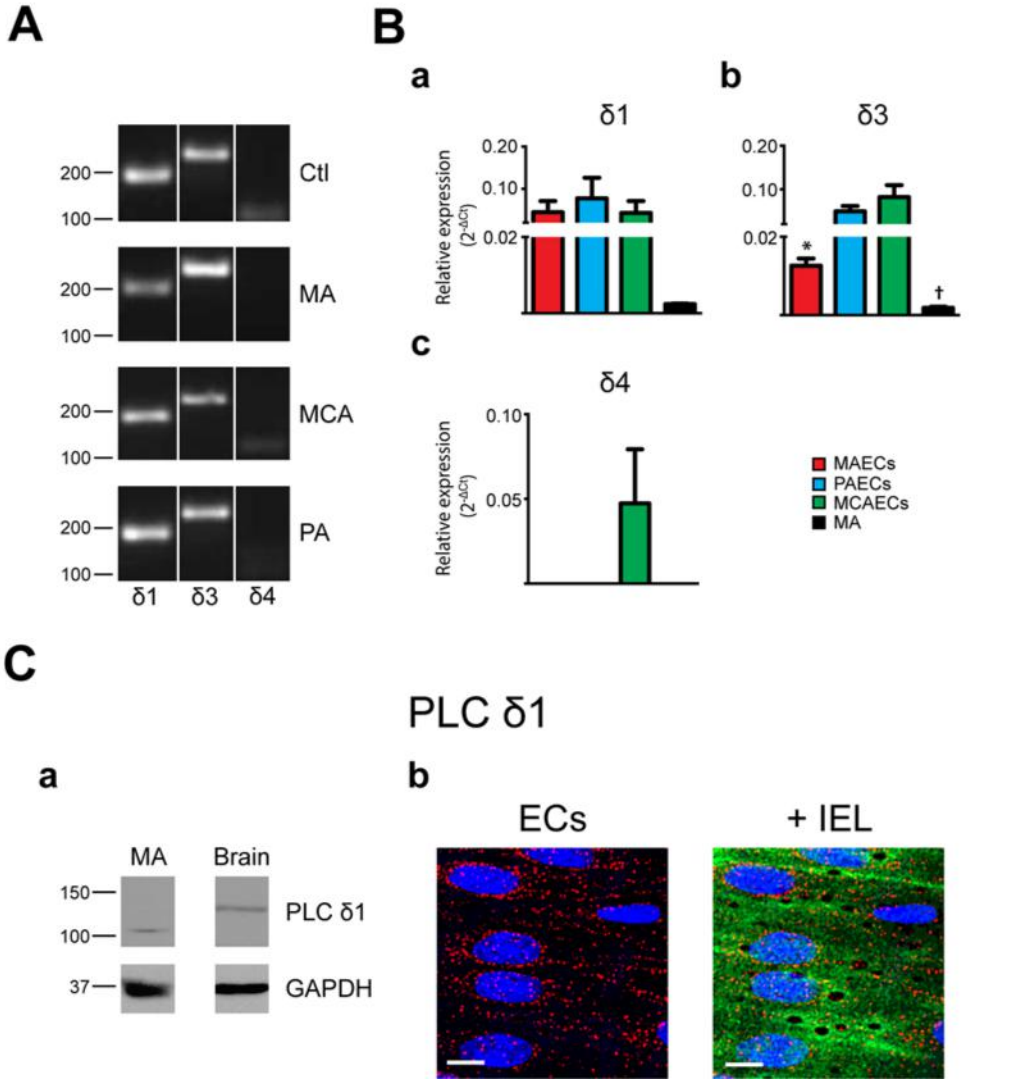

Fig 3. Characterization of phospholipase C δ isoforms in native arteries. A. The presence of mRNA for phospholipase C (PLC) δ isoforms was determined in mesenteric arteries (MA), pulmonary arteries (PA) and middle cerebral arteries (MCA) by PCR. Typical agarose gel electrophoresis of the PCR products showed the expression profile of PLCδ isoforms in the different vascular beds and brain was used as control tissue. n = 3. B. Quantitative real time PCR analysis of mRNA expression levels of PLCδ isoforms in MA and freshly isolated endothelial cells (ECs) from MA, PA and MCA. Bar graphs showed the expression profile of PLCδ1 (a), δ3 (b) and δ4 (c) isoforms in MAECs, PAECs, MCAECs and MA. n = 3. * P<0.05 between MAECs and MCAECs; † P<0.05 between MCAECs and MA. C. (a) Representative immunoblots of murine MA and brain that were analyzed using the primary antibody anti-PLCδ1 (Abcam #ab154610). GAPDH was used as reference protein. Relevant molecular weight markers are indicated on the left. n = 3. (b) Intracellular distribution of PLCδ1 immunoreactivity in ECs. (Left) Typical image showing labelling of PLCδ1 in red and nuclei in blue; scale = 10 μm. (Right) Labelling of PLCδ1 (red) overlay with internal elastic lamina (IEL; green) where voids correspond to potential myoendothelial projections; nucleus in blue; scale = 10 μm; n = 4.

doi:10.1371/journal.pone.0123769.g003

Protein expression of PLC isoforms

The three main PLC families are PLCβ, PLCγ and PLCδ [26]. However, investigation of PLC isoform expression at the protein level was limited to the commercially available antibodies: PLCβ3, PLCγ2 and PLCδ1. Western blotting was thus used to elucidate the expression of these

Table 2. Summary of mRNA expression for phospholipase C isoforms.

	qPCR				PCR		
	MAECs	PAECs	MCAECs	MA	MA	PA	MCA
PLCβ1	+	+	+	+	+	+	+
PLCβ2	-	-	-	-	-	+	-
PLCβ3	+	+	+	+	+	+	+
PLCβ4	+	+	+	+	+	+	+
PLCγ1	+	+	+	+	+	+	+
PLCγ2	+	+	+	+	+	+	+
PLCδ1	+	+	+	+	+	+	+
PLCδ3	+	+	+	+	+	+	+
PLCδ4	-	-	+	-	-	-	+
PLCε	+	+	+	+	+	+	+
PLCζ	-	-	-	-	-	-	-
PLCη1	-	+	+	+	-	+	+
PLCη2	-	+	-	-	-	+	-

MAECs, mesenteric arteries endothelial cells; PAECs, pulmonary arteries endothelial cells; MCAECs, middle cerebral arteries endothelial cells; MA, mesenteric arteries; PA, pulmonary arteries; MCA, middle cerebral arteries.

doi:10.1371/journal.pone.0123769.t002

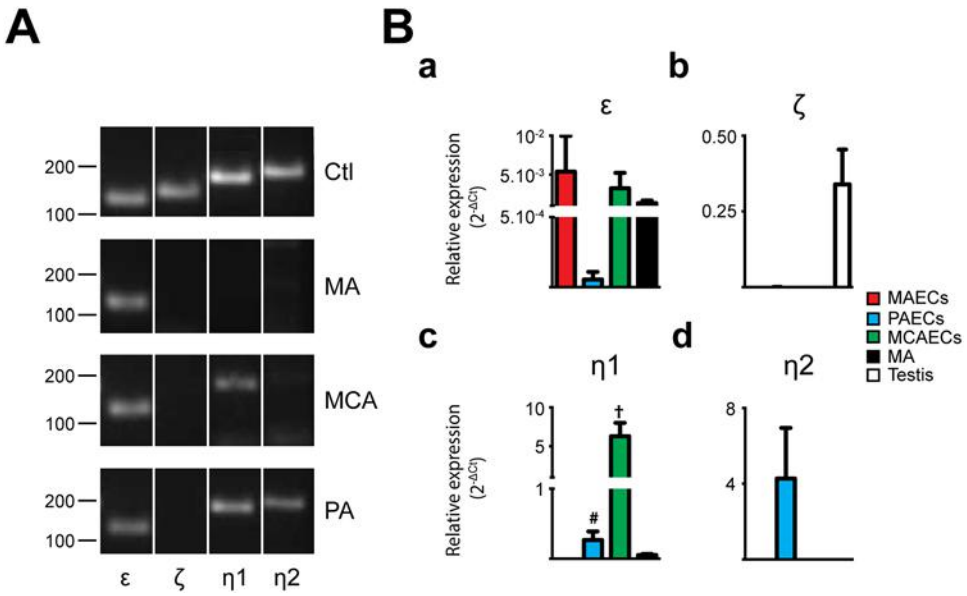

Fig 4. Characterization of phospholipase C ε, ζ and η isoforms in native arteries. A. The presence of mRNA for phospholipase C (PLC) ε, ζ, η1 and η2 isoforms was determined in mesenteric arteries (MA), pulmonary arteries (PA) and middle cerebral arteries (MCA) by PCR. Typical agarose gel electrophoresis of the PCR products showed the expression profile of PLCε, ζ, η1 and η2 isoforms in the different vascular beds and brain or testis were used as control tissue. n = 3. B. Quantitative real time PCR analysis of mRNA expression levels of PLCε, ζ, η1 and η2 isoforms in MA and freshly isolated endothelial cells (ECs) from MA, PA and MCA. Bar graphs show the expression of PLCε (a), ζ (b), η1 (c) and η2 (d) isoforms in MAECs, PAECs, MCAECs, MA and testis as positive control for ζ. n = 3. * P<0.05 between MAECs and MCAECs; # P<0.05 between PAECs and MCAECs; † P<0.05 between MCAECs and MA.

doi:10.1371/journal.pone.0123769.g004

PLC isoforms in MA at the protein level. As shown in Fig 1Ca, PLCβ3 antibodies revealed a band of 150-kDa in MA extracts. PLCδ1 and PLCγ2 antibodies revealed bands of 100-kDa and 150-kDa, respectively (Figs 2Ca and 3Ca).

Subcellular distribution of PLC isoforms

Since PLCβ3, γ2 and δ1 were detected in MA by western blotting, we next determined their respective presence and subcellular distribution. Immunofluorescence experiments were per-formed on MA sections dissected and immobilized with the endothelium in an en face configuration. All isoforms displayed a similar intracellular distribution. PLCβ3 (Fig 1Cb), γ2 (Fig 2Cb) and δ1 (Fig 3Cb) were homogeneously distributed in intact endothelium of MA.

Discussion

PLCs are crucial components of the phosphoinositide signalling pathway through their hydro-lysis of PIP_2 into IP_3 and 1,2-DAG. The 13 mammalian PLC isozymes identified so far are or-ganized within 6 families: β(1–4), γ(1–2), δ(1,3,4), ε, z and η(1–2) [5]. PLC isoforms are distinct in their activation mode, expression levels, catalytic regulation, cellular localization and tissue distribution. PLCβ and γ are considered as "first line PLCs" as they are activated by extracellular stimuli. In contrast, PLCδ, ε, η and z are secondary PLCs, being activated by intra-cellular Ca^{2+} [27]. For example, PLCγ isoforms are activated by tyrosine kinase receptors while members of the PLCβ family are activated by G protein-coupled receptors [28,29]. These dis-tinct characteristics allow PLC activity to be involved in a wide range of functions in both phys-iology and pathophysiology [30]. For example, each neuronal PLC isoform selectively couples with a specific neurotransmitter and contributes to distinct functions. PLCβ1 knockout mice are afflicted with epilepsy while abnormal activity and expression level of PLCγ1 are detected in pathologies including Huntington's disease, depression and Alzheimer's disease [7,31]. These numerous pathophysiological roles illustrate the extensive variety of cellular functions associated with each individual PLC isoform. Despite their crucial role in cellular signalling, the expression pattern of PLC isozymes remains to be established in native ECs. This study is the first study of PLC isoform expression at the mRNA level in murine resistance arteries from 3 distinct vascular beds: MA, PA and MCA. We also examined PLC expression pattern in freshly isolated ECs from these arterial beds. Finally, we demonstrated the presence of immu-noreactivity for 3 major PLC isoforms (β3, γ2 and δ1) in MA and their homogenous subcellular distribution in MA endothelium.

Recently, Lo Vasco and coll. Report that of 10out of 13 PLC isoforms are expressed in HUVECs, a cultured ECs model [18]. Interestingly, our data slightly differs from that of Lo Vasco et al.: PLCβ1 and ε are expressed in native ECs from all vascular beds tested but not in HUVECs. However, β2 is absent from freshly isolated murine ECs but is expressed in HUVECs. Also, η1 and η2 are expressed in HUVECs but were not detected in the 3 types of na-tive ECs. These discrepancies might be explained by the alteration of endothelial phenotype maintained in culture [32]. In vitro, ECs lose their MEP, an essential architecture for the com-munication with vascular SMCs. Therefore, in addition to passaging, culture media and the ab-sence of shear stress, the loss of cellular polarity may contribute to the observed differences in PLC expression in native and cultured ECs. Moreover, while we used arterial tissues in the present study, Lo Vasco and coll. used cells from veins. Hence, arteries to veins differences may also explain the different expression reported.

Employing qPCR allowed us to identify the PLC isoforms expressed specifically in freshly isolated ECs from MA, PA and MCA. Three of the four known PLCβ isoforms were detected in all ECs tested: PLCβ1, β3 and β4. Moreover, PLCβ3 expression was also found at the protein

level with immunoblots and confocal imaging. This is an interesting finding since PLC β3 is in-volved in the VEGF-dependent inhibition of vascular permeability [33]. However, the roles of endothelial β1 and β4 remain to be determined. Undetectable expression of PLC β2 from ECs was anticipated considering its involvement in platelets and hematopoietic cells chemotaxis [5,34–36]. Both PLCγ isoforms were detected in native ECs. PLCγ1 appears to be required for normal development as knockout mice do not survive beyond E9, due to a generalized growth failure attributed to the loss of both erythroid progenitors cells and ECs necessary for erythro-poiesis and vasculogenesis [37,38]. On the other hand, PLCγ2 appears to be selectively express-ed in blood cells, spleen and thymus [39]. The present study is the first report of PLCγ2 expression in native ECs. Detection of PLCγ2 expression by qPCR was further supported by immunoblotting. Moreover, immunostaining showed a homogeneous endothelial distribution of the enzyme. Obviously, the specific role of PLCγ2 in ECs is yet to be elucidated. Consistent with reports of PLCδ subtypes being expressed in porcine aortic ECs [40], we detected all three PLCδ isoforms in MCAECs whilst PLCδ4 was absent from MAECs and PAECs. PLCδ isoforms are among the most sensitive to Ca^{2+}, suggesting a potential role downstream of changes in en-dothelial Ca^{2+} dynamics [41,42]. However, elucidating the role of PLCδ4 specific function in MCAECs will require additional investigation. Studies employing a PLCδ4-null mouse have shown PLCδ4 to be involved in the initial stages of fertilization [6] but its role in endothelial function remains to be established. Immunoblotting of PLC δ1 revealed differences in apparent molecular weight in MA and brain. This can be explained by various types of post-translational modification, such as multiple phosphorylations as described by Fujii et al. [43]. Finally, we de-tected PLCε, but not PLCz, in freshly isolated ECs from all vascular beds. In contrast, while PLCη2 is only expressed in PAECs, PLCη1 was not detected in MAECs. Similar to δ4, there is currently no information available regarding the expression or function of PLCε, z, η1 and η2 in ECs. However, the function of these PLC isoforms has been examined in other cell types. For example, PLCε-null mice show abnormal development of the aortic and pulmonary valves [9], while PLCz expression/function was reported as sperm-specific [44] and PLCη1 and η2 seem to be involved in neural system regulation [5]. In summary, very little is known about the function of PLC isoforms in ECs, and further studies are therefore required to investigate their respective and specific roles.

ECs are heterogeneous both in structure and function across the vascular tree under normal or pathological conditions [20,21]. For example, rat PAECs have a broader and shorter shape than rat aortic ECs [45]. ECs are involved in several physiological functions, the relative impor-tance of which varies according to blood vessel type (conduit vs. resistance) or vascular bed, in-cluding vascular permeability, hemostasis or vasomotor tone in response to the specific requirements of the perfused organ. For example, pulmonary vasculature is exposed to a low-pressure, high flow of oxygen-deprived blood. Therefore, the proteins expressed in ECs will have varied in order to adapt to the needs of their particular vascular bed of origin [19]. We deter-mined the expression of all known mammalian PLC isoforms in native ECs of resistance arteries from three different vascular beds (MA, PA and MCA) by qPCR and observed a similar pattern of expression in each case. For 10 isoforms, the pattern of expression was constant between the 3 vascular beds (8 isoforms detected while 2 other were not detected). However, we observed slight differences for 3 isoforms: PLCδ4 and η2 were detected exclusively in MCAECs and PAECs, re-spectively, whereas PLCη1 was expressed in MCAECs and PAECs but not MAECs.

Endothelial PLC might be involved in the modulation of Ca^{2+} dependant vasoregulatory signals. In fact, the release of Ca^{2+} through IP_3 receptors in the ER membrane is stimulated by the IP_3 generated upon activation of membrane receptors leading to activation of PLC.
PLC are known to regulate Ca^{2+} levels and thus might be involved in the modulation of intra-cellular Ca^{2+} dynamics. In 2013, De Bock and coll. reviewed the signalling pathways

including PLCs pathway leading to intracellular Ca^{2+} elevation in blood-brain-barrier ECs [46]. Although all PLCs are Ca^{2+}-dependent, they vary with respect to their sensitivity to Ca^{2+}. PLCδ and η are the most sensitive to Ca^{2+} and are involved in potentiating Ca^{2+} signalling [47,48]. In a recent study, PLCβ1 and β4 were shown to be involved in distinct histamine-induced Ca^{2+} oscillations [49].

In ECs, increased IP_3 production results in the release of Ca^{2+} from intracellular stores [50] and the IP_3R is the only ER Ca^{2+} channels expressed in these cells [51]. IP_3 is generated through activation of G protein-coupled receptors or tyrosine kinase receptors which activate PLCβ and γ respectively [52]. Multiple cellular functions are regulated by changes in intracellular Ca^{2+}. Therefore, specificity of the Ca^{2+} signal is often achieved through spatial and temporal compartmentalization of Ca^{2+} signals. Several different patterns of Ca^{2+} dynamics have recent-ly been described in ECs: Ca^{2+} pulsars, TRPV4- and TRPA1-sparklets or wavelets, each gener-ated by a specific pathway [11,12,14,53]. Ca^{2+} pulsars are MEP localized signals consisting of a spontaneous Ca^{2+} release from IP_3 receptors [11]. Limited information is currently available on the regulatory mechanisms of Ca^{2+} pulsars. However, specific PLC activation could be re-sponsible for localized Ca^{2+} signalling such as Ca^{2+} pulsars. Cytoplasmic gradients of IP_3 would result in a limited activation of IP_3R and restricted propagation of the signal. Although our immunochemistry data showed a homogeneous distribution of PLCβ3, γ2 and δ1 in ECs, PLC partners and modulators could be heterogeneously distributed within the cell. Microdo-mains would then result from these associations as well as the distribution of proteins involved in Ca^{2+} sequestration. For example, Gonzales and coll. have recently shown colocalization of PLCγ1 with IP_3R, TRPM4 and TRPC6 in VSMC from cerebral arteries and elegantly demon-strated its requirement for pressure-induced membrane depolarization and myogenic vasocon-striction [13]. Moreover, TRPV4 channels responsible for Ca^{2+} sparklets are clustered in EC microdomains at MEP where they are modulated by PLC isoforms [54,55]. As for TRP chan-nels, specific PLC isoforms can be localized in microdomains to have a pivotal role in the mod-ulation of Ca^{2+} pulsars [56]. Moreover, our investigation of the subcellular localization of PLC was limited to three isoforms due to a lack of commercially available, reliable antibodies for the other isoforms. Therefore, the subcellular distribution of other members of the PLC family in native endothelium remains to be determined.

In summary, in this study we established for the PLCs that are expressed in native endothe-lium and freshly isolated ECs. We showed that 8 out of the 13 mammalian PLC isoforms are expressed in MAECs and 10 in PAECs and MCAECs. These results represent an important step forward in our understanding of the intracellular signalling pathways and their role in the regulation of endothelial microdomains. Further investigation of the subcellular distribution and biological function of these PLC isoforms is required in order to have a better understand-ing of their relative involvement in regulating endothelial function.

Supporting Information

S1 Fig. Purity of freshly isolated endothelial cells samples. Quantitative real time PCR analysis of mRNA expression levels of CD31, an endothelial-specific marker, and SM22, a smooth muscle cell-specific marker. (A) Pie chart illustrating the relative expression of CD31 to SM22 (CD31/SM22 ratio) in mesenteric arteries (MA) and in endothelial cells isolated from mesenteric arteries (MAECs). (B) Pie chart illustrating CD31/SM22 ratio in pulmonary arteries (PA) and in endothelial cells from pulmonary arteries (PAECs). (C) Pie chart illustrating CD31/SM22 in middle cerebral arteries (MCA) and in endothelial cells from middle cerebral arteries (MCAECs). n = 3.

Acknowledgments

The authors are grateful to Maya Mamarbachi and Louis R. Villeneuve for their helpful assis-tance in molecular biology and confocal microscopy. The authors are also thankful to Dr. Bruce G. Allen for his greatly appreciated critical editing of the manuscript.

Author Contributions

Conceived and designed the experiments: DMB JL. Performed the experiments: DMB FT AB. Analyzed the data: DMB FT. Contributed reagents/materials/analysis tools: DMB FT NRD CC JCT. Wrote the paper: DMB JCT JD JL.

References

1. Berridge MJ, Irvine RF. Inositol trisphosphate, a novel second messenger in cellular signal transduc-tion. Nature. 1984; 312: 315–321. PMID: 6095092
2. Nishizuka Y. The molecular heterogeneity of protein kinase C and its implications for cellular regulation. Nature. 1988; 334: 661–665. PMID: 3045562
3. Kishimoto A, Takai Y, Mori T, Kikkawa U, Nishizuka Y. Activation of calcium and phospholipid-depen-dent protein kinase by diacylglycerol, its possible relation to phosphatidylinositol turnover. J Biol Chem. 1980; 255: 2273–2276. PMID: 7358670
4. Rohacs T. Phosphoinositide regulation of non-canonical transient receptor potential channels. Cell Cal-cium. 2009; 45: 554–565. doi: 10.1016/j.ceca.2009.03.011 PMID: 19376575
5. Suh PG, Park JI, Manzoli L, Cocco L, Peak JC, Katan M, et al. Multiple roles of phosphoinositide-specif-ic phospholipase C isozymes. BMB Rep. 2008; 41: 415–434. PMID: 18593525
6. Fukami K, Nakao K, Inoue T, Kataoka Y, Kurokawa M, Fissore RA, et al. Requirement of phospholipase Cdelta4 for the zona pellucida-induced acrosome reaction. Science. 2001; 292: 920–923. PMID: 11340203
7. Kim D, Jun KS, Lee SB, Kang NG, Min DS, Kim YH, et al. Phospholipase C isozymes selectively couple to specific neurotransmitter receptors. Nature. 1997; 389: 290–293. PMID: 9305844
8. Li Z, Jiang H, Xie W, Zhang Z, Smrcka AV, Wu D. Roles of PLC-beta2 and -beta3 and PI3Kgamma in chemoattractant-mediated signal transduction. Science. 2000; 287: 1046–1049. PMID: 10669417
9. Tadano M, Edamatsu H, Minamisawa S, Yokoyama U, Ishikawa Y, Suzuki N, et al. Congenital semilu-nar valvulogenesis defect in mice deficient in phospholipase C epsilon. Mol Cell Biol. 2005; 25: 2191– 2199. PMID: 15743817
10. Jiang H, Kuang Y, Wu Y, Xie W, Simon MI, Wu D. Roles of phospholipase C beta2 in chemoattractant-elicited responses. Proc Natl Acad Sci U S A. 1997; 94: 7971–7975. PMID: 9223297
11. Ledoux J, Taylor MS, Bonev AD, Hannah RM, Solodushko V, Shui B, et al. Functional architecture of inositol 1,4,5-trisphosphate signaling in restricted spaces of myoendothelial projections. Proc Natl Acad Sci U S A. 2008; 105: 9627–9632. doi: 10.1073/pnas.0801963105 PMID: 18621682
12. Sonkusare SK, Bonev AD, Ledoux J, Liedtke W, Kotlikoff MI, Heppner TJ, et al. Elementary Ca2+ sig-nals through endothelial TRPV4 channels regulate vascular function. Science. 2012; 336: 597–601. doi: 10.1126/science.1216283 PMID: 22556255
13. Gonzales AL, Yang Y, Sullivan MN, Sanders L, Dabertrand F, Hill-Eubanks DC, et al. A PLCgamma1-dependent, force-sensitive signaling network in the myogenic constriction of cerebral arteries. Sci Sig-nal. 2014; 7: ra49. doi: 10.1126/scisignal.2004732 PMID: 24866019
14. Sullivan MN, Gonzales AL, Pires PW, Bruhl A, Leo MD, Li W, et al. Localized TRPA1 channel Ca2+ sig-nals stimulated by reactive oxygen species promote cerebral artery dilation. Sci Signal. 2015; 8: ra2. doi: 10.1126/scisignal.2005659 PMID: 25564678
15. Bhattacharya R, Kwon J, Li X, Wang E, Patra S, Bida JP, et al. Distinct role of PLCbeta3 in VEGF-medi-ated directional migration and vascular sprouting. J Cell Sci. 2009; 122: 1025–1034. doi: 10.1242/jcs. 041913 PMID: 19295129
16. Lawson ND, Mugford JW, Diamond BA, Weinstein BM. phospholipase C gamma-1 is required down-stream of vascular endothelial growth factor during arterial development. Genes Dev. 2003; 17: 1346– 1351. PMID: 12782653
17. Crljen V, Visnjic D, Banfic H. Presence of different phospholipase C isoforms in the nucleus and their activation during compensatory liver growth. FEBS Lett. 2004; 571: 35–42. PMID: 15280014

18. Lo Vasco VR, Pacini L, Di Raimo T, D'Arcangelo D, Businaro R. Expression of phosphoinositide-specif-ic phospholipase C isoforms in human umbilical vein endothelial cells. J Clin Pathol. 2011; 64: 911– 915. doi: 10.1136/jclinpath-2011-200096 PMID: 21742750

19. Cines DB, Pollak ES, Buck CA, Loscalzo J, Zimmerman GA, McEver RP, et al. Endothelial cells in physiology and in the pathophysiology of vascular disorders. Blood. 1998; 91: 3527–3561. PMID: 9572988

20. Aird WC. Phenotypic heterogeneity of the endothelium: I. Structure, function, and mechanisms. Circ Res. 2007; 100: 158–173. PMID: 17272818

21. Aird WC. Phenotypic heterogeneity of the endothelium: II. Representative vascular beds. Circ Res. 2007; 100: 174–190. PMID: 17272819

22. Kirby BS, Bruhl A, Sullivan MN, Francis M, Dinenno FA, Earley S. Robust internal elastic lamina fenes-tration in skeletal muscle arteries. PLoS One. 2013; 8: e54849. doi: 10.1371/journal.pone.0054849 PMID: 23359815

23. Socha MJ, Hakim CH, Jackson WF, Segal SS. Temperature effects on morphological integrity and Ca (2)(+) signaling in freshly isolated murine feed artery endothelial cell tubes. Am J Physiol Heart Circ Physiol. 2011; 301: H773–783. doi: 10.1152/ajpheart.00214.2011 PMID: 21705671

24. Johnson RP, El-Yazbi AF, Takeya K, Walsh EJ, Walsh MP, Cole WC. Ca2+ sensitization via phosphor-ylation of myosin phosphatase targeting subunit at threonine-855 by Rho kinase contributes to the arte-rial myogenic response. J Physiol. 2009; 587: 2537–2553. doi: 10.1113/jphysiol.2008.168252 PMID: 19359365

25. Takeya K, Loutzenhiser K, Shiraishi M, Loutzenhiser R, Walsh MP. A highly sensitive technique to measure myosin regulatory light chain phosphorylation: the first quantification in renal arterioles. Am J Physiol Renal Physiol. 2008; 294: F1487–1492. doi: 10.1152/ajprenal.00060.2008 PMID: 18400874

26. Kadamur G, Ross EM. Mammalian phospholipase C. Annu Rev Physiol. 2013; 75: 127–154. doi: 10.1146/annurev-physiol-030212-183750 PMID: 23140367

27. Yang YR, Follo MY, Cocco L, Suh PG. The physiological roles of primary phospholipase C. Adv Biol Regul. 2013; 53: 232–241. doi: 10.1016/j.jbior.2013.08.003 PMID: 24041464

28. Smrcka AV, Sternweis PC. Regulation of purified subtypes of phosphatidylinositol-specific phospholi-pase C beta by G protein alpha and beta gamma subunits. J Biol Chem. 1993; 268: 9667–9674. PMID: 8387502

29. Kim HK, Kim JW, Zilberstein A, Margolis B, Kim JG, Schlessinger J, et al. PDGF stimulation of inositol phospholipid hydrolysis requires PLC-gamma 1 phosphorylation on tyrosine residues 783 and 1254. Cell. 1991; 65: 435–441. PMID: 1708307

30. Gresset A, Sondek J, Harden TK. The phospholipase C isozymes and their regulation. Subcell Bio-chem. 2012; 58: 61–94. doi: 10.1007/978-94-007-3012-0_3 PMID: 22403074

31. Jang HJ, Yang YR, Kim JK, Choi JH, Seo YK, Lee YH, et al. Phospholipase C-gamma1 involved in brain disorders. Adv Biol Regul. 2013; 53: 51–62. doi: 10.1016/j.jbior.2012.09.008 PMID: 23063587

32. Grant DS, Tashiro K, Segui-Real B, Yamada Y, Martin GR, Kleinman HK. Two different laminin do-mains mediate the differentiation of human endothelial cells into capillary-like structures in vitro. Cell. 1989; 58: 933–943. PMID: 2528412

33. Hoeppner LH, Phoenix KN, Clark KJ, Bhattacharya R, Gong X, Sciuto TE, et al. Revealing the role of phospholipase Cbeta3 in the regulation of VEGF-induced vascular permeability. Blood. 2012; 120: 2167–2173. doi: 10.1182/blood-2012-03-417824 PMID: 22674805

34. Mao GF, Kunapuli SP, Koneti Rao A. Evidence for two alternatively spliced forms of phospholipase C-beta2 in haematopoietic cells. Br J Haematol. 2000; 110: 402–408. PMID: 10971398

35. Sun L, Mao G, Kunapuli SP, Dhanasekaran DN, Rao AK. Alternative splice variants of phospholipase C-beta2 are expressed in platelets: effect on Galphaq-dependent activation and localization. Platelets. 2007; 18: 217–223. PMID: 17497434

36. Tang W, Zhang Y, Xu W, Harden TK, Sondek J, Sun L, et al. A PLCbeta/PI3Kgamma-GSK3 signaling pathway regulates cofilin phosphatase slingshot2 and neutrophil polarization and chemotaxis. Dev Cell. 2011; 21: 1038–1050. doi: 10.1016/j.devcel.2011.10.023 PMID: 22172670

37. Ji QS, Winnier GE, Niswender KD, Horstman D, Wisdom R, Magnuson MA, et al. Essential role of the tyrosine kinase substrate phospholipase C-gamma1 in mammalian growth and development. Proc Natl Acad Sci U S A. 1997; 94: 2999–3003. PMID: 9096335

38. Liao HJ, Kume T, McKay C, Xu MJ, Ihle JN, Carpenter G. Absence of erythrogenesis and vasculogen-esis in Plcg1-deficient mice. J Biol Chem. 2002; 277: 9335–9341. PMID: 11744703

39. Homma Y, Takenawa T, Emori Y, Sorimachi H, Suzuki K. Tissue- and cell type-specific expression of mRNAs for four types of inositol phospholipid-specific phospholipase C. Biochem Biophys Res Com-mun. 1989; 164: 406–412. PMID: 2553017

40. Fu Y, Cheng JX, Hong SL. Characterization of cytosolic phospholipases C from porcine aortic endothe-lial cells. Thromb Res. 1994; 73: 405–417. PMID: 8073393

41. Allen V, Swigart P, Cheung R, Cockcroft S, Katan M. Regulation of inositol lipid-specific phospholipase cdelta by changes in Ca2+ ion concentrations. Biochem J. 1997; 327 (Pt 2): 545–552. PMID: 9359428

42. Kim YH, Park TJ, Lee YH, Baek KJ, Suh PG, Ryu SH, et al. Phospholipase C-delta1 is activated by capacitative calcium entry that follows phospholipase C-beta activation upon bradykinin stimulation. J Biol Chem. 1999; 274: 26127–26134. PMID: 10473563

43. Fujii M, Yi KS, Kim MJ, Ha SH, Ryu SH, Suh PG, et al. Phosphorylation of phospholipase C-delta 1 reg-ulates its enzymatic activity. J Cell Biochem. 2009; 108: 638–650. doi: 10.1002/jcb.22297 PMID: 19681039

44. Saunders CM, Larman MG, Parrington J, Cox LJ, Royse J, Blayney LM, et al. PLC zeta: a sperm-specific trigger of Ca(2+) oscillations in eggs and embryo development. Development. 2002; 129: 3533–3544. PMID: 12117804

45. Kibria G, Heath D, Smith P, Biggar R. Pulmonary endothelial pavement patterns. Thorax. 1980; 35: 186–191. PMID: 7385090

46. De Bock M, Wang N, Decrock E, Bol M, Gadicherla AK, Culot M, et al. Endothelial calcium dynamics, connexin channels and blood-brain barrier function. Prog Neurobiol. 2013; 108: 1–20. doi: 10.1016/j. pneurobio.2013.06.001 PMID: 23851106

47. Rebecchi MJ, Pentyala SN. Structure, function, and control of phosphoinositide-specific phospholipase C. Physiol Rev. 2000; 80: 1291–1335. PMID: 11015615

48. Vines CM. Phospholipase C. Adv Exp Med Biol. 2012; 740: 235–254. doi: 10.1007/978-94-007-2888-2_10 PMID: 22453945

49. Ishida S, Matsu-Ura T, Fukami K, Michikawa T, Mikoshiba K. Phospholipase C-beta1 and beta4 con-tribute to non-genetic cell-to-cell variability in histamine-induced calcium signals in HeLa cells. PLoS One. 2014; 9: e86410. doi: 10.1371/journal.pone.0086410 PMID: 24475116

50. Clapham DE. Calcium signaling. Cell. 1995; 80: 259–268. PMID: 7834745

51. Ledoux J, Bonev AD, Nelson MT. Ca2+-activated K+ channels in murine endothelial cells: block by intracellular calcium and magnesium. J Gen Physiol. 2008; 131: 125–135. doi: 10.1085/jgp.200709875 PMID: 18195387

52. Carafoli E, Santella L, Branca D, Brini M. Generation, control, and processing of cellular calcium sig-nals. Crit Rev Biochem Mol Biol. 2001; 36: 107–260. PMID: 11370791

53. Tran CH, Taylor MS, Plane F, Nagaraja S, Tsoukias NM, Solodushko V, et al. Endothelial Ca2+ wave-lets and the induction of myoendothelial feedback. Am J Physiol Cell Physiol. 2012; 302: C1226–1242. doi: 10.1152/ajpcell.00418.2011 PMID: 22277756

54. Garcia-Elias A, Mrkonjic S, Pardo-Pastor C, Inada H, Hellmich UA, Rubio-Moscardo F, et al. Phosphatidylinositol-4,5-biphosphate-dependent rearrangement of TRPV4 cytosolic tails enables channel activa-tion by physiological stimuli. Proc Natl Acad Sci U S A. 2013; 110: 9553–9558. doi: 10.1073/pnas.1220231110 PMID: 23690576

55. Sonkusare SK, Dalsgaard T, Bonev AD, Hill-Eubanks DC, Kotlikoff MI, Scott JD, et al. AKAP150-dependent cooperative TRPV4 channel gating is central to endothelium-dependent vasodilation and is disrupted in hypertension. Sci Signal. 2014; 7: ra66. doi: 10.1126/scisignal.2005052 PMID: 25005230

56. Dunn KM, Hill-Eubanks DC, Liedtke WB, Nelson MT. TRPV4 channels stimulate Ca2+-induced Ca2+ release in astrocytic endfeet and amplify neurovascular coupling responses. Proc Natl Acad Sci U S A. 2013; 110: 6157–6162. doi: 10.1073/pnas.1216514110 PMID: 23530219